# COLLECTED PAPERS

ON

# COHERENT OPTO-ELECTRONICS

## Volume 4

## July 1988—July 1989

Associate Professor

Motoichi OHTSU

TOKYO INSTITUTE OF TECHNOLOGY

THE GRADUATE SCHOOL AT NAGATSUTA

4259 Nagatsuta, Midori-ku, Yokohama,

Kanagawa 227, JAPAN

## PREFACE

This is a research review on coherent opto-electronics by Assoc. Prof. M. Ohtsu, Tokyo Institute of Technology. It contains copies of technical papers published during July 1988 - July 1989, and is composed of three parts, which correspond to research fields of M. Ohtsu. They are (1) Improvements in coherence of lasers, (2) Analyses of laser dynamics, and (3) Applications of coherent lasers.

## MEMBERS

Associate Professor

| | | |
|---|---|---|
| Motoichi OHTSU | ( Dr. Eng. ) | |

Research Associate

| | | |
|---|---|---|
| Ken'ichi NAKAGAWA | ( Dr. Sci. ) | ( 1989.4- ) |

Graduate Students ( Doctor Candidates )

| | | |
|---|---|---|
| Katsuhiko KUBOKI | ( M. Eng. )[a] | ( -1989.3 ) |
| Minoru HASHIMOTO | ( M. Eng. )[b] | ( -1989.3 ) |
| Hiroyuki FURUTA | ( M. Eng. ) | |
| Kaoru YOKOTANI | ( M. Eng. )[c] | ( -1989.2 ) |
| Chul Ho SHIN | ( M. Eng. ) | |
| Hideo KUSUZAWA | ( M. Eng. ) | ( 1989.4- ) |
| Shudong JIANG | ( M. Eng. ) | ( 1989.4- ) |

Graduate Students ( Master Course )

| | | |
|---|---|---|
| Morihiro MURATA | ( B. Eng. )[d] | ( -1989.3 ) |
| Eiji IKEGAMI | ( B. Eng. ) | |
| Motonobu KOUROGI | ( B. Eng. ) | |
| Isao KOSHIISHI | ( B. Eng. ) | |
| Hiromasa SUZUKI | ( B. Eng. ) | ( 1989.4- ) |
| Mitsuhiro TESHIMA | ( B. Eng. ) | ( 1989.4- ) |
| Naoyuki TOMITA | ( B. Eng. ) | ( 1989.4- ) |

Undergraduate Students

| | |
|---|---|
| Keiji YAMAMOTO | ( 1989.4- ) |
| Akihiro KIYOHARA | ( 1989.4- ) |

Visiting Researchers

| | |
|---|---|
| Toru IMAI[e] | |
| Togar PANGARIBUAN[f] | ( 1988.10 - 1988.12 ) |
| Budi PARDONO[g] | ( 1989.4 - 1989.6 ) |

a) Presently with Central Research Lab., Hitachi, Ltd.

b) Presently with Sony, Ltd.

c) Presently with Defense Academy

d) Presently with Yamaha, Ltd.

e) Permanent Address : Tokyo Aircraft Instrument Co. Ltd., Tokyo, Japan

f) Permanent Address : Graduate School, University of Indonesia, Jakarta, Indonesia

g) Permanent Address : Indonesian Institute of Sciences, Serpong, Indonesia

# LIST OF PAPERS

## [I] IMPROVEMENTS IN COHERENCE OF LASERS

### (a) Journal Papers

[1] M. Ohtsu, "Frequency stabilization in semiconductor lasers", Optical and Quantum Electronics, Vol.20, (1988) pp.283 - 300 ( Tutorial review )

[ pp. 1 - 18 ]

[2] C.-H. Shin, K. Kuboki and M. Ohtsu, "Simulation for the Heterodyne Type Optical Phase-Locked Loop by Semiconductor Lasers", Trans. IEE Japan, Vol. 108-C, No.9, (1988) pp. 678 - 684 ( in Japanese )

[ pp.19 - 25 ]

[3] L. Hollberg and M. Ohtsu, "Modulatable narrow-linewidth semiconductor lasers", Appl. Phys. Lett., Vol.53, No.11, (1988) pp.944 - 946

[ pp.26 - 28 ]

[4] M. Ohtsu, "Improvements of coherence in semiconductor lasers for optical sensing", Optronics, No.9, (1988) pp.97 - 101 ( Review paper, in Japanese )

[ pp.29 - 33 ]

[5] M. Ohtsu, "Light emitting devices for optical sensing", New Glass, Vol.3, No.2, (1988) pp.64 - 71 ( Review paper, in Japanese )

[ pp.34 - 41 ]

[6] M. Ohtsu, "Spectral properties of semiconductor lasers under electrical negative feedback", University and Science, Vol.2, (1988) pp.46 - 57 ( Review paper, in Japanese )

[ pp.42 - 53 ]

[7] M. Ohtsu and E.Ikegami, "Frequency stabilization of 1.5 um DFB laser using internal second harmonic generation and atomic $^{87}$Rb line", Electron. Lett., Vol. 25, No. 1, (1989) pp.22 - 23

[ pp.54 -55 ]

[8] C.H. Shin, M. Teshima and M. Ohtsu, "Novel measurement method of linewidth enhancement factor in semiconductor lasers by optical self-locking", Electron. Lett., Vol. 25, No. 1, (1989) pp.27 - 28

[ pp.56 - 57 ]

[9] M. Ohtsu, "Realization of Hyper-Coherent Light", Science ( Japanese version of "Scientific American" ), March (1989) pp.64 - 73 ( Review paper, in Japanese )

[ pp.58 - 67 ]

(b) International Conferences

[1] K. Kuboki, C.-H. Shin, T, Kato and M. Ohtsu, "Proposal of heterodyne type optical phase locked loop by semiconductor lasers", Proceedings of The 26th International Conference on Quantum Electronics ( IQEC'88 ), July 1988, Tokyo, Japan TuP58, pp.446 - 447

[ pp.68 - 69 ]

[2] M. Ohtsu, K. Kuboki, C.H. Shin and M. Murata, "Frequency Control of Semiconductor Lasers", Proceedings of the Fourth

Symposium on Frequency Standards and Metrology, September 1988, Ancona, Italy, Ed. by A. De Marchi ( Springer-Verlag, Berin ) pp.242 - 246

[ pp.70 - 74 ]

[3] M. Ohtsu and E. Ikegami, "Novel frequency control Scheme for a 1.56 um DFB laser using an internal second harmonic and atomic rubidium line", Proceedings of the Conference on Lasers and Electro-Optics ( CLEO'89 ), April 1989, Baltimore, Maryland, TUD4

[ pp.75-76 ]

[4] M. Ohtsu, M. Murata and M. Kourogi, "Subkilohertz linewidth of a semiconductor laser by electrical feedback and its network analysis", Proceedings of the Conference on Lasers and Electro-Optics ( CLEO'89 ), April 1989, Baltimore, Maryland, THK30

[ pp.77 - 78 ]

[5] M. Ohtsu, "Progress toward Highly Coherent Semiconductor Lasers", Proceedings of The Seventh International Conference on Integrated Optics and Optical Fiber Communication ( IOOC'89 ), July 1989, Kobe, Japan, 19A3-1 ( Invited ), pp.14 - 15

[ pp. 79 - 80 ]

[6] C.H. Shin, M. Teshima and M. Ohtsu, "Modulatable, High Coherent and Compact Semiconductor Laser Modules", Proceedings of The Seventh International Conference on Integrated Optics and Optical Fiber Communication ( IOOC'89 ), July 1989, Kobe, Japan, 21D4-5, pp.116 - 117

[ pp.81 - 82 ]

## [II] ANALYSES OF LASER DYNAMICS

(a) Journal Papers



## [III] APPLICATIONS OF COHERENT LASERS

(a) Journal Papers

(b) International Conference

[1] M. Hashimoto and M. Ohtsu, "Improvements in Short- and Long-Term Frequency Stabilities of Diode Laser Pumped Rubidium Atomic Clock", Proceedings of the Fourth Symposium on Frequency Standards and Metrology, September 1988, Ancona, Italy ( Ed. by A. De Marchi ( Springer-Verlag, Berlin ) pp.434 - 435

[ pp.115 - 116 ]

[III] Appendix

(a) Review Papers

[1] M. Ohtsu, "Frequency stabilization of semiconductor lasers for coherent optical communication and sensing", Anritsu Technical, No.56, (1988) pp.7 - 17 ( in Japanese )

[ pp.117 - 127 ]

[2] M. Ohtsu, "Development of a Hyper-coherent Optical Sweep Generator Using Semiconductor Lasers", Vol.9, No.45, (1989) pp.4 - 9

[ pp.128 - 133 ]

[V] Awards

[1] Japan IBM Science Award, Category of Electronics, on "Generation of Ultra-high Coherent Light from Semiconductor Lasers", November, 1988

## [VI] PRESENTED PH.D. THESES

[1] Katsuhiko KUBOKI, "Study on Heterodyne-type Frequency Locked Loop by Semiconductor Lasers", January 1989.

[2] Minoru HASHIMOTO, "Study on Applications of Semiconductor Lasers to Rubidium Atomic Clocks", January 1989.

[3] Yoshiaki AKIMOTO, "Study on Methane-stabilized Helium Neon Lasers for Optical Frequency Standards", April 1989

*Optical and Quantum Electronics* **20** *(1988) 283–300*

TUTORIAL REVIEW

# Frequency stabilization in semiconductor lasers

MOTOICHI OHTSU
*Graduate School at Nagatsuta, Tokyo Institute of Technology, 4259 Nagatsuta-cho, Midori-ku, Yokohama 227, Japan*

AN INVITED PAPER

*Received 22 June 1987; revised 18 November 1987; accepted 11 December 1987*

Three promising methods of improving temporal coherence in semiconductor lasers are reviewed. They are the development of novel laser devices, a technique of optical feedback and a technique of electrical feedback. The main discussion in this paper is focused on the technique of electrical feedback. The theoretical limit of frequency stability and recent experimental results are presented with respect to the following five subjects which are indispensable in the realization of highly coherent lasers: (a) frequency stabilization; (b) improvements in frequency reproducibility; (c) linewidth reduction; (d) frequency tracking; and (e) stable, accurate and wideband frequency sweep.

## 1. Introduction

One of the advantageous properties of the light emitted from a laser is its high temporal coherence; that is, the light is monochromatic and its frequency and phase are stable. Attempts at further improvements of this property have been continuously carried out since the advent of lasers [1–3]. Furthermore, high temporal coherence of semiconductor lasers has been required recently for applications to coherent optical communication [4, 5], coherent optical sensing, and so on. However, since cavity structures and oscillating mechanisms of semiconductor lasers are considerably different from those of other kinds of lasers, techniques for improving their temporal coherence also be different from those for other lasers.

In this paper a technique of improving temporal coherence – that is, to stabilize the frequency of semiconductor lasers – are reviewed. In Section 2 basic concepts of frequency stabilization and three promising methods of achieving it are presented. The theoretical limit of ultimate frequency stability expected by a technique of negative electrical feedback is also estimated. In Section 3 the discussion is focused on negative electrical feedback, and experimental results on five subjects are presented, which are essential in the realization of a highly coherent laser. Section 4 is provided to introduce the development of novel integrated laser devices, which are compatible with a technique of negative electrical feedback. Several applications of the frequency-stabilized laser are given in Section 5. Discussions in the present paper are summarized in Section 6.

0306-8919/88 $03.00 + .12 

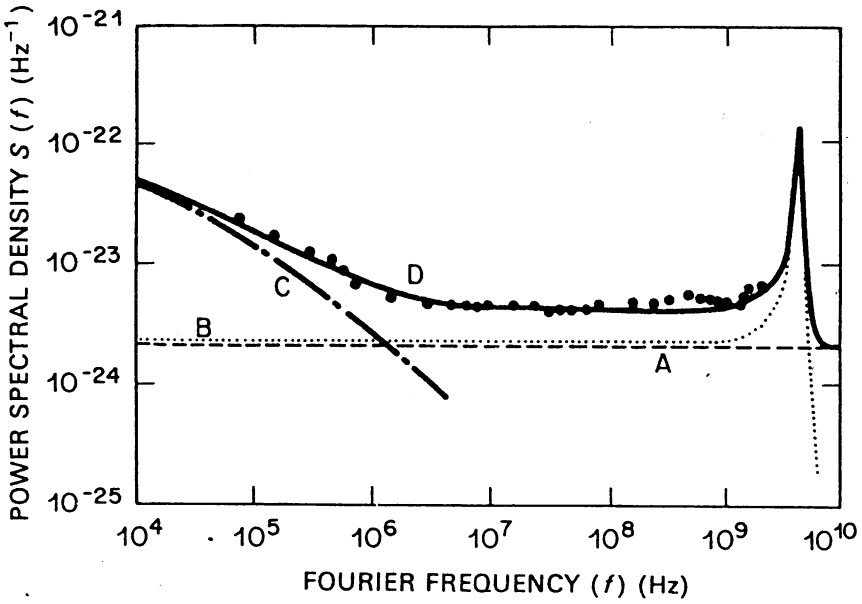


*Figure 1* Power spectral density of frequency fluctuation in a 0.8 $\mu$m AlGaAs laser [6]. A, Fluctuation induced by spontaneous emission; B, fluctuation induced by carrier density fluctuation, which is also induced by the spontaneous emission; C, fluctuation induced by current fluctuation, which is induced by carrier density fluctuation of curve B; and D, total frequency fluctuation given by the sum of A to C. Close circles represent experimental results.

## 2. Fundamental concepts of frequency stabilization

In the following discussion it is assumed that the semiconductor laser oscillates with a single longitudinal mode and with the lowest transverse mode. The fundamental driving forces for frequency fluctuations in semiconductor lasers are spontaneous emission and carrier density fluctuations. Since this carrier density fluctuation is also induced by the spontaneous emission [6], it should be noted that the most fundamental intrinsic noise source — the quantum noise source — is the spontaneous emission. Fig. 1 shows the power spectral density of frequency fluctuations in an AlGaAs laser driven by these noise sources [6]. In addition to these intrinsic noise sources there are several external noise sources, such as ambient temperature fluctuations, injection current fluctuations due to the noises from a power supply, and so on. The contributions form all the noise sources to the frequency fluctuations of a free-running laser are shown by curve E of Fig. 2 [7]. In this figure $\sigma$ represents the square root of the Allan variance $\sigma^2$ [8] which is a measure commonly used to evaluate the frequency stability of stable oscillators. The quantity $\tau$ in abscissa represents the integration time of the measurements. As shown by curves $A_1$, $B_1$, $C_1$ and D, the measured values of $\sigma$ are larger than $10^{-8}$. These values can be regarded as the magnitude of fluctuation of the centre frequency of the field spectrum actually observed for free-running lasers.

The linewidth of the field spectrum takes the value of between several megahertz and several hundred megahertz, which is also governed by the magnitudes of spontaneous emission and carrier density fluctuations. For this linewidth the power spectral density of frequency fluctuations in Fig. 1 at the Fourier frequency range of $f \leqslant 100$ MHz gives a main contribution. In other words, the value of $\sigma$ in Fig. 2 at the integration time range of $\tau \geqslant 10$ ns gives the main contribution.

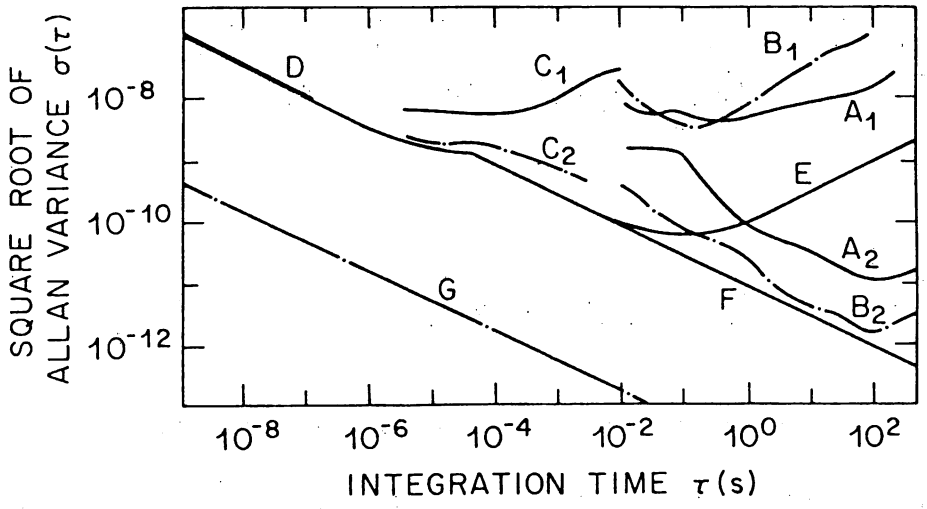


*Figure 2* Experimental and theoretical results of frequency fluctuation in a 0.8 $\mu$m AlGaAs laser [7]. $\sigma$ and $\tau$ represent the square root of the Allan variance and integration time of measurement, respectively [8]. $A_1$, $B_1$, $C_1$, D, Experimental results for free-running laser; $A_2$, $B_2$, $C_2$, experimental results stabilized by using absorption spectral lines in $H_2O$ vapour, Rb vapour and a resonance spectral line of a rigid Fabry–Perot interferometer, respectively; E, calculated result of the magnitude of the frequency fluctuation in a free-running laser; F, calculated result of the magnitude of the frequency fluctuation induced by quantum noise sources – that is, spontaneous emission and carrier density fluctuation; and G, calculated result of ultimate limit of residual frequency fluctuation in a frequency-stabilized laser. This value is governed by a detector shot noise in the feedback loop.

The reproducibility of a semiconductor laser frequency is lower than that of other kinds of lasers, because of scattering of cavity dimensions and scattering of mole-fractions in composite semiconductor materials. Furthermore, a large magnitude of long-term frequency drift can be observed for $\tau$ as long as several months. For example, it has been observed that the centre frequency of the field spectrum in an AlGaAs laser showed a blue shift of several megahertz per hour for a period of 1 month [9].

As can be recognized from the discussions described above, the magnitude of the centre frequency fluctuations and the linewidth of the field spectrum can be essential measures in the evaluation of the temporal coherence of the laser. However, the experimentally observed values of these measures are still unsatisfactorily large for applications to coherent optical communication, coherent optical sensing, and so on. For example, by a brief estimation, the value of $\sigma$ and the linewidth have to be lower than $10^{-9}$ and 100 kHz, respectively, for these applications. There are three promising methods to satisfy these demands: (a) to develop a novel device; (b) to improve temporal coherence by optical feedback; and (c) by electrical feedback. Among these methods the third is most promising at the present stage, because of its high stability and reliability. Therefore, the remainder of this paper focuses on this technique. A technique of optical feedback is also described in Section 5, and this is compared with the electrical feedback. Developments of novel devices are introduced in Section 4.

Fig. 3 is a block diagram of negative electrical feedback system in which several external electrical and optical components are connected to the laser. To reduce the frequency fluctuation it is necessary to detect its magnitude precisely, and the detected signal has to be negatively fed back to the operating parameter of the laser to countermodulate the laser frequency. As such an operating parameter, temperature or injection current has commonly been used. That is, the laser frequency is varied through the variations of refractive index

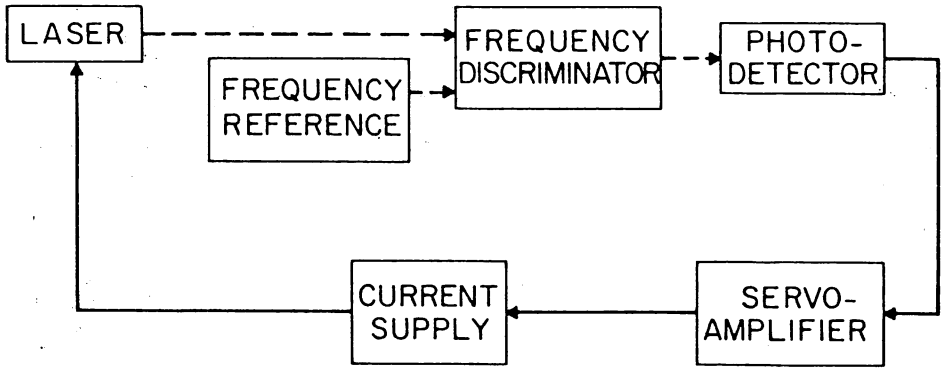


*Figure 3* Block diagram of negative electrical feedback for frequency stabilization.

and cavity length, which are induced by the variations of temperature or injection current. For example, a red shift of about $10\,\mathrm{GHz\,K^{-1}}$ and about $10\,\mathrm{GHz\,mA^{-1}}$ can be induced by variations of temperature and injection current, respectively. However, since the response time constant of the temperature variation is rather long, it is more favourable to control the injection current to realize a wide bandwidth of the negative electrical feedback loop.

Variations of laser frequency by the injection current modulation are due to the temperature variation at the p–n junction (temperature effect) and the carrier density variations in the active waveguide (carrier effect). As is shown by Fig. 4a, the f.m. response due to the temperature effect has low-pass characteristcs with a cut-off frequency of several megahertz. The f.m. response due to the carrier effect also shows low-pass characteristics with a cut-off frequency of several gigahertz, which corresponds to the resonance frequency of relaxation oscillation [10]. Fig. 4b shows a phase delay of f.m. response [11]. It should be noted that both the temperature and the carrier effects induce the phase delay. External servo-amplifiers for negative electrical feedback should be designed by taking these f.m. response characteristics of the laser into account.

As was described above, the frequency fluctuations due to quantum noise sources (spontaneous emission and carrier density fluctuations) can be detected by the experimental set-up of Fig. 3, and the laser frequency can be countermodulated by a macroscopic operating parameter — the injection current — to compensate for these fluctuations. In this situation an effect of this negative electrical feedback can be expressed by following the quantum-mechanical Langevin equation of motion if the bandwidth of the feedback loop is assumed to be infinite [12]:

$$\delta\nu(t) = \Gamma_s(t) + \Gamma_c(t) - \int_0^\infty h(t')[\delta\nu(t - t') + \Gamma_n(t')]\mathrm{d}t' \qquad (1)$$

where $\delta\nu(t)$ is the frequency fluctuation at time $t$. The Langevin forces $\Gamma_s$ and $\Gamma_c$ represent the two quantum noise sources for the free-running laser due to spontaneous emission and carrier density fluctuations, respectively. The convolution integral on the right-hand side of this equation represents the effect of negative electrical feedback, where $\delta\nu(t - t')$ is the detected frequency fluctuation, $\Gamma_n$ is the noise magnitude generated from the feedback loop, and $h(t')$ is the impulse response of the feedback loop. The Fourier transform of Equation 1 gives

$$F(f) = \frac{\Pi_s(f)}{1 + H(f)} + \frac{\Pi_c(f)}{1 + H(f)} - \frac{H(f)}{1 + H(f)}\Pi_n(f) \qquad (2)$$

where $F$, $\Pi_s$, $\Pi_c$, $\Pi_n$ and $H$ represent the Fourier transform of $\delta\nu$, $\Gamma_s$, $\Gamma_c$, $\Gamma_n$ and $h$,

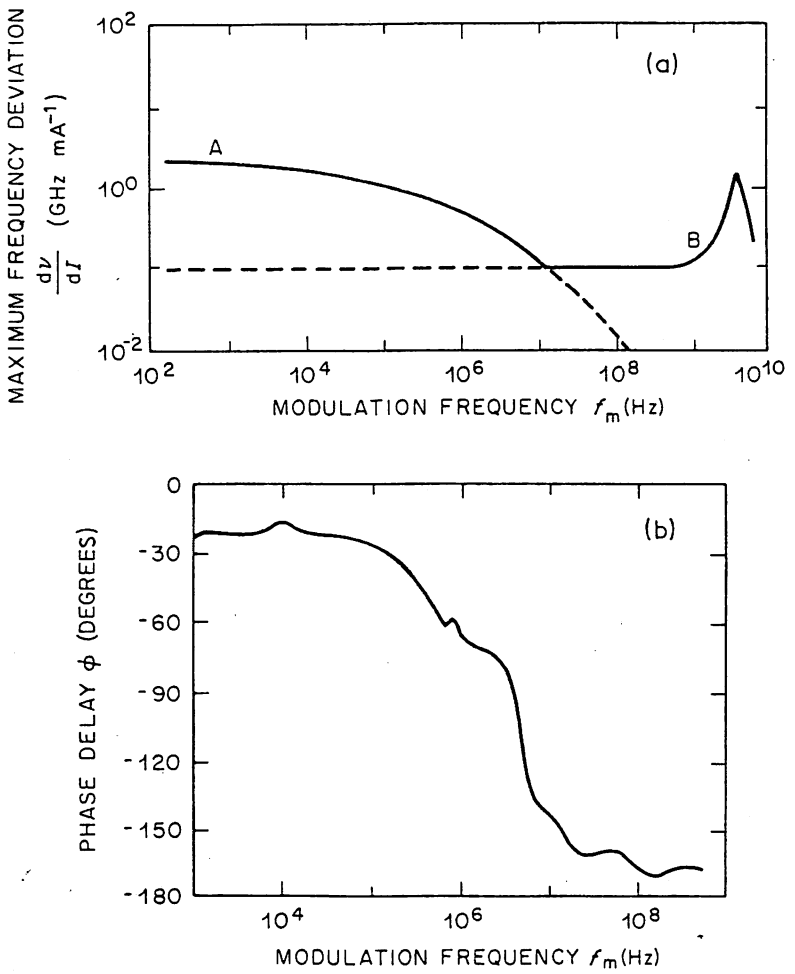


*Figure 4* Frequency-modulated response characteristics of a 0.8 $\mu$m AlGaAs laser, given as a function of modulation frequency $f_m$ of the injection current. (a) Maximum deviation of the laser frequency per a unit change of the amplitude of modulated injection current [10]. Curves A and B represent contributions from thermal effect and carrier effect, respectively. (b) Phase delay of the f.m. response with respect to the phase of the modulated injection current [11].

respectively. In Equation 2 the values of the first and second terms of the right-hand side approach zero in the infinite gain of the feedback loop ($|H| \rightarrow \infty$), while that of the third term approaches $|\Pi_n|$. This means that the contributions from the two quantum noise sources can be suppressed by a high gain of feedback, and the magnitude of the frequency fluctuation can ultimately be reduced to a value limited by the noise magnitude generated from the feedback loop. In other words, if a high-gain and low-noise feedback loop is employed, a very high temporal coherence and high frequency stability can be artifically realized, resulting in lower frequency fluctuations than the quantum noise level of the free-running laser. For this reason it can be claimed that the negative electrical feedback is a promising technique in the realization of a high frequency stability in semiconductor lasers.

Since the negative electrical feedback can improve the frequency stability to a value limited by the noise magnitude generated from the feedback loop, curve G of Fig. 2 represents such a stability limit governed by the shot noise of the photodetector in the feedback loop. This limit of frequency fluctuations is expressed as $\sigma = 1.7 \times 10^{-14}\tau^{-1/2}$ [7], which is as low as that of a hydrogen maser. Furthermore, as is described in Section 3,

the linewidth of the field spectrum can also be reduced to 58 mHz to 2.9 Hz by the negative electrical feedback [13], which is as narrow as that of a frequency-stabilized gas laser. From these results of estimation, it can be concluded that a semiconductor laser has a possibility of becoming a quite highly stabilized oscillator by negative electrical feedback.

## 3. Techniques for frequency stabilization

By an analogy with a well-developed technique for highly stabilized microwave oscillators (hydrogen masers, caesium and rubidium atomic clocks [1], and so on) and by the requirements from several applications, five subjects described in the following subsections should be carried out for semiconductor lasers to improve their frequency stability and temporal coherence.

### 3.1. Improvements in stability of the centre frequency of the field spectrum

For improvements in stability of the centre frequency of the field spectrum, components of the frequency fluctuation at the Fourier frequency range $f \leqslant 1$ MHz should be reduced. Temperature fluctuation in the free-running laser can give a major contribution at such a low Fourier frequency range, and this fluctuation would induce a frequency drift. It is effective to employ an analogue integrator as an external servo-amplifier in Fig. 3 for negative feedback to reduce this drift. Furthermore, it is effective to use an analogue proportional amplifier and differentiator in parallel with the integrator, to expand the bandwidth of the feedback loop.

One of the simplest frequency references in Fig. 3 is a passive external cavity, for example, a Fabry–Perot interferometer. However, its resonance frequency would drift with an ambient temperature fluctuation. This can degrade the long-term frequency stability of the laser under feedback conditions. Temperature stabilization of the interferometer would be required in order to obtain a higher frequency stability. However, since the effect of this drift is negligibly small at the Fourier frequency of $f \geqslant 100$ Hz (that is, at the integration time of $\tau \leqslant 10$ ms), a simple Fabry–Perot interferometer – for example, one made of a rigid cylindrical quartz block – has commonly been used to improve short-term frequency stability within this Fourier frequency range. Curve $C_2$ of Fig. 2 represents the experimental result obtained by using such a compact interferometer as a frequency reference.

For higher frequency stability a more stable frequency reference should be employed. For the semiconductor lasers of wavelength 0.7 to 1.6 $\mu$m, spectral lines of combination tones or higher harmonics of vibration–rotation transitions in organic molecular vapour (for example, $H_2O$ and $NH_3$ [14, 15]) can be used as such a stable frequency reference. Since a great number of these lines are found in the near-infrared wavelength range, the frequency of each semiconductor laser can be tuned to at least one of them, which makes these lines popular and stable frequency references. Curve $A_2$ of Fig. 2 represents the experimental results obtained by using an absorption spectral line in $H_2O$ vapour as a frequency reference. The frequency shift of the AlGaAs laser locked to the $H_2O$ vapour has been accurately measured, and a value of $1 \times 10^{-8}\,K^{-1}$ was obtained, which was attributed to temperature-dependent pressure shift in $H_2O$ vapour [16]. A problem of employing the absorption spectral lines in these organic molecular vapours is that the sensitivities of the frequency discrimination of these references are rather low because of their low absorption coefficients. In contrast, resonance spectral lines of electronic transitions in alkali vapours (for example, Cs and Rb) can be used as a highly sensitive frequency reference, because they

exhibit large absorption coefficients at the wavelength range of 0.8 $\mu$m [17, 18]. Curve $B_2$ of Fig. 2 represents the experimental result obtained using an absorption spectral line in Rb vapour as a frequency reference. It can be seen that this result shows a higher stability than that of curve $A_2$, which is due to the higher sensitivity of frequency discrimination by Rb vapour. Furthermore, for the 0.8 $\mu$m wavelength range, strong spectral lines due to the optogalvanic effect in inert gases can be also used as a sensitive frequency reference [19]. Since the wavelengths of these lines have been well calibrated by a conventional technique of spectroscopy, they can be used as a frequency reference with a high frequency accuracy. However, the problem in employing optogalvanic spectral lines is that the resonance frequencies of these lines are shifted by a variation of the discharge current, as was the case of a traditional Lamb-dip stabilized He–Ne gas laser at wavelength 633 nm. This shift in reference frequency would limit the frequency stability of semiconductor laser at $\sigma \geqslant 10^{-9}$ to $10^{-10}$.

The minimum of $\sigma$ on curve $B_2$ of Fig. 2 is $1.4 \times 10^{-12}$ at the integration time of 100 s, which is as low as that of the theoretically estimated value governed by spontaneous emission and carrier density fluctuations (curve F of Fig. 2). This means that the frequency drift due to temperature fluctuation in the free-running laser was sufficiently suppressed by the negative electrical feedback, and the quantum noise limit has already been realized. Further improvements can be expected by improving the performances of feedback systems, and frequency fluctuation as low as that limited by the detector shot noise (curve G in Fig. 2) can be expected in the future. For 1.5 $\mu$m wavelength InGaAsP lasers, absorption spectral lines in $H_2O$ and $NH_3$ have also been used as frequency references, and the frequency fluctuation as low as that given by curve $A_2$ of Fig. 2 has been realized [14, 20].

For detecting the spectral lines mentioned above, the technique of absorption spectroscopy has commonly been employed. To improve the sensitivity and resolution of this detection, a technique of frequency-modulation spectroscopy was recently employed, and preliminary experiments were demonstrated [21].

## 3.2. Improvements in reproducibility of the centre frequency of the field spectrum

A high gain of the analogue integrator is required at a low Fourier frequency range in order to reduce the frequency drift caused by temperature fluctuation. However, since the gain of the commercially available analogue integrator has an upper limit at a very low Fourier frequency range, it has been empirically found that the low frequency roll-off of the negative feedback is about 1 mHz. In other words, it is rather difficult to improve the long-term frequency stability at the integration time $\tau \geqslant 1000$ s by using conventional electronic circuits. This is the main cause limiting the frequency reproducibility of the stabilized laser. Developments of a d.c. amplifier, having a larger gain at an ultra-low frequency range, would be required to improve the reproducibility.

On the other hand, as described in Section 2, a long-term blue shift has been observed, which was attributed to slow temporal decreases of thermal resistance due to oxidation of the indium bonding layer of thermal effects induced by non-radiative recombinations of carrier near the facets [22]. Decreases and stabilization in thermal resistance and screening of laser devices are required at the stage of device fabrication, in order to reduce these uncontrollable frequency variations and to improve the frequency reproducibility.

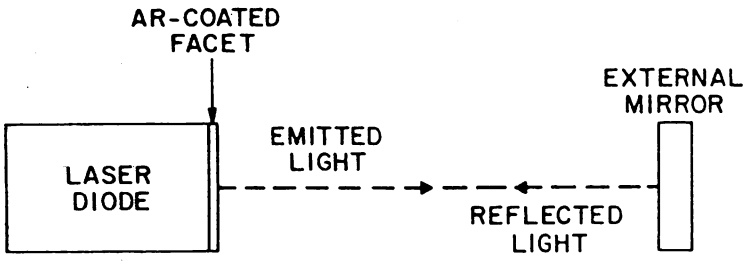


*Figure 5* Experimental set-up of extended cavity laser, which employs an optical feedback effect induced by the reflected light from an external mirror.

### 3.3. Linewidth reduction of the field spectrum

Frequency fluctuation at the Fourier frequency range of $f \leqslant \Delta\nu_{FR}$ has to be reduced for linewidth reduction of the field spectrum by the negative electrical feedback, where $\Delta\nu_{FR}$ represents the linewidth of the free-running laser. However, since the linewidth at an early period of the development of semiconductor laser devices was as wide as 100 MHz, a bandwidth wider than 100 MHz has been required for the feedback system. Since the design of such a wideband feedback system was not technically easy, an alternative technique – optical feedback – has so far been preferably employed. The experimental set-up for optical feedback is shown in Fig. 5. The principle of operation is that the frequency fluctuation induced by randomly generated photons due to the spontaneous emission process was decreased by increasing the photon lifetime in the laser cavity. In this figure an external mirror was used to form a large volume of extended cavity, by which the photon lifetime in the cavity was increased. The linewidth has been reduced to as little as 10 kHz by this technique [23]. Furthermore, as an equivalent configuration an optical fibre was connected at one of the laser facets, and one of the polished edges of the fibre was used as an external mirror to form a long extended cavity. Using this configuration a linewidth of 30 kHz was realized [24]. If the position of the external mirror was not stabilized within the accuracy of the optical wavelength, then this extended-cavity laser would induce several instabilities in oscillation characteristics induced by variations of operating parameters of the laser. For example, the linewidth fluctuates due to the mechanical vibration of the external mirror. Furthermore, inappropriate values of operating parameters (cavity length, laser power coupling between the laser diode and external mirror, injection current, and so on) would sometimes induce chaotic instability [25] or coherence collapse [26]. This configuration has further problems, such as the increase in the cavity volume, decreases in the direct frequency modulation efficiency, and so on. In spite of these disadvantageous properties, it has commonly been used for several applications because of its technical simplicity.

On the other hand, the performances of laser devices have been improved drastically in recent years by the progress of device fabrication techniques, and a linewidth as narrow as several tens of megahertz has recently been demonstrated for a free-running laser. This means that the requirement of the bandwidth for negative electrical feedback becomes less severe. By following this trend, an approach of negative electrical feedback was tried [27] to overcome difficulties presented by the optical-feedback technique. Its principle of operation is similar to that of frequency stabilization described in Section 3.1 (Fig. 3) except that its feedback bandwidth is expanded to as much as several tens of megahertz. To realize this bandwidth expansion, the feedback loop length was decreased and a phase compensating

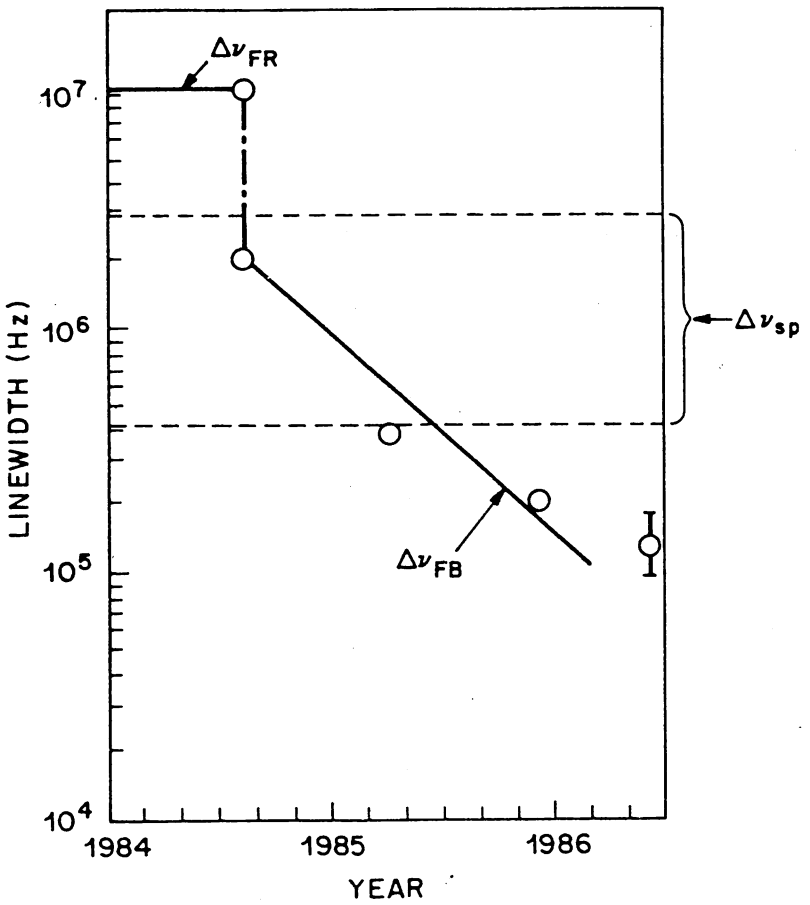


*Figure 6* Progress of the experimental results of the linewidth reduction of a 1.5 $\mu$m InGaAsP laser by employing negative electrical feedback [13, 29, 31]. $\Delta\nu_{FR}$, Linewidth of a free-running laser; $\Delta\nu_{FB}$, linewidth under feedback condition. The value of the linewidth between the two broken lines represents the value of $\Delta\nu_{sp}$, which is the linewidth governed by spontaneous emission; that is, by the most fundamental quantum noise source.

circuit was employed to compensate for the phase delay shown in Fig. 4b. For frequency reference and discriminator, a compact Fabry–Perot interferometer [27–29] or heterodyning with a highly coherent reference laser [30] has been employed. Fig. 6 shows the progress of the authors' experimental results of linewidth reduction by employing a compact 3 cm long Fabry–Perot interferometer as a frequency reference. It is seen from this figure that the linewidth of between 150 and 360 kHz has recently been obtained for a 1.5 $\mu$m InGaAsP laser [13, 29, 31]. This is 1/65 to 1/27 times the linewidth of the free-running laser. The profile of the field spectrum was very stable in spite of ambient temperature fluctuations, mechanical vibrations and acoustic vibrations in the laboratory. That is, its linewidth was kept constant for more than 40 h [13]. Such a high stability can be attributed to the fact that the electrical feedback employed was inherently negative. It was not always possible to obtain such a high stability by optical feedback.

The linewidth of the free-running laser has been given by the modified Schawlow–Townes formula [32], which is expressed as

$$\Delta\nu_{FR} = \Delta\nu_{sp}(1 + \alpha^2) \tag{3}$$

In this equation $\Delta\nu_{sp}$ represents a contribution from the most fundamental quantum noise source — that is, the spontaneous emission — which corresponds to $|\Pi_s|$ in Equation 2. The quantity $\alpha$ is a linewidth-enhancement factor due to carrier density fluctuation induced by

the spontaneous emission [32], and $\Delta\nu_{sp}\alpha^2$ corresponds to $|\Pi_c|$ in Equation 2. Reported values of the linewidth-enhancement factor of 1.5 $\mu$m InGaAsP laser is $1.5 \leqslant \alpha \leqslant 5.0$ [33]. This leads to $1/3.3 \geqslant 1/(1 + \alpha^2) \geqslant 1/26$. Therefore, the factor of 1/65 to 1/27 shown above implies that the linewidth realized by the present feedback is narrower than the value of $\Delta\nu_{sp}$ determined from the magnitude of the spontaneous emission – that is, the most fundamental quantum noise source. This fact is consistent with the result of the theoretical discussion in Section 2.

At the present stage the linewidth obtained experimentally is still limited by the insufficient bandwidth of the negative electrical feedback loop, which is mainly caused by the response time delay of the wideband servo-amplifier. If the present amplifier is replaced by a faster GaAs amplifier [34], then the total delay time of the feedback loop can be decreased to as short as 0.6 ns even if electrical and optical path lengths in the feedback loop are as long as 12 cm. By a precise network analysis based on the value of this delay time, it has been estimated that a linewidth as narrow as 15 kHz can be expected by using the presently employed discrete electrical and optical components; that is, without employing any novel optoelectronic integrated circuits [13].

Furthermore, if a sufficiently wide bandwidth of the feedback is maintained by employing a fast GaAs servo-amplifier as described above, it can be expected that the value of the noise-limited linewidth, corresponding to $|\Pi_n|$ in Equation 2, can be reduced by increasing the sensitivity of the frequency discriminator for the negative feedback. For example, this increase in the sensitivity can be realized by reducing the resonant spectral linewidth $\Delta\nu_{FP}$ of the Fabry–Perot interferometer used as a frequency reference and discriminator. However, if the value of $\Delta\nu_{FP}$ is reduced too much, then the bandwidth of the feedback loop will be limited by the bandwidth of the Fabry–Perot interferometer itself. This would violate the assumption, made for the present discussion, of a sufficiently wide bandwidth of the feedback loop. In such a case further decreases in the noise-limited linewidth will be prohibited. This means that there is an optimum value of $\Delta\nu_{FP}$ to give the minimum of noise-limited linewidth of the laser. Calculations were carried out to demonstrate this possibility [13], and it was found that the noise-limited linewidth took a minimum of 58 mHz to 2.9 Hz if $\Delta\nu_{FP}$ is between 820 kHz and 6.8 MHz. These values of $\Delta\nu_{FP}$ correspond to the length of the Fabry–Perot interferometer of 9.3 to 1.1 m for a mirror reflectivity of 80%. A fibre ring cavity [35] can be used to reduce a volume of such a long Fabry–Perot interferometer. From this estimation it can be concluded that quite a narrow linewidth of the field spectrum is expected by an optimum condition of negative electrical feedback.

It can be pointed out that the technique of negative feedback has several advantages. For example, the laser cavity structure does not have to be modified, is more stable than the technique of optical feedback, and so on. Even though the frequency fluctuations at the tail of the field spectrum are not reduced because of the finite bandwidth of the electrical feedback loop, it has been confirmed that the profile around the peak of the field spectrum can be well approximated as a very narrow Lorentzian [27–29]. Therefore, electrical feedback can be an effective technique to improve temporal coherence of light sources, especially for narrow bandwidth sensing systems and for low to medium bit-rate coherent optical communication systems.

### 3.4. Frequency tracking to a stable master laser

It is possible to control a laser (a slave laser) so that its frequency tracks that of a highly stable laser (a master laser). Here it is assumed that the stable master laser has been

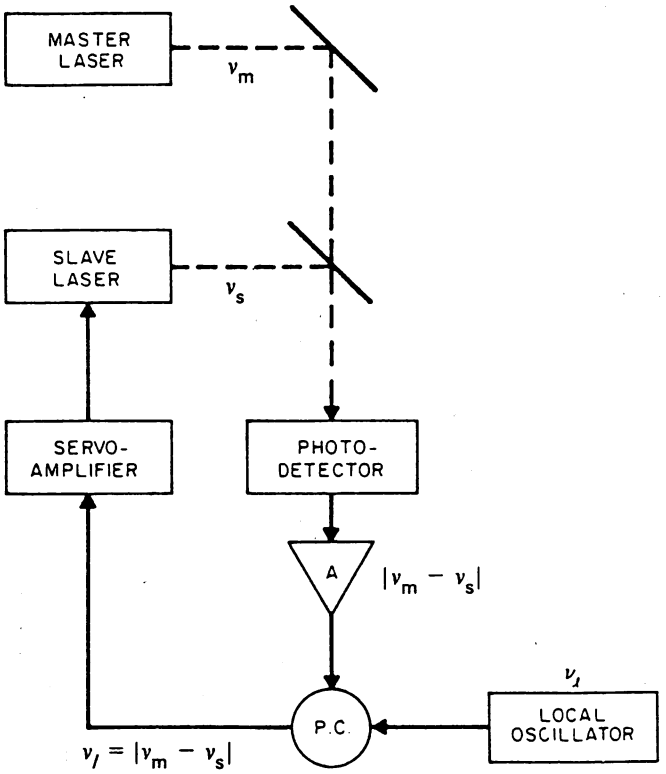


*Figure 7* Experimental set-up for frequency offset locking [37]. P.C., Phase comparator; $\nu_m$, $\nu_s$, $\nu_l$, frequency of a master laser, a slave laser and a microwave local oscillator, respectively.

prepared by the techniques of Sections 3.1 to 3.3. This tracking means that a high temporal coherence of the master laser can be transferred to the slave laser, which would be useful for heterodyne or homodyne detection in coherent optical communication systems, direct optical amplification, coherent optical sensing, and so on. The technique of such a frequency tracking has been well developed for microwave oscillators.

One of the techniques commonly used for frequency tracking is a non-linear optical effect called injection locking [36]. That is, if the light from the master laser is injected into the slave laser, then the slave laser frequency is locked to that of the master laser. Under this condition the slave laser frequency tracks the master laser frequency. In spite of the phenomenon of injection locking being physically interesting, it presents several difficulties if it is used as a practical technique for accurate frequency tracking and transfer of high temporal coherence. This is because the lock range depends on the powers of both lasers, which would require a high power of the master laser and low power fluctuations of the two lasers. These requirements make the practical experimental apparatus complicated.

A technique of frequency offset locking has been proposed to overcome these difficulties [37]. Fig. 7 shows an experimental set-up of this technique, in which the slave laser frequency is controlled so that the beat frequency between the two lasers is locked to the frequency of a microwave local oscillator. Similar techniques for frequency tracking have been reported for FSK heterodyne detection of coherent optical communication systems [38, 39]. In the present experimental set-up the phase of the beat signal was controlled instead of controlling its frequency to increase the accuracy of tracking. A digital phase comparator for the beat signal was developed for this purpose, which had a dynamic range of $2\pi \times 2^{11}$ rad. It can easily be seen from this figure that this system is analogous to a heterodyne stabilizer of a microwave phase-locked loop [40]. Therefore, this system can be considered as an optical phase-locked loop (OPLL). A network analysis was carried out for

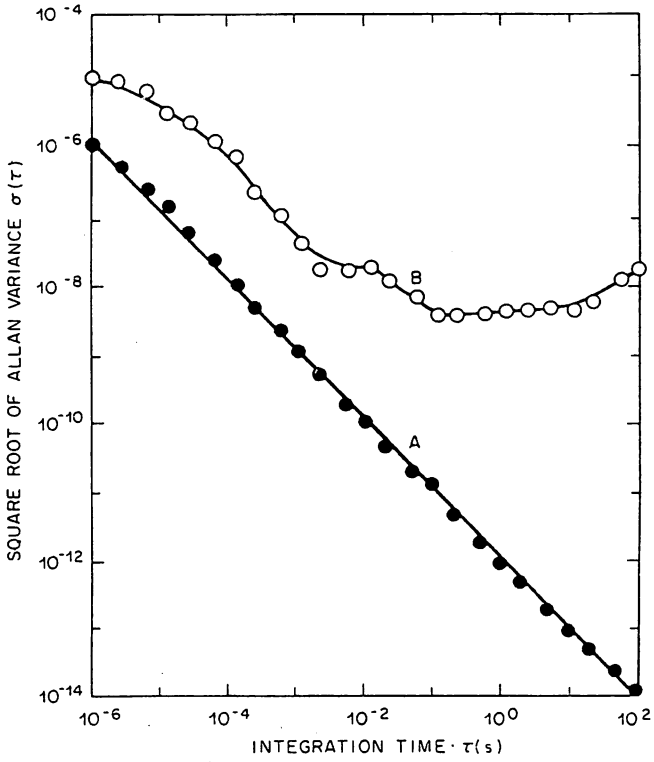


*Figure 8* Square root of the Allan variance $\sigma^2$ for the frequency fluctuation of the beat signal between the master and slave lasers. Here the beat frequency fluctuation was normalized to the optical frequency. A, under the condition of frequency offset locking; and B, free-running.

the OPLL to find an open-loop transfer function and the optimum loop gain to realize the most effective reduction of beat frequency fluctuations. Under the optimum gain a capture range as wide as 1 GHz was obtained. Furthermore, as shown by curve A of Fig. 8, the beat frequency fluctuation was reduced to as low as $\sigma = 1.0 \times 10^{-12}\tau^{-1}$ [41], where this value of $\sigma$ represents the beat frequency fluctuation normalized to optical frequency. This value of $\sigma$ is lower than that of the master laser given by curve $B_2$ of Fig. 2, which means that the frequency fluctuation of the slave laser was reduced to as low as that of the master laser. In other words, the slave laser frequency tracked the master laser frequency very accurately, and the high temporal coherence of the master laser was transferred to the slave laser.

The limit of reduction of the phase or frequency fluctuation of the slave laser was governed by the linewidth of the master laser and by the optimum loop gain of the frequency offset lock loop. Fig. 9a shows a probability density of the residual phase fluctuation of the slave laser, which was calculated by using a Fokker–Planck equation to discuss the effect of the linewidth of the master laser [41]. It is seen from this figure that the probability density has a Gaussian profile whose width depends on the linewidth of the master laser. The square root of the variance of the residual phase fluctuations $\sigma_\phi^2$ can be obtained from this probability density, which is shown in Fig. 9b. It is seen from this figure that $\sigma_\phi$ is proportional to the square root of the linewidth of the master laser. It has been confirmed by the preliminary experiments that the result of Fig. 9b agreed with experimental results [41].

## 3.5. Stable, accurate and wideband frequency sweep

An extended-cavity laser has commonly been employed for wideband frequency sweep by replacing the external mirror in Fig. 5 by a diffraction grating. In this configuration a

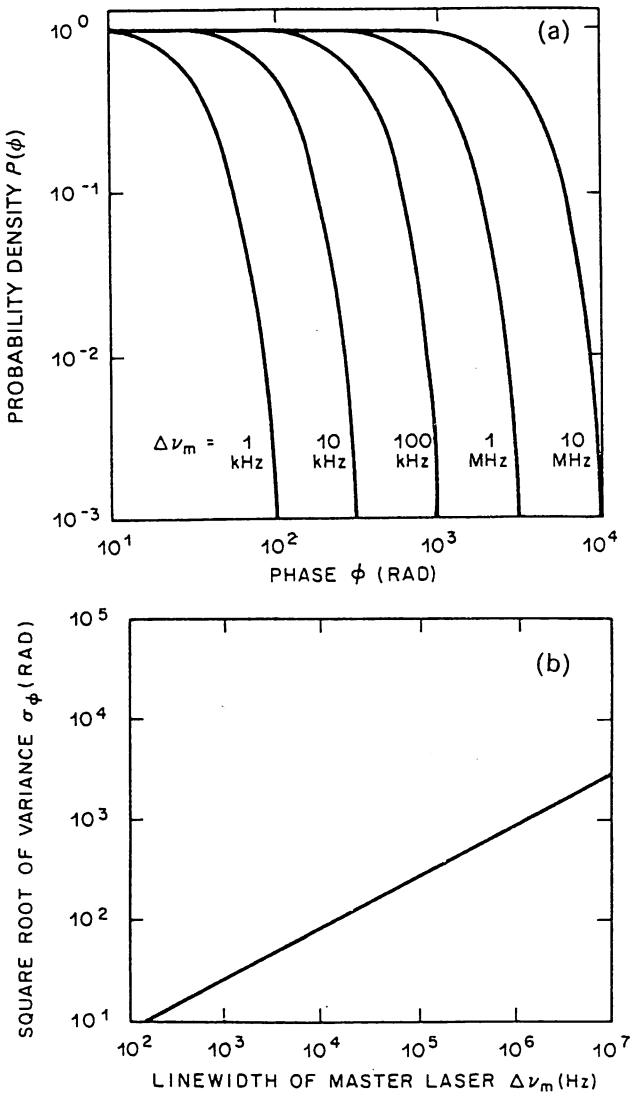


*Figure 9* (a) Probability density function $P(\phi)$ for the residual phase fluctuation of the slave laser, which was calculated by using a Fokker–Planck equation [41]. $\Delta\nu_m$, Linewidth of the master laser. (b) Relationship between the linewidth of the master laser $\Delta\nu_m$ and the square root of variance of residual phase fluctuation of the slave laser $\sigma_\phi^2$, which was calculated using $P(\phi)$ in (a).

longitudinal mode of extended cavity was selected for coarse frequency tuning by rotating a diffraction grating. For fine tuning a Fabry–Perot etalon was sometimes installed inside the extended cavity. The frequency of a 1.5 $\mu$m InGaAsP laser has been swept for 67 GHz (0.5 nm in wavelength) by this configuration [42]. This is a popular and convenient technique of frequency sweep, which has commonly also been employed for infrared gas lasers and visible dye lasers.

It has been proposed that the frequency offset locking in the previous section can be used as an effective technique to realize a more stable and accurate frequency sweep. That is, if the frequency of the microwave local oscillator in Fig. 7 is swept under the condition of frequency offset locking, then the slave laser frequency can be swept while its frequency stability is maintained as high as that of the master laser. Therefore, this technique is analogous to that for the lock-box in the heterodyne stabilizer of the microwave phase-locked loop [40]. It was confirmed by experiments for 0.8 $\mu$m AlGaAs lasers that the lock range of the beat frequency (that is, the frequency range in which the beat frequency was swept was as wide as 1.8 GHz, and that the residual frequency fluctuation of the beat signal was as low as given by curve A of Fig. 8 [41]. These results mean that the slave laser frequency was swept in a very stable manner within the frequency range of 3.6 GHz with respect to the master laser frequency.

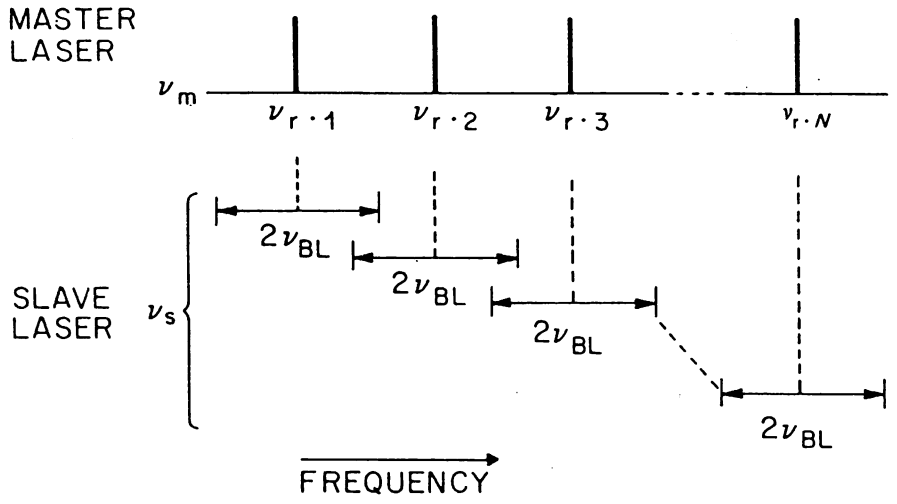


*Figure 10* A method of extending the tuning range of the slave laser frequency [41]. The master laser frequency $\nu_m$ is successively locked to one of the frequency $\nu_{r,k}$ ($k$ = 1, 2, 3, . . . , $N$) of equidistantly distributed frequency reference grids. Frequency offset locking is provided for the slave laser frequency $\nu_s$ with respect to the master laser frequency $\nu_m$ which is locked to $\nu_{r,k}$. $\nu_{BL}$ is the lock range of the beat frequency. If $2\nu_{BL} \geqslant \nu_{r,k+1} - \nu_{r,k}$, then the total tuning range of the slave laser frequency is given by $\nu_{r,N} - \nu_{r,1}$.

The value of this lock range was limited by the response bandwidth of the photodetector used to observe the beat signal. As is shown in Fig. 10, one of the effective methods to extend the tunable range of the slave laser frequency is to make a discrete tuning of the master laser frequency by locking it to one of the equidistantly distributed frequency reference grids. If frequency offset locking is applied to the slave laser under this condition, then its tunable range can be extended. Therefore, this discrete locking is analogous to varying the order of harmonics of the reference oscillator in the heterodyned stabilizer of the microwave phase-locked loop [40]. For these frequency reference grids, absorption spectral lines of combination tones or higher harmonics of vibration–rotation transitions in organic molecular vapours can be employed. This is because a great number of these spectral lines are distributed with several gigahertz or several tens of gigahertz interval in the near-infrared wavelength range, and because some of their absolute frequencies have already been calibrated with an accuracy of $1 \times 10^{-6}$ to $7 \times 10^{-8}$ [14, 15]. Equidistantly distributed resonance frequencies of a Fabry–Perot interferometer can be also used as a simpler frequency reference grid. An experiment using this interferometer showed that the master laser frequency could be locked to its 15 successive resonance frequencies. For each locked frequency of the master laser, frequency offset locking was applied to the slave laser. Using this method the range of stable frequency sweep of the slave laser was extended to 54 GHz [41]. The number of frequency reference grids to which the master laser frequency was locked was limited by a mode-hopping phenomenon in the master laser. It would be effective for extending this range to use a laser which does not show mode-hopping. A recently developed 1.5 $\mu$m InGaAsP distributed feedback (DFB) laser may be favourably used for this purpose because its wavelength can be continuously tuned to 15 nm under free-running conditions by varying the ambient temperature without inducing mode-hopping. This corresponds to the continuous frequency sweep range of 2 THz [43]. A stable, accurate and wideband frequency sweep can be expected if this kind of laser is employed for frequency offset locking in the future.

## 4. Design of novel semiconductor lasers to improve frequency stability

It is desirable to obtain a low-noise and single-mode laser at the stage of device fabrication to realize a high frequency stability. For this purpose a distributed feedback (DFB) laser [44], distributed Bragg reflector (DBR) laser [44] and a laser employing a quantum-well structure [45] have been proposed. Furthermore, it is also desirable to develop novel laser devices whose structures and oscillation characterstics are compatible with negative electrical feedback. As an example of such a device, an external waveguide was integrated together with the laser device to reduce the linewidth of the field spectrum [46, 47], which is analogous to the optical-feedback scheme of Fig. 5.

On the other hand, several external components for feedback in Fig. 3 can also be integrated together with the laser devices. As an example of such devices, a multi-electrode DBR laser [48] and a multi-electrode DFB/DBR hybrid laser [49] have been fabricated, with which an intracavity phase modulator was integrated. A multi-electrode DFB laser has been also developed [50, 51], in which non-uniform f.m. response characteristics due to thermal and carrier effects (Fig. 4) were compensated by adjusting the d.c. current injected into the phase modulator. A flat f.m. response characteristic was realized by this adjustment.

As can be recognized by this example, it is advantageous to have a phase modulator inside the laser cavity because the f.m. response characteristics can be modified so as to be appropriate for negative electrical feedback. However, if the current injected into this phase modulator is varied, then the laser power can be varied simultaneously, due to the variation of the cavity loss. Such a power variation would induce several practical difficulties for the design of the negative-feedback system for these lasers. To overcome this difficulty the phase modulator should be integrated outside the laser cavity as an advanced device in the future. As a primitive scheme of such an external modulator, the use of a bulky external modulator has already been popular for frequency-stabilized gas and dye lasers, whose linewidths have been reduced to less than 1 Hz to realize a ultra-high frequency stability [52].

In addition to integrating a phase modulator, it is also possible to integrate the photodetector and a servo-amplifier of Fig. 3 together with the laser device [53]. It can be expected that a more sophisticated laser device will be realized to improve the frequency stability in the future, in which several components of Fig. 3 are integrated together.

## 5. Applications of frequency-stabilized semiconductor lasers

Semiconductor lasers have commonly been used for several practical and industrial applications because of their small size, low power consumption and long life. If their frequency stability is improved in addition to these advantageous characteristics, then further applications will be found. Several candidates for such applications are: coherent optical communication (optical fibre communication [4, 5] an optical intersatellite link [54]); Doppler velocimeter to measure flow velocity and anemometry [55]; holography; optical distance measurements; alignment of a mask with a pattern on the substrate for semiconductor device fabrication; a fibre gyroscope for inertial navigation [56], earthquake prediction [35], and a measurement for a polar motion of the Earth; laser radar for pollutant gas monitoring in the atmosphere [57]; optical pumping of stable microwave

caesium and rubidium atomic clocks [58]; high-resolution laser spectroscopy; and standardization of length.

## 6. Summary

Three promising methods were reviewed to improve temporal coherence in semiconductor lasers. These were the development of novel laser devices, a technique of optical feedback and a technique of electrical feedback. The main discussion here is focused on the technique of electrical feedback. This was because of its high stability and reliability, as has been proved for frequency stabilization in conventional microwave oscillators. For further improvements in this technique, it is important to develop novel laser devices which are compatible with the technique of electrical feedback.

The technique of optical feedback, based on a non-linear optical phenomenon associated with the mechanism of laser oscillation, is physically interesting. However, it still presents several technical difficulties to assure high stability and reliability. Further investigations of laser oscillation mechanisms and developments of novel optoelectronic integrated circuits are awaited, to find an improved optical feedback technique which is more reliable to improve the temporal coherence in semiconductor lasers.

Furthermore, developments of several optical components, such as a reliable optical isolator, are also essential to utilize a highly coherent laser realized by using the techniques presented in this paper.

## Acknowledgements

The author would like to thank his graduate students, S. Kotajima, K. Kuboki, M. Hashimoto, S. Araki, N. Tabuchi and T. Ouchi for their intensive support to this work. This work was partially supported by a Grant-in-Aid for Scientific Research from the Ministry of Education, Science and Culture of Japan.

## References

1. M. OHTSU, 'Lasers and Atomic Clocks' (Ohm-sha Publishing, Tokyo, 1986) (in Japanese).
2. M. OHTSU, S. KATSURAGI and T. TAKO, 'Performances of a Frequency Offset Locked He-Xe Laser System at 3.51 $\mu$m', *IEEE J. Quantum Electron.* **QE-17** (1981) 1100.
3. A. BRILLET and P. CEREZ, 'Laser Frequency Stabilization by Saturated Absorption', *J. de Physique* **42** (1981) 73.
4. Y. YAMAMOTO, 'Receiver Performance Evaluation of Various Digital Optical Modulation-Demodulation Systems in the 0.5–10 $\mu$m Wavelength Region', *IEEE J. Quantum Electron.* **QE-16** (1980) 1251.
5. T. OKOSHI and K. KIKUCHI, 'Heterodyne-Type Optical Fibre Communications', *J. Opt. Commun.* **2** (1981) 82.
6. Y. YAMAMOTO, S. SAITO and T. MUKAI, 'AM and FM Quantum Noise in Semiconductor Lasers Part II: Comparison of Theoretical and Experimental Results for AlGaAs Lasers', *IEEE J. Quantum Electron.* **QE-19** (1983) 47.
7. M. OHTSU, H. FUKADA, T. TAKO and H. TSUCHIDA, 'Estimation of the Ultimate Frequency Stability of Semiconductor Lasers', *Jpn J. Appl. Phys.* **22** (1983) 1157.
8. D. W. ALLAN, 'Statistics of Atomic Frequency Standards', *Proc. IEEE* **54** (1966) 221.
9. M. OHTSU, M. HASHIMOTO and H. OZAWA, 'A Highly Stabilized Semiconductor Laser and its Application to Optically Pumped Rb Atomic Clock', *Proc. 39th A. Symp. Frequency Control*, Philadelphia, 1985, p. 43.
10. S. KOBAYASHI, Y. YAMAMOTO, M. ITO and T. KIMURA, 'Direct Frequency Modulation in AlGaAs Semiconductor Lasers', *IEEE J. Quantum Electron.* **QE-18** (1982) 582.
11. G. JACOBSEN, H. OLESEN and F. BIRKEDAHL, 'Current/frequency-modulation Characteristics for Directly Optical Frequency-Modulated Injection Laser at 830 nm and 1.3 $\mu$m', *Electron. Lett.* **18** (1982) 874.
12. Y. YAMAMOTO, O. NILSSON and S. SAITO, 'Theory of a Negative Frequency Feedback Semiconductor Laser', *IEEE J. Quantum Electron.* **QE-21** (1985) 1919.

13. M. OHTSU and N. TABUCHI, 'Electrical Feedback and its Network Analysis for Linewidth Reduction of a Semiconductor Laser', *J. Lightwave Technol.* **6** (1988) 357.
14. M. OHTSU, H. KOTANI and H. TAGAWA, 'Spectral Measurements of $NH_3$ and $H_2O$ for Pollutant Gas Monitoring by 1.5 $\mu$m InGaAsP/InP Lasers', *Jpn. J. Appl. Phys.* **22** (1983) 1553.
15. K. FUKUOKA, M. OHTSU and T. TAKO, 'Accurate Wavelength Measurement of the Absorption Lines in $H_2O$ Vapour by a 0.8 $\mu$m AlGaAs Laser', *Jpn. J. Appl. Phys.* **23** (1984) L117.
16. V. PEVTSCHIN and S. EZEKIEL, 'Investigation of Absolute Stability of Water-vapour-stabilized Semiconductor Laser', *Optics Lett.* **12** (1987) 172.
17. T. YABUZAKI, A. IBARAGI, H. HORI, M. KITANO and T. OGAWA, 'Frequency-Locking of a GaAlAs Laser to a Doppler-free Spectrum of the Cs-$D_2$ Line', *Jpn. J. Appl. Phys.* **20** (1981) L451.
18. H. TSUCHIDA, M. OHTSU, T. TAKO, N. KURAMOCHI and M. OURA, 'Frequency Stabilization of AlGaAs Semiconductor Laser Based on the $^{85}$Rb-$D_2$ Line', *Jpn. J. Appl. Phys.* **21** (1982) L561.
19. S. YAMAGUCHI and M. SUZUKI, 'Frequency Stabilization of a Diode Laser by use of the Optogalvanic Effect', *Appl. Phys. Lett.*, **41** (1982) 597.
20. T. YANAGAWA, S. SAITO and Y. YAMAMOTO, 'Frequency Stabilization of 1.5 $\mu$m InGaAsP Distributed Feedback Laser to $NH_3$ Absorption Lines' *Appl. Phys. Lett.*, **45** (1984) 826.
21. A. SOLLBERGER, A. HEINAMAKI and H. MELCHIOR, 'Frequency Stabilization of Semiconductor Lasers for Applications in Coherent Communication System' *J. Lightwave Technol.* **LT-5** (1987) 485.
22. F. FAVRE and D. LE GUEN, Emission Frequency Stability in Single-mode-fibre Optical Feedback Controlled Semiconductor Lasers', *Electron. Lett.* **19** (1983) 663.
23. R. WYATT and W. J. DEVLIN, '10 kHz Linewidth 1.5 $\mu$m InGaAsP External Cavity Laser with 55 nm Tuning Range', *Electron. Lett.* **19** (1983) 110.
24. F. FAVRE, D. LE GUEN and J. C. SIMON, 'Optical Feedback Effects upon Laser Diode Oscillation Field Spectrum', *IEEE J. Quantum Electron.* **QE-18** (1982) 1712.
25. R. LANG and K. KOBAYASHI, 'External Optical Feedback Effects on Semiconductor Injection Laser Properties, *IEEE J. Quantum Electron.* **QE-16** (1980) 347.
26. D. LENTRA, B. H. VERBEEK and A. J. DEN BOEF, 'Coherence Collapse in Single-Mode Semiconductor Lasers Due to Optical Feedback', *IEEE J. Quantum Electron.* **QE-21** (1985) 674.
27. M. OHTSU and S. KOTAJIMA, 'Linewidth Reduction of a 1.5 $\mu$m InGaAsP Laser by Electrical Feedback', *Jpn J. Appl. Phys.* **24** (1985) L256.
28. M. OHTSU, 'Linewidth Reduction of a Semiconductor Laser by Electrical Feedback', *Dig. Tech. Papers, Conf. Lasers and Electro-Optics*, Baltimore, 1985, Postdeadline Paper THZ5.
29. M. OHTSU and S. KOTAJIMA, 'Linewidth Reduction of a Semiconductor Laser by Electrical Feedback', *IEEE J. Quantum Electron.* **QE-21** (1985) 1905.
30. S. SAITO, O. NILSSON and Y. YAMAMOTO, 'Frequency Modulation Noise and Linewidth Reduction in a Semiconductor Laser by Means of Negative Frequency Feedback Technique', *Appl. Phys. Lett.* **46** (1985) 3.
31. M. OHTSU, 'Demonstration and Application of Frequency Stabilization and Linewidth Reduction in Semiconductor Lasers', *Dig. Tech. Papers, Conf. Lasers and Electro-Optics*, San Francisco, 1986, p. 154.
32. D. WELFORD and A. MOORADIAN, 'Output Power and Temperature Dependence of the Linewidth of Single-frequency CW (GaAl)As Diode Laser', *Appl. Phys. Lett.* **40** (1982) 865.
33. M. OSINSKI and J. BUUS, 'Linewidth Broadening Factor in Semiconductor Lasers – An Overview', *IEEE J. Quantum Electron.* **QE-23** (1987) 9.
34. D. HORNBUCKLE, 'GaAs IC Direct-Coupled Amplifiers', *IEEE MTT-S Int. Microwave Symp. Dig.*, Washington, DC, 1980, p. 387.
35. M. OHTSU and S. ARAKI, 'Using a 1.5 $\mu$m DFB InGaAsP Laser in a Passive Ring Cavity-type Fibre Gyroscope', *Appl. Optics*, **26** (1987) 464.
36. S. KOBAYASHI and T. KIMURA, 'Injection Locking in AlGaAs Semiconductor Laser', *IEEE J. Quantum Electron.* **QE-17** (1981) 681.
37. K. KUBOKI and M. OHTSU, 'Frequency Offset Locking of AlGaAs Semiconductor Lasers', *IEEE J. Quantum Electron.* **QE-23** (1987) 388.
38. K. EMURA, M. SHIKADA, S. FUJITA, I. MITO, H. HONMOU and K. MINEMURA, 'Novel Optical FSK Heterodyne Single Filter Detection System Using a Directly Modulated DFB-laser Diode", *Electron. Lett.* **20** (1984) 1022.
39. F. FAVRE and D. LE GUEN, 'Spectral Narrowing by Optical Feedback', *Proc. Int. Conf. Lasers*, San Francisco, 1983, p. 79.
40. F. M. GARDNER, 'Phaselock Technique' (John Wiley & Sons, New York, 1979).

41. M. OHTSU, 'Ultrahigh Coherence in Semiconductor Lasers', *Tech. Dig. Optical Fibre Communication Conf./ Sixth Int. Conf. on Integrated Optics and Optical Fibre Communication*, Reno, 1987, Paper TUC5, p. 52.
42. K. H. CAMERON, M. R. MATTHEWS, T. G. HODGKINSON and W. J. DEVLIN, 'Frequency-Stable Packaged 20-kHz Linewidth 1.5 $\mu$m InGaAsP External Cavity Laser Used in an Experimental Heterodyne Optical Fibre System', *Tech. Dig. Conf. Lasers and Electro-Optics*, Baltimore, 1985, Paper **TUC5**.
43. B. BROBERG, F. KOYAMA, Y. TOHMORI and Y. SUEMATSU, '1.53 $\mu$m DFB Lasers by Mass Transport', *Electron. Lett.* **20** (1984) 692.
44. Y. SUEMATSU, 'Semiconductor Lasers and Optical Integrated Circuits' (Ohm-sha Publishing, Tokyo, 1984) (in Japanese).
45. Y. ARAKAWA and A. YARIV, 'Enhanced Modulation Performance and Reduced Quantum Noise in Quantum Well Lasers', *Tech. Dig. Conf. Lasers and Electro-Optics*, Baltimore, 1985, Paper **WH5**, p. 90.
46. T. FUJITA, J. OHYA, K. MATSUDA, M. ISHINO, H. SATO and H. SERIZAWA, 'Narrow Spectral Linewidth Characteristics of Monolithic Integrated-passive-cavity InGaAsP/InP Semiconductor Lasers', *Electron. Lett.* **21** (1985) 374.
47. S. MURATA, S. YAMAZAKI, I. MITO and K. KOBAYASHI, 'Spectral Characteristics for 1.3 $\mu$m Monolithic External Cavity DFB Lasers', *Electron. Lett.* **22** (1986) 1197.
48. T. TOHMORI, Y. SUEMATSU, H. TSUSHIMA and S. ARAI, 'Wavelength Tuning of GaInAsP/InP Integrated Lasers with Butt-jointed Built-in Distributed Bragg Reflector", *Electron. Lett.* **19** (1983) 656.
49. L. D. WESTBROOK, A. W. NELSON, P. J. FIDDYMENT and J. V. COLLINS, 'Monolithic 1.5 $\mu$m Hybrid DFB/ DBR Lasers with 5 nm Tunining Range', *Electron. Lett.* **20** (1984) 957.
50. Y. YAMAZAKI, K. EMURA, M. SHIKADA, M. YAMAGUCHI and I. MITO, 'Realization of Flat FM Response by Directly Modulating a Phase Tunable DFB Laser Diode', *Electron. Lett.* **21** (1985) 283.
51. Y. YOSHIKUNI and G. MOTOSUGI, 'Multielectrode Distributed Feedback Laser for Pure Frequency Modulation and Chirping Suppressed Amplitude Modulation', *J. Lightwave Technol.* **LT-5** (1987) 516.
52. J. L. HALL, D. HILLS, C. SALOMON and M. RAYMAN, 'Stable Lasers: Progress and Applications', *Tech. Dig. Conf. Lasers and Electro-Optics*, Baltimore, 1985, Paper **FM3**, p. 294.
53. K. IGA and B. I. MILLER, 'GaInAsP/InP Laser with Monolithically Integrated Monitoring Detector', *Electron. Lett.* **16** (1980) 342.
54. V. W. S. CHAN, 'Space Coherent Optical Communication Systems — An Introduction', *J. Lightwave Technol.* **LT-5** (1987) 633.
55. F. DURNST, A. MELLING and J. H. WHITELAW, 'Principle and Practice of Laser-Doppler Anemometry' (Academic Press, New York, 1976).
56. T. G. GIALLORENZI, J. A. BUCARO, A. DANDRIDGE, G. J. SIGEL, Jr, J. H. COLE, S. C. RASHLEIGH and R. C. PRIEST, 'Optical Fiber Sensor Technology', *IEEE J. Quantum Electron.* **QE-18** (1982) 626.
57. N. TAKEUCHI, H. BABA, K. SAKURAI and T. UENO, 'Diode-laser random-modulation cw lidar', *Appl. Opt.* **25** (1986) 63.
58. M. HASHIMOTO and M. OHTSU, 'Experiments on a Semiconductor Laser Pumped Rubidium Atomic Clock', *IEEE J. Quantum Electron.* **QE-23** (1987) 446.

UDC 621.375.826 : 621.383.5 : 537.533.621.3.018.5

論　文

# 半導体レーザによるヘテロダイン形光位相同期ループの実現のためのシミュレーション

正員　申　哲浩　(東京工業大)
非会員　久保木勝彦　(東京工業大)
正員　大津元一　(東京工業大)

## 1. まえがき

光位相同期ループ (Optical Phase Locked Loop, OPLL)[1]~[5]は光周波数制御，コヒーレント光計測および周波数基準分野への応用上重要である。半導体レーザによる OPLL は小形で高い変調効率，大きい制御利得，注入電流による出力光の直接変調可能などの半導体レーザのもつ利点が十分活かされるし，更に，光通信にも応用される。特に，半導体レーザによるヘテロダイン形 OPLL は広帯域・精密周波数掃引の可能な光周波数シンセサイザ／光トラッキングジェネレータとして有望である。

そこで，筆者らはヘテロダイン形 OPLL の予備実験として半導体レーザを用いた周波数オフセット・ロックの方法を開発し，積分時間1秒で主，従レーザの間のビート周波数揺らぎを約 200 Hz まで抑圧した[6]~[8]。これを更に改良し，二つのレーザの間の同期誤差が ±1 ラジアン以内であるヘテロダイン形光位相同期ループを実現するためには半導体レーザの固有の位相雑音や制御系各部の性能および同期誤差との相互関係を明らかにする必要があるが，これについては従来，詳細な報告がない。

そこで，本研究ではフォッカ・プランク法[9]による理論解析，および OPLL の光学部を電子回路で置き換えたモデルによるシミュレーションを行った。2節ではフォッカ・プランク法による理論解析とその結果，3節ではシミュレーション系の構成およびシミュレーションとその結果をそれぞれ示した。4節では半導体レーザを用いた実際の実験データをシミュレーションの結果と比較し，本シミュレーションの妥当性を明らかにした。そして，5節には本研究の結果をまとめてヘテロダイン形 OPLL の実現のための条件を提示した。

## 2. フォッカ・プランク法による理論解析

不規則雑音の存在下においての位相同期ループの動特性の解析にフォッカ・プランク法を利用するのが一般的である[9]。この方法を用いてヘテロダイン形 OPLL において主レーザの線幅と位相誤差分散との関係を求めた。更に，線形化ループ・モデルを用い，従レーザの影響も明らかにした。

半導体レーザを用いたヘテロダイン形 OPLL の構成を図1(a)に示す。主レーザと従レーザの光ビート信号を光検出器 (Photo Detector ; PD) で検出して分周器で位相比較器の応答速度に合わせ適当に分周する。分周率 $M$ で分周されたビート信号と安定な基準マイクロ波発振器からの信号を位相比較器に入力して位相誤差信号を得る。位相誤差信号は能動ループ・フィルタを通して従レーザの注入電流を制御する。この一連の動作によってビート信号が基準発振器からの基準信号に位相同期されれば主レーザと従レーザの間も位相同期される。すなわち，二つのレーザの間の位相差の揺らぎの抑圧限界は基準マイクロ波発振器の位相安定度に左右される。

図1(a)のヘテロダイン形 OPLL は図1(b)の等価解析モデルで表せる。ここで，$\omega_M$, $\omega_R$, $\omega_S$ はそれぞれ主レーザ，基準マイクロ波発振器，従レーザの角

Simulation for the Heterodyne Type Optical Phase-Locked Loop by Semiconductor Lasers. By *Chul-Ho Shin*, Member, *Katsuhiko Kuboki*, Non-member & *Motoichi Ohtsu*, Member (The Graduate School at Nagatsuta, Tokyo Institute of Technology).

申　哲浩：正員，東京工業大学総合理工学研究科物理情報工学専攻
久保木勝彦：非会員，東京工業大学総合理工学研究科物理情報工学専攻
大津　元一：正員，東京工業大学総合理工学研究科物理情報工学専攻

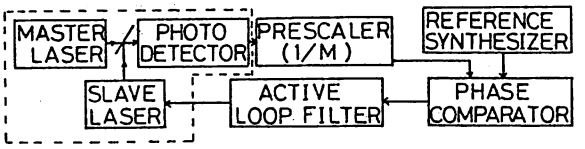


(a) ヘテロダイン形位相同期ループ

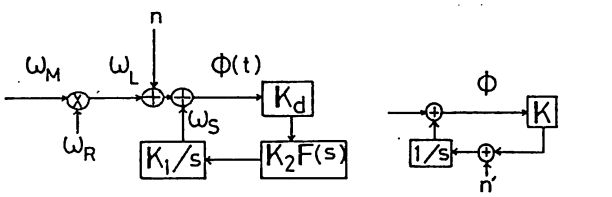


(b) 主レーザの位相雑音を考慮した(a)の等価解析モデル　(c) 従レーザの位相雑音を考慮したループの等価解析モデル

図 1 ヘテロダイン形光位相同期ループのブロック図と理論解析モデル

Fig. 1. Block diagram and analytical models of heterodyne optical phase-locked loop.

周波数である。$K_1$, $K_2$, $K_d$ は従レーザの電流/周波数変換利得，能動ループ・フィルタの利得，PFC の位相差/電圧変換利得をそれぞれ表す。$F(s)$ は能動ループ・フィルタの伝達特性を，$\phi(t)$ は位相差をそれぞれ表す。主レーザの位相揺らぎを表す $n$ は白色雑音とみなすことができるので図1(b)のモデルによりループの動作方程式は

$$\phi(t)+\frac{K_1K_2K_dF(s)\phi(t)}{s}=\{\omega_S-(\omega_L+n)\}t+\theta \quad \cdots\cdots(1)$$

と書ける[9]。ここで，$\theta$ は $\omega_L(=\omega_M-\omega_R)$ がもつ初期位相である。$\phi(t)$ も $n$ と同様の不規則過程に従うとし，更に $F(s)=1$ の1次ループ近似を用いると(1)式から次の微分方程式が得られる。

$$\frac{d\phi(t)}{dt}=(\omega_S-\omega_L)-K\left\{\phi(t)+\frac{n}{K}\right\} \quad \cdots\cdots(2)$$

ここで，$K=K_1K_2K_d$ である。$n$ が完全な白色雑音と仮定すると $n$ の両側パワー・スペクトル密度は

$$S_n=2\pi\Delta\nu_M \ [\mathrm{rad^2\cdot Hz}] \quad (-\infty\leqq f\leqq\infty) \quad \cdots\cdots(3)$$

と表せる[10][11]。ここで，$\Delta\nu_M$ は主レーザの発振スペクトル線幅である。$\phi(t)$ と $d\phi(t)/dt$ がマルコフ過程に従うと考えると，(2)，(3)式を用いて位相誤差の確率密度関数 $p(\phi,t)$ は

$$\frac{\partial p(\phi,t)}{\partial t}=\{\omega_S-\omega_L+K\phi(t)\}p(\phi,t)+\frac{1}{2}(2\pi\Delta\nu_M)\frac{\partial^2p(\phi,t)}{\partial\phi^2} \quad \cdots(4)$$

のフォッカ・プランク方程式で記述できる。

定常解を求めるため，$dp/dt=0$ と置くと(4)式は

$$\frac{d}{d\phi}\left\{(\alpha\phi-\beta)p(\phi)+\frac{dp(\phi)}{d\phi}\right\}=0 \quad \cdots\cdots(5)$$

となる。ただし，

$$\alpha=\frac{K}{\pi\Delta\nu_M},\quad \beta=\frac{\omega_L-\omega_S}{\pi\Delta\nu_M} \quad \cdots\cdots(6)$$

である。境界条件および規格化条件

$$p(\pi)=p(-\pi) \quad \cdots\cdots(7a)$$

$$\int_{-\pi}^{\pi}p(\phi)d\phi=1 \quad \cdots\cdots(7b)$$

を用い，更に，$\omega_S=\omega_L$，すなわち，あらかじめ二つのレーザの周波数がロックされていると仮定して解くと

$$p(\phi)=\frac{e^{-\alpha\phi^2/2}}{2\sqrt{(2\pi/\alpha)}\cdot\{G(\pi\sqrt{\alpha})-1/2\}} \quad (0\leqq\phi\leqq\pi) \quad \cdots\cdots(8)$$

の確率密度関数が得られる。ここで，

$$G(x)\equiv\frac{1}{\sqrt{2\pi}}\int_{-\infty}^{x}e^{-t^2/2}dt \quad \cdots\cdots(9)$$

である。一方，$\Delta\nu_M$ による $\phi$ の揺らぎの分散は

$$\sigma_{\phi M}{}^2=\int_{-\pi}^{\pi}\phi^2p(\phi)d\phi=\frac{1}{\sqrt{(2\pi/\alpha)}\cdot\{G(\pi\sqrt{\alpha}(-1/2\}}\times\int_0^{\pi}\phi^2e^{-\alpha\phi^2/2}d\phi \quad \cdots\cdots(10)$$

となる。

ここで，$F(s)=1$ の1次ループ近似を導入したので，それに対応する1次ループにおいてのループ帯域 $B_L$ は

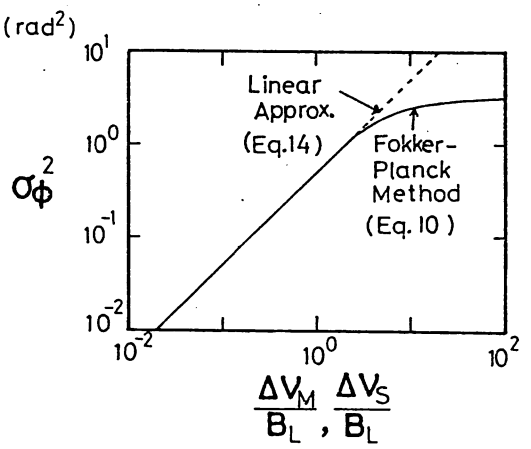


図 2 位相誤差の分散 $\sigma_\phi{}^2$ とループ帯域幅で規格化したレーザの線幅 $\Delta\nu_S/B_L$, $\Delta\nu_M/B_L$ との関係

Fig. 2. Phase error variance $\sigma_\phi{}^2$ vs. $\Delta\nu_M/B_L$, $\Delta\nu/B_L$ which are linewidths of the master and the slave laser normalized by loop bandwidths, respectively. A solid curve and a dashed one were obtained by the Fokker-Planck method and by using the Parseval theorem, respectively, for the 1st order loop.

$$B_L = K/(2\pi)\ [\mathrm{Hz}] \quad \cdots\cdots(11)$$

と表せる[11][12]。図2の実線は(10)式の数値計算の結果であり，$B_L$ で規格化した $\Delta\nu_M$ によるループの位相誤差分散 $\sigma_{\phi M}{}^2$ を示す。(7b)式の規格化条件と $\omega_L=\omega_S$ の初期条件のため，$\Delta\nu_M/B_L$ が大きくなると $\sigma_\phi{}^2$ は $-\pi$ から $\pi$ にわたって均一に分布された確率変数の分散である $\pi^2/3$ の一定値になる[9]。

一方，線幅 $\Delta\nu_S$ の従レーザのもつ位相雑音による位相誤差の解析は図1(c)の線形化モデルを使用した。図のモデルによって位相誤差 $\phi$ は次の動作方程式で記述できる。

$$\phi = (K\phi + n')/s \quad \cdots\cdots(12)$$

ここで，$n'$ は従レーザの位相雑音でその両側パワー・スペクトル密度 $Sn'$ は(3)式と同様に $2\pi\Delta\nu_S$ [rad²·Hz] $(-\infty \leqq f \leqq \infty)$ である。この関係とパセバル(Parseval)定理[9]を利用すると(12)式から従レーザの位相雑音による位相誤差の分散 $\sigma_{\phi S}{}^2$ は

$$\sigma_{\phi S}{}^2 = (2\pi\Delta\nu_S)\frac{1}{2\pi}\int_{-\infty}^{\infty}\frac{1}{\omega^2+K^2}d\omega$$
$$= \pi\Delta\nu_S/K\ [\mathrm{rad}^2] \quad \cdots\cdots(13)$$

になる。(11)式の関係を用いると(13)式は

$$\sigma_{\phi S}{}^2 = \Delta\nu_S/(2B_L) \quad \cdots\cdots(14)$$

となる。図2の破線は(14)式から求めたもので，この図から $\Delta\nu_M$ と $\Delta\nu_S$ がループの位相誤差に及ぼす影響は $\sigma_\phi{}^2 < 1\ \mathrm{rad}^2$ のとき同じであることがわかる。したがって，主，従レーザの位相雑音による OPLL の位相誤差の分散は

$$\sigma_\phi{}^2 = \frac{\Delta\nu_M + \Delta\nu_S}{2B_L}\ [\mathrm{rad}^2] \quad \cdots\cdots(15)$$

と近似できる。これは文献(11)の結果と一致する。$K_1K_d \gg K_2$ の場合，能動ループ・フィルタを使った2次 PLL の雑音帯域が1次ループのそれに近似できる[9][19]から(15)式はヘテロダイン形 OPLL において近似式として十分使える。

結局，位相誤差の分散を1ラジアン以下にするためには図2からわかるように $B_L \geqq (\Delta\nu_M + \Delta\nu_S)/2$ 以上の条件が必要である。この結果は小節 3·5 の図 10 で電子回路モデルによるシミュレーション結果と比較する。

## 3. シミュレーション

この節では電子回路モデルによるシミュレーション系の構成についてまず記し，これを用いて能動ループ・フィルタの帯域幅と従レーザの主レーザへの線幅追随性との関係，能動ループフィルタの制御帯域と利得との関係，ビート信号の分周率と位相誤差との関係，レーザの線幅で規格化した能動ループ・フィルタの帯域幅とビート信号の揺らぎとの関係などを明らかにする。

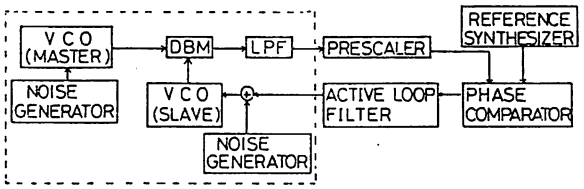


図 3 ヘテロダイン形光位相同期ループの電子回路によるシミュレーション系のブロック図

Fig. 3. Block diagram of the simulation loop by electronic circuits corresponding to the heterodyne OPLL of fig. 1 (a).

〈3·1〉 シミュレーション系の構成　シミュレーション系は図1(a)の破線で囲まれた部分，すなわち，実際の系で広い範囲にわたって実験条件を変えるのが必ずしも容易ではない半導体レーザと光検出器(Photo Detecter : PD) とからなる光学部を図3の破線で囲まれた部分のように電圧制御発振器 (Voltage Controlled Oscillator : VCO)，雑音発生器，DBM (Double Balanced Mixer) により置換えて構成した。電流制御発振器 (Current Controlled Oscillator : CCO) である半導体レーザは VCO とそれに位相雑音を与える雑音発生器で，PD は DBM と低域通過フィルタ (Low Pass Filter : LPF) で置換えた。

VCO の中心周波数は数 MHz の値に設定した。雑音発生器より発生させた peak-to-peak 値 0～1 V の出力の白色ガウス雑音 (雑音帯域 50 kHz) によって，VCO の発振スペクトル線幅の半値全幅 (FWHM) は数 100 Hz～約 300 kHz の範囲で任意に設定した。

図3中の能動ループ・フィルタは図1(a)のそれと同型であり，利得可変できるものを3台用意して帯域幅と利得に関係するシミュレーションに使用した。これらの能動ループ・フィルタの制御帯域幅 $Bn$ はそれぞれ 0.47 kHz，7 kHz，25 kHz であり，その伝達特性は $H(s) = K_2/\{1 + s/(2\pi Bn)\}$ である。位相比較器は筆者らが考案し，半導体レーザを用いた実験に使用したもの，すなわち，$\pm 2\pi \times 2^{11}$ ラジアンの範囲にわたって直線比較特性をもつデジタル形位相周波数比較器 (Phase/Frequency Comparator : PFC) を使用した。この動作原理は文献(7)に説明されている。

VCO の発振スペクトルの線幅は RF スペクトラム・アナライザで，ビート信号の揺らぎは著者らにより開発されたアラン分散実時間測定装置 (Allan variance Real time Processing System : ARPS)[13] で測定した。

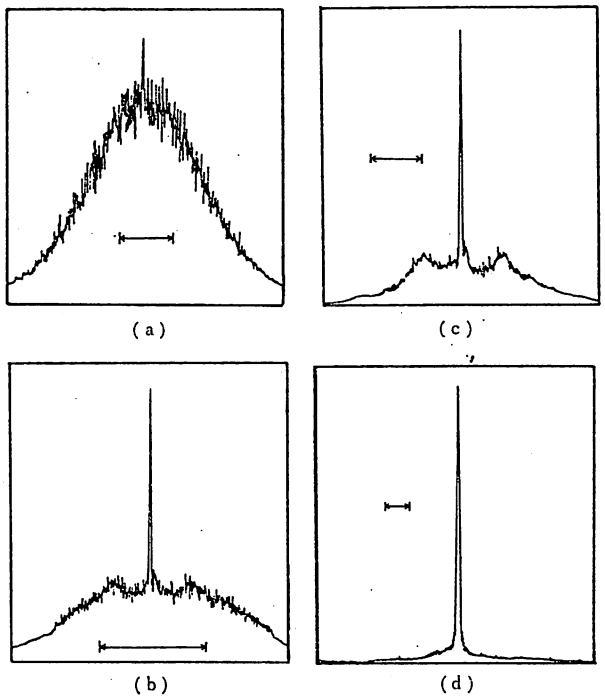


図 4　主レーザを基準として制御された従レーザのスペクトル。ここで，能動ループ・フィルタの帯域幅で規格化したフリー・ランニング時の従レーザの線幅 $\Delta\nu_S/Bn$ はそれぞれ (a) 3.2, (b) 2.2, (c) 1.2, (d) 0.06 である。矢印で表したスケールはそれぞれフリー・ランニング時の従レーザの線幅を示す。

Fig. 4. Controlled spectra of the slave laser referring to that of the master laser. Normalized linewidths $\Delta\nu_S/Bn$ of the slave laser by the bandwidth of the active loop filter employed in this simulation loop were selected (a) 3.2, (b) 2.2, (c) 1.2, and (d) 0.06 respectively. A scale indicated by an arrow in every figures is the linewidth of a free-runned slave alser.

〈3・2〉 従レーザとビート信号のスペクトル線幅制御　高安定な主レーザの位相に従レーザの位相を追随させるのはヘテロダイン形 OPLL の主な目的の一つである。半導体レーザの中心周波数の安定化[14][15]および線幅狭窄化[16]~[18]は現在も更に改善されつつあるので安定な主レーザとして使用できる。しかし，従レーザとして現在入手しうるフリー・ランニング時の半導体レーザの線幅は数 MHz～数 10 MHz の大きな値をもっているのが現状である。したがってヘテロダイン形 OPLL によって主レーザの全スペクトル特性を従レーザに伝達するためには広い能動ループ・フィルタの帯域が必要になる。

図 4 は主レーザを基準として狭窄化された従レーザのスペクトル形状と $Bn$ との関係のシミュレーション結果を示す。$\Delta\nu_S/Bn>3$ のときは図 4 (a) のようにスペクトルの中心付近少ししか制御が掛からない。すなわち，中心周波数がロックされているにもかかわらず線幅は狭くならない。しかし，図 4 (b), (c), (d) のように能動ループ・フィルタの制御帯域を広くすることによって主レーザの線幅 $\Delta\nu_M$ と同等の値まで狭くなるのがわかる。結局，電気的負帰還による線幅狭窄化のとき[16]と同様に $Bn>\Delta\nu_S$ である十分広い制御帯域を必要とする。かつ，図 4 (b), (c) に残っているスペクトルの裾の部分の雑音を抑制するためには，もっと広く例えば図 4 (d) の場合のように $Bn$ を $\Delta\nu_S$ の 10 倍以上取らなければならない。図 5 は帯域幅の異なる三つの能動ループ・フィルタを使用して，それぞれの $\Delta\nu_S/Bn$ と $\Delta\nu_{S,L}/\Delta\nu_M$ との関係を示す。ここで，$\Delta\nu_S$ と $\Delta\nu_{S,L}$ はそれぞれフリー・ランニングとロックされたときの従レーザの線幅である。図 4 (a) と (b) の境界は図 5 からわかるように $\Delta\nu_S/Bn$ が 1.2～3 程度である。すなわち，$Bn\geqq\Delta\nu_S/(1.2\sim3)$ であれば図 4 (b)-(d) のように $\Delta\nu_M$ 値まで小さくなる。

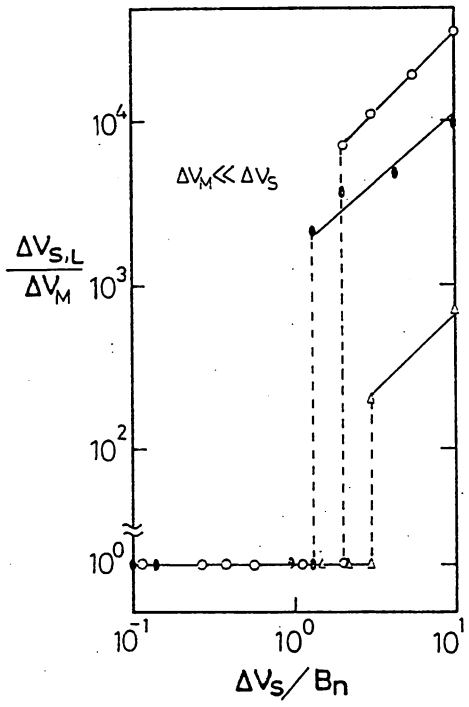


図 5　ロックされた従レーザの線幅と主レーザの線幅との比 $\Delta\nu_{S,L}/\Delta\nu_M$ と従レーザの規格化線幅 $\Delta\nu_S/Bn$ との関係

Fig. 5. Ratio $\Delta\nu_{S,L}/\Delta\nu_M$ of linewidth of the slave laser locked and linewidth of the master laser vs. normalized linewidth $\Delta\nu_S/B_n$ of the slave laser in free-run.

図 6 は $\Delta\nu_B/\Delta\nu_R$ と $\Delta\nu_S/Bn$ の関係を示す。$\Delta\nu_B$ と $\Delta\nu_R$ はそれぞれビート信号と基準マイクロ波発振器の線幅である。ここでは $\Delta\nu_M$ を固定し，$\Delta\nu_S$ を変化したときであるが，$\Delta\nu_S$ を固定し，$\Delta\nu_M$ を変化し

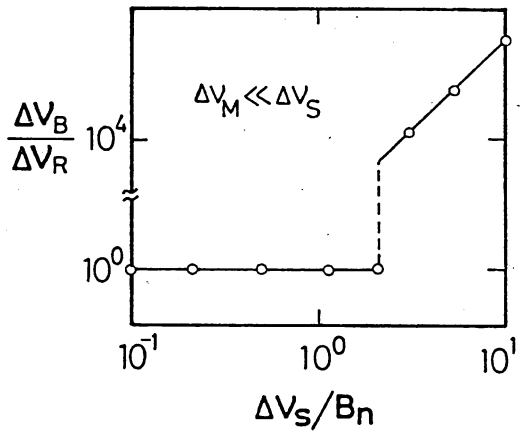


図 6 基準マイクロ波発振器の線幅とレーザのビート・スペクトルの線幅との比 $\Delta\nu_B/\Delta\nu_R$ と従レーザの規格化線幅 $\Delta\nu_S/Bn$ との関係

Fig. 6. Ratio $\Delta\nu_B/\Delta\nu_R$ of spectral linewidth of the laser beat between the slave and the master lasers and linewidth of the reference microwave synthesizer vs. normalized linewidth $\Delta\nu_S/B_n$ of the slave laser.

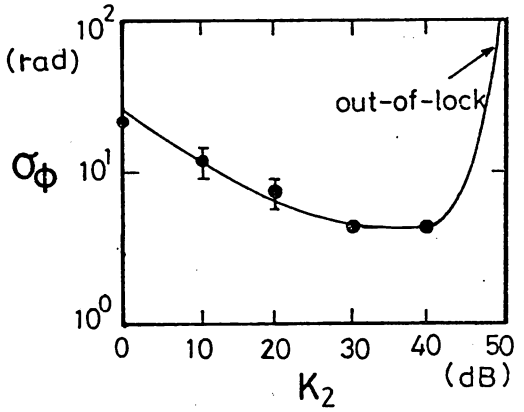


図 7 ループの位相誤差分散の平方根 $\sigma_\phi$ と能動ループ・フィルタの利得値 $K_2$ との関係

Fig. 7. Square root of phase error variance $\sigma_\phi$ of the loop vs. gain $K_2$ of the active loop filter.

たときも図6の結果と同じであった。これは2節の理論解析の結果と同様に $\Delta\nu_S$ と $\Delta\nu_M$ のループ制御に及ぼす影響は同じであることを示す。この図からわかるように $\Delta\nu_S/Bn \leqq 2$, $\Delta\nu_M/Bn \leqq 2$ であれば $\Delta\nu_B$ は $\Delta\nu_R$ と一致するまで小さくなる。したがって，この条件下ではビート信号は基準マイクロ波信号と同程度まで高安定になり，結局 $\nu_S$ が $\nu_M$ に高精度で追随することになる。

〈3・3〉 能動ループ・フィルタの利得と帯域幅

唯一の最適系または最適化手順はあり得なく，最適値の範囲は相当広いのが一般的であるので[19]，我々の実験系で使用している利得可変可能な能動ループ・フィルタの制御帯域において位相誤差を最小にする最適

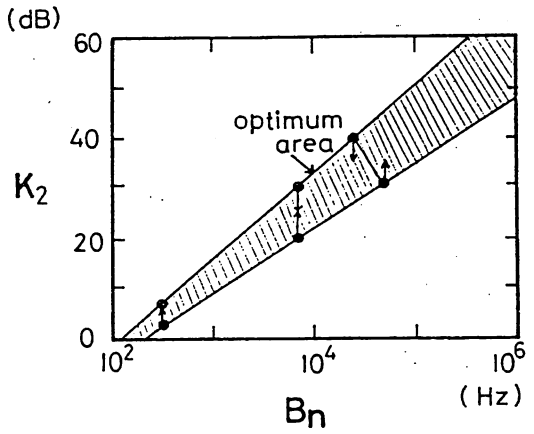


図 8 最適利得値 $K_2$ と能動ループ・フィルタの帯域幅 $Bn$ との関係

Fig. 8. Gain $K_2$ vs. bandwidth Bn of the active loop filter. Optimal gains are indicated by a hatched area.

利得をシミュレーションで求めた。その結果を図7に示す。この図からもわかるようにやはり最適利得値は30～40 dB の範囲にある。すなわち，その範囲の幅は10 dB であり相当広い。利得が足りないと位相誤差が増加し，結局，ビート信号の揺らぎが抑えられなくなり，ロックが外れる。利得の過多はループの伝播時間遅延または外部要因による移相による発振を引起こし[3]，ビートのスペクトルに鋭いサイド・バンドを形成して，ついにはロックが外れる。

以上のような方法で求めた能動ループ・フィルタの帯域 $Bn$ と利得 $K_2$ の最適値との関係を図8の斜線部に示す。この図からわかるように $Bn$ を広くすることによって高利得が必要であり，更に，最適値の範囲も広くなる。レーザの線幅が広くなるとその分広帯域で，高利得の能動ループ・フィルタが要る。

〈3・4〉 分周率と位相誤差　二つのレーザ間のビート周波数 $\nu_B$ を大きくすると，すなわち，従レーザの中心周波数を主レーザのそれからの周波数オフセット値を大きくするとデジタル位相周波数比較器 (PFC) の周波数応答速度を越えることがある。それと，現在市販の半導体レーザの広い線幅と中心周波数の大きい揺らぎのため周波数オフセットは数 10 MHz 以下には設定できないので，これも PFC に直接入力するには高過ぎる。結局，$\nu_B$ を適当に分周しなければならない。

ループの位相誤差は分周率 $M$ と共に大きくなる。この様子を表すシミュレーション結果を図9に示す。この図からわかるように $M$ を大きくするほど $\sigma_\phi$ は大きくなり近似的に

$$\sigma_{\phi D} = M^{0.5}\sigma_{\phi_0} \quad \cdots\cdots (16)$$

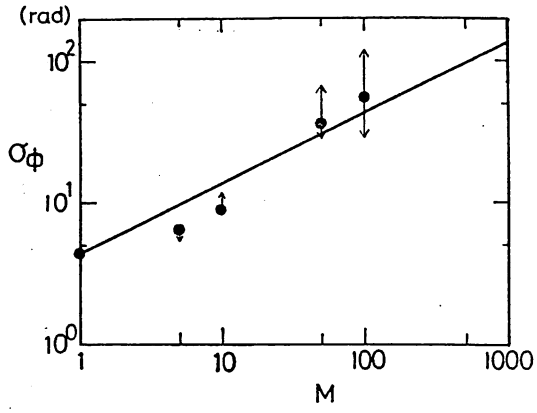


図 9 ループの位相誤差分散の平方根 $\sigma_\phi$ と分周率 $M$ との関係

Fig. 9. Square root of phase error variance $\sigma_\phi$ vs. division ratio $M$ in prescaling laser beats.

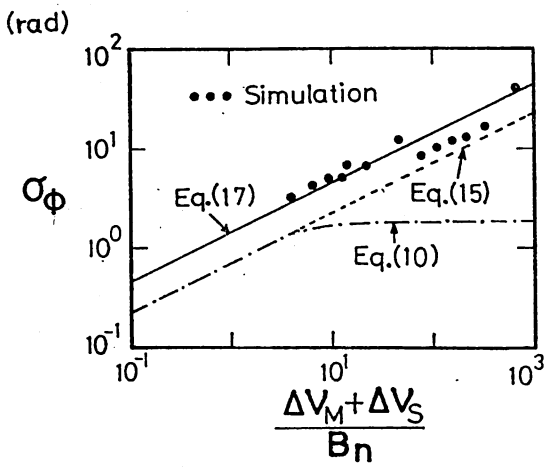


図 10 ループの位相誤差分散の平方根 $\sigma_\phi$ と規格化レーザ線幅の和 $(\Delta\nu_M+\Delta\nu_S)/Bn$ との関係（シミュレーション結果と理論計算値との比較）

Fig. 10. Square root of phase error variance $\sigma_\phi$ vs. the sum of normalized linewidths $(\Delta\nu_M+\Delta\nu_S)/B_n$ of the master and the slave laser by bandwidths of the active loop filter. The calculated results for the 1st loop in Fig. (2) are also indicated for the comparison with those of the simulation.

と書ける。ここで，$\sigma_{\phi D}$, $\sigma_{\phi_0}$ はそれぞれ分周率 $M$ のときと分周器を使用しないときのループの位相誤差分散の平方根である。したがって，PFC の応答速度が許容する限りできるだけ $M$ を小さくするのが望ましい。更にこの図からわかるように $M$ が大きいほど $\sigma_\phi$ の測定値のばらつきが大きくなり，ループのロッキング状態が不安定になる。この不安定の原因は分周後の周波数がループの帯域に比べ十分高くないため，ループ帯域内に残る信号周波数成分による位相リップルが増加する[20]からであると思われる。

〈3・5〉 レーザの線幅と位相誤差　半導体レーザの位相雑音が非常に大きいため，ループの位相誤差に与える影響はループの回路雑音の影響よりずっと大きい。

図 10 は能動ループ・フィルタの帯域幅で規格化された二つのレーザのスペクトルの線幅の和 $(\Delta\nu_M+\Delta\nu_S)/Bn$ とループの位相誤差に相当するビート信号の位相揺らぎのアラン分散の平方根 $\sigma_\phi$（積分時間 $\tau$ は1秒）との関係を示す。全体的な $\sigma_\phi$ の傾向は $(\Delta\nu_M+\Delta\nu_S)/Bn$ に依存しているのが明らかでありフォッカ・プランク法や線形化モデルからの結果とよく一致している。この図からわかるようにシミュレーションの結果から，位相誤差の分散を1ラジアン以下にするためには $(\Delta\nu_M+\Delta\nu_S)/Bn\leqq 0.5$，すなわち，ループ・フィルタの制御帯域は $(\Delta\nu_M+\Delta\nu_S)$ の2倍以上必要であることがわかる。これは理論解析の要求である0.5倍に比べるともっと厳しい値である。しかし，理論解析は1次ループ近似の結果であるので，シミュレーションの方がより高い信頼性をもつ。図 10 のシミュレーション結果から位相誤差の分散は

$$\sigma_\phi{}^2=\frac{2(\Delta\nu_M+\Delta\nu_S)}{Bn}\ [\mathrm{rad}^2] \quad \cdots\cdots\cdots\cdots (17)$$

と近似できる。文献(21)にも類似な理論解析結果が出ている。

レーザの線幅の値が大きくなると能動ループ・フィルタの帯域幅も広くする必要がある。すると，小節〈3・3〉で示したように $K_2$ も大きくしなければならない。更に，$Bn$ が広くなると回路雑音を拾込みやすくなるし，PD のショット雑音による位相誤差も増加する。もし，フリー・ランニング時の半導体レーザを従レーザとして採用すると $\Delta\nu_M$ が非常に狭いと仮定しても $\Delta\nu_S$ の2倍である数 10 MHz の $Bn$ が要り，それに応じて必要とする $K_2$ は 60〜80 dB となる。しかし，このような広帯域，高利得の能動ループ・フィルタの製作は現実上難しいと思われる。したがって，レーザの線幅はできるだけ狭い方がよいが，従レーザ用として狭い線幅を持つ半導体レーザを求めるのも決して簡単ではない。結局，この相反関係を折衷する必要がある。GB 積（利得×帯域幅）が 1 GHz の広帯域で dc 利得の高い OP アンプを用いて能動ループ・フィルタを構成すると $Bn$ が (2〜3) MHz で，$K_2$ が約 50 dB であるものは実現できると考えられる。この場合は $(\Delta\nu_M+\Delta\nu_S)$ が約 1 MHz であればよいが，これは市販の半導体レーザと著者らの線幅狭窄化技術より[16]実現可能である。以上により現在使用しうる技術を組合せて位相誤差の分散が1ラジアン以下であるヘテロダイン形 OPLL が実現できる。

## 4. 実際系の実験データとの比較

シミュレーションの結果の妥当性を確認するために波長 0.8 μm AlGaAs 半導体レーザの周波数オフセットロックシステム(図1(a)に相当)を用いた予備実験の実験結果[8]とシミュレーションの結果を比較した。この予備実験では二つのフリー・ランニング半導体レーザを使用し，$\Delta\nu_M$, $\Delta\nu_S$ はそれぞれ約 15 MHz であった。一方，$Bn$ が 25 kHz であったので，$(\Delta\nu_M+\Delta\nu_S)/Bn$ が約 1,000 であり，したがって図10から $\sigma_\phi$ は80～100ラジアンになると推定される。また，実験ではビート信号を 1/500～1/2,000 程度分周して位相比較器に入力した。このとき，ビート周波数の残留揺らぎは図9によると分周しないときの 22～45 倍増加する。以上よりこの実験系に対しシミュレーションから予想される $\sigma_\phi$ 値は $(1.76\sim4.5)\times10^3$ ラジアンである。一方，実験結果は二つのレーザ信号間の同期誤差であるビート信号の残留位相揺らぎのアラン分散の平方根が $1\sim2\times10^3$ ラジアン（積分時間1秒）であったので[8]，シミュレーションからの予想と符合する。

## 5. あとがき

1次能動ループ・フィルタを用いた半導体レーザによるヘテロダイン形 OPLL において位相誤差が1ラジアン以下になるために必要な条件を求めることを目的として，フォッカ・プランク法による理論解析，および光学部を電子回路で置換えたモデルによるシミュレーションを行った。

ビート信号の位相を基準マイクロ波発振器の位相に同期させ，主レーザの周波数安定性を従レーザのに移乗するためには少なくとも能動ループ・フィルタの帯域幅は $Bn\geqq\Delta\nu_S/(1.2\sim3)$ である必要がある。特に，ループの同期誤差であるビート周波数の揺らぎを1ラジアン以下にするためには $Bn$ を $(\Delta\nu_S+\Delta\nu_M)$ の2倍以上にすること，更に能動ループ・フィルタの設計上の制約（すなわち，利得と帯域においての制約）を考慮すると $(\Delta\nu_S+\Delta\nu_M)$ を約 1 MHz 以下にすることが要求される。

位相比較器の応答速度の制限より分周器を使用するときは，位相誤差は分周率 $M$ の 0.5 乗に比例して増加するので，できるだけ $M$ を小さくするのが望ましい。一方，能動ループ・フィルタの利得は $Bn$ が広いほど大きく取らなければならないことも注目する必要がある。

上記の条件を満たすことによって，半導体レーザを用いたヘテロダイン形光位相同期ループの実現が期待でき，精密な光トラッキングジェネレータ/光シンセサイザとして応用できると考えられる。

(昭和63年2月22日受付)

## 文　献


(1) L.H. Enloe & J.L. Rodda: "Laser Phase Locked-Loop", Proceedings of IEEE, 165-166 (1965)

(2) W.R. Leeb, H.K. Philipp, A.L. Scholtz & E. Bonek: "Frequency Synchronization and Phase Locking of $CO_2$ Lasers", *Appl. Phys. Lett.*, 41(7), 592-594 (1982)

(3) J.L. Hall, L.S. Ma & G. Kramer: "Principles of Optical Phase-Locking; Application to Internal Mirror He-Ne Lasers Phase-Locked via Fast Control of the Discharge Current", *IEEE J. of Quantun Electron.*, **QE-23**, 4, 427-437 (1987)

(4) R.C. Steele: "Optical Phase-Locked Loop using Semiconductor Laser Diodess", *Eletron. Lett.*, **19**, 2, 69-71 (1983)

(5) D.J. Malyon, D.W. Smith & R. Wyatt: "Semiconductor Laser Homodyne Phase Lock Loop", CLEO '86, San Francisco, THJ 1, 270-271 (1986)

(6) 久保木・大津:「半導体レーザの周波数オフセット・ロックに関する研究」, 信学技報, **MW 85-29**, 99-104 (1985)

(7) K. Kuboki & M. Ohtsu: "Frequency Offset Locking of AlGaAs Semiconductor Lasers", *IEEE J. of Quantum Eletron.*, **QE-23**, 4, 388-394 (1987)

(8) 久保木・加藤・申・大津:「半導体レーザの周波数オフセット・ロック」, 応用物理学会量子エレクトロニクス研究会「レーザ・原子発振器の周波数制御と応用」第2回シンポジューム予稿集, 67-68 (昭62)

(9) A.J. Viterbi: "Phase-Locked Loop Dynamics in the presence of Noise by Fokker-Planck Techniques", Proceedings of IEEE, 1737-1753 (1963)

(10) L.G. Kazovsky: "Impact of Laser Phase Noise on Optical Heterodyne Communication systems", *J. of Opt. Commun.*, 2, 7, 66-78 (1986)

(11) K. Kikuchi, T. Okoshi, M. Nagamatsu & N. Henmi: "Degradation of Bit-Error Rate in Coherent Optical Communications Due to Spectral Spread of the Transmitter and the Local Oscillator", *IEEE J. of Lightwave Tech*, **LT-2**, 6, 1024-1033 (1984)

(12) A. Blanchard: "Phase-Locked Loops", John Willey & Sons, New York, 61-62 (1976)

(13) 加藤・久保木・大津:「周波数オフセットロックシステムの性能評価」, 第48回応用物理学会学術講演会予稿集, 第3分冊, 20p-ZQ-4, 701 (昭62)

(14) M. Ohtsu, H. Fukuda, T. Tako & H. Tsuchida: "Estimation of the Ultimate Frequency Stability of Semiconductor Lasers", *Jpn. J. of Appl. Phys.*, **23**, 7, 1157-1166 (1983)

(15) Y.C. Chung & T.M. Shay: "450-Hz frequency stability in a GaAlAs injection laser", CLEO '86, San Francisco, WB 3, 154 (1986)

(16) M. Ohtsu & S. Kotajima: "Linewidth Reduction of a Semiconductor Laser by Electrical Feedback", *IEEE J. of Quantum Electron.*, **QE-21**, 12, 1905-1912 (1985)

(17) H. Yasaka, Y. Yoshikuni, Y. Nakano & K. Oe: "Optical Frequency Stabilization and Linewidth Reduction of a Multielectrode DFB Laser with Current Feedback", *Electron. Lett.*, **23**, 21, 1161-1162 (1987)

(18) 大津元一:「周波数可変調可能な狭スペクトル線幅半導体レーザ」, 信学技報, **OQE 87-135**, 35-40 (昭62)

(19) F.M. Gardner: "Phaselock Techniques 2ed.", John Willey & sons, New York, 31, 143 (1979)

(20) 畑・古川:「PLL-IC の使い方」, 産業報知センター, 東京, 102 (昭60)

(21) L.G. Kazovsky: "Performance Analysis and Laser Linewidth Requirements for Optical PSK Heterodyne Communications Systems", *J. of Lightwave Tech.*, **LT-4**, 4, 415-425 (1986)

# Modulatable narrow-linewidth semiconductor lasers

L. Hollberg and M. Ohtsu[a)]
*National Bureau of Standards, Boulder, Colorado 80303*

(Received 28 March 1988; accepted for publication 5 July 1988)

We find that using the technique of optical feedback locking, to narrow semiconductor linewidths, does not sacrifice the ability to modulate the laser's frequency via the injection current. The frequency of a laser is stabilized to a separate Fabry–Perot reference cavity using resonant optical feedback and can be modulated efficiently at frequencies related by rational fractions to the free-spectral range of the reference cavity. This system can provide an array of narrow-linewidth, frequency-stable laser lines and shows promise for applications in frequency-division-multiplexed coherent communications, as well as laser frequency control and precision measurement systems.

Optical feedback locking of semiconductor lasers provides a powerful means for stabilizing the frequency and narrowing the linewidth of diode lasers.[1-3] This optical technique can reduce laser linewidths by more than a factor of 1000, thus achieving linewidths of a few kilohertz. We consider here the interesting and useful modulation characteristics of these optically stabilized semiconductor lasers (OSSL). Direct modulation of the injection current of these lasers can provide a high FM modulation index while the very narrow linewidth and frequency stabilization produced by the optical feedback lock is maintained.

The high-speed frequency and amplitude modulation capabilities of semiconductor lasers are important attributes of these lasers relative to other optical sources. Unfortunately, the FM capabilities are usually sacrificed when the laser linewidths are reduced by optical means.[4] With most frequency stabilization schemes there is a trade-off between the diode laser's linewidth and its FM modulation capabilities. Usually a one-to-one correspondence exists between these quantities; that is, if the laser linewidth is reduced by a factor of 10, its FM sensitivity to injection current (typically $\sim 3$ GHz/mA) is also reduced by roughly this same factor of 10. In the case of the OSSL the modulation characteristics are definitely altered by the optical locking process, but we find that the modulation sensitivity is not necessarily reduced when the linewidth is narrow. In fact, we find that the modulation characteristics of the OSSL have a predictable resonant frequency dependence.

The concept behind the optical feedback locking technique is to establish weak resonant feedback from a high $Q$ (relative to the $Q$ of the diode laser cavity) optical resonator. Figure 1 is a diagram of a system which gives enhanced optical feedback when the laser frequency matches the cavity resonance and effectively zero-feedback off resonance. Here a beamsplitter picks off a small amount of the laser output ($\sim 4\%$) and couples it off axis into a confocal optical resonator. This geometrical arrangement ensures that the laser sees positive optical feedback precisely when the laser frequency matches the cavity resonance frequency. The optical lock usually operates in the low feedback limit and typically requires an optical feedback power of about $10^{-4}$ of the laser output power.[2] At resonance the spectrally cleaned laser field which has built up in the reference cavity leaks back through the cavity input mirror and returns to the laser where it increases the laser gain at that frequency. This frequency-selective gain enhancement forces the laser to lock to the cavity resonance frequency. The result is that the semiconductor laser's frequency is stabilized to the cavity resonance, and its 20 MHz linewidth is reduced to less than 10 kHz. Related work has also been reported for semiconductor laser frequency control using optical feedback from optical waveguides[5] and fiber cavities.[6]

We have used a variety of optical geometries and reference cavities for these optical locking systems. The free-spectral ranges (FSR) of the reference cavities were between 7.5 GHz and 250 MHz with cavity resonance widths varying from 75 MHz to 20 kHz. The commercial lasers were single-mode AlGaAs lasers operating near 850 nm and were not modified in any way. For applications requiring higher spectral purity and low residual phase noise at high frequencies, it is useful to send all of the laser power into and through the high-efficiency reference cavity. The cavity then acts as a

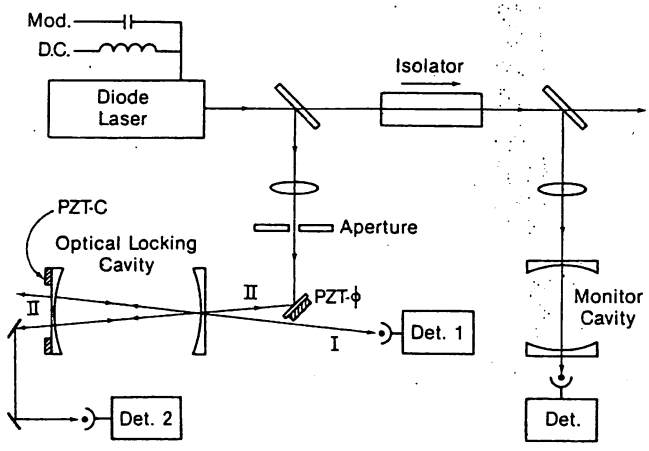


FIG. 1. Experimental diagram of an optically stabilized semiconductor laser (OSSL). Approximately 4% of the laser output power is coupled off-axis into the confocal optical locking cavity. In this geometry resonant optical feedback returns to the laser and automatically locks the laser frequency to the cavity resonance. Piezoelectric ceramics PZT-C and PZT$\phi$ are used to control the cavity frequency and optimize the feedback phase, respectively. An additional monitor cavity is used for spectral analysis and is separated from the laser by an optical isolator. rf modulation is added to the dc injection current through the modulation port (mod.). Photodiode detectors (det.) monitor the transmission and reflection signals from the cavities.

[a)] Permanent adress: Tokyo Institute of Technology, Graduate School at Nagatsuta, Midori-ku, Yokohama, Kanagawa 227, Japan.

  

bandpass filter and removes the excess laser phase noise at very high frequencies. This scheme uses the reference cavity as a spectral and spatial filter as well as the frequency discriminator for the optical feedback lock using the weak reflection.

Modulation of the injection current of nonstabilized semiconductor lasers results in both amplitude and frequency modulation of the laser output. At least in the limit of low modulation index the temporal characteristics of the laser electric field can be represented by

$$E(t) = A\,[1 + m\cos(\omega_m t)]\sin[\omega t + \beta\cos(\omega_m t + \theta)]\,. \tag{1}$$

Here $A$ is the field amplitude, $\omega/(2\pi)$ is the laser carrier frequency, $\omega_m/(2\pi)$ is the modulation frequency, and $m$ and $\beta$ represent the amplitude and frequency modulation indices, respectively.[7,8] The resulting frequency-domain spectra can be described by the usual sum of AM plus FM sidebands (with Bessel function amplitudes) except that the relative phase $\theta$ between AM and FM is frequency dependent. When a diode laser is operating well above threshold, a small modulation of the injection current results in a modulation of the laser field that is predominantly FM with the ratio of $\beta$ to $m$ typically in the range of 10 to 20. However, when the modulation index is large ($\beta > 2$), the situation can be considerably more complicated.

When the OSSL is modulated at low frequencies, typically $\omega_m < 200$ MHz, the frequency modulation is suppressed by the optical lock relative to that of an unstabilized laser.[9] On the other hand, there are special modulation frequencies that strongly affect the frequency modulation characteristics of the OSSL. With certain modulation conditions some or all of the modulation sidebands can resonate with the reference cavity (with or without the carrier), in which case they return to the laser and reinforce the optical lock. In particular optical sidebands at frequencies that correspond to the FSR (or its harmonics) of the reference cavity are simultaneously resonant with the cavity and are fed back to the laser with the carrier. In this way it is possible to modulate the laser current with a high modulation index $\beta$ and generate many sidebands without disrupting the frequency stabilization and linewidth narrowing provided by the optical feedback lock.

Figure 2 shows the resonances in the optical locking process that one observes as a function of the applied rf modulation frequency. The tallest, evenly spaced, sharp resonances in this figure occur when the modulation is at frequencies integrally related to the cavity FSR of 245 MHz. Good optical locking is observed at the modulation frequencies corresponding to these resonances. Also, the power transmitted through the cavity is maximized because the laser carrier and the sidebands match cavity resonances.

All of the cavity transmission resonances shown in Fig. 2 correspond to modulation frequencies that are related to the reference cavity FSR by rational numbers, that is, when the modulation frequency is

$$\omega_m/(2\pi) = (a/b)(\mathrm{FSR}), \quad a,b = 1,2,3,\ldots\,. \tag{2}$$

The smaller resonances shown in Fig. 2 occur when the ratio $(a/b)$ is not an integer. This rational relationship between

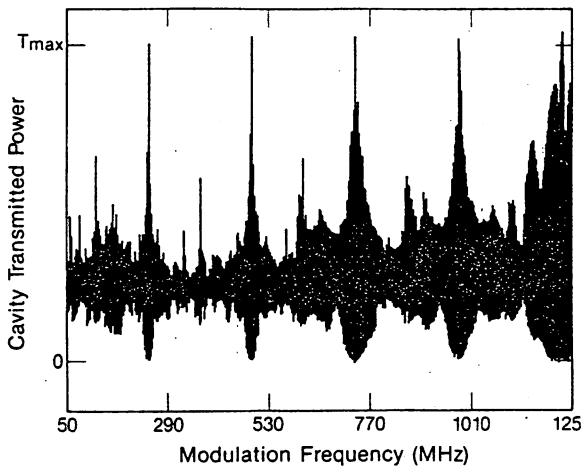


FIG. 2. Power transmitted through the optical locking cavity (FSR = 245 MHz, finesse = 10) as seen by detector 2 (Fig. 1) as a function of the frequency of the modulation applied to the injection current. The modulation frequency is swept slowly from 50 to 1250 MHz. Points of zero and maximum transmission are indicated on the vertical axis. The sharp peaks indicate the resonant nature of the stability of the optical lock as a function of modulation frequency. The large evenly spaced peaks correspond to modulation at the frequency of the cavity free-spectral range (245 MHz) and its harmonics. The smaller resonant peaks occur when the modulation frequency is related to the cavity FSR by a noninteger rational number. A modulation current of ~5 mA was added to the dc current of 95 mA (~1.7 times threshold).

the modulation frequency and the cavity FSR for stable optical locking is easily understood: that is, under the conditions of Eq. (2) every $b$ th sideband can resonate with every $a$th cavity mode. For example, modulation at 367 MHz corresponds to $a/b = 3/2$ and means that when the carrier is resonant with a cavity mode, every other sideband will be simultaneously resonant with every third cavity mode. This situation gives stable optical locking with roughly half of the available power resonant with the cavity. We have observed these resonant enhancements in the optical lock for many modulation frequency to FSR ratios, including those with $a = 1$–$9$ and $b = 1$–$5$. In principle, some optical locking occurs for any modulation frequency that is related to the cavity FSR by a rational number $(a/b)$, but in general as the denominator $b$ gets larger, less and less of the available optical power is resonant with the cavity modes and hence the optical lock is less effective. The strength of a particular resonance depends on the number and size of the sidebands that are resonant with cavity modes and thus depends strongly on the modulation index $\beta$ and the value of $b$.

The frequency domain power spectra of an optically locked laser that is modulated at one of the resonances [consistent with Eq. (2)] consist of an array of frequency stabilized, narrow-linewidth laser lines separated by the modulation frequency. Figure 3 shows sideband spectra of a modulated OSSL taken with an optical spectrum analyzer (see Fig. 1). The optical spectrum analyzer that is used to display the modulation sidebands is not capable of measuring the very narrow laser linewidth because of the limited resolving power when a large FSR (7.5 GHz) is required. In order to measure the laser linewidth we use heterodyne methods to detect the beat note between two OSSL's.[2] We find that the locked laser linewidths are less than 10 kHz and

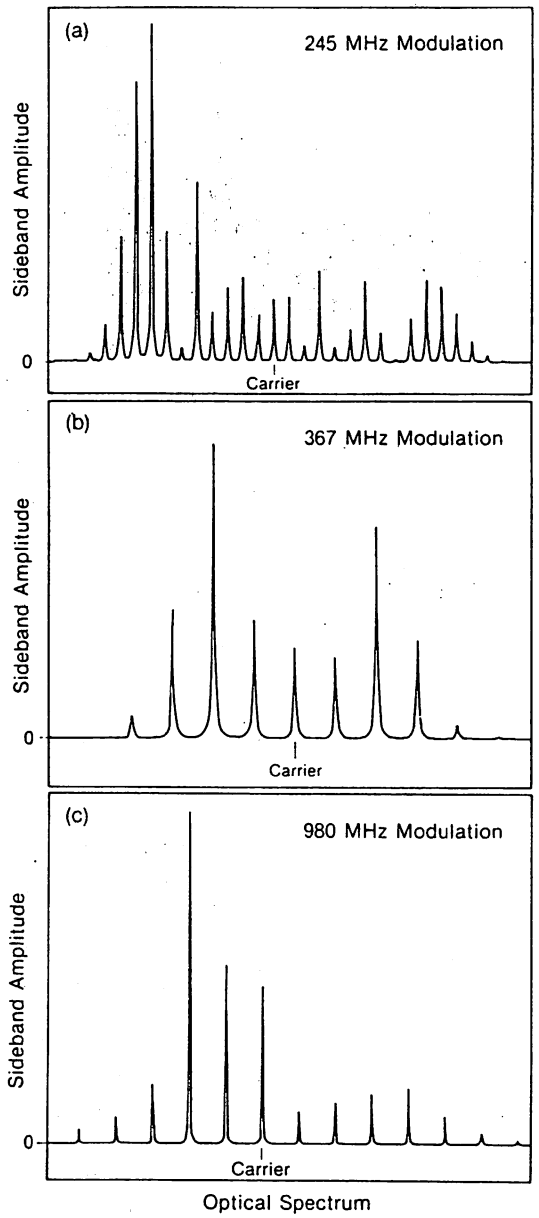


FIG. 3. Sideband structure of a modulated, optically locked, semiconductor laser taken with an optical spectrum analyzer (FSR = 7.5 GHz, finesse = 150) for three of the resonant modulation frequencies. In all of these cases a high-modulation index $\beta$ is obtained while maintaining the narrow laser linewidth and center frequency stabilization. In (a) the modulation frequency is equal to the locking cavity FSR of 245 MHz. Here a modulation current of ~7 mA is added to the dc bias of 97 mA. We see that more than 20 narrow-linewidth, frequency stable, sidebands are produced. In (b) the 4 mA of modulation current is at a frequency of 367 MHz which is 3/2 the cavity FSR. In (c) the laser is modulated with ~10 mA at 980 MHz (four times the FSR), and the laser generates more than ten useful sidebands covering a total frequency range of more than 10 GHz (in this case the overlapping sidebands from the adjacent 7.5 GHz FSR have been removed for clarity).

that the linewidth is unchanged when the laser is modulated at frequencies that correspond to the locking resonances that are shown in Fig. 2. This is to be compared with linewidths that are measured to be 20 MHz when the laser is not locked or is strongly modulated at a frequency that is not an optical locking resonance frequency. When modulated at such nonlocking frequencies the OSSL's linewidth degrades progressively from 10 kHz to 20 MHz as the modulation index is increased.

A good optical lock occurs when the laser is modulated at a resonance frequency consistent with Eq. (2). However, these resonances are fairly narrow in modulation frequency and depend directly on the $Q$ of the cavity, the modulation index, and the optical feedback level. For example, with a locking cavity $Q \sim 10^7$ (corresponding to a cavity finesse of 10 and a FSR of 245 MHz) and an optical feedback power ratio of about $10^{-4}$, the modulation frequency range for good optical locking is approximately 6 MHz wide (centered at the modulation resonance frequency at 245 MHz; see Fig. 2). This range is for a modulation index $\beta \simeq 8$ and increases, as we might expect with smaller modulation index. This resonant character of the laser's FM modulation response limits the modulation formats that can be employed with the OSSL.

Using the technique of optical feedback locking, we find that it is possible to simultaneously have a narrow-linewidth semiconductor laser with a high-sensitivity frequency modulation capability. Frequency modulation induced via the injection current is compatible with the optical stabilization (and narrow linewidth) when the ratio of the modulation frequency to cavity FSR is a rational number. One of the promising applications is to use the modulated OSSL to provide an array of frequency-stabilized local oscillators for frequency-division-multiplexed coherent communication systems. There is also the potential for measuring optical absorption and dispersion with high sensitivity using the techniques of optical heterodyne spectroscopy[10] as well as applications in precision laser measurements and frequency control.[11,12]

We would like to thank J. L. Hall, R. Drullinger, B. Dahmani, and A. Clairon for constructive discussions, and J. L. Hall and the Joint Institute for Laboratory Astrophysics for making this collaboration possible.

[1]D. Hjelme, A. Mickelson, L. Hollberg, and B. Dahmani, in *Digest of Topical meeting on Semiconductor Lasers* (Optical Society of America, Washington, DC, 1987), p 15.
[2]B. Dahmani, L. Hollberg, and R. Drullinger, Opt. Lett. **12**, 876 (1987).
[3]H. R. Telle and H. Li, IEEE J. Quantum Electron. (to be published).
[4]M. Ohtsu and S. Kotajima, IEEE J. Quantum Electron. **21**, 1905 (1985).
[5]N. A. Olsson, C. H. Henry, R. F. Kazarinov, H. J. Lee, B. H. Johnson, and K. J. Orlowsky, Appl. Phys. Lett. **51**, 1141 (1987); R. F. Kazarinov and C. H. Henry, IEEE J. Quantum Electron. **23** 1401 (1987); R. F. Kazarinov, C. H. Henry, and N. A. Olsson, IEEE J. Quantum Electron. **23**, 1419 (1987).
[6]F. Favre and D. Le Guen, IEEE J. Quantum Electron. **21**, 1937 (1985).
[7]S. Kobayashi, Y. Yamamoto, M. Ito, and T. Kimura, IEEE J. Quantum Electron. **18**, 582 (1982).
[8]W. Lenth, Opt. Lett. **8**, 575 (1983).
[9]A. Clairon, B. Dahmani, Ph. Laurent, and Ch. Breant, in Proceedings of the 2nd European Frequency and Time Forum, Neuchatel, Switzerland, 1988; and Ph. Laurent, A. Clairon, and Ch. Breant (unpublished).
[10]J. L. Hall, L. Hollberg, T. Baer, and H. G. Robinson, Appl. Phys. Lett. **39**, 680 (1981).
[11]R. W. P. Drever, J. L. Hall, F. V. Kowalski, J. Hough, G. M. Ford, A. J. Munley, and H. Ward, Appl. Phys. B **31**, 97 (1983).
[12]R.G. Devoe, C. Fabre, K. Jungmann, J. Hoffnagle, and R. G. Brewer, Phys. Rev. A **37**, 1802 (1988).

特集　光波センシング技術の応用

# センシング応用のための半導体レーザの高コヒーレント化

東京工業大学　大津　元一

## 1. はじめに

「コヒーレント」という言葉の意味は，「周波数揺らぎが少ない」，「位相の揃ったきれいな波」，さらには「干渉性に富んだ波」，と理解されている。高精度の光波センシングシステムにはこのようなコヒーレントな光波を発生する半導体レーザ光源が必須である。そのようなシステムは共振形ファイバジャイロスコープ，測長，分光分析，その他，非常に多岐の分野にわたる。コヒーレント光源として満たすべき性質としては図1に示すように次の4点が挙げられる。すなわち，

(1) 主レーザの発振スペクトルの中心周波数 $\nu_m$ が安定な基準周波数値 $\nu_r$ に安定化されること。

(2) 主レーザの発振スペクトル線幅 $\Delta\nu_m$ が狭いこと。

(3) 従レーザの発振スペクトルの中心周波数 $\nu_s$ が主レーザのそれに高精度で追随し，さらに発振スペクトル線幅 $\Delta\nu_s$ が主レーザのそれと同様に狭いこと。

(4) (3)の状態を保ったまま，従レーザの周波数 $\nu_s$ が高精度，広帯域にわたり掃引されること。

以上の4点は従来，マイクロ波周波数領域において高精度発振器を実現する際に行われていた項目に対応する。すなわち，光周波数シンセサイザ・光トラッキングジェネレータを実現することに他ならない。そこで本稿ではこれを実現するために従来行われている研究開発の現状と将来展望について概説する。対象とする半導体レーザは主に波長1.5$\mu$mのInGaAsPレーザ，および0.8$\mu$mのAlGaAsレーザである。

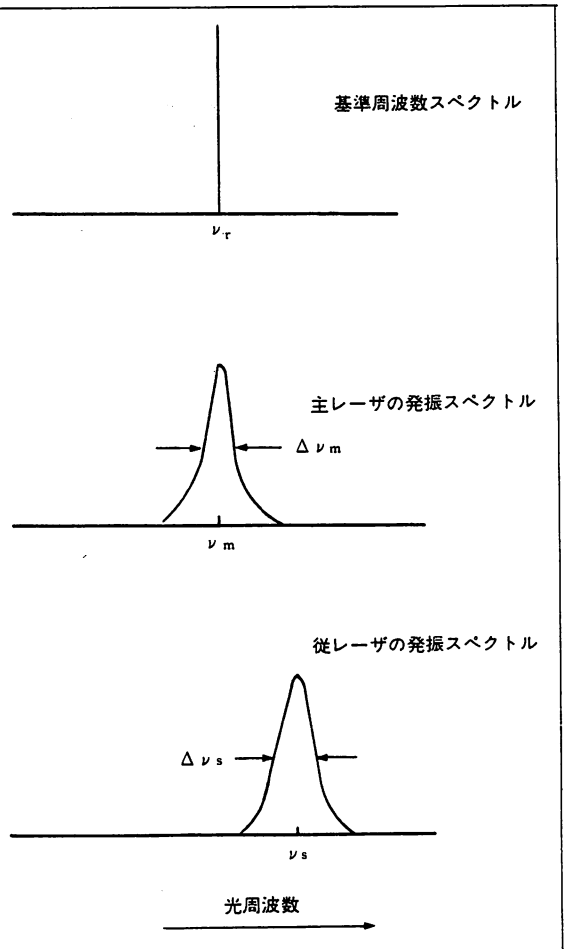


図1　コヒーレントな光を発生するためのレーザとしての必要4項目の説明

## 2. 光帰還法

前節で示した4点のうち(2)のスペクトル線幅を狭くする簡便な方法が過去約20年にわたって採用されている[1]。それは図2（a）に示すようなもので，光帰還法と呼ばれる。これはレーザからの出射光を外部反射面にあて，その反射光をレーザに再注入させる方法である。この場合レーザ本体と反射面とにより大きな共振器が構成され，これによって共振器の損失が減少して周波数揺らぎ，すなわちスペクトル線幅が狭くなる。図2（b）に示すよ

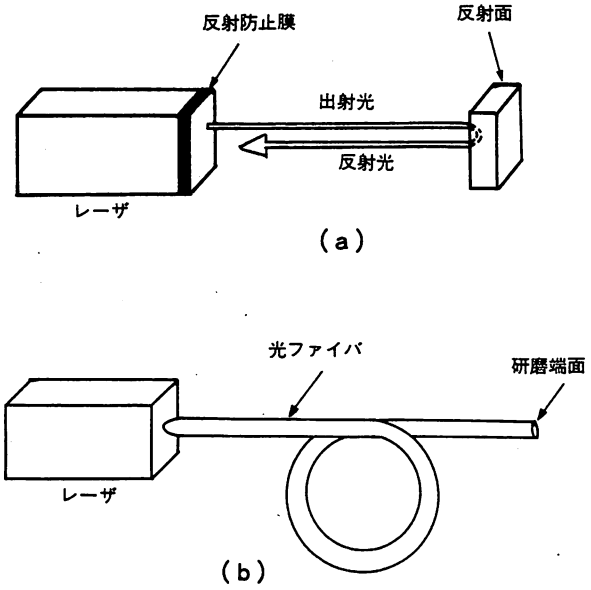


図2　光帰還法の説明。(a) 外部反射面からの反射光をレーザに再注入する方法。(b) レーザに光ファイバを接続し，その研磨端面からの反射光をレーザに再注入する方法。

うに反射面のかわりに端面を研磨した光ファイバをレーザに接続する方法も採用されている[2]。この方法により10 kHz ～30 kHz の線幅が得られている[2]。さらに，外部反射面を半導体レーザ本体とモノリシックに集積化することも試みられている[3]。

図2の方法は簡便であるのでしばしば用いられるが，欠点としては決定論的不安定の発生[4]，単一縦モード性の崩壊，直接周波数変調効率の消滅，などを有する。そこでこれを補う方法として図3 (a) に示すようにレーザ外部に置かれた共焦点形ファブリ・ペロー共振器（以後「FP 共振器」と記す）からの反射光をレーザに再注入する方法が提案されている[5]。FP 共振器からの反射率は周波数依存性を持つので図2の場合より安定に線幅を狭くすることができる。図3 (b) に示すように20 kHz の線幅が得られている。この場合，FP 共振器とレーザ本体とは光学的に弱結合なのでレーザの単一縦モード性が保存される。さらに FP 共振器の自由スペクトル域の周波数値の有理数倍の変調周波数でレーザの注入電流を変調すると直接周波数変調が可能となる[6]。この FP 共振器を用いた光帰還法は有望な方法であり，図4に示すように分布グレーティング反射器と導波路をレーザ本体とモノリシックに集積化することが試みられている[7]。

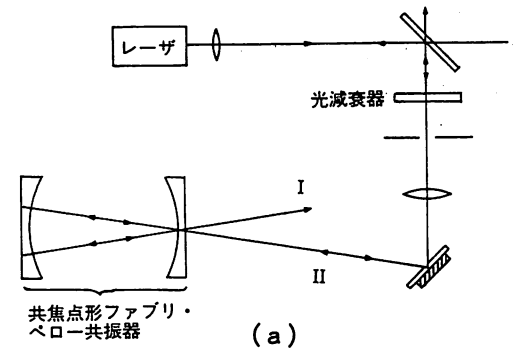


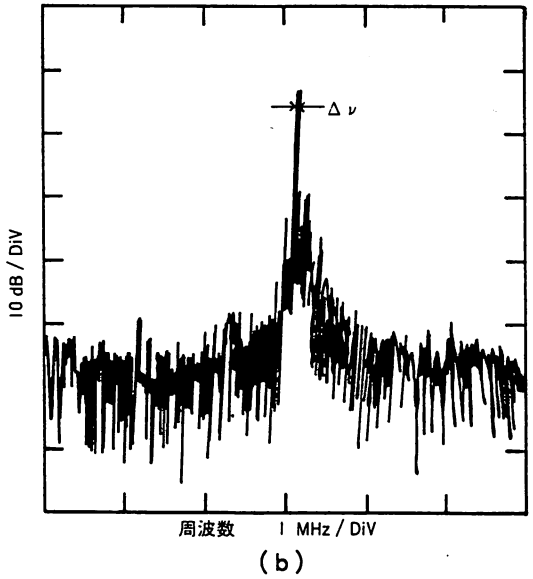


図3　(a) 共焦点形ファブリ・ペロー共振器からの反射光をレーザに再注入する方法の原理図[5]。この図では2種類の反射光 I，II のうち共振器内で共振してしみだした光 II をレーザに再注入する。(b) 得られた発振スペクトル。線幅 Δν の値は20 kHz。

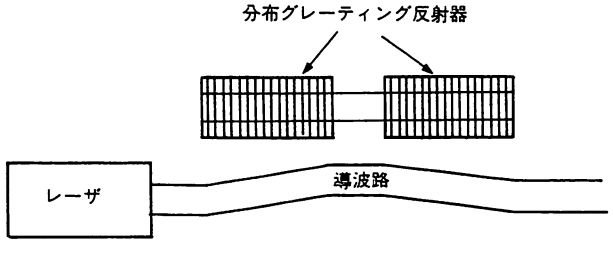


図4　図3 (a) の装置を集積化したもの[7]。分布グレーティング反射器が図3 (a) のファブリ・ペロー共振器に対応している。

## 3. 電気的負帰還法

光帰還法は負帰還制御法ではないので不安定性が残る。そこで図5に示すように積極的に負帰還制御を施して周波数揺らぎを抑える方法が考案されている[8]。すなわち，適当な光周波数復調器でレーザの周波数揺らぎを検出し，その検出器出力を増幅してレーザの注入電流に負帰還することによりレーザ固有の周波数揺らぎを抑圧するものである。この方法の主な利点は次の4つである。(1)本質的に負帰還なので安定性が高い。(2)非制御時のレーザ固有の量子雑音による周波数揺らぎレベル以下の，非常に周波数揺らぎの小さい状態を実現しうる。(3)制御システムの計算機シミュレーションを行うと制御時の周波数揺らぎの抑圧度を推定することができ，これが実験結果とよく合う。すなわち，実験を行うまでもなくCAD(Computer Aided Design)により周波数揺らぎ特性の改善の様子が推定できる。(4)1節で述べた4項目を同時に実現する統合システムの構築が可能である。

特に上記の利点(4)に対応する統合システムのブロック図を図6に示す[8]。図中のブロック(1)～(4)が各々1節で述べた4項目に対応する。本節ではこれらの各部について実験結果等を説明する。

### 3．1　主レーザの中心周波数安定化

図6のブロック(1)において，制御帯域 $f \leqq \Delta\nu_{FR}$（非制御時のレーザのスペクトル線幅）であるような低速制御を施すと主レーザの発振スペクトル中心周波数が安定化される。この場合安定な周波数基準が必要であり，そのような基準としてはアルカリ金属蒸気の吸収スペクトル線などが採用されている[8]。ルビジウム(Rb)の吸収スペクトルを使った実験では周波数安定度 $2\times10^{-12}$ が得られている。制御系の最適化により将来は $1\times10^{-15}$ が可能であると試算されている。

### 3．2　主レーザの発振スペクトル線幅の狭窄化

図6のブロック(2)において，制御帯域 $f \geqq \Delta\nu_{FR}$ であるような高速制御を施すと主レーザの発振スペクトル線幅が狭窄化される。この場合，高感度な光周波数復調器としてFP共振器を使うのが便利である。このFP共振器にレーザ光を入射させ，その透過光パワーの揺らぎを測定することによりレーザ周波数揺らぎを検出できる。この方法により線幅は100kHzまで狭くなっている[9]。さらに，広帯域制御をほどこすには透過光よりも反射光パワーの揺らぎを測定する方が有利である[10]。反射光揺らぎには周波数揺らぎの微分が含まれているからである。この原理にもとづき，高フィネスFP共振器からの反射光を利用した電気的負帰還を施した結果，図7に示すように線幅としては世界で最も狭い値，880Hzが実現している[11]。制御系の最適化により将来は1Hz以下の線幅が可能であると試算されている[8]。

### 3．3　従レーザの周波数追随

3．1，3．2節で実現した高コヒーレントな主レー

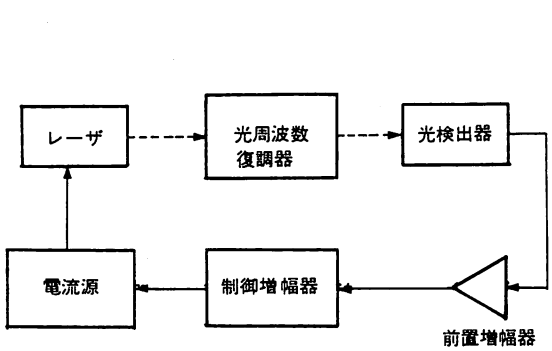


図5　電気的負帰還法の原理

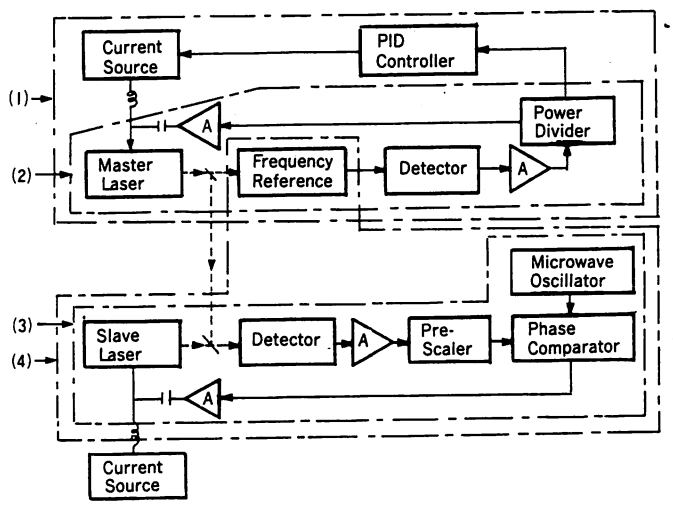


図6　1節の4つの課題を電気的負帰還法によって同時に実現する統合システムの原理[8]。

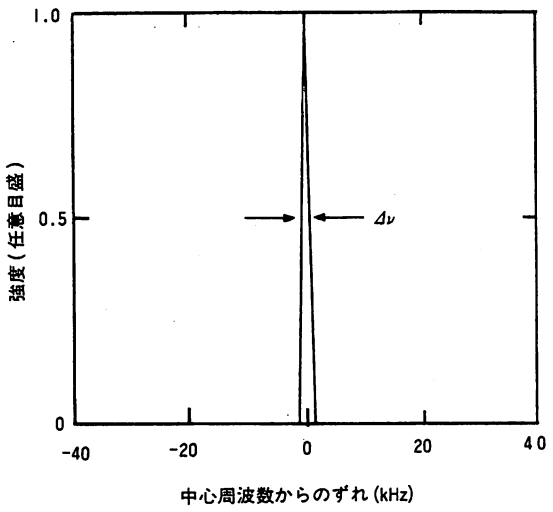


**図7**　高フィネスファブリ・ペロー共振器からの反射光を利用した電気的負帰還法の結果得られたスペクトル[11]。線幅 Δν の値は880 Hz。

ザの周波数に従レーザの周波数を追随させるには図6のブロック(3)を用いる。すなわち，主，従レーザの間のビート信号を検出し，その周波数が別に用意するマイクロ波局部発振器の周波数と一致するように従レーザの注入電流を負帰還制御する。実際には追随精度を向上させるために，周波数ではなく位相を検出し，制御している。この結果，ビート周波数の安定度は $6\times10^{-15}$ に達している[12]。この安定度は3．1で得た主レーザの安定度よりすぐれている。このことは従レーザ周波数揺らぎは主レーザの周波数揺らぎと同等なレベルまで抑圧され，従レーザ周波数は主レーザ周波数に高精度に追随していることを意味している。この制御系の性能をさらに向上させるとヘテロダイン形光位相同期ループが実現し，ビート信号の位相揺らぎ1ラジアン以下，周波数安定度 $1\times10^{-17}$ が可能であると試算されている[13]。

### 3．4　従レーザ周波数の高精度・広帯域掃引

3．3の制御を保ったまま，マイクロ波局部発振器の周波数を掃引するとビート周波数，従って従レーザ周波数が高精度に掃引される。一回の掃引範囲はビート信号検出用の光検出器の応答周波数帯域によって決まり，約2 GHz である。さらに掃引範囲を拡大するためには3．1節において主レーザ周波数を安定化するときに用いた基準周波数として，周波数軸上に等間隔に多数分布しているもの（例えば有機分子の振動回転準位間での遷移による吸収スペクトル線周波数[8]，FP 共振器の共振周波数）を用い，その隣合う基準周波数に主レーザ周波数を次々に安定化していきながら，同時に3．3節の制御を従レーザに施し，マイクロ波局部発振器の周波数を掃引すればよい。この方法により60GHz の範囲にわたって従レーザ周波数が高精度かつ連続的に掃引されている[12]。この周波数範囲はレーザのモードホッピング特性により制限されているので，モードホッピングのない動的単一モードレーザ[14]を使えば約1 THz の掃引範囲が可能であると試算されている[8]。

**表1**　電気的負帰還法による半導体レーザの高コヒーレント化の現状と将来

| 事　項 | 現在の値 | 将来予測 |
|---|---|---|
| (1) 中心周波数安定度 | $2\times10^{-12}$ | $1\times10^{-15}$ |
| (2) スペクトル線幅狭窄化 | 880 Hz | 1 Hz |
| (3) 周波数追随精度 | $6\times10^{-15}$ | $1\times10^{-17}$ |
| (4) 高精度周波数掃引範囲 | 60 GHz | 1 THz |

以上の4つの小節に示した数値を表1にまとめる。この表からもわかるようにきわめて高精度のコヒーレント半導体レーザ光源が実現しているといえる。

## 4．性能向上のための課題

さらに一層の性能の向上のために必要な技術的課題は次のとおりである。

(1)　周波数確度の向上。すなわち，光周波数は非常に高い（約100THz）のでマイクロ波に比べ絶対測定が難しい。現在のところその測定確度は約 $1\times10^{-8}$ である[15]。光周波数多重化技術によってセンシング精度を向上させる場合には周波数測定確度はさらに2桁以上向上する必要がある。より実用的な周波数または波長測定法の開発[16]が不可欠となろう。

(2)　電気的負帰還を施す場合，その制御帯域をできるだけ拡大し，かつ制御利得を増大させるには半導体レーザの直接周波数変調効率は広い変調周波数にわたって均一であることが望ましい。しかし従来のレーザ素子では低変調周波数領域では熱効果，高変調周波数ではキャリヤ効果によって変調が生ずるので，その特性は均一ではない。この特性を均一化することは次世代のコヒーレント半導体レーザ実現のために重要な課題である。現在までに，DFB レーザの電極を分割し，キャリヤ密度の空間的分布を調節して周波数変調特性の均一化を試みた例がある[17]。今後，

この種のレーザ素子の開発の一層の進展が望まれる。

(3) 光源のコヒーレント性を表す尺度として，単に発振スペクトル線幅のみでなく，発振器のQ値も考えられる。即ち，

$$Q=\frac{(\text{発振スペクトル中心周波数})}{(\text{発振スペクトル線幅})}$$

である。制御を施さない時のレーザについてのQ値は発振波長に反比例することが理論的に示されている[18]。従って，将来，よりコヒーレント特性の優れたレーザ素子を得るためには短波長レーザの開発が重要である。現在，AlGaInP半導体レーザが最も短波長であり，室温では波長約670 nmで発振する[19]。将来はこのレーザの単一縦モード化，さらに，より短波長のレーザ素子の開発が望まれる。

## 5. まとめ

コヒーレント光センシングに使うための半導体レーザのコヒーレント特性を向上させるための技術について概説した。このような技術の性能を十分発揮するには現在の半導体レーザ素子の性能は十分完備されているとはいえない。今後はこの技術の向上とともにこの技術に適した半導体レーザ素子の開発を並行して行うことがますます重要になると考えられる。本稿では半導体レーザのコヒーレント特性の基礎，およびその応用については省略したが，これらの詳細については文献20を参照されたい。

### 参考文献


1) 大津，光ファイバセンサ，第3章，(大越編，オーム社)，1986年

2) F. Favre, D. Le Guen and J. C. Simon, IEEE J. Quantum Electron., QE-18 (1982) 1712

3) T. Fujita, J. Ohya, K. Matsuda, M. Ishino, H. Sato and H. Serizawa, Electron. Lett., 21 (1985) 374

4) 大津，月刊フィジックス，海洋出版，6 (1985) 297

5) B. Dahmani, L. Hollberg and R. Drullinger, Opt. Lett., 12 (1987) 876

6) 大津，電子情報通信学会技術報告，1987年12月，QOE 87-135

7) N. A. Olsson, C. H. Henry, R. F. Kazarinov, H. J. Lee, B. H. Johnson and K. J. Orlowsky, Appl. Phys. Lett., 51 (1987) 1141

8) M. Ohtsu, J. Lightwave Technol., 6 (1988) 245

9) 加藤，久保木，大津，第35回応用物理学関係連合講演会，1988年3月，29P-ZP-12

10) 村田，大津，第35回応用物理学関係連合講演会，1988年3月，29P-ZP-9

11) 大津，村田，興梠，第1回光波センシング技術研究会，1988年6月，LST 1-3

12) K.Kuboki, C. H. Shin, T. Kato, and M. Ohtsu, Digest of 1988 Conference on Precision Electromagnetic Measurements, June 1988, Tsukuba, p. 24

13) 申，久保木，加藤，大津，第35回応用物理学関係連合講演会，1988年3月，29P-ZP-14

14) Y. Tohmori, Ph. D. thesis, Tokyo Institute of Technology, Tokyo, Japan, 1986

15) M. Ohtsu, H. Kotani, and H. Tagawa, Jpn. J. Appl. Phys., 22 (1983) 1553

16) M. Ohtsu, H. Tagawa, and H. Kotani, Jpn. J. Appl. Phys., 22 (1983) 1876

17) Y. Yoshikuni and G. Motosugi, J. Lightwave Technol., LT-5 (1987) 516

18) 大津，レーザーと原子時計，オーム社，1986年，第5章

19) 例えば，日経エレクトロニクス，no. 427, Aug. 10, 1987, p. 127

20) M. Ohtsu and T. Tako, Progress in Optics, vol. XXV, Chapter II, Elsevier Science Pub., Amsterdam, 1988



〈著　者〉　オオツ　モトイチ（東京工業大学　総合理工学研究科）

〈連絡先〉　045－922－1111

# センサー用発光素子

東京工業大学　総合理工学研究科　大　津　元　一

## 1．まえがき

光センサーシステムにおいて光源は不可欠な基本要素であり，システムの性能は光源の性能により制限されるといっても過言ではなかろう．光源には各種の発光素子が使われているが，産業用には小型，低消費電力，長寿命等の利点を有する半導体レーザが適している．ところで，従来より，レーザから出て来る光は周波数または位相の揃ったきれいな波であるといわれているが，実際の光センサシステムに半導体レーザを用いるとき，戻り光誘起不安定などを避けるためにそのコヒーレント性を下げて使うことがしばしば行われている．しかし，光センサシステムの精度，分解能を向上させるにはレーザのもつコヒーレント性を積極的に利用するのが妥当な方法である．本稿ではこの認識にもとづき半導体レーザの高コヒーレント化の実現をめざした研究の現状について述べる．

レーザの周波数変動の大きさを表す標準偏差値$\sigma$の値は図1に示すようにレーザ発明当時(1960年)は約$10^{-7}$(すなわち，レーザ周波数100THzに対して10MHzの揺らぎ)であったが，その後この揺らぎを小さくするための努力が継続してなされ，昨年7月の時点でのトップデータとしてはすでに$10^{-16}$が実現している[1)]．つまり揺らぎはわずか0.01Hzにまで抑えられている．これは計測などで頻繁に使われている気体レーザの値であるが，この図によると$\sigma$の値は10年間ごとに約5桁ずつ減少しており，現在もその減少のようすに頭打ちが見られない．もちろんこのような高度の安定度を得るにはレーザ物理，分光，制御技術などの進歩に負うところが大きいが，約30年にわたってこのように順調に進歩した技術の例は少ないのではなかろうか．この図をもとにした技術予測によると特に大きな壁にぶつかることなく21世紀初頭には$10^{-18}$～$10^{-21}$が達成しうるといわれている[1)]．

このような順調な進歩はつぎのような考察によって理解できる．即ち，レーザに限らず，一般の非線形自励発振器が外部の制御装置によって周波数制御を施されているとき，時刻tにおける周波数変動$\delta\nu(t)$は

$$\delta\nu(t)=\varkappa\cdot\Gamma_0-\int_0^\infty h_f(\tau)\cdot\{\delta\nu(t-\tau)+\Gamma_n(\tau)\}d\tau \qquad (1)$$

と表される[2)]．ここで$\varkappa$はレーザ共振器の損失，$\Gamma_0$は量子効果(自然放出光揺らぎ)に起因する非制御時のレーザ周波数揺らぎを引き起こす雑音源，$\delta\nu(t-\tau)$は制御装置内の周波数揺らぎ検出系により検出された周波数揺らぎ，$\Gamma_n$は制御装置内で発生する雑音，$h_f$は制御装置のインパルス応答，を表す．この式をフーリエ変換して整理すると，

$$F(f)=\frac{1}{1+H(f)}\cdot\varkappa\Pi_0(f)-\frac{H(f)}{1+H(f)}\cdot\Pi_m(f) \qquad (2)$$

を得る．ここで，F，$\Pi_0$，$\Pi_n$，Hは各々(1)式中の$\delta\nu$，$\Gamma_0$，$\Gamma_n$，$h_f$のフーリエ変換である．ここで制御利得Hを大きくすると($|H|\to\infty$)この式右辺第1項は0に漸近する．一方第2項は$|\Pi_n|$に漸近する．このことは高利得の制御装置を用いて制御を施せば，量子効果に起因する非制御時の周波数揺らぎの値以下の値が実現でき，それは究極的には制御系の雑音によって制限される値をとることを意味する．

さて，この原理は工業的な応用上重要な半導体レーザにも当然当てはまる．半導体レーザの周波数揺らぎは非制御時には非常に大きいが，制御を施すことによりこれを抑圧でき，きれいな光波を得ることが可能である．これが実現すれば高性能

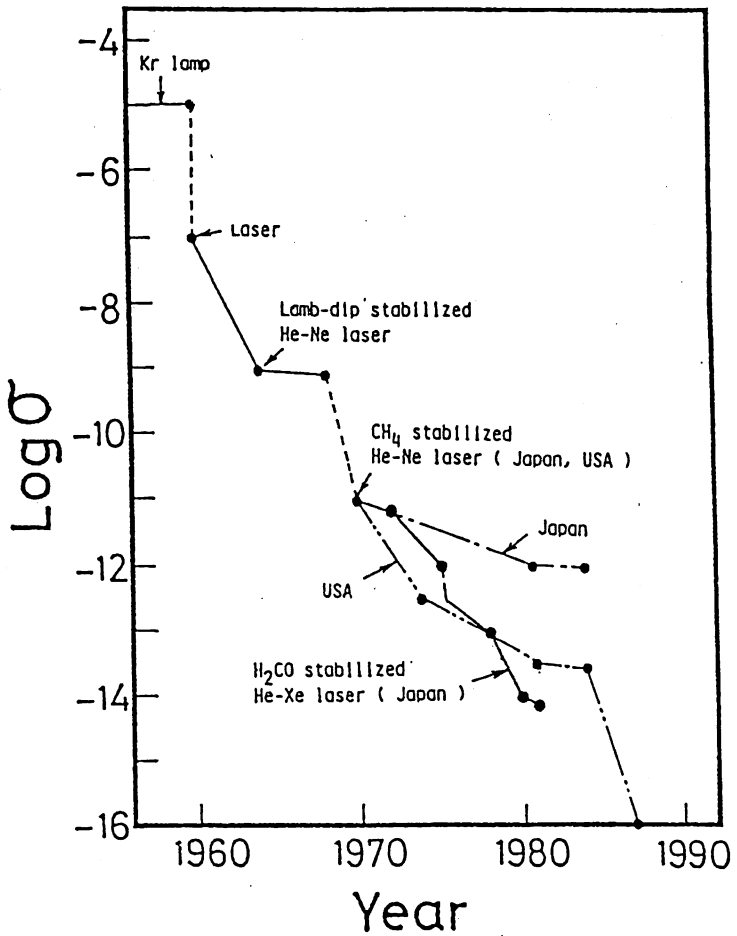


図1．He-Neレーザの周波数変動の大きさを表す標準偏差値σの値の進歩．

の光周波数シンセサイザ，光トラッキングジェネレータとして光センサシステムにおいて威力を発揮する．

そこで以下の節では半導体レーザの周波数制御方法とその特性，および問題点を順次列挙したい．ただし，2節では単一縦レード発振する半導体レーザについて議論する．この単一縦モード性に関する問題点は3節で取り上げる．尚，半導体レーザの周波数特性の基礎については文献3）～5）を，理論と実験の詳細については文献6），7）を参照されたい．

## 2．半導体レーザの周波数制御の実際

半導体レーザを使う場合，その周波数が一定値を取ること，その値が正確にわかっていること，すなわち，安定性と再現性が高いことが望まれる．さらに，これらとは一見相反するように感じられるが，周波数が広範囲にわたって掃引しうること，が挙げられる．これらの周波数制御性を実現するためには，従来マイクロ波発振器に対し確立している周波数制御技術[8]との類推により，以下の各小節で述べるような各項目を実行すればよい．

### 2．1．発振スペクトル中心周波数の安定化

周囲温度変化，自己発熱などによりレーザ発振スペクトルの中心周波数が少なくとも$10^{-7}$程度ドリフトするのでこれを抑える必要がある．

使用目的にもよるが，約1MHzの帯域の低周波制御装置が必要になる．レーザのヒートシンクの温度を制御してもよいが，高精度制御のためには注入電流制御の方がよい．周波数固定のための周波数基準として，簡便なものでは小型ファブリ・ペロー共振器が使われるが，周囲温度変化などによるこの共振周波数自身のドリフトがあるので，達成しうる安定度は$10^{-9}$が限界である[9]．より高度の安定度を得るには現在のところ原子，分子気体の吸収スペクトルが使われている．たとえば波長0.8μm～1.6μmの領域には$H_2O$,$NH_3$,$CO_2$を始めとする多数の有機分子の振動回転遷移の高調波，結合調の吸収スペクトル線が約10GHz間隔で分布している．これらは多数分布しているので各半導体

レーザ素子は少なくとも1本の吸収線に同調，安定化でき，都合がよい．これにより波長0.8μmのAlGaAsレーザ，1.5μmのInGaAsPレーザともに$10^{-11}$の周波数安定度が得られている[10,11]．この場合の問題点として，吸収強度が小さいので制御利得がやや小さいこと，吸収線の同定がまだ不十分なので周波数再現性がよくないこと，などが挙げられる．

波長0.8μm付近にはRb,Csなどのアルカリ金属の共鳴スペクトルがあり，この吸収強度は大きく，また同定も行われているので周波数基準としては有利である．これを用い$10^{-12}$の周波数安定度が得られている[12]．この場合の問題点はスペクトル線の数が少ない為に同調しうるレーザ素子が限られることである．原理的には（2）式の$\Pi_n$で決まる値，すなわち$10^{-15}$の安定度が可能であると推定されている[13]．ただし，この限界に達するにはさらに制御利得を増加させる必要があり，そのためにはFM分光法のような高感度な吸収スペクトル線検出法を採用する必要があろう[14]．

以上のような原子分子を周波数基準に用いた場合の共通の問題点としては，吸収スペクトル周波数が気体圧力によりシフトすることである[15]．これらは$10^{-12}$より良い長期周波数安定度，$10^{-11}$より良い周波数再現性を得ようとするとき問題になる．外部環境の変化に対してより安定な原子分子の探索が今後必要となろう．さらに，安定化された周波数の測定精度は現在のところ約$10^{-7}$である[16]．干渉測長への応用の際，この値は長さ絶対値の確度を制限するので十分でない．$10^{-10}$程度の精度の波長測定装置の開発が必要である．

### 2．2．発振スペクトル線幅の狭窄化

より高速の周波数揺らぎの成分はレーザ発振スペクトル線の幅をひろげる．非制御時の線幅は数MHz～100MHzである．共振型ファイバジャイロ，ヘテロダイン形干渉測長，コヒーレント・ライダーなどの広帯域光計測用光源としてはこのような線幅を狭窄化する必要がある．2．1節のような電流負帰還制御を施す場合，広帯域制御回路の設計は必ずしも容易ではないので10年以上前から現在まで，別の簡便な方法が採られてきた．これは(2)式において，H＝0（負帰還制御はしない）とするがその代わりに$x$を小さくする（レーザ共振器損失を小さくする）ものである．こうするとレーザ共振器の帯域全範囲で周波数揺らぎが小さくなり，スペクトル線幅も狭くなる．これを実行するには図2のようにレーザの一方の端面に反射防止膜を塗り，その代わりにレーザ長以上離れたところに反射鏡または回折格子を置く．こうしてレーザ単体のときにくらべ格段に長い共振器を構成し，これにより$x$を小さくする．この方法により数10kHzの線幅が実現している[17]．鏡を置く代わりにレーザ端面にファイバを接続した例[18]や，外部導波路をレーザと一緒に集積化した例もある[19]．この場合の問題点は系の安定性である．すなわち，負帰還制御を施していないので外部鏡，ファイバなどの機械的振動，熱膨張などの影響により線幅が時間的に変化する．これを抑えるためにレーザ端面の反射防止を強化し，レーザへの戻り光量を増す方法が採られるが[20]，それでもその安定性は実用的な光計測への応用には不十分である．その他の問題として，注入電流を変調してもレーザ周波数が変調されなくなること，縦モード周波数間隔が狭くなるので単一モード発振が保証されなくなること，などが挙げられる．

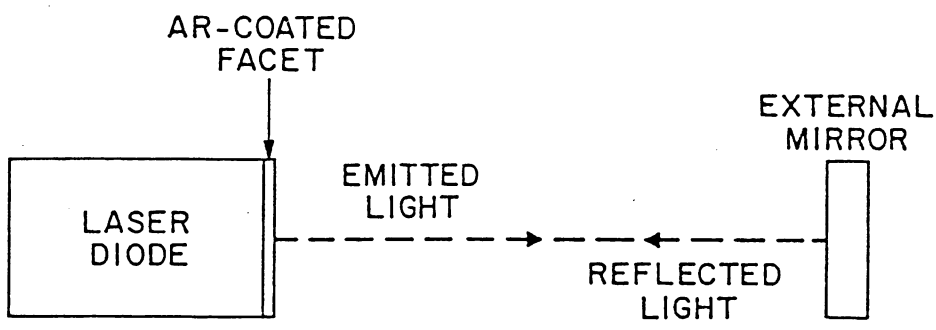


図2．外部反射体を用いた光帰還法により線幅を狭窄化する方法の原理．

これらの欠点のうち，とくに系の不安定性をおさえるには2．1節と同様，負帰還制御を施すのがよい．この場合は制御帯域は少なくとも非制御時の発振スペクトル線幅の値と同程度必要である．しかし最近のレーザの線幅は10MHz以下のものが多くなってきているので，あまり広い制御帯域は必要にならず，負帰還制御が容易になった．その制御装置の代表例を図3に示す．周波数揺らぎの検出には2．1節でも述べた簡単な小型ファブリ・ペロー共振器の透過光を用いる．波長0.8$\mu$mのAlGaAsレーザの場合，制御により線幅は100kHzまで狭くなった．これは非制御時の1／50である．また，この図ではファブリ・ペロー共振器の反射光を用いたもう一つの負帰還制御回路により同時に発振スペクトル中心周波数も安定化している．このような負帰還制御により線幅は安定に狭窄された．

図3の制御装置では(2)式の$\Pi_n$の値によって決まる線幅狭窄の限界は約1kHzであるが，現在のところ，この値に達していない．それは制御装置の制御帯域が約20MHzであり，これは十分広くないので制御利得もまだ不十分であることによる．レーザの周波数応答特性も含めた回路解析によると，制御系の遅延時間が0.6ns以内になれば十分な制御帯域が確保でき，従って制御利得もより増加できて上記限界に達する．この遅延時間を実現するにはたとえばGaAsなどの高速ICを用いて制御増幅器を作り(この場合遅延時間は約0.2ns)，さらに制御ループの光路長，電気長を12cm以内(遅延時間は0.4ns)にすればよい．こうすれば光集積回路などを用いた制御系の集積化などに頼る事なく，現在入手しうる光学，電気要素の組合せで図2の方法よりも狭い線幅が実現しうる．さらに図3のファブリ・ペロー共振器の周波数弁別感度の最適化により(2)式の$\Pi_n$によって決まる線幅狭窄化の限界は約1Hzという小さな値になる[21]．制御帯域を広げるためにはレーザそのものの周波数応答特性も重要で，特にその位相遅れが均一である方が有利である．最近はそれを実現するためにレーザの電極を2つに分割し，各々に流す直流電流値を調節することにより位相遅れ特性を改良する試みがなされている[22]．この電気的な負帰還制御の問題点はやはり制御帯域が有限なことである．従って，制御帯域外，すなわちレーザ発振スペクトルの裾を構成す

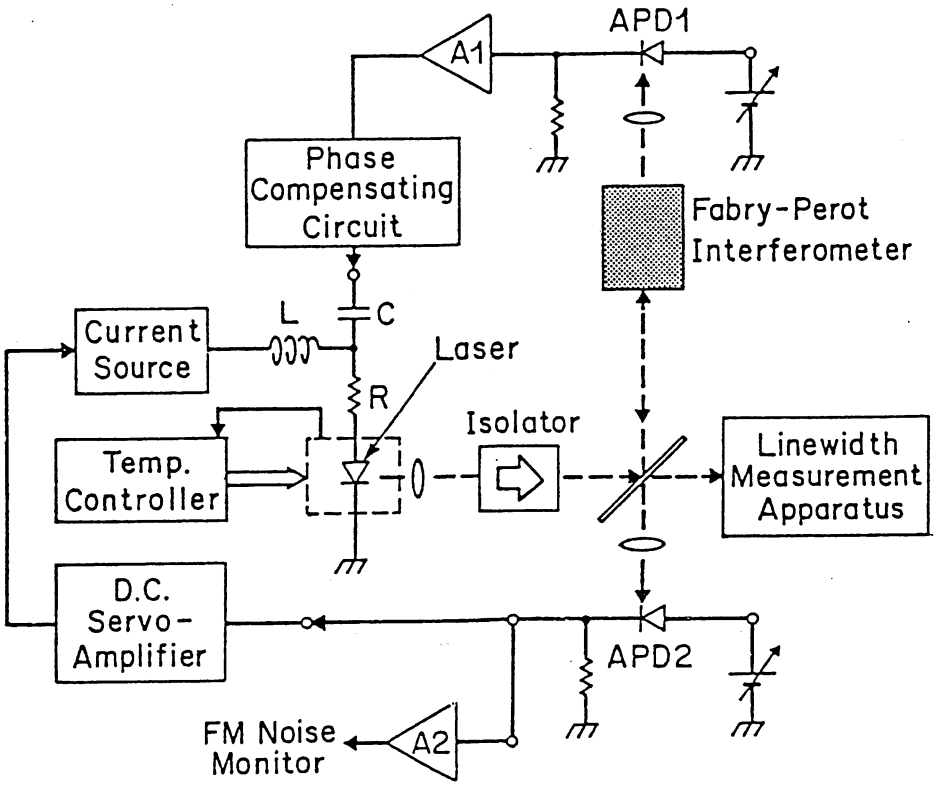


図3．電気的負帰還制御法の実験装置．

る周波数揺らぎは抑圧されない．そこで図２の光帰還の方法と図３の電気的負帰還の方法とその利点を生かした複合法を採用するのがよい．その例として図４に示すように外部ファブリ・ペロー共振器からのわずかな量の戻り光をレーザに再注入して(2)式の$x$の値を減少させ，同時にレーザとファブリ・ペロー共振器との距離を電気的に負帰還制御して系の安定性を保つ方法が提案された[23]．これにより比較的安定に線幅20kHzが実現した．また，戻り光量が少ないので縦モード周波数間隔はレーザ単体のままに保たれており，単一モード性は失われない．さらにレーザの電流をファブリ・ペロー共振器の自由スペクトル域の値の有理数倍の値の周波数で変調するとレーザ周波数は変調される[24]，などの利点を有する．

### ２．３．周波数の精密な追随

ヘテロダイン形の光計測では周波数の安定な主レーザに従レーザの周波数を高精度で追随させることが必要である．このためには従来注入同期現象が利用されていた[25]．これは非線形光学効果にもとづく現象なので物理的には興味深いが安定性などの点で実用上問題がある．

図５はそれに変わるもので，マイクロ波におけるヘテロダイン形位相同期ループに対応するものである．すなわち，主，従レーザのヘテロダイン信号の位相が局部発振器であるマイクロ波シンセサイザの位相に同期するよう従レーザの注入電流を制御するものである[26]．ここで主レーザとしては２．１節および２．２節で示したように周波数安定度を向上させたレーザを用いればよい．この位相同期法のキャプチャ・レンジは約1.2GHzであった．また，ヘテロダイン信号周波数の安定度として１×$10^{-14}$が得られている．この安定度は２．１節で示した主レーザの発振スペクトル中心周波数の安定度よりよい．このことは従レーザの周波数は主レーザのそれに忠実に追随していること，言い替えれば主レーザの高安定性が従レーザに移乗していることを意味する．このことから良質の光トラッキング・ジェネレータが実現していることが確認される．周波数追随の制御帯域を広げ，利得を増加させることによりヘテロダイン信号の位相揺らぎを１ラジアン以下にするような位相同期ループを構成することが原理的に可能である．さらにこのように位相同期の成立するレーザを多数用意し，それら全てのレーザ光を重ね合わせると，これはモード同期レーザからの光と同じ特性を示す．すなわち，非線形光学効果を使わずにフェムト秒程度の超短光パルス発生が可能である．

### ２．４．安定な周波数掃引

周波数を安定に，かつ広帯域に掃引することは分光計測などには必須である．たとえば図２で示した光帰還法において，外部反射鏡のかわりに回折格子を使い，その面を回転させると周波数掃引が可能になる．波長1.5$\mu$mのInGaAsPレーザではこの方法により67GHz(波長に換算すると0.5nm)にわたり周波数掃引された例がある[27]．しかしこの場合には周波数の安定度として２．１節で示した値は得られておらず，きわめて荒っぽい掃引で

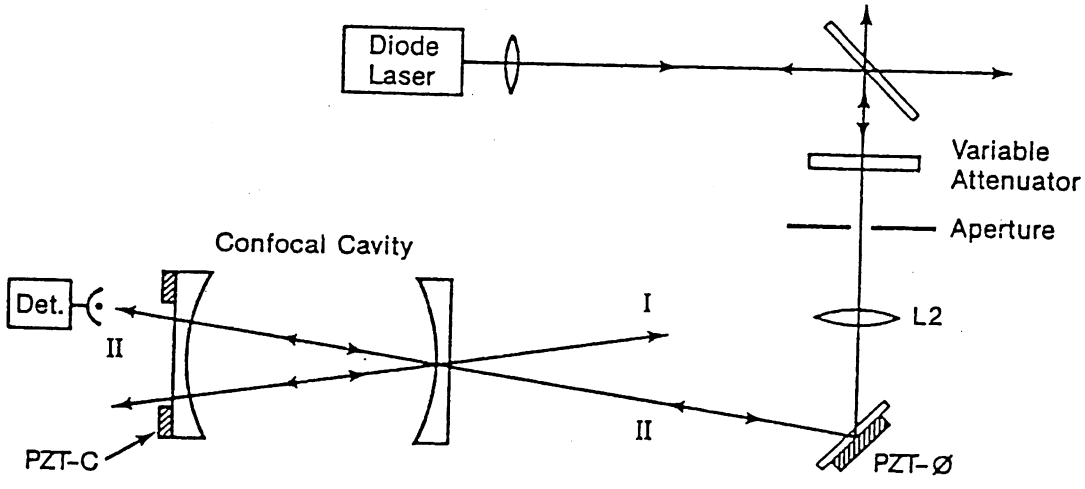


図４．外部共焦点ファブリ・ペロー共振器からの光帰還による線幅狭窄化の実験装置[23]．

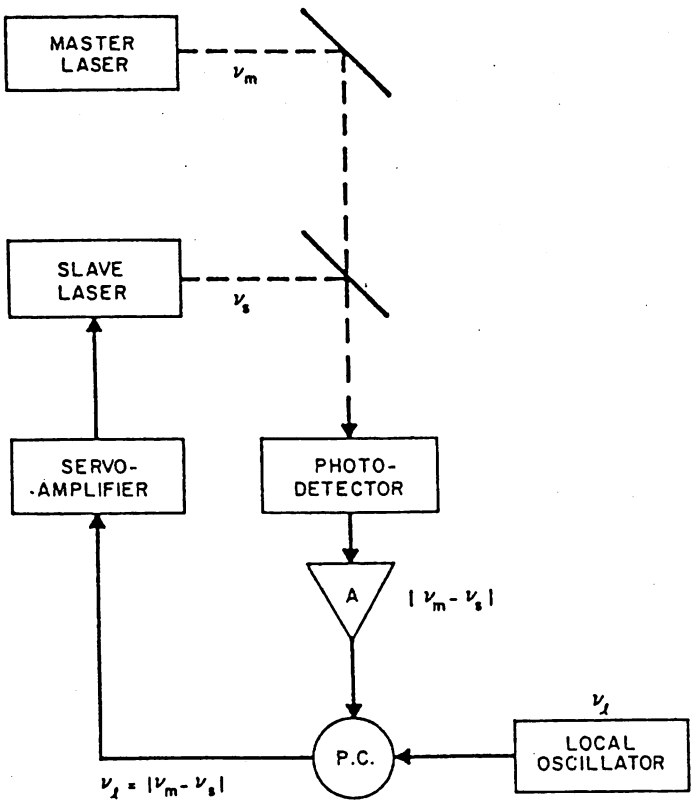


図5．周波数追随の原理[26]．P.C.：位相比較器．$\nu_m$，$\nu_s$，$\nu_l$，は各々主レーザ，従レーザ，マイクロ波シンセサイザの周波数．

ある．従って，掃引中の周波数の校正もされていない．周波数掃引をより高精度に行うには2．4節の光位相同期の系を用い，局部発振器としてのマイクロ波シンセサイザ周波数を掃引すればよい．これにより2．3節で示した安定度を保ったまま53GHzの範囲にわたって連続掃引された[26]．この場合，掃引可能範囲はレーザのモードホッピング特性により制限されている．従って，モードホッピングのない単一モードレーザを使えば[28]，原理的には1THzの範囲にわたって周波数連続掃引可能である．

## 3．半導体レーザの周波数制御のための問題点

光計測システムへの応用のために2節で述べたような周波数制御をする際，半導体レーザデバイスに関連した問題点を挙げるとつぎのようになろう．

### (1)縦モードの単一性

今までは半導体レーザが単一縦モード発振するという仮定のもとに議論を進めてきた．しかし，DFB形のように注意深く作られた単一モードレーザでも自然放出光揺らぎの混入により従モードが過渡的に発振し，このモードとの非線形モード結合により主モードパワーが過渡的に減少するパワー・ドロップアウトが見られる[29,30]．ドロップアウトの深さは10%～60%，持続時間は数μs～数nsであり，これらはバイアス電流に依存する．従って，このような時間範囲内では主モードの単一モード性は保証されない．使用する光計測システムの特性にもよるが，このドロップアウトを抑えるには主モード，従モードのパワーの時間平均値の比が40dB以上必要である[29,30]．デバイス試作段階ではこのような高パワー比をもったレーザは得られるが，このようなデバイスは実用的な光計測システムにはまだ十分安定に供給されていない．このようなドロップアウトが起こる一要因として，レーザの発振利得スペクトル幅にくらべ縦モード間隔が狭すぎ，隣合う縦モード間の利得差が少ないことが挙げられる．

例えば波長0.8μmのAlGaAsレーザの場合，発振利得スペクトル幅，縦モード間隔は波長単位で表すと各々500Å，3Åである．

一方長さ15cmの単一モードHe-Neレーザではそれらは各々，1GHz，1GHzである．縦モード間

隔はレーザの長さに反比例するので，短いレーザのほうが単一縦モード性に優れているが，両レーザのこれらの数値を比較し，半導体レーザをそれと等価なHe-Neレーザに置き換えてみると，その長さはなんと25mにもなる．さらに，より詳しい議論をするとHe-Neレーザの縦モード間の結合は弱く，2つ以上の縦モードは同時に安定なパワーで発振しうるが，半導体レーザではその結合は強く，縦モード間でパワー・スイッチング現象を示す[31]．これを考慮すると半導体レーザは長さ約100mのHe-Neレーザに対応する．だれもこのような巨大なレーザは使いたくないので，今後単一モード性を改善するには縦モード間隔を大きくするか，発振利得スペクトルを狭くすべきである．縦モード間隔を大きくするにはレーザ長を短くすればよいが，パワー低下，周波数揺らぎ増加を引き起こすので不利である．むしろ量子井戸など[32]の新構造，さらには新材料を用いて発振利得スペクトルを狭くすべきである．

(2) 周波数の長期シフト

半導体レーザの周囲温度揺らぎを$10^{-5}$℃以内，さらに注入電流揺らぎを0.6nA／$\sqrt{\text{Hz}}$以内に抑圧した超高安定環境下で約6カ月の長期にわたり周波数のドリフトを測定すると，約20MHz／hのブルーシフトが見られる[33]．これはInボンディング層の酸化による熱抵抗の変化，レーザ端面付近でのキャリヤの非放射再結合による熱効果などによると言われている[34]．光計測では発振周波数，波長の絶対値の再現性に対する要求が今後一層強くなると考えられるので，このような再現性，すなわちスペクトル寿命を向上させるためにデバイス設計製作の段階での熱抵抗の低減，スクリーニングなどの配慮が必要である．

(3) 半導体レーザ装置の寸法

(1)では縦モードの単一性の面から半導体レーザ素子の等価的寸法がまだ非常に大きいことを指摘した．さらに指摘すべきことは，半導体レーザ素子の実際の寸法が小さい(長さ数100$\mu$m)ので(2)式の$x$の値が大きく，従って周波数揺らぎが大きいために，その揺らぎを抑えるには図2，3のような外付け光電回路が必要となり，結果的には半導体レーザ装置全体の寸法はHe－Neレーザ装置程度の大型になってしまうということである．装置全体を小型化するには外付け回路の集積化のみでなく，広帯域の位相変調器の開発，さらにより重要な課題として周波数制御利得の高い半導体レーザを実現することが必要である．すなわち，2．2節でも述べたように電極を分割するなどして周波数変調効率が高く，その位相遅れ特性の均一なレーザの開発が望まれる．

## 4．あとがき

本稿ではまず半導体レーザは原理的にきわめて周波数安定度の高い光源となりうる可能性を理論的に示し，さらに4項目に関しその実験結果を示した．これらの実験結果により現在のところ簡易形の気体レーザなみの性能が得られていることがわかる．一方，半導体レーザデバイスそのものに注目すると，いくつかの問題があり，周波数安定性の点ではまだ不十分な段階である．これらの問題を克服し，より信頼性の高い周波数安定半導体レーザを実現するためには新デバイス設計，周辺デバイスの高性能・集積化，制御法の改良，などを有機的に行う必要があろう．このような技術の積み上げのもとに光センサシステム用の実用的な光源が実現することを期待したい．

## 参考文献


1) J.L.Hall : US-Japan Seminar, Quantum Mechanical Aspects of Quantum Electronics, July 1987, Monterey, CA, Paper III-4

2) M.Ohtsu, K.Kuboki, N.Tabuchi : Sixth International Congerence on Integrated Optics and Optical Fiber Communication, January 1987, Reno, Nevada, TUC5

3) 大津元一：「レーザーと原子時計」，1986年，オーム社，第6章

4) 大越孝敬編：「光ファイバセンサ」，1986年，オーム社，第3章

5) 応用物理学会編：「半導体レーザの基礎」，1987年，オーム社，第2章

6) M.Ohtsu : IEEE J.Lightwave Technology, January 1988, in press

7) M.Ohtsu and T.Tako : Progress in Optics, 25,

Elsevier, Amsterdam, 1988
8) P.Kartaschoff : Frequency and Time, Academic Press, London, 1978
9) K.Kuboki, M.Ohtsu, N.Tabuchi, and Ouchi : Proceedings of SPIE (The International Society for Optical Engineering) Vol.723, Progress in Semiconductor Laser Diodes, September 1986, Cambridge, MA, 73
10) H.Tsuchida, M.Ohtsu, and T.Tako : Jpn, J.Appl, Phys., 21(1982) L1
11) M.Ohtsu, H.Kotani, and H.Tagawa : Jpn, J.Appl, Phys., 22(1983) 1553
12) H. Tsuchida, M. Ohtsu, T. Tako, N. Kuramochi, and N. Oura : Jpn, J.Appl, Phys., 21 (1982) 1561
13) M. Ohtsu, H. Fukada, T. Tako, and H. Tsuchida : Jpn, J. Appl, Phys., 22 (1983) 1157
14) G.C.Bjorklund : Opt, Lett., 5 (1980) 15
15) 吉田浩之，橋本実，大津元一：第48回応物学会学術講演予稿，1987年10月，17a-ZC-2
16) K.Fukuoka, M.Ohtsu, and T.Tako : Jpn, J.Appl, Phys., 23 (1984) L117
17) R.Wyatt and W.J.Devlin : Electron. Lett., 19 (1983) 110
18) F.Favre, D.Le Guen, and J.C.Simon : IEEE J.Quantum Electron., QE-18 (1982) 1712
19) T.Fujita, J.Ohya, K.Matsuda, M.Ishino, H.Sato and H.Serizawa : Electron, Lett., 21 (1985) 374
20) N.A.Olsson and J.P.van der Ziel : IEEE J, Lightwave Technol., LT-5 (1987) 509
21) M.Ohtsu : Technical Digest of Conference on Lasers and Electro-Optics, June 1986, San Francisco, CA, WB4
22) H.Yasaka, Y.Yoshikuni, Y.Nakano, and K.Oe : Electron. Lett., 23 (1987) 1161
23) B.Dahmani, L.Hollberg, and R.Drullinger : Opt, Lett., 12 (1987) 876
24) 大津元一：電子情報通信学会光量子エレクトロニクス研究会技術報告，1987年12月，OQE87-135
25) S.Kobayashi and T.Kimura : IEEE J.Quantum Electron., QE-18 (1982) 575
26) K.Kuboki and M.Ohtsu : IEEE J.Quantum Electron., QE-23 (1987) 388
27) K. H. Cameron, M. R. Mattews, T. G. Hodgkinson and W. J. Devlin : Technical Digest of Conference on Lasers and Electro-Optics, Baltimore, MA, 1985, TUC5
28) Y.Tohmori : Ph. D.Thesis, Tokyo Institute of Technology, Tokyo, Japan, March 1986
29) R. Linke, B. L. Kasper, C. A. Burrus, I. P. Kaminov, J. S. Ko, and T. P. Lee : IEEE J. Lightwave Technol., LT-3 (1985) 711
30) 大津元一：電子情報通信学会光量子エレクトロニクス研究会技術報告，1987年12月，OQE87-136
31) M.Ohtsu, Y.Teramachi, Y.Otsuka, and A.Osaki : IEEE J.Quantum Electron., QE-22 (1986) 535
32) R.Chin, N.Holonyak, Jr. and B.A.Vojak : Appl, Phys, Lett., 36 (1980) 19
33) M.Ohtsu, M.Hashimoto, and H.Ozawa : Proceedings of the 39th Annual Frequency Control Symposium, May 1985, Philadelphia, PA, p.43
34) F.Farve and D.Le Guen : Electron, Lett., 19 (1983) 663

〔著 者 紹 介〕

大津元一(おおつ もといち)
昭48年東工大電子卒．昭53同大学大学院博士課程終了．同年東工大助手．昭57年同大助教授．現在に至る．この間，昭61年～62年米国AT＆Tベル研究所研究員．工学博士．

# 1. 電流負帰還半導体レーザのスペクトル特性

大津元一
(おおつ　もといち)
東京工業大学総合理工学研究科助教授

## 周波数の安定度

以前から、レーザは非常にきれいな波で、その周波数は一定値をとり、あまり乱れないといわれてきました。その特性を使って、コヒーレント光通信や、コヒーレント光計測などに利用されるようになりました。光の場合、周波数は$10^{14}$Hzくらいですが、その周波数がたいへん高く、かつ、きれいな波である特徴を利用する応用が活発になっています。

図1は、世界のトップデータとして、もっとも高性能のレーザでどの程度周波数が安定しているかをまとめたものです。横軸は年号で、縦軸はレーザの周波数に対する揺らぎの割合($\sigma$)を対数で表しています。1960年、レーザの発明当初は、周波数安定度は$1\times10^{-7}$ほどで、約10MHzの変動がありました。ちなみに、このレーザを発振器とした腕時計を作ると、1秒狂うのにちょうど1年かかることになります。それが、現在のトップレベルのレーザでは周波数安定度が$1\times10^{-16}$となり、揺らぎはわずか0.01Hzです。この場合の時計は、1秒狂うのに10億年も必要となり、非常に高性能となっています。

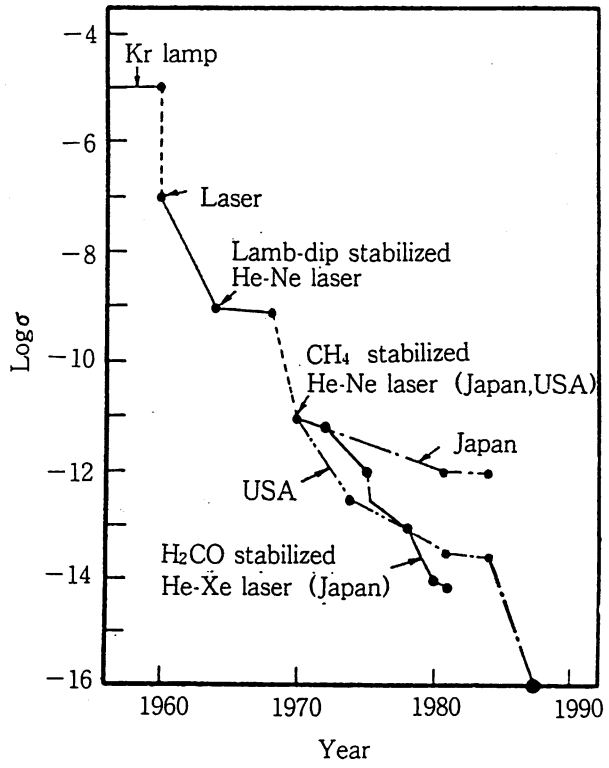


図1　レーザの周波数安定度向上の様子

ところで、図1のカーブには凹凸がありますが、ほぼ10年ごとに約5桁の割合で進歩していることがわかります。昨年の専門家会議の技術予測によると、21世紀に向かって特に大きな技術の壁にあたることなく、さらに2桁、つまり周波数安定度は$1\times10^{-18}$〜$1\times10^{-21}$が達成できるといわれています。その場合、その用途は重力波の検出や、情報量の大きいコヒーレント光通信などになると思われます。

このように、頭うちのない技術の進歩がみられたのは、レーザ発振のメカニズムに対する基礎的な学問や、エンジニアリング的手法の自動制御が進歩したためです。このことを別にしても、レー

ザ発明後、その性能が30年間近く進歩し続けた技術分野は、他にあまり例をみないと思います。

ではなぜ、このような高性能が次々と達成されたのでしょうか。このことについて、半導体レーザの場合で考えてみることにします。

## 自然放出揺らぎ

まず、レーザのある時間tにおける周波数の揺らぎ$\delta\nu(t)$は、何に起因するのでしょうか。それはレーザの量子力学的な発振原理に基づいています。つまり、自然放出という周波数がランダムに変化する光の影響をうけて揺らぎます(自然放出光揺らぎ$\Gamma_s$)。また、活性層のなかの電子密度、キャリア密度が時間的に変動する効果もあります(キャリア密度揺らぎ$\Gamma_c$)。その二つの効果に、レーザ共振器性能の大きさ、つまり共振器の損失を表す$\varkappa$が、レーザの周波数揺らぎを誘発する原因になっています。

そのため、なんらかの制御を加えなければ、レーザ発明当時の性能しか発揮できません。しかし、私たちはエンジニアリングの有力な方法として、自動制御という人為的に制御を施す技術をしっています。そこで、周波数の揺らぎを抑圧する方法を次に考えてみることにします。

抑圧の効果は、次式で表されます。

$$\delta\nu(t)=\varkappa[\Gamma_s(t)+\Gamma_c(t)]-\int_0^\infty h(\tau)\{\delta\nu(t-\tau)+\Gamma_n(\tau)\}\,d\tau \cdots\cdots(1)$$

この(1)式の積分記題のなかで、$\delta\nu(t-\tau)$は、自動制御をレーザに施したことにより、検出される周波数揺らぎの測定量です。$\Gamma_n(\tau)$は制御系で発生する雑音の大きさを表し、$h(\tau)$は制御系のインパルス応答で、制御系の利得のようなものです。そして、積分記号の前にマイナス記号がはいっていることは、自動制御の効果により、固有の揺らぎ$\Gamma_s$、$\Gamma_n$が抑圧されることを表しています。

(1)式をフーリエ変換して整理すると、次式のようになります。

$$F(f)=\frac{\varkappa\Pi_s(f)}{1+H(f)}+\frac{\varkappa\Pi_c(f)}{1+H(f)}-\frac{H(f)}{1+H(f)}\cdot\Pi_n(f) \cdots\cdots(2)$$

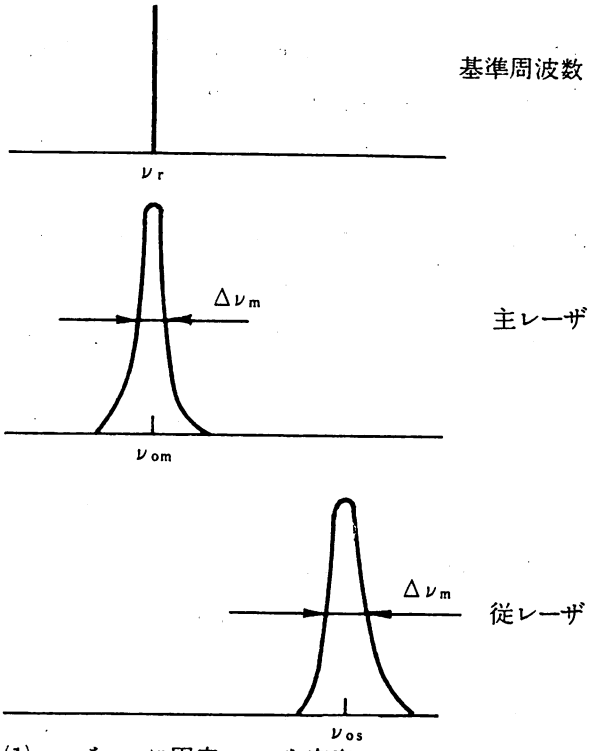


(1) $\nu_{om}$ を $\nu_r$ に固定、$\nu_{om}$ を安定に
(2) $\Delta\nu_m$ を小さく
(3) $\nu_{os}$、$\Delta\nu_s$ を $\nu_{om}$、$\Delta\nu_m$ に追随
(4) $\nu_{os}$： 高精度掃引

**図2 レーザの時間的コヒーレンス向上のための四つの課題**

ここでF、$\Pi_s$、$\Pi_c$、$\Pi_n$、Hはそれぞれ(1)式の$\delta\nu$、$\Gamma_s$、$\Gamma_c$、$\Gamma_n$、hのフーリエ変換を表します。

まず第1に、自然放出揺らぎ、キャリア密度揺らぎの効果は、(2)式の右辺の第1、2項で表されるように、分母に制御の利得(H)がはいってきます。したがって、非常に大きい利得をもつ制御系を使うと、レーザ固有の雑音の大きさをゼロにすることができます。最終的に残るのは第3項です。つまり、制御ループの雑音の大きさがはいっており、その係数として分母、分子に制御の利得の効果がはいっています。そのため、利得を大きくすると、(2)式第3項の値は制御系の雑音自体によってきまることになります。

いいかえれば、レーザ固有の量子力学的な雑音の揺らぎの源は、レーザの周波数を揺るがせる本質的な原因にはなっていなくて、制御を施せば周波数の揺らぎを小さくすることができるわけです。原則的には、制御系の性能によりきまる雑音の大きさまで小さくできます。つまり、利得の非常に

大きく、雑音が非常に小さい高質の制御系を使えば、レーザ本来のもつ量子力学的な揺らぎ以下の高コヒーレントなレーザができることになります。このことが、過去27年間にわたって周波数の揺らぎの大きさが$1\times10^{-7}$から$1\times10^{-16}$へと進歩した、物理的な基礎となっています。

ただし、このような原理に基づきレーザの時間的コヒーレンスを向上させようとすると、いくつかの課題があります。それは、どのように応用するかによっても異なってきますが、図2に示すように次の4点に大別できます。

第1に、基準となる周波数($\nu_r$)をきめ、それに開発しようとしているレーザの発振スペクトルの発振周波数($\nu_{om}$)を絶えず固定させることです。つまり、レーザの中心周波数($\nu_{om}$)を安定させて使いやすくするわけです。

第2に、光の波のきれいさを表すスペクトル線幅を、できるだけ狭くすることです。ただし、周波数が固定されたきれいな波のレーザであるだけでは周波数が可変でないので、かならずしも使いやすくありません。そこで、使いやすいレーザを開発するには、従レーザの周波数やスペクトル線幅を主レーザに追随させることが必要です。これが第3の課題です。

第4に、従レーザを主レーザの性能と同じ程度に保ったまま、周波数を広帯域に掃引することです。これにより応用上、周波数の多重通信やセンシングなどに使い勝手のよい光源ができると思います。

ただし、以上の4課題を別々に解決していたのではよいレーザがえられないため、ある程度系統的なシステムを組んで、それらを同時に解決するほうが有利になります。そのことを図3で示します。それは、主レーザについて第1、第2の課題が(1)(2)のブロックのなかのシステムで解決され、従レーザに対して、第3、第4の課題が(3)(4)のブロックで解決されることを模式的に示しています。これらの(1)から(4)までの個々の実験結果と、理論的な限界を表1に示します。

## 基準周波数による制御

最初の課題は、主レーザの中心周波数の揺らぎを適当な基準周波数値に固定することです。その方法は簡単で、自動制御の基本そのものです。つまり、レーザの揺らぎを適当な基準周波数と比較することにより検出し、それに比例した信号をレーザの注入電流に負帰還して揺らぎを抑圧します。この注入電流を変化させると、半導体の温度やキ

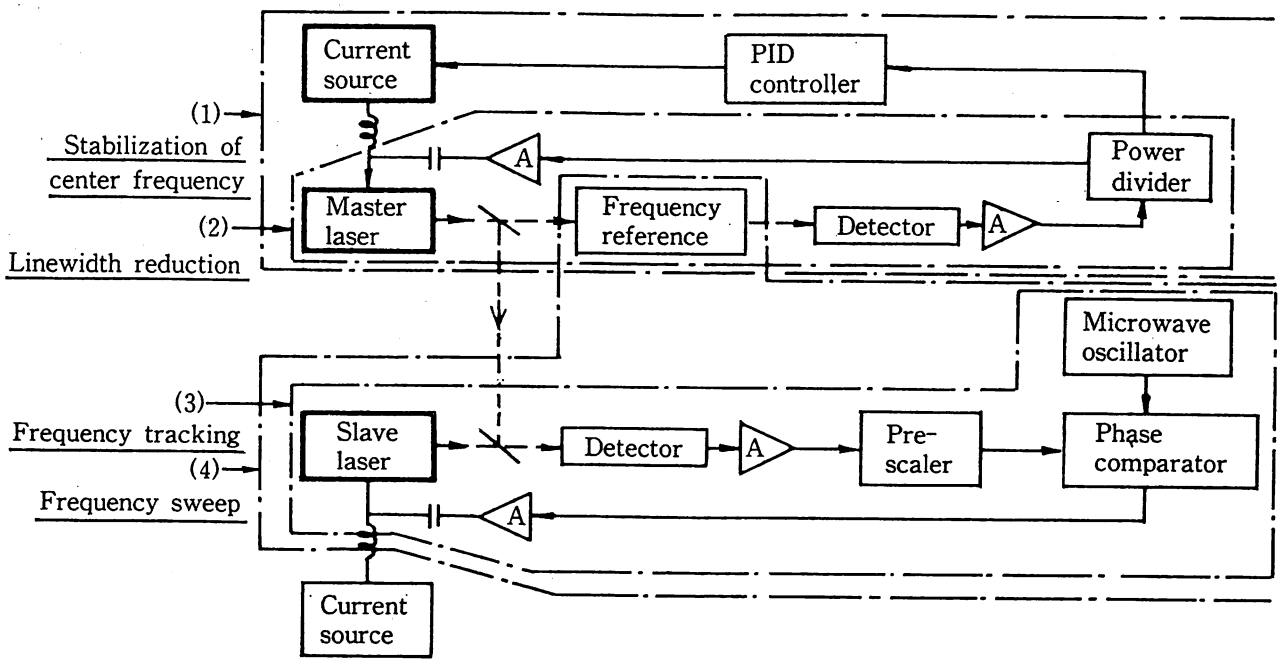


図3　四つの課題を同時に解決するための、電気的負帰還法による系統的システム

| | Experimental results | Theoretical limits |
|---|---|---|
| (1) Frequency stabilization | $2\times10^{-12}$ | $1\times10^{-15}$ (at $\tau=100$s) |
| (2) Linewidth reduction | 0.9kHz | 1Hz |
| (3) Frequency tracking | $1\times10^{-14}$ | $2.7\times10^{-16}$ (at $\tau=100$s) |
| (4) Frequency sweep | 53.4GHz | 1THz |

**表1　四つの課題の実験結果と理論的限界**

ヤリア密度などが変化して、周波数がかわります。このようにすることで、周波数が制御できます。

問題は、基準周波数です。半導体レーザの波長は約0.7～1.6$\mu$mです。現在私たちがみいだしている高性能の周波数基準は、アンモニアや水蒸気、炭酸ガス、それ以外の有機気体や金属蒸気の吸収スペクトルです。アンモニアは約10GHzの周波数間隔で、この波長帯に非常に多くの吸収線が分布し、これらの波長が有効数字8桁くらいで測定されており、基準周波数として使われています(表2)。より簡便な例として、ファブリ・ペロー干渉計といわれる光学素子のもつ共振周波数を基準に使うこともできます。

| | No. | Wavelength in the air (pm) | Wavelength in vacuum (pm) |
|---|---|---|---|
| ($NH_3$) | 1. | 1496315.8±0.8 | 1496311.1±0.8 |
| | 2. | 1498610.7±0.7 | 1498605.9±0.7 |
| | 3. | 1498713.4±0.4 | 1498708.6±0.4 |
| | 4. | 1498743.3±0.4 | 1498738.5±0.4 |
| | 5. | 1498802.8±0.8 | 1498798.0±0.8 |
| | 6. | 1503013.7±0.6 | 1503008.9±0.6 |
| | 7. | 1503032.6±1.0 | 1503027.8±1.0 |
| | 8. | 1503051.9±1.2 | 1503047.1±1.2 |
| | 9. | 1503084.9±0.9 | 1503080.1±0.9 |
| | 10. | 1503097.1±0.8 | 1503092.3±0.8 |
| | 11. | 1503125.1±0.8 | 1503120.3±0.8 |
| | 12. | 1503137.3±0.5 | 1503132.5±0.5 |
| | 13. | 1503195.6±1.3 | 1503190.8±1.3 |
| | 14. | 1503200.5±1.6 | 1503195.7±1.6 |
| | 15. | 1503207.1±0.9 | 1503202.3±0.9 |
| | 16. | 1503226.7±1.0 | 1503221.9±1.0 |
| | 17. | 1503232.6±0.5 | 1503227.8±0.5 |
| | 18. | 1503342.6±0.9 | 1503337.8±0.9 |
| | 19. | 1503354.0±1.0 | 1503349.2±1.0 |
| | 20. | 1503431.7±0.7 | 1503426.9±0.7 |
| | 21. | 1503506.6±1.1 | 1503501.8±1.1 |
| ($H_2O$) | | 1496508.9±0.9 | 1496504.2±0.9 |

M. Ohtsu et al., Jpn. J. Appl. Phys., 22, 1983, p.1553

**表2　アンモニアおよび水の蒸気の吸収スペクトル波長**

半導体レーザ周波数がどの程度の揺らぎになっているかを、図4で示します。図の縦軸は揺らぎの大きさ$\sigma$、横軸は$\sigma$の値を測定するのに要した時間です。何の制御も与えないと、揺らぎは$A_1$、$B_1$、$C_1$、Dのように約$1\times10^{-8}$になります。したがって、1M～10MHz程度の周波数分だけ揺らいでいることになります。

それに対して、基準周波数を使って制御すると、横軸の値$\tau$にもよりますが、周期が100秒くらいのゆっくりした揺らぎは非常によく抑圧され、何も制御しないときの4桁から5桁くらい性能がよくなります。曲線$B_2$に示されるように$2\times10^{-12}$くらいの振幅の揺らぎに抑圧されています。

これ自体は制御系の雑音によりきまる値よりもかなり大きく、制御系の最適化などを行うと、理論的には3桁くらい、つまり曲線Gに示されるように、$10^{-15}$くらいの値がえられると予測されます。

## スペクトル線幅の制御

次に、レーザスペクトル線幅を狭くする話に移ります。スペクトル線幅の原因は、周波数の非常に速い周波数変動成分です。その成分を抑圧して、スペクトル線幅を狭くすることに関しては、先ほどよりも帯域の広い自動制御系が必要となっています。

5年くらい前まで、半導体レーザのスペクトル線幅は10M～100MHzという大きな値でした。それを狭くしようとすると、自動制御系としても制御帯域を100MHzと広くとる必要がありました。このような制御系の設計はむずかしいため、過去20年間ほどは簡便な方法がとられていました。そ

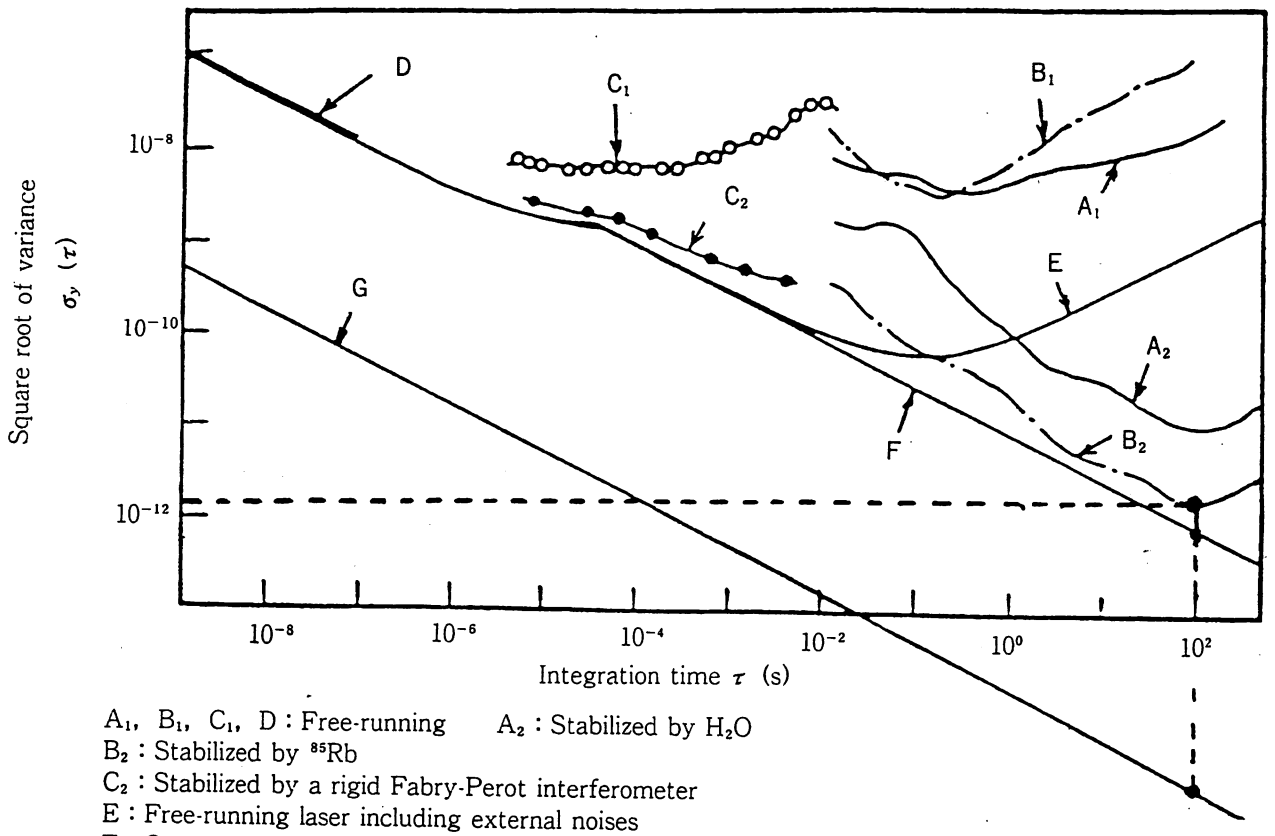


$A_1$, $B_1$, $C_1$, D : Free-running　　$A_2$ : Stabilized by $H_2O$
$B_2$ : Stabilized by $^{85}Rb$
$C_2$ : Stabilized by a rigid Fabry-Perot interferometer
E : Free-running laser including external noises
F : Quantum noises in free-running laser　G : Detector noise limited
(M. Ohtsu, et. al. : Jpn. J. Appl. Phys., 22 (1983) p.1157)

**図4　周波数安定化の実験結果**

れはレーザを自動制御するのではなく、共振器の損失($\kappa$)を小さくすることにより、自然放出光揺らぎが混入する割合を小さくしようという方法です。

原理的には簡単で、図5で示すようになっています。つまり、半導体レーザの両端面が光を反射する鏡になっていますが、そのうち一方の端面の反射率をゼロにするように適当な膜をぬっておきます。そして、レーザの長さよりも十分に離れた点に鏡をおきます。そのようにすると、光が鏡に反射するようになり、2枚の鏡の間が共振器となります。

こうすると、レーザと外部鏡により構成される共振器が非常に長くなるので、共振器の損失、つまり$\kappa$が小さくなり、線幅を狭くすることができます。ただし、この方法には主に三つの問題があります。まず第1は、構造的に不安定性をともなうことです。周囲の温度の影響や機械的振動により、スペクトル線幅が狭くなるのとは逆に、従来の10倍、100倍も広くなってしまいます。第2に、注入電流を変調しても、レーザの周波数には変調はかからなくなります。第3に、共振器が長くなることにより、単一縦モード性が本質的に失われる欠点があります。

したがって、このような方法は簡便で、チャンピオンデータとしては最小値10kHzという狭い幅がえられていますが、本質的には使えません。過去20年間はだましだまし使っていたわけです。

ところで最近では、デバイスそのものの性能が上がっており、何も制御しないでも線幅が約10MHzのレーザがえられるようになってきました。そのため、先ほどの自動制御系の帯域が狭くても十分働くことになり、安定性、信頼性の高い

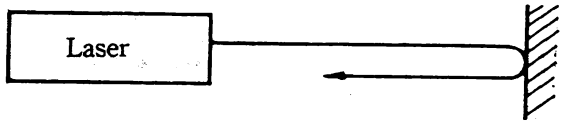


**図5　光帰還による方法の原理図**

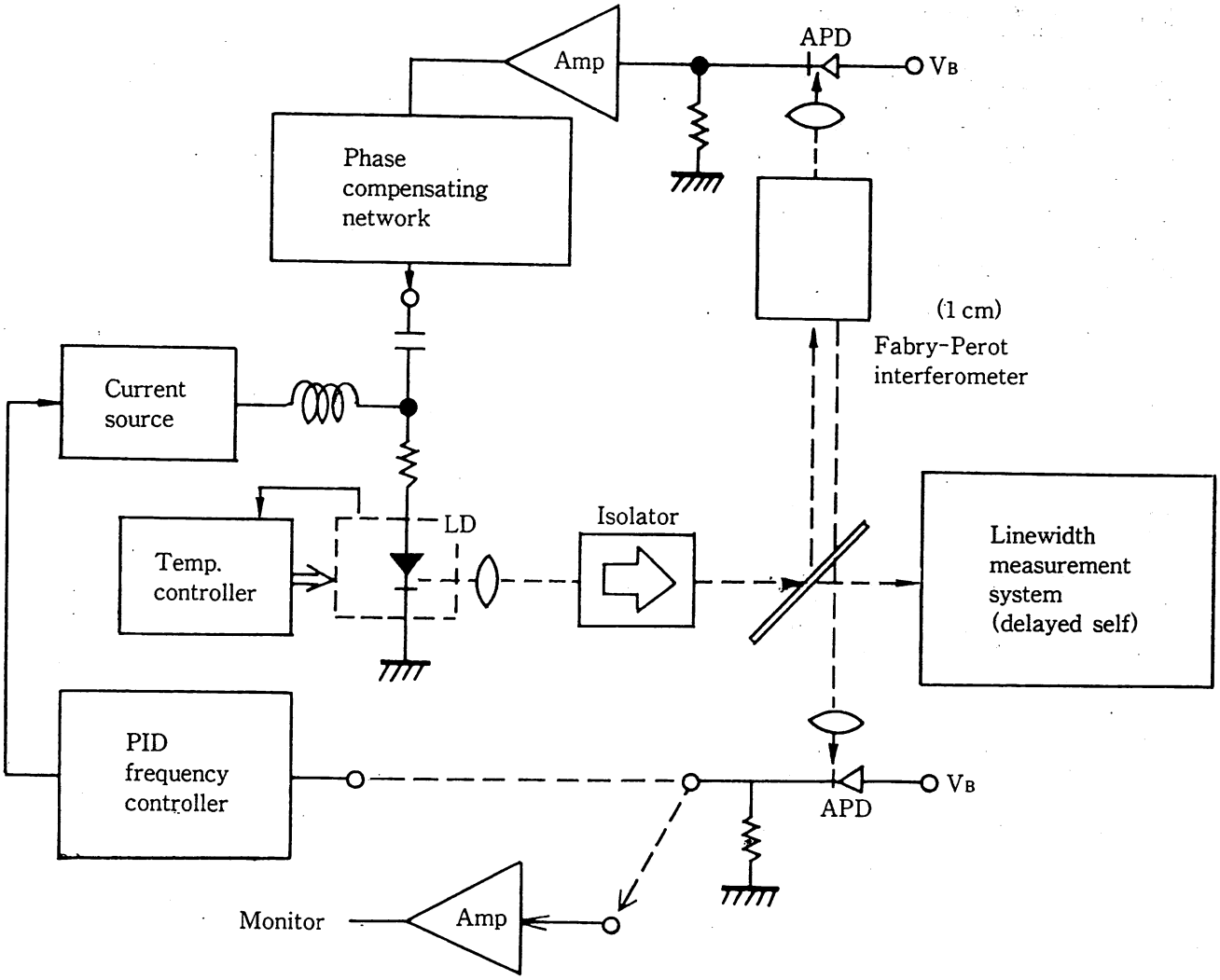


図6　線幅狭窄化のための実験装置

自動制御の手法がまた見直されてきたわけです。自動制御の方法でレーザの線幅を狭くする具体的な装置を図6に示します。これは第1の課題と本質的には同じですが、レーザの周波数揺らぎを、長さ1cmくらいの円柱でできた簡単なファブリ・ペロー干渉計という、光学素子を使って検出しています。周波数の揺らぎを検出したら、それに比例する電流をレーザに流して自動制御します。

ファブリ・ペロー干渉計については、横軸にレーザの周波数またはレーザの電流をとり、透過光の強度をモニターすると、図7で示す実線のようになります。図において、白丸の点周囲でレーザの周波数が変動すると透過光が変動し、揺らぎの検出ができます。自動制御を行わない状態では、レーザ発振スペクトルは図8(a)のような形状で、約10MHzくらいの線幅です。それを制御すると図8(b)のように狭くなります。

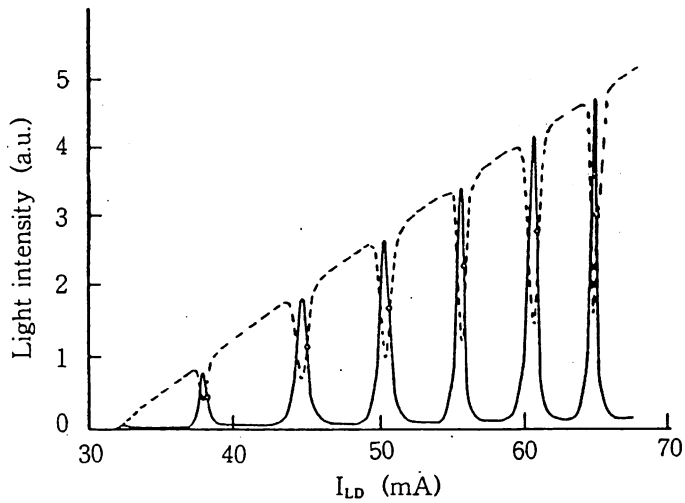


図7　ファブリ・ペロー干渉計の共振曲線

図9は、市販されている波長0.8$\mu$mのAlGaAsレーザに自動制御を施したときの線幅のデータです。何も制御しないと5MHzから20MHzくらいの値ですが、制御すると約100kHzとなり、制御

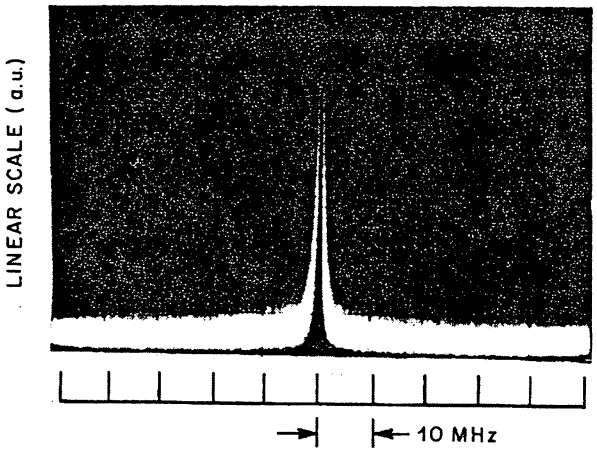


(a)フリーランニング時

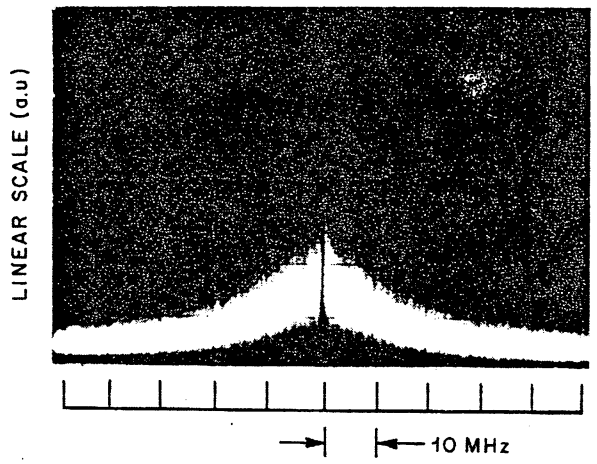


(b)制御時

図8　レーザの発振スペクトル

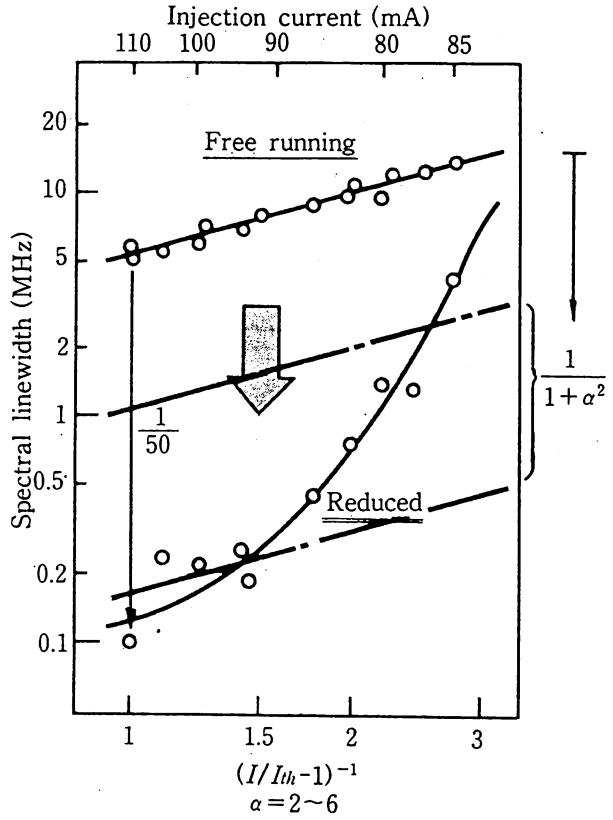


図9　スペクトル線幅と注入電流との関係

しないときの50分の1ほどの値がえられています。

図で示されている二つの1点鎖線は、レーザ固有の自然放出の揺らぎ源により生ずる、周波数揺らぎが与えるスペクトル線幅の範囲を表しています。この実験でえられた100kHzという値はこの範囲以下なので、このことは自然放出光揺らぎの原因はレーザの線幅をきめる根本的なものではなく、制御により線幅が狭くなることを示唆しています。

先ほどの実験では、中心周波数を安定することも同時に行いました。ファブリ・ペロー干渉計からの反射光を用いて、中心周波数を自動制御しているわけです(図6参照)。そのようにすると、スペクトルの中心周波数は安定し、制御もかなり容易になります。その結果、線幅は数日間にわたり安定して狭くなります。従来の光を戻す方法では働かないような不安定な周囲環境下でも、100kHzのスペクトル線幅がレーザを制御しているかぎり続くという、信頼性の高いシステムになっています。

1986年半ばまでの実験結果の進歩の様子を図10で示します。横軸が年代で、縦軸がスペクトル線幅です。制御しない10MHzから徐々に狭くなり、86年半ばの時点では60～80kHzくらいの値になっています。ただし、長さ1cmのファブリ・ペロー干渉計を使った現在のシステムでは、もっと性能が上がるはずで、1kHzくらいまで可能です。

現在60～80kHzにとどまっている理由は、制御系の帯域が広くないため、制御利得がかぎられていることに起因しています。つまり、可能であるべき1kHzが60～80kHzにとどまっているわけです。図11は、レーザの電流を変調したときに、周波数がどのように変調されるかを示すレーザのもつ周波数特性の例です。その他制御系の性能等を検討して、回路解析のようなことを行っていますが、その結論として、表3に示すように1kHzの線幅を現在の装置で実現するには、ループ内を信号が伝播する際の遅延時間が0.6ns以内であれば可能です。

実験では、シリコン系のアンプを使った自動制

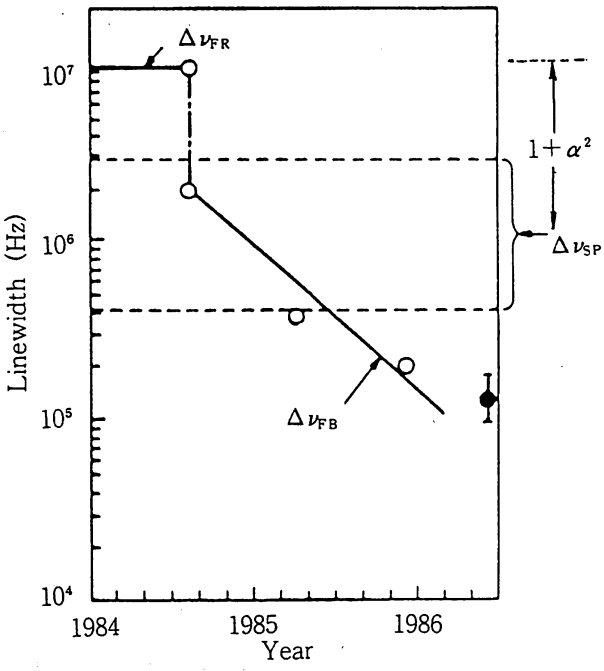


**図10　線幅狭窄化の実験結果の進歩の様子**
$\Delta\nu_{SP}$は自然放出光の揺らぎの大きさによってきまる線幅の値

御系を使っていますが、それをGaAs ICにかえて、遅延時間を0.2nsにします。また、フィードバックループの長さや、レーザから受光器の同軸ケーブルまでの長さを12cmほどに短くすると、光がそこを伝播する時間は0.4nsくらいになるので、全部で0.6nsくらいになります。このように現在の装置を使って1kHzくらいの値を実現する見通しがたてられてきました。

さらに極限的なデータをねらうには、簡便なファブリ・ペロー干渉計をもう少し高級にして、周波数の揺らぎを検出する感度をもう少し上げればよいということです。図12の横軸はファブリ・ペロー干渉計の共振曲線の幅、縦軸は制御しないときのレーザのスペクトルの線幅で、規格化した制御時のレーザのスペクトル線幅です。ファブリ・

| |
|---|
| Network analysis |
| ↓ Delay time $\tau d \leq 0.6$ns |
| ● 0.2ns : GaAs IC Servo-amplifier |
| ● 0.4ns : Optical & electrical path length $\leq$12cm |

**表3　線幅1 kHzを実現するために必要な条件**

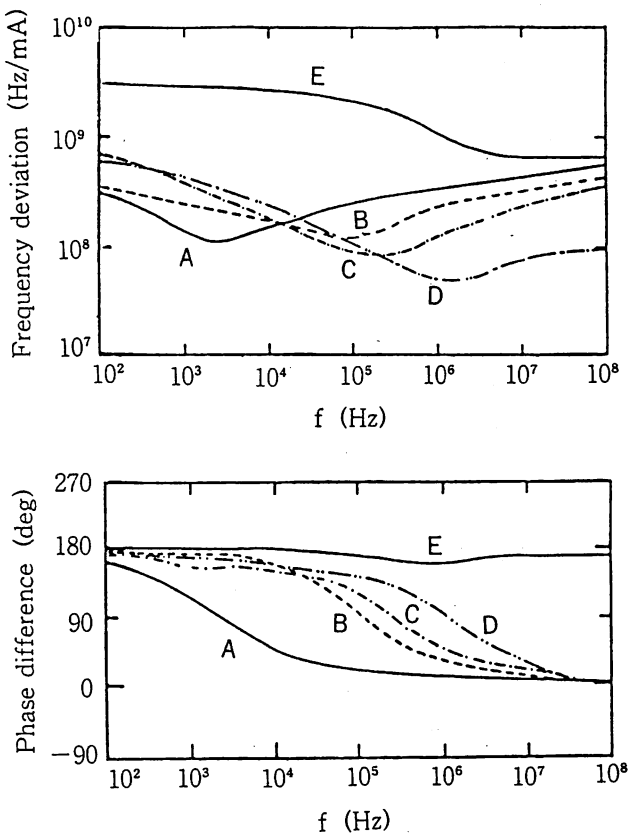


**図11　レーザの周波数変調特性の例**

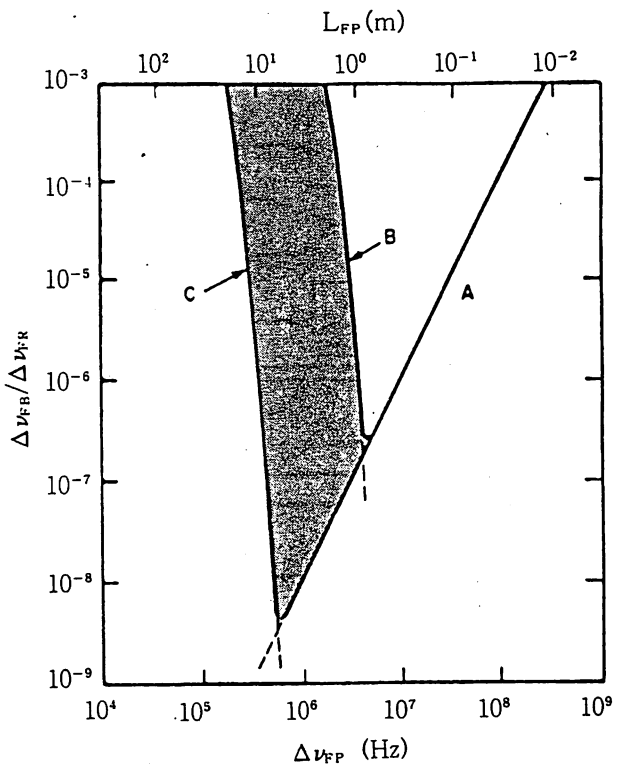


**図12　周波数揺らぎ検出用ファブリ・ペロー干渉計の共振曲線の幅$\Delta\nu_{FP}$に対する制御時、フリーランニング時のレーザスペクトル線幅$\Delta\nu_{FB}$、$\Delta\nu_{FR}$の比の値の計算結果**

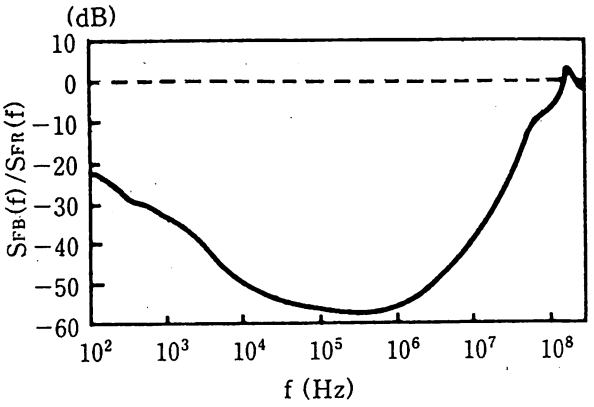


**図13　電流負帰還による周波数揺らぎのパワースペクトル密度の抑圧の様子**

ペロー干渉計の共振曲線の幅を狭くしていくと周波数揺らぎ検出感度が向上し、曲線Aのように線幅が狭くなることがわかります。しかし、ファブリ・ペロー干渉計は制御ループ内では一つのフィルタの役割を果たしており、感度を上げすぎるとフィルタの帯域が狭くなります。そうなると干渉計自体により制御ループの帯域が制限されます。したがって、図の横軸の値をあまり小さくしすぎると、線幅は逆に広がってしまう効果があり、それが曲線BとCで囲まれた領域です。したがって、性能としてはVの字形となります。その最小値は$10^{-6}$～$10^{-8}$くらい、すなわち1Hzくらいの値が実現可能です。

実際に1Hzは実現できないと思われる方も多いと思いますが、実は1986年半ばにえられた100kHzの値に比べるとかなり1Hzに近い値が、私たちの実験ですでに実現しています。

すなわち、最適化された高フィネスのファブリ・ペロー干渉計と普通のアンプ、市販されている0.8$\mu$mの半導体レーザを組み合わせると、図13に示すように制御時の周波数揺らぎのパワースペクトル密度の値は、制御しないときに比べて−57dBまで小さくなっています。つまり、線幅は6桁狭くなっています。これは線幅が約0.9kHzになっている状態です。これは1988年初頭にえられた世界最高の値です。

## 従レーザの追随性と周波数の掃引性

3番目は、主レーザとして、上記のような方法で

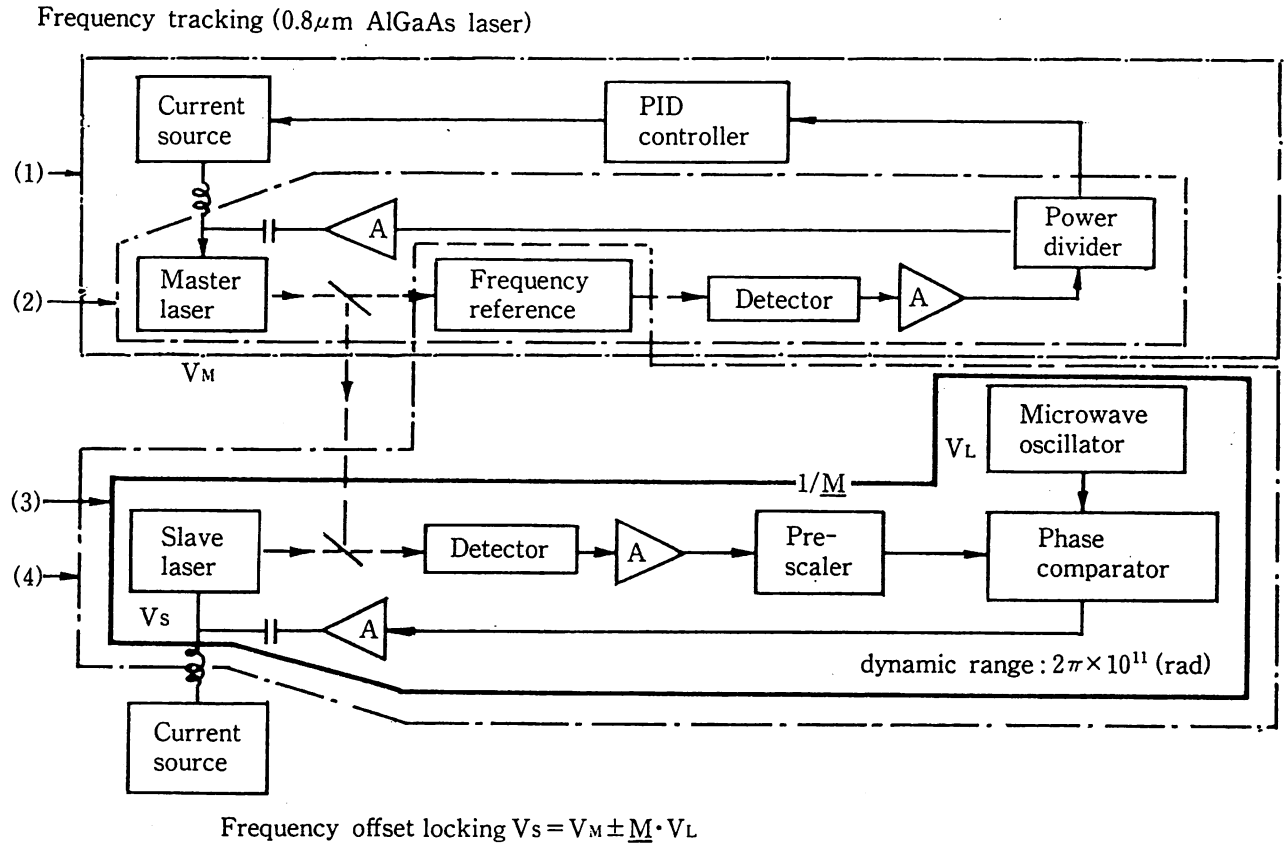


**図14　周波数追随の原理**

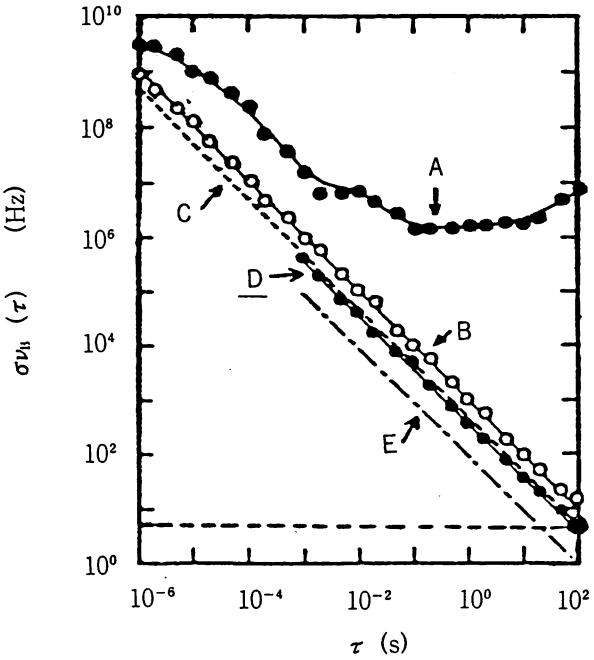


$\sigma$ : Square root of variance
$\tau$ : Integration time

$$\{\sigma_{yB}^2 << \sigma_{yM}^2\}$$

$$\sigma_{yS}^2 = \sigma_{yM}^2 + \sigma_{yB}^2 \cong \sigma_{yM}^2$$

Slave Master Beat Master

**図15　周波数追随時のビート周波数揺らぎの値**

高性能のレーザを開発したときに、従レーザの周波数を主レーザに追随させる話題についてお話しします。

これはマイクロ波などのネットワーク技術を使って、ある程度簡単にできます。具体的には、2台のレーザのビートの周波数をとり、それがマイクロ波局部発振器の周波数と一致するように従レーザの電流を制御するものです(図14)。これ自体は高性能位相制御系になっており、ビート周波数揺らぎを表す$\sigma$の値は、$\tau$=100秒で数Hzになり、追随精度は$1\times10^{-14}$です(図15)。

従レーザの揺らぎの大きさは、主レーザの揺らぎの大きさとビートの周波数の揺らぎの大きさの二つできまります。ビート周波数揺らぎのほうは$10^{-14}$となり、主レーザの周波数揺らぎの値$10^{-12}$に比べて2桁小さくなっているため、結局は従レーザと主レーザの揺らぎは同程度になっているといえます。いいかえると、非常に揺らぎの小さい主レーザに、従レーザの周波数が高精度に追随しているということです。

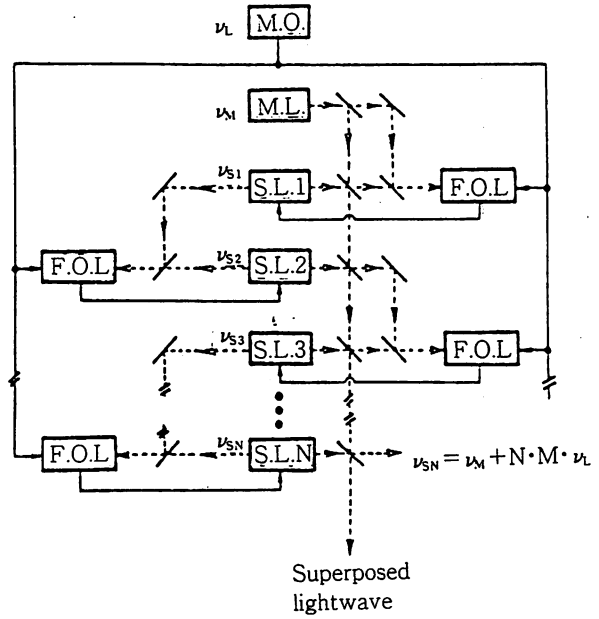


**図16　周波数追随の原理を利用した超短光パルス発生の原理**

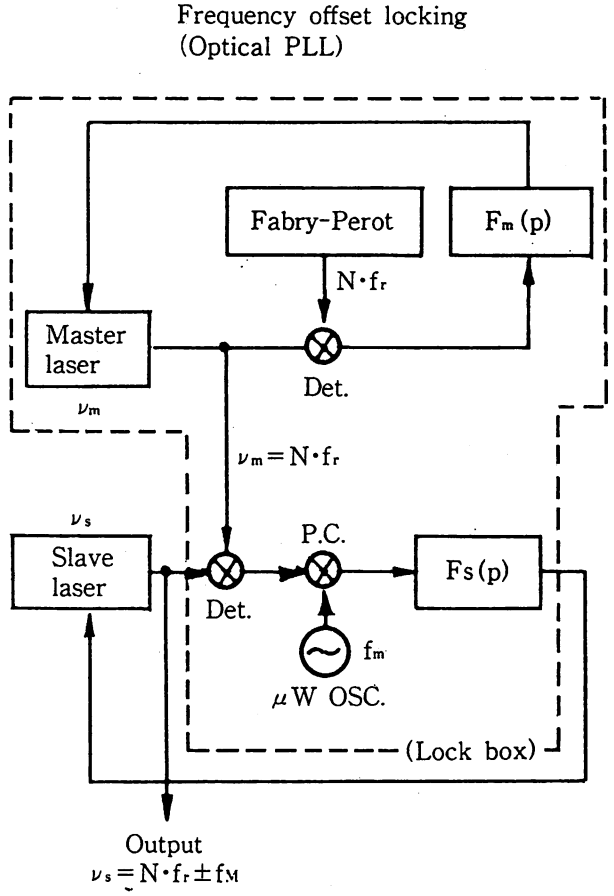


**図17　周波数掃引の原理**

余談ですが、このような主レーザと従レーザをいくつか用意して、発振器のチェーンを作って、すべてのレーザを重ねあわせると、モードロックレーザを使って作り出した光と等価になります(図16)。モードロックレーザは、非常に短い幅の

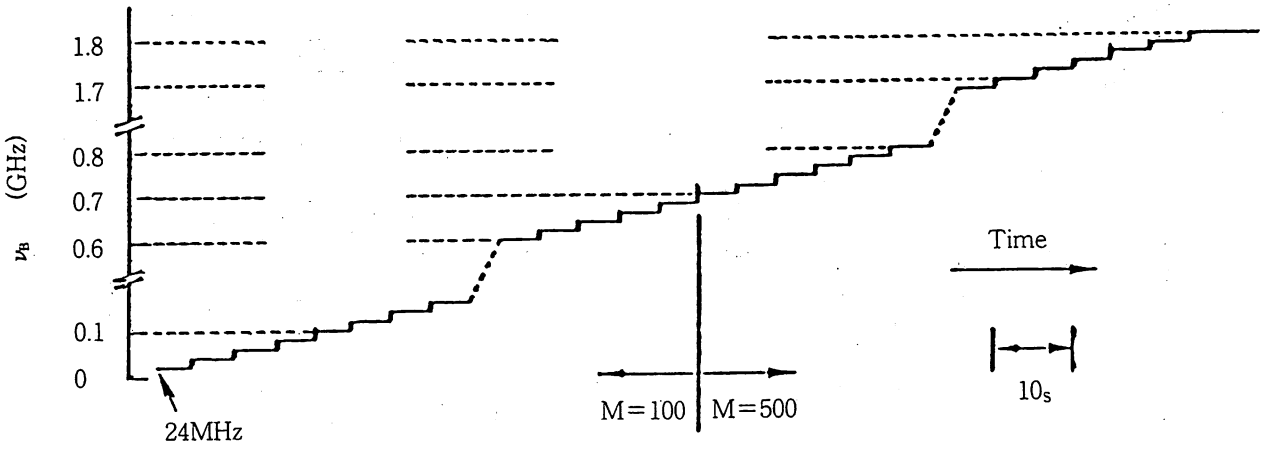


Lock range of the beat frequency : 1.78GHz
Frequency tunable range of the slave laser : 3.56GHz

**図18　周波数掃引の様子**

パルス、例えばフェムト秒のパルスを実現するのに、レーザのもつ非線形の効果を使っていたため、システムが複雑になっていますが、この方法ではそれに比べ線形な方法を使っているのでシステムが簡単です。

最後は、周波数の掃引についてです。原理的には先ほどと同一の技術が使えます。図17のように、主レーザと従レーザがあり、その間にマイクロ波の発振器を介して周波数を固定します。そして、マイクロ波の周波数を掃引すると、従レーザの周波数は主レーザのそれと同じくらいの揺らぎの少なさを保ったまま、マイクロ波の発振器と同じ程度の精度で周波数が可変になります。

例えば、コヒーレント光通信等で、一つの究極的な性能の周波数超多重通信などを行う場合、周波数のグリッドを作るときには、非常に再現性が高くなります。このマイクロ波の発振器を5秒おきにきざみ、幅20MHzくらいでかえていくと、2台のレーザのビート周波数が安定して掃引されます(図18)。連続掃引の幅は、現在約60GHzになっています。不連続でよければ、掃引可能な範囲はもっと広くなります。この範囲がその程度にとどまっている理由は、使ったレーザが普通の0.8$\mu$m単位のAlGaAsレーザであるため、電流をかえていくと、あるところで波長が跳ぶ、いわゆるモードホッピングという現象が起こるためです。動的単一モードレーザというようなシングルモード性の高いレーザを使うと、安定性を保ったまま1THzくらい、つまり$10^{12}$Hz程度くらいの連続掃引が可能です。

## まとめ

以上の話を簡単にまとめます。4点の課題があるといいましたが、現在の実験結果は表1に示すようなものです。主レーザの中心周波数の安定度は、現在約$2\times10^{-12}$、理論限界は$1\times10^{-15}$です。主レーザの線幅の値は、1988年初頭では0.9kHzで、理論的には1Hzが予測されています。

従レーザの周波数の追随性は、実験的には約$1\times10^{-14}$、理論限界は$2.7\times10^{-16}$くらいです。周波数掃引可能範囲は連続的には60GHzくらいで、理論的、技術予測は1THzくらいです。

以上の手法の特徴は、次のようになります。第1に、たいへん安定性が高いこと、再現性がよいことです。第2は、応用に際して、例えば1Hzの線幅は不必要な場合に、1MHz、10kHzくらいですますときに、単に制御系のゲインを調節するだけで希望の線幅がえられ、レーザの構造そのものをかえる必要がないことです。

第3は、従来の電子回路の自動制御方法とのアナロジーがきくことです。したがって、自動制御のシステムを作るときに、実験しなくてもよいわ

けです。つまりCADができることで、計算機上でシミュレーションをして、その結果に基づき装置を設計、製作して、それを用いて実験を行うと、直接実験した結果と一致します。

第4は、システムの小型化をすると制御帯域が非常に広がることで、OEIC等とこの手法はコンパチブルであるということです。応用範囲は、センシングやコヒーレント光通信で、特に、低ビットレートから中ビットレート程度のコヒーレント光通信には十分に使えると思います。

# Q&A

—Q—

スペクトルの幅を狭くする技術は、一つはキャビティ長を大きくする方法、もう一つは本方法のように、あるディテクタをつけてフィードバックしていくことだと思いますが、できることならレーザ単体で狭くしたほうがよいと思います。レーザの長さはどのくらいがよいのでしょうか。

—A—

実際には、レーザの長さそのものよりは、共振器の損失を少なくするために、レーザ内部での吸収や散乱の損失を少なくすること、端面の反射率を上げることが有効です。長くすることはそれほど本質的なことではないと思います。共振器の反射率を100%にすれば、もちろん光はでてこないので、問題があります。したがって、反射率の上限は使う側からきまります。デバイスだけでは、共振器長をむやみに長くすることでも考えないかぎり、約1MHzから200～300kHzくらいになると思います。それから先は、どうしても本発表のような方法が必要ではないかと思います。

—Q—

ループゲインとしては、どのくらい必要ですか。

—A—

これは非常に簡単で、デバイスの性能で何もしないときの線幅が1MHzあるとすると、応用上でそれを1kHzにしたいときは、線幅を1000分の1にしたいわけです。制御ゲインは簡単に1000で30dBにすればよいことになります。アンプだけで、30dBを実現することは場合によりむずかしい場合がありますが、今述べたように、光電変換をしているわけです。そこで、ファブリ・ペロー干渉計などでゲインをかなりかせげます。

光電変換は、レーザの周波数の揺らぎを検出するためにファブリ・ペロー干渉計を使っています。レーザの周波数が揺らげばファブリ・ペロー干渉計を通り抜ける光のパワーも揺らぎ、ここで光をAPDでうけて、電気量に変換します。そのときのファブリ・ペロー干渉計はよいものを使って、ここで制御原因をあげる工夫ができます。技術的な問題はいくらでも融通がきくということです。

—Q—

アイソレータに対する要求はどのくらいですか。

—A—

それが一番のネックで、従来手にはいるアイソレータは一つあたりだいたい30dBくらいで、1Hzとか極限的なことをやろうとするときには、2台くらい必要です。30dBのアイソレーター一つでは少し不安というのが現状です。その点は確かにネックだと思います。

—Q—

線幅を狭窄化したときに、強度はどうなりますか。

—A—

質問の主旨は、レーザの周波数の揺らぎを小さくするように電流をかえていると、逆にレーザのパワーの揺らぎが大きくなるのではないかということです。ですが、実際の数値は、レーザの周波数の揺らぎがかりにゼロになったとしても、パワーの揺らぎの大きさは何もしないときの約10%増加するだけです。いいかえると、レーザの周波数のゆらぎが何MHzとしても、周波数の揺らぎの大きさで$10^{-7}$くらいで、レーザのパワーの揺らぎは何もしないときでも1000分の1くらいあるのではないでしょうか。ですから、そのようなことがいえるわけです。

# FREQUENCY STABILISATION OF 1·5 μm DFB LASER USING INTERNAL SECOND HARMONIC GENERATION AND ATOMIC $^{87}$Rb LINE

*Indexing terms: Semiconductor lasers, Lasers and laser applications*

Absorption spectral lines in $^{87}$Rb were measured by the internal second harmonic generated from a 1·56 μm GaInAsP DFB laser. This second harmonic frequency was locked to the centre of the $^{87}$Rb spectral line to stabilise the 1·56 μm fundamental radiation frequency. The resultant frequency stability was $9{\cdot}0 \times 10^{-12}$ at the integration time of 100 s.

*Introduction:* Coherent optical communication systems using 1·5 μm semiconductor lasers have many advantages including high sensitivity and minimum fibre loss. For these systems, frequency stabilisation of these lasers is an important problem to be solved. Absorption spectral lines of combination tones or the higher harmonics of vibration–rotation transitions in gaseous organic molecules ($NH_3$, $H_2O$, etc.), have been used as frequency references for the stabilisation.[1] However, there are problems in their low absorption coefficients and the difficulty of spectral assignments, which could limit the sensitivity of frequency discrimination and frequency reproducibility, respectively.[2,3] On the other hand, atomic spectra offer a few and relatively strong lines in comparison with the organic molecular spectra, which can be easily identified, facilitating their use as frequency references in lightwave communication systems. For example, an optogalvanic spectral line in atomic krypton has been used as a frequency reference.[4] However, the problem in using this line should be the frequency shift induced by the change of discharge current of the hollow cathode lamp, as has been found in the Lamb-dip stabilised HeNe lasers at 633 nm.[5,6]

On the other hand, at 0·8 μm wavelength region, there are several stable frequency references, for example, Rb and Cs atomic lines, which show very strong absorptions.[2,3] In particular, because it has been confirmed that the magnitude of frequency shift in Rb by the change of its ambient temperature was far lower than 0·8 MHz/K,[7] a spectral line in Rb can be used as a very stable and accurate frequency reference. In this letter, we propose a novel and simple method of stabilising the frequency of a 1·5 μm GaInAsP DFB laser by locking onto a Rb absorption spectral line by using internal second harmonic (ISH) generated from this laser.

*Experiment:* The experimental set-up is shown in Fig. 1. A 1·56 μm wavelength GaInAsP DFB laser [flat-surface buried heterostructure (FBH) type][8] was used. The temperature of the laser heat sink was regulated within 1 mK at the room temperature. The threshold current was 14 mA at 298 K. The output power was 11 mW at the DC injection current of 6·9 times the threshold. This laser was oscillating in a single longitudinal mode with a sidemode suppression ratio of 60 dB. The frequency tunability of the laser was −1·1 GHz/mA and −20 GHz/K. Since the laser material had a large second-order nonlinear susceptibility and optical field strength in the active waveguide of the laser is strong enough, the second harmonic with the wavelength of 780 nm could be generated in the laser and was emitted from the laser facet. This ISH was transmitted through a compact glass cell (35 mm long) of a $^{87}$Rb atomic vapour (temperature of 296 K), and then, the absorption spectral profile in $^{87}$Rb could be measured by sweeping the laser injection current. The ISH power was high

enough to be detected by a conventional photomultiplier (PM), or even by a compact Si avalanche photodiode, which made the experimental set-up simple. Laser frequency was modulated by dithering the injection current (1 kHz frequency and 2 $mA_{p-p}$ amplitude) in order to lock the ISH frequency to the centre of the first derivative of the absorption spectral profile in $^{87}Rb$. This derivative was obtained by a lock-in amplifier (time constant 30 ms) and employed as the frequency fluctuation discriminator. After the output signal from the lock-in amplifier was processed by a proportional amplifier and an integrator, the resultant error signal was added to the injection current. The output signal from the lock-in amplifier was sent also to the Allan variance real-time processing system (ARPS)[9,10] to estimate the frequency stability.

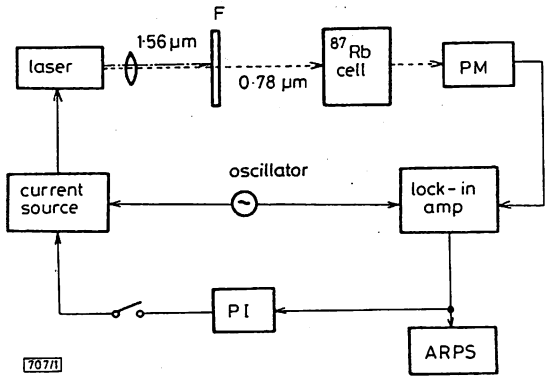


**Fig. 1** *Experimental set-up*

F = infra-red cut filter, PM = photomultiplier, PI = proportional amplifier and integrator, ARPS = Allan variance real-time processing system[10]

*Results and discussions:* A relation between the fundamental radiation power of the laser $P_f$ and its ISH power $P_{ish}$ was measured to be $P_{ish} = 2{\cdot}0 \times 10^{-8} \times P_f^2$ ($P_f$, $P_{ish}$ expressed in W). The maximum of $P_{ish}$ obtained was 2·0 pW at $P_f$ = 10 mW. Although the ISH has been observed for other kinds of semiconductor lasers,[11,12] the present work is, to the authors' knowledge, the first report for quantitative evaluation and application of the ISH of a 1·5 μm single mode DFB laser.

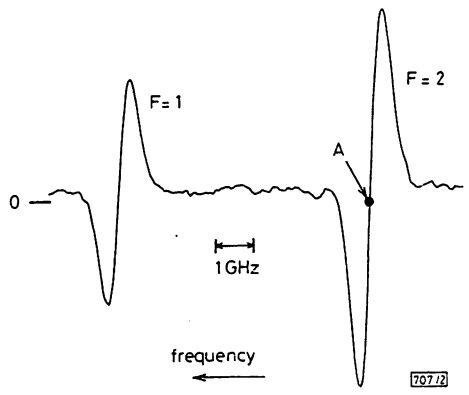


**Fig. 2** *First derivative signal of $^{87}Rb$–$D_2$ spectral lines*

ISH frequency locked to point A

Fig. 2 shows the first derivative signal of the $^{87}Rb$–$D_2$ spectral line ($^5S_{1/2}$–$^5P_{3/2}$ transitions) measured by the ISH. Two spectral components in this Figure correspond to the transitions from the hyperfine levels of $F = 1$ and 2 in the ground state ($^5S_{1/2}$). This Figure shows clearly that the spectral profile of $^{87}Rb$ was measured with a high signal-to-noise ratio.

Frequency of the ISH was locked to the centre of the transition from the $F = 2$ level (the point $A$ in Fig. 2) by closing the feedback loop of Fig. 1. Fig. 3 shows the square root of the Allan variance $\sigma_y^2(\tau)$ of the ISH frequency fluctuation,[9] which corresponds to that of the 1·56 μm fundamental radiation, measured by the ARPS. Comparison between the curves *a* and *b* in this Figure show that the frequency stability was improved substantially by the present frequency control scheme. The minimum of $\sigma_y$ on the curve *a* was $9{\cdot}0 \times 10^{-12}$ at the integration time $\tau$ of 100 s. This minimum of $\sigma_y$ obtained by this simple experimental set-up is 1/3 times that by using the $NH_3$ molecular vapour as a frequency reference.[1] This would be attributed to the large absorption in $^{87}Rb$ atoms. Our results indicate that the $^{87}Rb$ atoms offer a reliable frequency reference and that the present method is very useful to realise a high frequency stability.

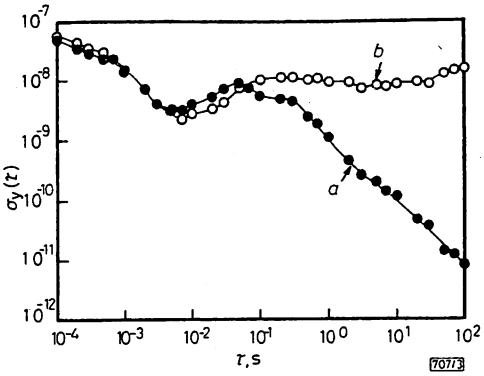


**Fig. 3** *Square root of Allan variance $\sigma_y^2(\tau)$ of frequency fluctuation*

*a* Frequency-stabilised laser
*b* Free-running laser

*Summary:* The maximum power of the ISH of a 1·56 μm GaInAsP DFB laser was 2·0 pW in this work. Absorption spectral line in $^{87}Rb$ atoms was measured by this ISH, and the ISH frequency was locked to the centre of the one of the spectral component to stabilise the 1·56 μm fundamental radiation frequency. The resultant frequency stability was $9{\cdot}0 \times 10^{-12}$ at the integration time of 100 s, which was estimated from the error signal of the feedback loop.

*Acknowledgment:* We thank Dr. H. Ishikawa of Fujitsu Laboratories for discussions on DFB lasers.

M. OHTSU
E. IKEGAMI

*Graduate School at Nagatsuta*
*Tokyo Institute of Technology*
*4259 Nagatsuta, Midori-ku*
*Yokohama, Kanagawa 227, Japan*

*28th October 1988*

## References

1 OHTSU, M., KOTANI, H., and TAGAWA, H.: 'Spectral measurements of $NH_3$ and $H_2O$ for pollutant gas monitoring by 1·5 μm InGaAsP/InP lasers', *Jpn. J. Appl. Phys.*, 1983, **22**, pp. 1553–1557
2 OHTSU, M.: 'Realization of ultrahigh coherence in semiconductor lasers by negative electrical feedback', *J. Lightwave Technol.*, 1988, **2**, pp. 245–256
3 OHTSU, M., and TAKO, T.: 'Coherence in semiconductor lasers', *in* WOLF, E. (Ed.): 'Progress in optics XXV' (Elsevier Science Publisher, Amsterdam, 1988)
4 CHUNG, Y. C., and ROXLO, C. B.: 'Frequency-locking of a 1·5 μm DFB laser to an atomic krypton line using optogalvanic effect', *Electron. Lett.*, 1988, **24**, pp. 1048–1049
5 LEE, P. H., and SKOLNIK, M. L.: 'Saturated neon absorption inside a 6238-Å laser', *Appl. Phys. Lett.*, 1967, **10**, pp. 303–305
6 BAGAEV, S. N., KOLOMNIKOV, Y. D., LISITSYN, V. N., and CHEBOTAEV, V. P.: 'Stabilization of reproducibility of frequencies of He–Ne lasers at 0·63 μ', *IEEE J. Quantum Electron.*, 1968, **QE-4**, pp. 868–870
7 FURUTA, H., and OHTSU, M.: 'Evaluation of frequency shift and stability in rubidium-vapor-stabilized semiconductor lasers', submitted to *Applied Optics*
8 KIHARA, K., KAMITE, K., SUDO, H., TANAHASHI, T., KUSUNOKI, T., ISOZUMI, S., ISHIKAWA, H., and IMAI, H.: 'High-power, wide-bandwidth, 1·55 μm-wavelength GaInAsP/InP distributed feedback laser', *Electron. Lett.*, 1987, **23**, pp. 941–942
9 ALLAN, D. W.: 'Statistics of atomic frequency standards', *Proc. IEEE*, 1966, **54**, pp. 221–230
10 KUBOKI, K., and OHTSU, M.: 'Development of Allan variance real time processing system to estimate laser frequency stabilities', submitted to *IEEE Transactions on Instrument Measurement*
11 FURUSE, T., and SAKUMA, I.: 'Internal second harmonic generation in InGaAsP DH lasers', *Opt. Commun.*, 1980, **35**, pp. 413–416
12 OGASAWARA, N., ITO, R., ROKUKAWA, H., and KATSURASHIMA, W.: 'Second harmonic generation in an AlGaAs double-heterostructure laser', *Jpn. J. Appl. Phys.*, 1987, **26**, pp. 1386–1387

# NOVEL MEASUREMENT METHOD OF LINEWIDTH ENHANCEMENT FACTOR IN SEMICONDUCTOR LASERS BY OPTICAL SELF-LOCKING

*Indexing terms: Semiconductor lasers, Optical measurement*

We propose a simple, accurate and novel method to measure the value of the linewidth enhancement factor in semiconductor lasers. It utilises the asymmetry of the frequency locking range of a semiconductor laser with the optical feedback from the external CFP cavity. The measured value for a 0·8 $\mu$m CSP-type AlGaAs laser was 3·07 $\pm$ 0·26, which showed good agreement with those measured by other conventional methods.

A number of semiconductor laser properties depend on the linewidth enhancement factor $\alpha$,[1,2] e.g. spectral linewidth and phase noise, correlation between FM and AM noises, oscillating wavelength, injection locking, optical feedback by the external mirror, light amplification etc. On the basis of these dependences, the value of $\alpha$ has been estimated by numerous authors.[2] In this letter we propose a novel method, which can determine precisely the value of $\alpha$ by a simple measuring apparatus. Furthermore, this method requires neither the values of structural parameters and material constants of the laser nor high-speed modulation of injection current.

In the injection locking of semiconductor lasers, the locking range shows a strong dependence on the value of $\alpha$,[3] by which Henry *et al.*[4] have measured the value of $\alpha$. Our method is similar to this from the viewpoint of using the frequency locking property of the laser; however, we utilised the frequency self-locking of a semiconductor laser by the reflected light from an external Fabry–Perot cavity. In this case, the locking range shows asymmetry for the resonance frequency of the cavity depending on the value of $\alpha$, which can thus be determined by this asymmetry.

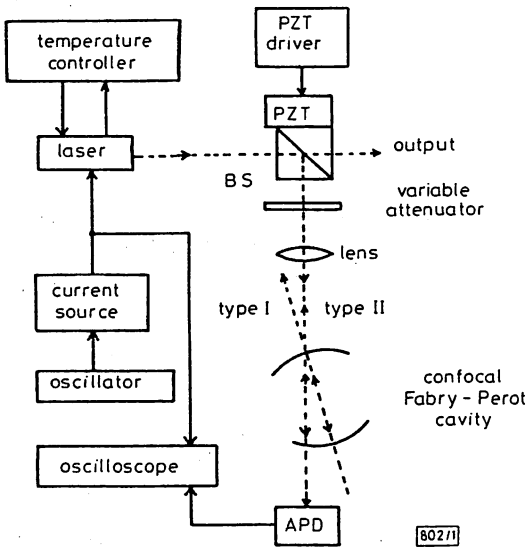


**Fig. 1** *Experimental apparatus*

BS and APD are beamsplitter and avalanche photodiode, respectively

The experimental set-up is shown in Fig. 1. A 0·83 $\mu$m AlGaAs (CSP type, Hitachi 8312E) semiconductor laser was used in this work. The laser was operated at room temperature, any fluctuation of which was suppressed within 1 mK by the temperature controller consisting of Peltier coolers and thermistor sensors. The DC bias current was 1·4 times the threshold level. The free spectral range and finesse of the confocal Fabry–Perot (CFP) cavity, used for optical feedback, were 1·5 GHz and 10, respectively. When laser output light couples to this cavity placed off-axis as shown in Fig. 1, two types of light are reflected from the cavity (types I and II). The power of the reflected light of type II has its maximum at the resonance frequency $\nu_c$ of the CFP cavity. Feedback of this light to the laser gives rise to locking of the laser oscillating frequency to $\nu_c$, and the linewidth of the laser becomes very narrow.[5] The linewidth of the optically self-locked semiconductor laser shown in Fig. 1 was 150 kHz, which was measured by the delayed self-homodyne method with a 2 km-long optical fibre. This narrow linewidth could be maintained stably up to 3 h by the phase control of feedback light to accomplish long-term stability. This could be done by automatic servo-control of the voltage applied to the PZT on which the beam splitter was mounted.

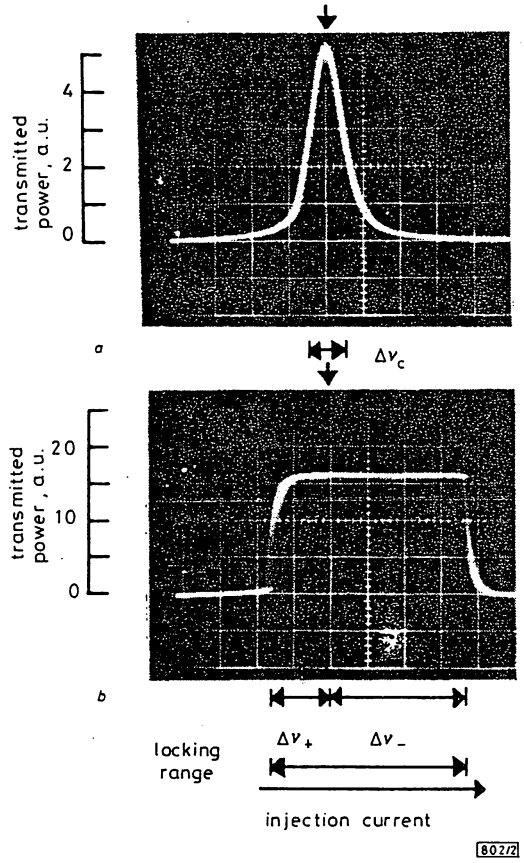


**Fig. 2** *Resonance curves of confocal Fabry–Perot cavity in (a) no feedback state (b) in optical feedback state*

Scale of horizontal axes is 0·055 mA/div. Arrow at top of (*a*) and (*b*) indicates $\nu_c$

The intensity of the transmitted light from the CFP cavity, i.e. its resonance curve, is shown in Fig. 2, which was detected by an avalanche photodiode, where the injection current was modulated slowly with a 1 kHz sawtooth wave. When the feedback light level is sufficiently low, the resonance curve of the CFP cavity has a conventional profile, as shown in Fig. 2*a*. The peak of this curve indicates the centre frequency $\nu_c$ of the resonance, and the resonance bandwidth (FWHM) $\Delta\nu_c$ of the cavity can be measured from this curve. By increasing the feedback light level, self-locking takes place. In the locking range, the laser frequency is locked to the cavity resonance irrespective of the injection current. The intensity of transmitted light thus becomes almost constant in the locking range as shown in Fig. 2*b*. By comparison between Figs. 2*a* and *b*, it is clear that the frequency locking range is $\Delta\nu_- + \Delta\nu_+$, because the oscillating frequency of the laser is invariant within the range $[\nu_c - \Delta\nu_-] \sim [\nu_c + \Delta\nu_+]$. Furthermore, it can also be seen from Fig. 2*b* that $\Delta\nu_- > \Delta\nu_+$, i.e. the locking range is asymmetric with respect to $\nu_c$. This phenomenon can be explained by the stationary solutions of an equation describing the complex laser field coupled with feedback light from the CFP cavity.[3,4,*] From such an analysis, $\Delta\nu_-$

* HOLLBERG, L.: private communication, 1988; LAURENT, P., CLAIRON, A., and BREANT, C.: 'Frequency noise analysis of optically self-locked diode lasers', submitted to *IEEE J. Quantum Electron.*, 1988

and $\Delta\nu_+$ are given by

$$\Delta\nu_- = F\sqrt{(1+\alpha^2)} + \Delta\nu_c/2 \quad (1)$$

and

$$\Delta\nu_+ = F + \Delta\nu_c/2 \quad (2)$$

respectively, where $F$ is the quantity proportional to the power of feedback light. Eliminating $F$ from eqns. 1 and 2, $\alpha$ is given by

$$\alpha = 2\sqrt{(\beta)}/(1-\beta) \quad (3)$$

where

$$\beta = \frac{\Delta\nu_- - \Delta\nu_+}{\Delta\nu_- + \Delta\nu_+ - \Delta\nu_c} \quad (4)$$

The values of $\Delta\nu_-$, $\Delta\nu_+$ and $\Delta\nu_c$ can be measured from Fig. 2; thus the value of $\alpha$ is determined by using these and eqns. 3 and 4. The average value of $\alpha$ obtained from the data of 15 successive measurements and its standard deviation were 3·07 and 0·26, respectively. This result shows good agreement with those reported so far, which are in the range 1·3–5·4.[2]

As seen from eqns. 3 and 4, the value of $\alpha$ can be determined by simple measurements of the values of $\Delta\nu_-$, $\Delta\nu_+$ and $\Delta\nu_c$ only, where the measurements and/or calculations of structural parameters or material constants of the semiconductor laser are not required at all. In the locking state, the voltage applied to the PZT shown in Fig. 1 was adjusted to an appropriate value, and then the transmission curve of the CFP cavity was very stable as shown in Fig. 2*a*. With a feedback light level sufficient to maintain the locking state, the measured values of $\alpha$ were independent of the feedback light level; thus it is clear that this method is very reliable. This method can be applied to all types of semiconductor laser, for which the optical self-locking system can be employed. Whereas the injection locking method requires a master laser, this method requires only a passive external Fabry–Perot cavity, which would not have to be of confocal type.

In conclusion, we have proposed a simple, accurate and novel method to measure the value of $\alpha$ by using the asymmetry of the frequency locking range of a semiconductor laser with optical feedback from an external CFP cavity. The measured value of $\alpha$ for the 0·8 $\mu$m CSP-type AlGaAs laser was $3{\cdot}07 \pm 0{\cdot}26$, which showed good agreement with those measured by other methods.

We thank Dr. L. Hollberg of NIST, Boulder, for fruitful discussions on the operating characteristics of the semiconductor laser coupled with the CFP cavity.

C. H. SHIN
M. TESHIMA
M. OHTSU

*Graduate School at Nagatsuta*
*Tokyo Institute of Technology*
*4259 Nagatsuta-cho, Midori-ku*
*Yokohama, Kanagawa 227, Japan*

*11th November 1988*

## References

1 HENRY, C. H.: 'Theory of the linewidth of semiconductor lasers', *IEEE J. Quantum Electron.*, 1982, **QE-18**, pp. 259–264
2 OSINSKI, M., and BUUS, J.: 'Linewidth broadening factor in semiconductor lasers—an overview', *ibid.*, 1987, **QE-23**, pp. 9–29
3 LANG, R.: 'Injection locking of a semiconductor laser', *ibid.*, 1982, **QE-18**, pp. 976–983
4 HENRY, C. H., OLSSON, N. A., and DUTTA, N. K.: 'Locking range and stability of injection locked 1·54 $\mu$m InGaAsP semiconductor lasers', *ibid.*, 1985, **QE-21**, pp. 1152–1156
5 DAHMANI, B., HOLLBERG, L., and DRULLINGER, R.: 'Frequency stabilization of semiconductor lasers by resonant optical feedback', *Opt. Lett.*, 1987, **12**, pp. 876–878

# ハイパー・コヒーレント光の実現

きれいな波と思われているレーザー光にも，量子力学的効果のため，基本的な周波数揺らぎが存在している。そこで，この揺らぎを正確に測定，レーザーの動作状態を制御し，揺らぎの影響を取り除いた。ここに，ハイパー・コヒーレント光が初めて発生したのである

大津　元一

温度揺らぎや機械的な振動などの外乱のため，きれいな波と考えられているレーザー光にも，揺らぎが存在している。この揺らぎを取り除くと，古典物理学によって表わされる「なめらかな波」と，量子雑音（不確定性原理から導かれる量子力学的な揺らぎ）とを合成した状態になる。これが，コヒーレント状態である。つまり，光を使った測定や通信の精度は，この量子雑音のために制限されているのである。

しかし最近，この量子雑音を制御，抑制できることがわかってきた。それは，量子雑音によって生じる光周波数の揺らぎを高精度に検出し，これがゼロになるよう，レーザーに流れる電流などをフィードバック回路を使って，自動制御すればよい。すると，コヒーレント状態の光よりもなめらかな，ハイパー・コヒーレント状態の光が実現できるのである。

筆者の実験により，現在までに，半導体レーザー光の光周波数揺らぎを，コヒーレント状態の100分の1以下にまで抑えることができるようになった。今後，この自動制御の精度や速度をさらに高めることにより，光周波数揺らぎを，いっそう小さくする可能性も残されている。

このハイパー・コヒーレント光を使えば，原子の冷却・静止，重力波の検出，相対論の検証，コヒーレント光通信などの研究を，大きく前進させることができるのである。

いろいろな物理量の精密測定や光通信など，非常にきれいで，なめらかな光の波を使いたい場合が数多くある。このためには，ネオンランプなどの光では不十分なため，普通はレーザーの光を利用している。

確かに，レーザーの光はきれいで，なめらかな波である。それでも実際は，温度揺らぎや機械的な振動などの外乱の影響を受け，わずかに揺らいでいる。そこで，フィードバック回路を用いた自動制御によってこの揺らぎを取り除くと，量子雑音以外の影響を排除できるのである。この量子雑音とは，不確定性原理から導かれる量子力学的揺らぎのことで，レーザーの光周波数揺らぎの基本的要因になっている。この量子雑音だけが残った状態が，コヒーレント状態である（66ページの図）。

一般に光の波は，古典物理学によって記述される「なめらかな波」と，量子力学によって記述される「揺らぎ」とを合成したものとして表わされる。これらの波に含まれている量子雑音は規則性をもたないため，光周波数もまた，ゆっくりとした揺らぎや，非常に速い揺らぎなど，不規則な揺らぎをもっている。この不規則な揺らぎは非常に取り扱いにくいこともあり，これまで，光を使った測定や通信の精度は，この量子雑音のために基本的に制限されてきた。それは，量子雑音を制御したり，抑圧したりすることは不可能だと考えられていたからである。

しかし最近，ひとつの解決策として，光の波のある部分の量子雑音を他の部分に分散した，いわゆる「スクイーズド光」と呼ばれる，非古典的な光を作り出すことが考案された（R. E. スラッシャー／B. ユーケ「量子雑音を克服する『スクイーズド光』」サイエンス1988年7月号参照）。つまり，スクイーズド光は，量子雑音の効果を低減するのではなく，量子雑音を光の波のいろいろな部分に分散させてしまうのである。しかし，光の波を一周期にわたって見てみると，ある部分では雑音の影響がコヒーレント状態よりも増加してしまっているため，使い方に注意しないと，測定や通信の精度は向上できない。

そこで，もうひとつの有力な解決策として，量子雑音の影響を人為的に減らし，光の波の一周期全体にわたって，揺らぎを小さくする方法が考案された。これが，ハイパー・コヒーレント光の発生である。

この方法は，量子雑音そのものを制御するのではない。それどころか，微視的な現象である量子雑音は自由に発生させたままにしておく。しかし一方で，その量子雑音が引き起こす光の周波数の揺らぎを，高精度で検出するのである（周波数の揺らぎは巨視的で，古典的な物理量なので検出できる）。この検出量に応じて，レーザー発振に係わりをもつ巨視的な物理量（たとえば，レーザーに流れる電流）などを変化させ，その結果，検出する光周波数揺ら

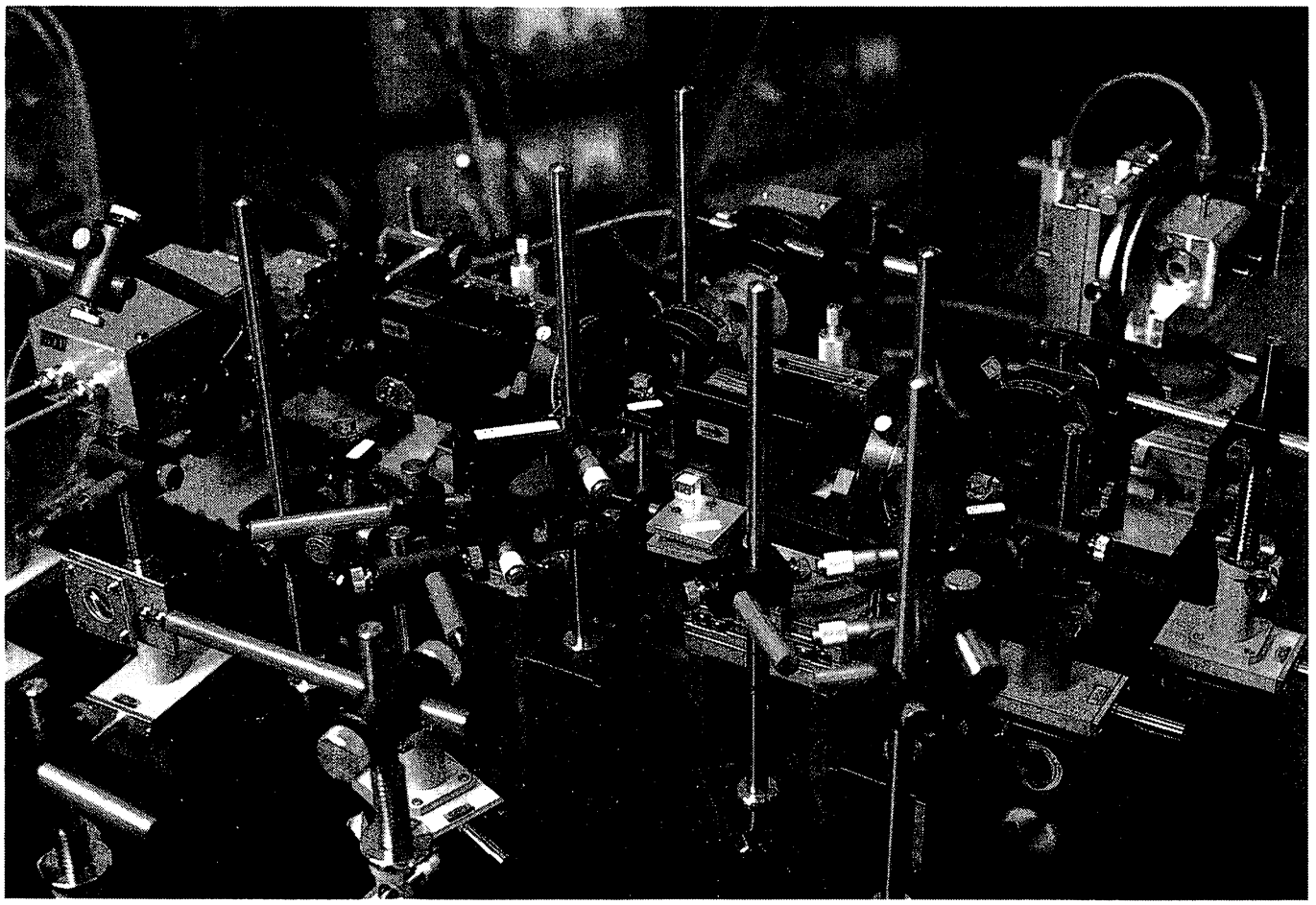

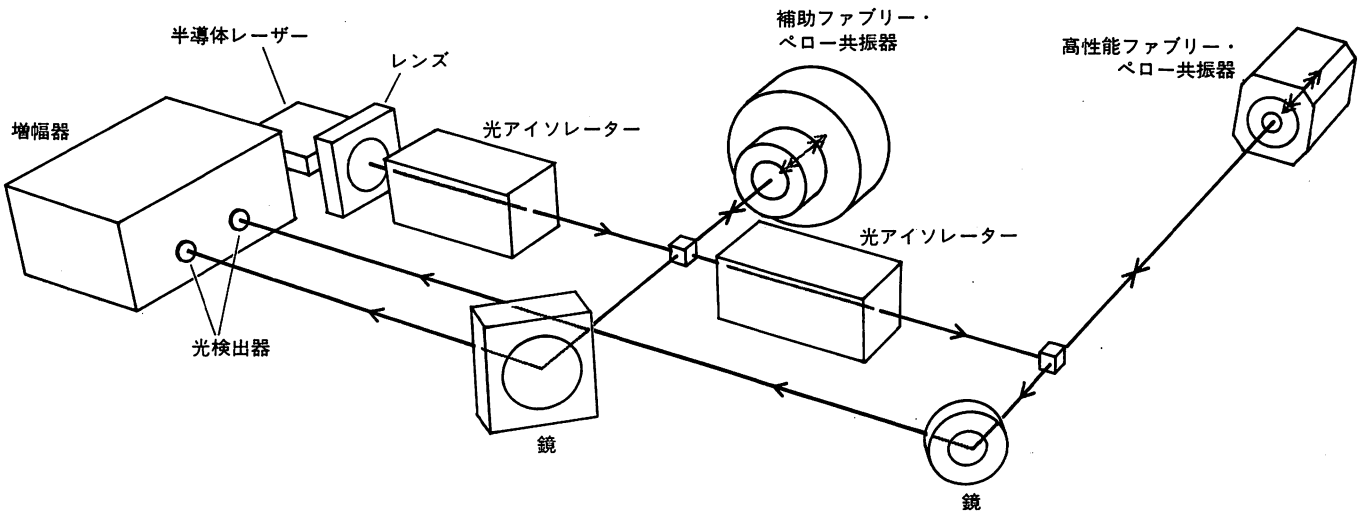


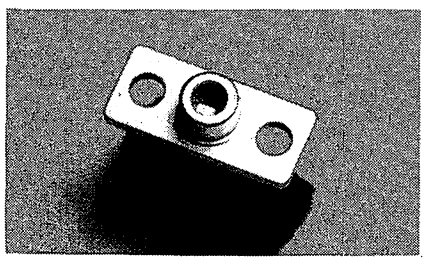

**ハイパー・コヒーレント光発生のための実験装置**　ここには，筆者が実際に使った実験装置と，その概念図を示す。実験に使われた半導体レーザー(左)は波長0.8ミクロンの近赤外光を出し，その出力は約10ミリワットで，コンパクト・ディスク（CD）プレーヤーなどにも使われているものである。さてこの装置では，半導体レーザーから出た光が外部反射面で反射して，レーザー本体に戻ってしまうのを防ぐために高性能光アイソレーターが使われている。周波数揺らぎ検出のためのファブリー・ペロー共振器は，反射率99.99%以上の高性能の2枚の鏡を互いに平行に向き合わせた構造をしている。レーザーの電流を自動制御するための増幅器は，計算機シミュレーションにより最適設計されている。レーザー本体の温度揺らぎは1000分の1度以下に抑えられている。

ぎがゼロになるように自動制御するという方法である。

この場合，結果的には，量子雑音の大きさはコヒーレント状態の場合と変わらない。つまり，量子雑音が光周波数揺らぎに及ぼす効果を低減するように，レーザーを制御しているだけなのである。これにより，コヒーレント状態，すなわち，制御しない場合の量子力学的限界よりも小さな光周波数揺らぎが実現できる。つまり，コヒーレント状態よりも古典的な波に近い，なめらかな波が作り出せるのである。

## 気体レーザーによる実験

レーザーが発明された1960年には，レーザーの光はなめらかで，すでに量子雑音によって決まる状態（コヒーレント状態）が実現していると思われていた。

しかし実際は，レーザー装置の周囲の温度揺らぎ，機械的な振動，レーザー発光媒質の密度揺らぎなどの外乱の影響を受け，コヒーレント状態とはほ

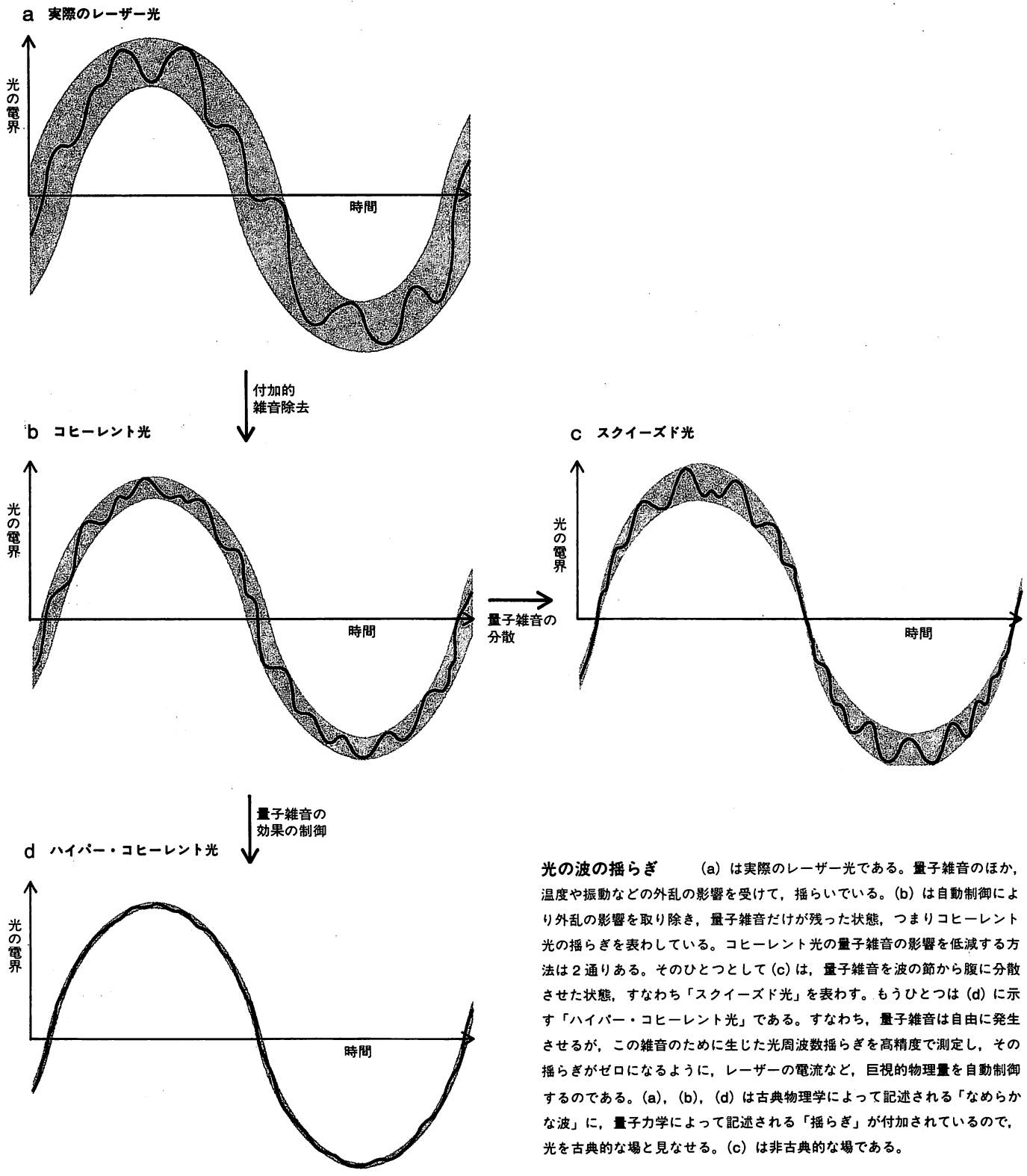


**光の波の揺らぎ**　(a) は実際のレーザー光である。量子雑音のほか，温度や振動などの外乱の影響を受けて，揺らいでいる。(b) は自動制御により外乱の影響を取り除き，量子雑音だけが残った状態，つまりコヒーレント光の揺らぎを表わしている。コヒーレント光の量子雑音の影響を低減する方法は２通りある。そのひとつとして (c) は，量子雑音を波の節から腹に分散させた状態，すなわち「スクイーズド光」を表わす。もうひとつは (d) に示す「ハイパー・コヒーレント光」である。すなわち，量子雑音は自由に発生させるが，この雑音のために生じた光周波数揺らぎを高精度で測定し，その揺らぎがゼロになるように，レーザーの電流など，巨視的物理量を自動制御するのである。(a)，(b)，(d) は古典物理学によって記述される「なめらかな波」に，量子力学によって記述される「揺らぎ」が付加されているので，光を古典的な場と見なせる。(c) は非古典的な場である。

ど遠いものであった。

たとえば，最もなめらかな波を出す気体レーザー（ヘリウム・ネオンレーザー，波長は0.6ミクロン）では，その光周波数（約100テラヘルツ；1テラは1兆）に含まれている揺らぎの割合は$10^{-7}$，光周波数揺らぎの大きさは10メガヘルツ（1メガは100万）だった。量子雑音の限界値は約$10^{-18}$～$10^{-19}$（光周波数揺らぎの大きさは$10^{-4}$～$10^{-5}$ヘルツ）であるから，当時は量子雑音限界よりも，ずっと大きな揺らぎであったことがわかる。

そこで，その揺らぎを小さくし，量子雑音限界，すなわちコヒーレント状態を実現する研究が始まったのである。現在，ヘリウム・ネオンレーザーを用いた最も高精度な実験は，米国国立標準局のホール（John L. Hall）が行なったものである（72ページの図）。

この実験ではヘリウム・ネオンレーザーの光周波数揺らぎを検出するために，ファブリー・ペロー共振器を使っている。この共振器は簡単にいえば，光に対するフィルターである。したがって，光周波数が揺らぐと，この共振器を通り抜ける光のパワーも揺らいでしまう。そして，このパワー揺らぎをフォトダイオードで測定すると，光周波数揺らぎが検出できるのである。

この共振器は，2枚の鏡を向き合わせて，固定したもので，鏡の反射率は99.99%以上ときわめて高い。このような高反射率を実現するには，世界最高の真空蒸着技術が必要である。鏡の間隔を固定するには，「ゼロデュア」と呼ばれる熱膨張係数が小さい，特殊なガラス系材料で作った円筒を，スペーサとして使っている。そして，この共振器の温度揺らぎは1000分の1度に抑えられている。

測定された光周波数揺らぎの大きさに応じて，たとえば巧妙な電子回路を使って，ヘリウム・ネオンレーザーに流れる放電電流の値を自動制御し，光周波数揺らぎを抑える。この装置全体は温度揺らぎ，音響振動，地面の振動などの外乱の影響を防ぐため，防振テーブルの上に置かれる。さらに，音響振動の影響も防ぐため，カエデ合板と鉛の板とを張り合わせた，大きな箱の中に設置してある。この箱を，「静かな家」と呼んでいる（次ページの図）。

こうした改良によりホールは，光周波数揺らぎの割合を$10^{-16}$まで低減することに成功した。これは，光周波数揺らぎの大きさ0.01ヘルツに相当する。

### コヒーレント状態は実現したのか

1960年当時から比べると，ヘリウム・ネオンレーザーの光周波数揺らぎの大きさは9桁も小さくなった。すなわち，光周波数揺らぎは，10年ごとに約3桁ずつ減少し，現在に至っている。

さらに，今後も技術的な壁に打ち当たることなく，実験結果はさらに進歩し，2000年には揺らぎの割合は$10^{-18}$～$10^{-20}$に達する，という将来予測もある。

その理由は――。レーザー自身には，量子雑音が生み出す電界ベクトルの位相の揺らぎを抑圧する制動力がない。すなわち，位相の揺らぎはちょうど，制動力のないブラウン運動と同じように振る舞うのである。したがって，このブラウン運動を規制するように，外部から強制的に自動制御すると（レーザーはこの制御効果を抑圧しないので），位相揺らぎをゼロに近づけることができる。これが自動制御によって位相揺らぎ，すなわち，これとほぼ同等な量である光周波数揺らぎが小さくなった理由である（69ページの図）。

ところで，ホールが実現した$10^{-16}$という光周波数揺らぎの割合の値は，はたしてコヒーレント状態に達しているのだろうか？

実は，ヘリウム・ネオンレーザーのように高品質のレーザーでは，コヒーレント状態に相当する光周波数揺らぎの割合はきわめて小さい。試算によると，その割合の値は$10^{-18}$～$10^{-19}$という。したがって，ホールが達成した揺らぎの値は世界最小ではあるが，ハイパー・コヒーレント光の発生という観点からすると，まだコヒーレント状態にも達していないといえる。

### 半導体レーザーでの挑戦

波長0.8ミクロン，出力10ミリワットの光を出す半導体レーザーは小形で，約40ミリアンペアのわずかな電流を流すだけで発光する。このレーザーは安価なので，近年いろいろな分野で使われるようになってきており，身近な例では，コンパクト・ディスク（CD）プレーヤーがある。

ただし，半導体レーザーは小形であるため，ヘリウム・ネオンレーザーなどに比べて性能が劣る部分もある。たとえば，量子雑音による光周波数揺らぎの大きさは，ヘリウム・ネオンレーザーに比べると，約8桁も大きい。これは半導体レーザーの光をコヒーレント状態にしたところで，依然として大きな光周波数揺らぎがあることを意味している。

したがって，半導体レーザーの場合，量子雑音は光周波数の大きな揺らぎを与える基本的要因であり，半導体レーザー使用者にとってこの問題は，避けて通れない“大きな壁”であった。こうしたことから，「半導体レーザーは火花放電にすぎない」と悪口をいう人さえもいた。

さらに，半導体レーザーの光周波数は，電流や温度がわずかに変化した程度でも，大きく変化してしまう。したがって，半導体レーザー単体を，高精度の光計測や通信に使うことはできず，技術的な工夫をする必要がある。

しかし最近になって，量子雑音で決まる光周波数の揺らぎは，制御・抑圧することができ，ハイパー・コヒーレント光を発生させられることがわかってきた。さらに，ハイパー・コヒーレント光の発生という目的から半導体レーザーを見直すと，これは非常に都合

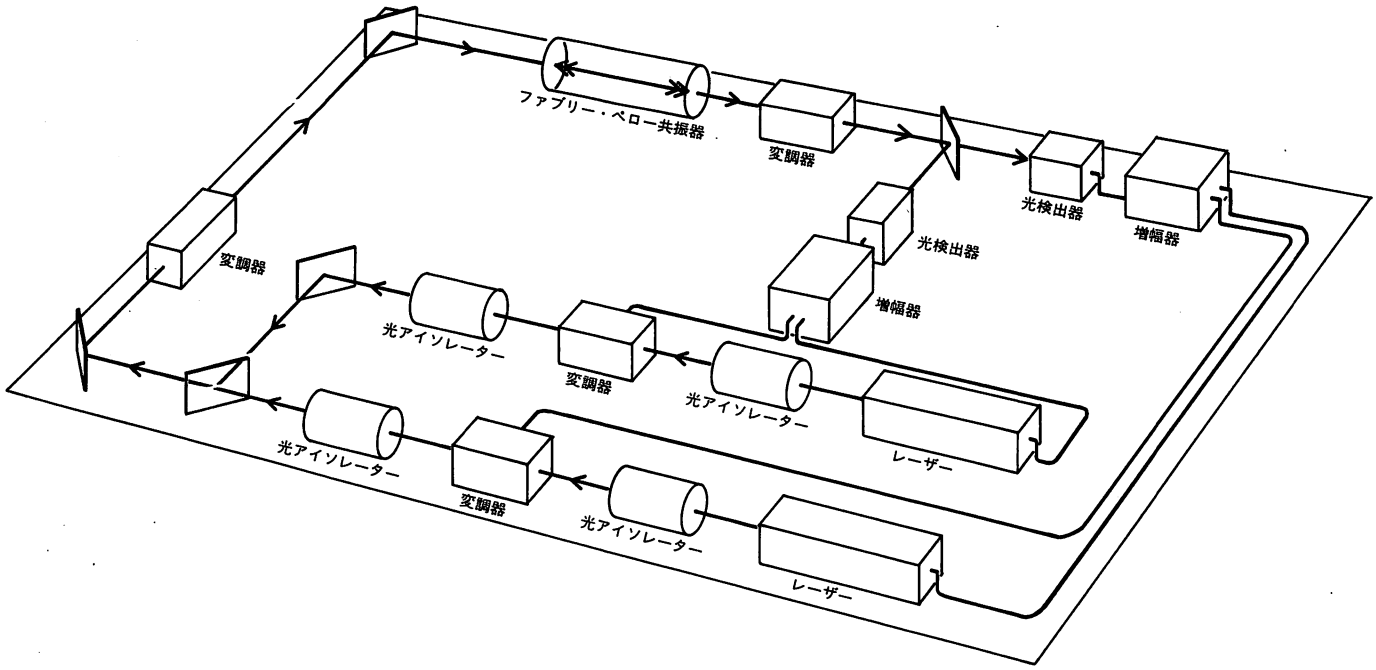


**光周波数揺らぎを抑圧する自動制御装置**　ヘリウム・ネオンレーザーの光周波数揺らぎを抑圧するため，ホールが開発した自動制御装置の概念図である。装置には，非常に注意深く設計されたヘリウム・ネオンレーザー，周波数変調器，ファブリー・ペロー共振器，増幅器などを使っている。これら全体は防振テーブルの上に置かれ，さらに音響振動の影響を防ぐため「静かな家」と呼ばれるカエデ合板と鉛板製の大きな箱の中に設置してある。

のよい装置であることもわかった。

つまり半導体レーザーは，量子雑音による光周波数揺らぎが大きいので，ヘリウム・ネオンレーザーの場合ほど精度が高い，特別な装置を使わなくても，量子雑音を直接，高精度に検出できるのである。さらに，この検出量に比例してレーザーの電流を変化させると，光周波数は容易に変化し，光周波数揺らぎをなくすこともできるのである。つまりこれは，巨視的な物理量である電流の制御により，微視的な量子雑音による効果を減らし，光周波数揺らぎをなくすことができることを意味している。すなわち，ハイパー・コヒーレント光を発生させることが，実際に可能なのである。

この事実には従来，誰も気づかなかったし，試みてもいなかった。これに対し，私たちの研究グループは数年前に，半導体レーザーを使ったハイパー・コヒーレント光の発生に，取り組み始めたのだった（65ページの図）。

### 周波数揺らぎの制御

半導体レーザーの電流を制御すると，光周波数が変化する。これは，電流が変化すると，レーザー媒質中の電子密度が変わり，このためにレーザー媒質の屈折率が変化するからである。この場合，効率よく制御するには，わずかな電流で光周波数が大きく変わること，さらに，電流を高速度で変化させた時に，光周波数も遅れずに変化すること，が大切である。

普通の半導体レーザーでは，この変化効率は電流１ミリアンペア当たり，約３ギガヘルツ（１ギガは10億）であり，変化の速さは約１ナノ秒（１ナノは10億分の１），つまり，応答帯域は約１ギガヘルツである。これは，十分によい性能である。

そこで問題は，量子雑音による光周波数揺らぎを，いかに高精度に検出するかに絞られてくる。そのために私たちは，非常に性能の高いファブリー・ペロー共振器を用いた。これは，ホールと同じように，反射率99.99％以上の高性能の鏡を2枚使って，作ったものである。

ファブリー・ペロー共振器を透過するか，反射する光の強度は，その光の周波数によって変化する。光の周波数がファブリー・ペロー共振器固有の共鳴周波数（これは２枚の鏡の距離によって決まる）に一致するとき，透過光強度は最大となり，反射光強度は最小となる。一方，一致しない場合は，これらの光強度は両周波数の差に比例して変化する。したがって，ファブリー・ペロー共振器は，透過光にとってはバンド通過フィルター，反射光にとってはバンド除去フィルターになる。

これらのフィルターのバンド幅は，鏡の反射率が高いほど狭く，鋭いフィルター特性をもつ。したがって，ここで用いた高性能ファブリー・ペロー共振器を透過，または反射してくる光の強度揺らぎを測定すれば，レーザーの光周波数揺らぎを高精度，高感度に検出できるのである（70ページの図）。

しかし，ここで新たな問題が生じた。それは，あまり高感度検出ができるような狭いバンド幅のファブリー・ペロー共振器を使うと，高速の検出ができなくなるということである。高速の検出ができないと，レーザーの電流変化に対して，レーザー光周波数がいくら

遅れずに変化しても，高速で，広い帯域の自動制御ができなくなってしまう。したがって，自動制御の効率もあがらず，光周波数揺らぎを十分に抑圧することもできないのである。

よく調べてみるとこの問題は，ファブリー・ペロー共振器からの透過光強度揺らぎを測定し，光周波数揺らぎを検出する場合に生じることがわかった。そこで，これを解決するため，透過光ではなく，反射光の強度揺らぎを測定することにした。

透過光と反射光とはあまり違いはないように思われるかもしれない。確かに，ゆっくり揺らいでいる光周波数を検出する場合には，ほとんど違いはない。光周波数揺らぎによって生ずる光強度揺らぎの符号が，互いに反対であるだけである。しかし，速く揺らいでいる光周波数を検出する場合には，大きな差がでてくる。

つまり，反射光というのはファブリー・ペロー共振器の入射端側の鏡から直接反射してきた光と，共振器内部を何回も往復して出てきた光とを合成したものである。前者の光は，“現時点での光周波数”をもっているが，後者の光は，往復にかかる時間だけ“過去の光周波数”をもっているのである。

すなわち，これらを合成した反射光では，現在と過去の周波数の差を測定していることになる。この差を測定するとき，現在と過去の時間間隔は，実は非常に小さいのである。したがって，この小さな時間間隔の中で発生する光周波数揺らぎ，つまり非常に速い揺らぎを測定することができる。

言い換えれば，反射光は，周波数揺らぎを，時間に関して微分する効果をもっているのである。この“微分効果”により，速く揺らいでいる光周波数をも，検出できることになる。一方，透過光は，ファブリー・ペロー共振器内を何回も往復した光だけで構成されているので，このような微分効果はもっていない。

ファブリー・ペロー共振器という装置は19世紀に考案され，物理の教科書にもよく載っているが，どの教科書も，光周波数の微分効果について触れたことはない。しかし，私たちは，教科書には書かれていない新しい見方をすることにより，この実験が進歩する糸口を得たのであった。

## ハイパー・コヒーレント光の実現

このようなファブリー・ペロー共振器からの反射光から光周波数揺らぎを検出し，自動制御の効率が最大に，そして同時に，制御速度が最高になるように，自動制御装置の最適設計を行なった。ただし，外乱の影響を極力抑えるため，半導体レーザーの温度揺らぎは1000分の１度以下に抑え，装置全体は防振テーブルの上に置き，シールドケースで覆うことにした。この自動制御は，いろいろな所で使われてきたアナログ電子回路とよく似ていることから，アナログ電子回路の最適設計のための計算機シミュレーション手法を利用したのである。

最適設計された装置を使うと，シミュレーションで予測した通り，周波数揺らぎを高精度に抑圧できるようになる。すなわち，この自動制御装置は，きわめて再現性に富んでいるといえる。こうして得られた最適の自動制御装置を使って実験し，レーザーの発振スペクトルの形状を測定した。

発振スペクトルとはレーザーの光周波数に対する光電界振幅の分布曲線のことで，どのような光周波数をもつ光電界振幅が，どのくらいの大きさになっているかを表わすヒストグラムである。したがって，その中心の周波数は，レーザーの発振周波数の平均値を表わ

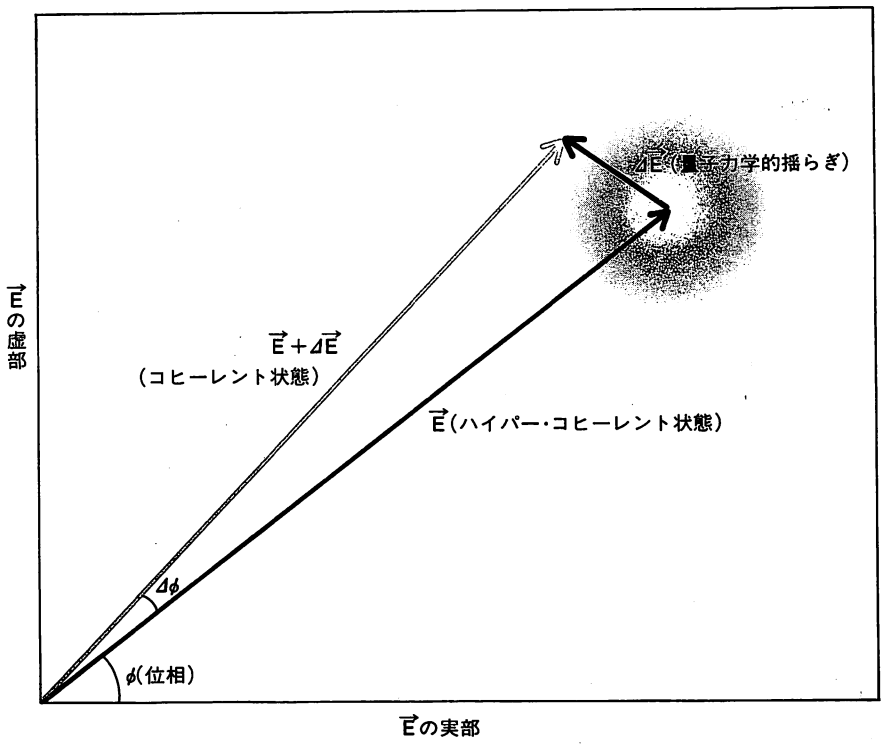


**光電界の位相変動のベクトルモデル**　光電界の位相変動の様子を，ベクトルを使って表わしたものである。電界を複素ベクトル表示したものが$\vec{E}$（青の矢印）であり，位相$\phi$をもつ。これに量子力学的揺らぎ$\Delta\vec{E}$が加わる。この揺らぎのベクトル$\Delta\vec{E}$の方向は不規則であるが，そのうちベクトルEと直交するものが位相$\phi$を$\Delta\phi$だけ揺るがせる。レーザー自身にはこの位相揺らぎを抑圧させる機構はないので，位相はちょうど，制動力のないブラウン運動をしているように，どんどん揺らいでいる。しかし，逆にもし，外部からこのブラウン運動を規制するように強制的な自動制御を施すと，レーザーはこの自動制御の効果を妨げることはしない。したがって，この自動制御により，位相揺らぎ，さらには周波数揺らぎをゼロに近づけることが可能である。ここで，青い矢印がハイパー・コヒーレント状態，赤い矢印がコヒーレント状態を示している。

している（次ページの図）。

波長0.8ミクロンの半導体レーザーの場合，それは375テラヘルツである。光の波が完全な正弦波であるならば，スペクトル幅はゼロになる。しかし，波の周波数が揺らいでいれば，その揺らぎに比例して，スペクトル幅は広くなる。したがって，スペクトル幅は周波数揺らぎの大きさを表わす尺度として使えるのである。

私たちが使った半導体レーザーでは，自動制御をしない場合には，スペクトル幅は5メガヘルツだった。一方，ファブリー・ペロー共振器の透過光を使って自動制御した結果，スペクトル幅はかなり狭くなったが，中心から±25メガヘルツ離れたところに，低いピークがいくつか見られた。これは，速い周波数揺らぎが検出できなかったため，それを十分抑圧できなかったことから生じたもので，スペクトル形状としてはやや，ゆがんでいる。

そこで，反射光を使って自動制御した結果，スペクトル幅はさらに狭くなったうえ，低いピークも見られなくなった。これは，速い周波数揺らぎを十分に検出でき，それを抑圧できたことを表わしている。

この値がもつ意味を考えてみよう。1984年6月以前，すなわち自動制御をする前のスペクトル幅は5メガヘルツだった。この値は，量子雑音のほかに，レーザー内の電子の密度揺らぎなどの付加的影響をも受けていることを示している。量子雑音によって決まるスペクトル幅，すなわちコヒーレント状態でのスペクトル幅は，レーザーの構造を詳しく解析することから推定できる。私たちが使用した半導体レーザーでは，そのスペクトル幅は，150キロヘルツから2メガヘルツの間に入ることがわかった。

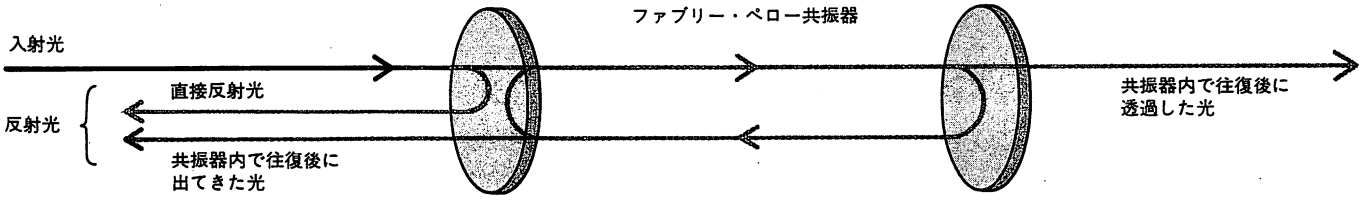


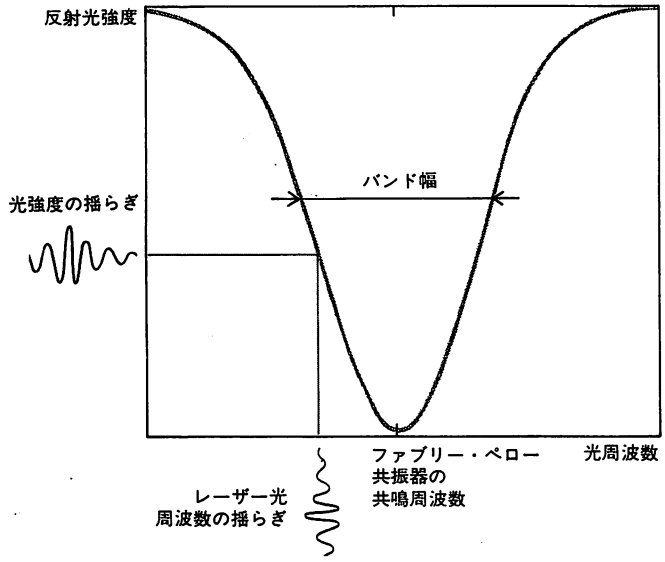


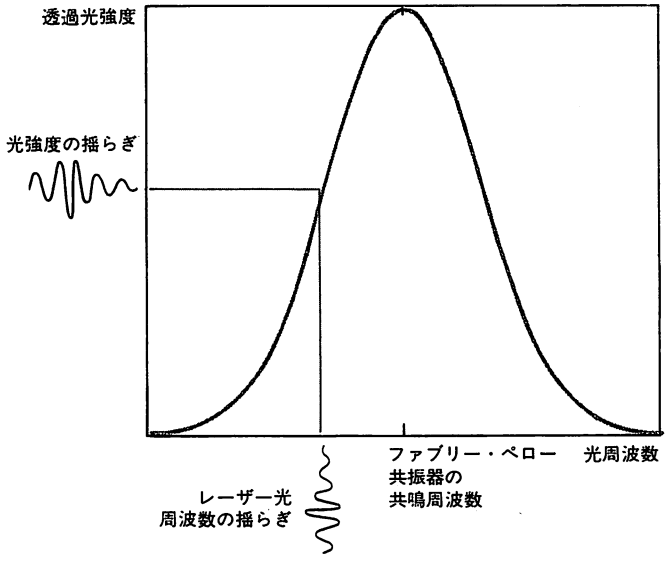


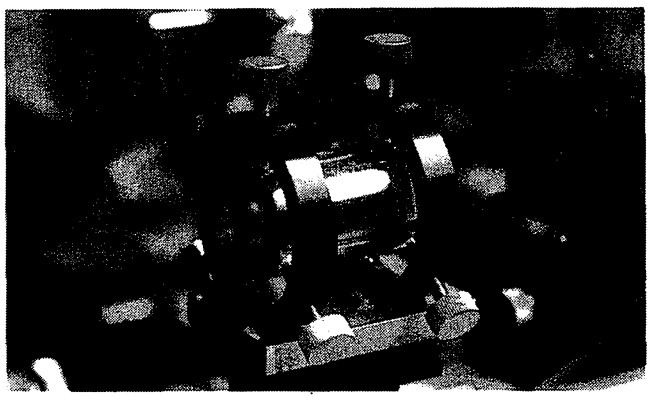

**ファブリー・ペロー共振器の透過光と反射光**　ファブリー・ペロー共振器を透過したり，反射したりする光の強度は，その光の周波数によって変化する。したがって共振器は，透過光にとってはバンド通過フィルター，反射光にはバンド除去フィルターとして働くのである。つまり，入射する光の周波数が揺らげば，これを透過，反射して出てくる光強度もまた，揺らいでしまう。すなわち，この光強度の揺らぎを測定すると，光周波数の揺らぎがわかる。これらのフィルターのバンド幅は，鏡の反射率が高いほど狭くなり，鋭いフィルター特性をもつようになる。したがって，光周波数揺らぎの検出感度は，高い反射率の鏡を使うほど良くなるのである。反射光を測定すると，光周波数揺らぎの微分が測定できる。この“微分効果”により，速く揺らいでいる光周波数も検出できるわけで，周波数揺らぎ抑圧のための自動制御には都合がよい。

1984年6月以後，自動制御でスペクトル幅は次第に小さくなり，1988年6月には880ヘルツにまで縮小した。これは，コヒーレント状態（制御をしない場合の量子力学的限界）でのスペクトル幅の1／100以下で，半導体レーザーのスペクトル幅としては世界最小である。これは，ハイパー・コヒーレント状態が初めて実現したことを示している。私たちの装置を改良すれば，さらにスペクトル幅を小さくすることも可能である（次ページの図）。

その限界値は周波数揺らぎを検出するための光検出器によって発生する量子雑音，すなわちショット雑音の大きさによって決まり，約1ヘルツである。しかし，このような小さな値を実現するためには，現在の半導体レーザーの構造と性能を，もっと高めなければならない。つまり，より一層，自動制御に適した特性をもつレーザー素子を開発する必要がある。

現在，国内外において，このようなレーザー素子の開発が活発に進められている。さらに，現在の実験装置では自動制御回路の長さが，まだ長すぎる。すなわち，制御のための電気信号がこの回路を一巡するための時間がかかりすぎ，十分高速の制御ができていないのである。

これを改良するには半導体デバイス加工技術を駆使して，制御回路を半導体レーザー本体とともに集積化，小型化する必要がある。日本は集積化技術の一部分では，他国に比べ，優れたものをもっている。このように最先端半導体デバイス技術を駆使することにより，近い将来，私たちはハイパー・コヒーレント状態の限界値を実現できるのではないかと期待される。

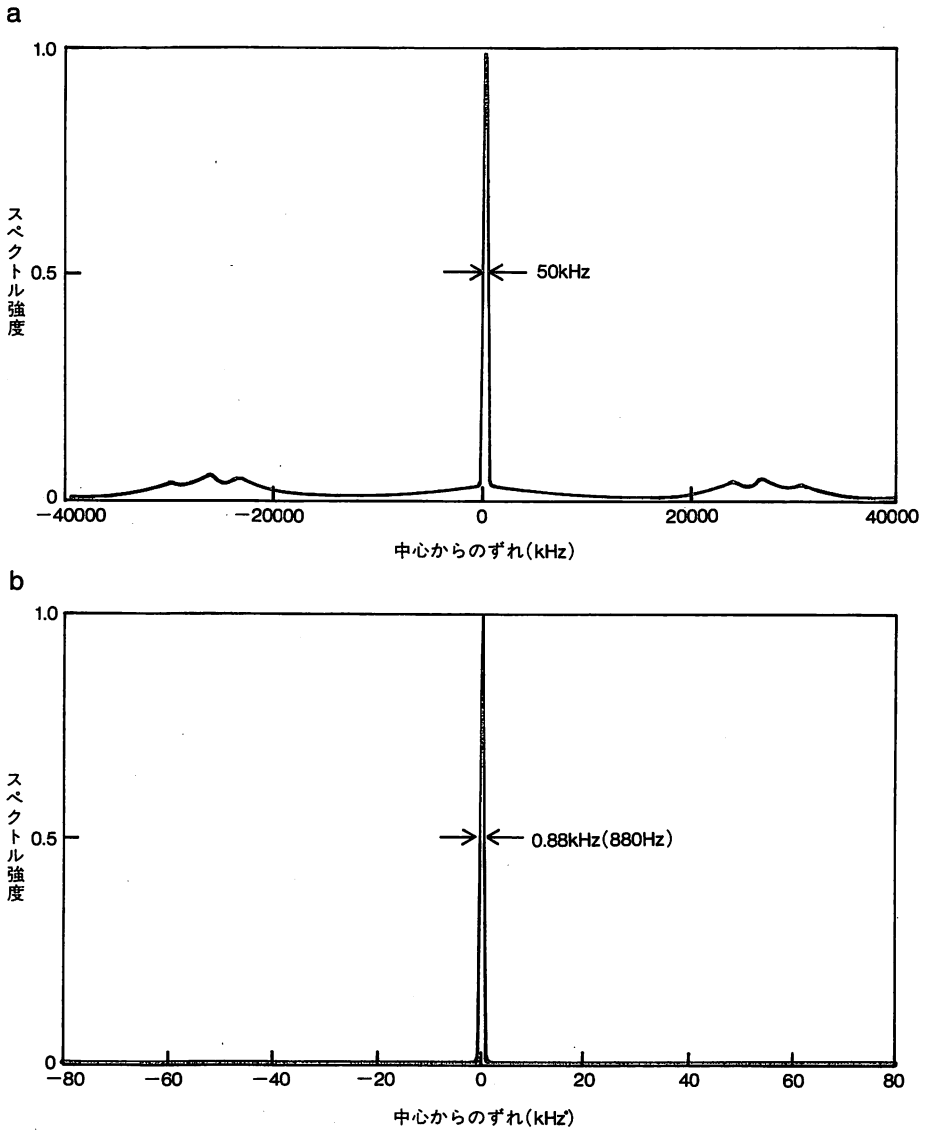


**自動制御された半導体レーザーの発振スペクトル**　自動制御しないとき，半導体レーザーの発振スペクトル幅は，5メガヘルツであった。ファブリー・ペロー共振器からの透過光強度の揺らぎにより光周波数揺らぎを検出し，自動制御した結果，スペクトル中心部から約±25メガヘルツ離れたところに，背の低いピークがいくつか見られる（a）。これは，この方法では速い光周波数揺らぎが検出できず，したがってそれを抑圧できなかったことを表わしている。ファブリー・ペロー共振器からの反射光強度の揺らぎにより光周波数揺らぎを検出し，自動制御した結果を（b）に示す。速い光周波数揺らぎを検出し，それを十分抑圧したので（a）のような背の低いピークなどは現われてこない。スペクトルの幅は880ヘルツまで狭くなっているのがわかる。

### ハイパー・コヒーレント光の用途

ハイパー・コヒーレント光の応用範囲は広い。その代表的な例をいくつか紹介しよう。第1は「レーザーの光による原子の冷却と静止」の実験である。これは，現在の最先端をいく，原子物理研究分野である。

熱エネルギーにより真空中を自由に飛び回る原子に，なめらかな光の波を当てる。このとき光の周波数は，原子中の電子振動で決まる原子固有の共鳴周波数よりやや小さくしておく。しかし，このように周波数がずれている場合でも，原子は熱運動の結果として生じるドップラー効果で，この光を吸収できる。

その後すぐに原子は光を放出する。この光は共鳴周波数と同じ周波数をもっている。この吸収・放出の過程を繰り返すことで，原子は熱エネルギーを次第に失っていく。そして最後には，熱エネルギーの値を表わす原子温度は，0.001K（絶対温度）以下になり，原子は極低温にまで冷却され，真空中に静止するのである。

このように，原子を静止させるための技法には，いくつかの種類がある。

その一例は，AT & T ベル研究所のチュー（Steven Chu）により，実験的に示された。真空中のナトリウム原子に，なめらかな波のレーザー光を照射した結果，原子の熱運動速度は減少し，原子集団は「光による糖蜜」と呼ばれる状態になって，原子雲はオレンジ色に光ったのである（次ページの上図）。

このように，原子の運動を制御すること自身が物理的に興味深いし，また，静止した原子は，固体結晶中の凝縮した原子のように振る舞うので，結晶物性研究の強力な道具となる。正確にいうと，原子は完全に静止するのではなく，わずかに揺らいでいる。しかし，照射する光の周波数揺らぎが少ないほど，静止状態に近い状態が実現するのである。すなわち，この実験には，ハイパー・コヒーレント光が重要な役割を演ずるといえる。

第2の例は，「重力波検出」の実験である。アインシュタインが予言したように，宇宙のかなたで発生した重力波が地球に到来した場合，それを検出する方法として，なめらかな波の光を出すレーザー光を使った干渉計を用意しておく（A. D. ジェフリーズ／P. R. ソ

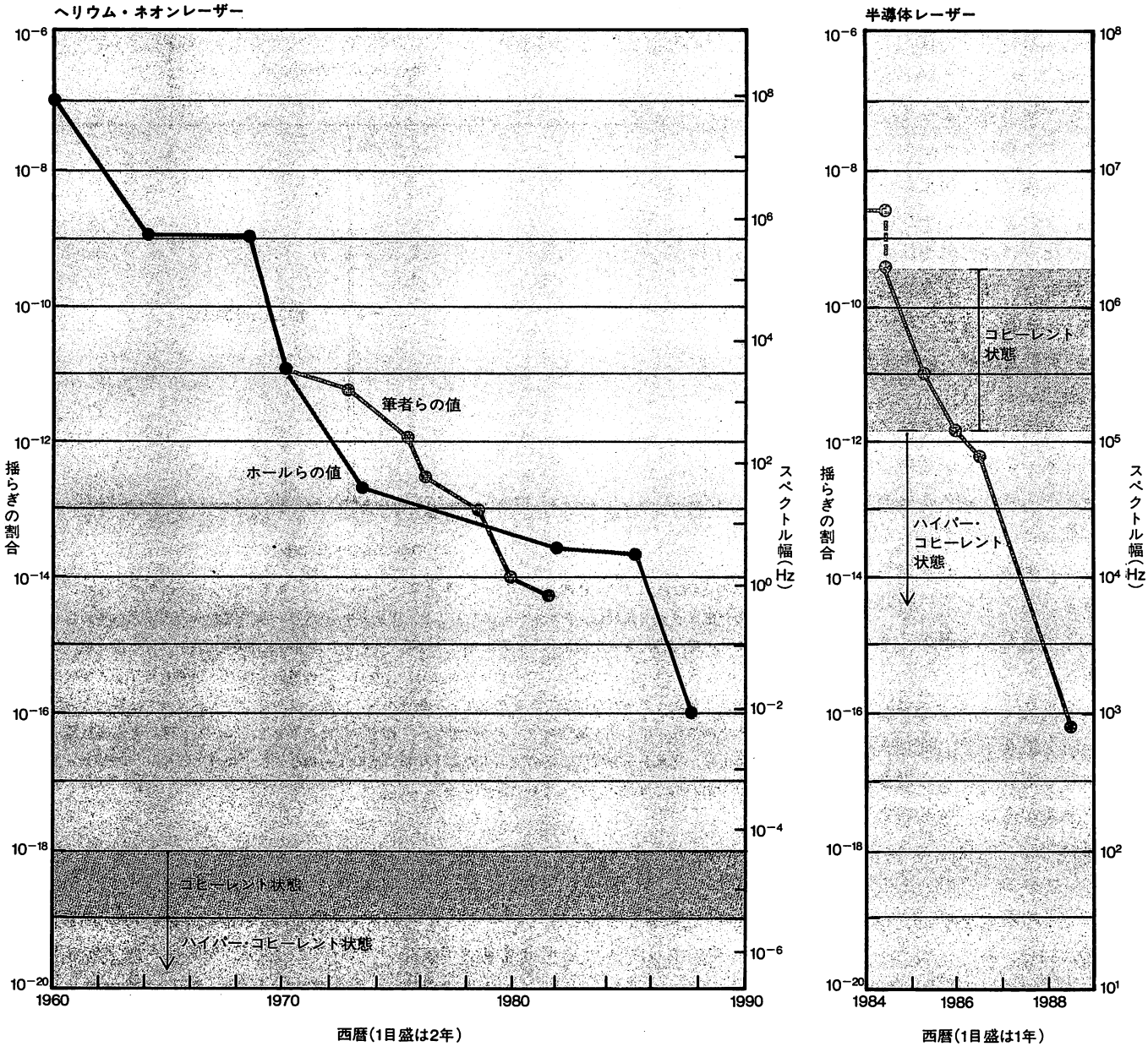


**レーザーの光周波数揺らぎ・スペクトル幅の減少の経緯**　1960年にレーザーが発明されたとき，光周波数のうちの揺らぎの割合の値は，$10^{-7}$であった。その後，世界の各地で，この値を小さくするための研究が行なわれた。1970年以降，米国国立標準局のホール（John L. Hall）が次々にトップデータを更新し，現在の$10^{-16}$という値を得た。この間，筆者らのグループは，1980年に当時の世界最高値である$10^{-14}$を報告した。ただし，これらの値はまだ，ヘリウム・ネオンレーザーの量子雑音によって決まるコヒーレント状態（紫色の領域）には達していない。一方，半導体レーザーのスペクトル幅を比較してみる。自動制御をしないとき（1984年以前）のスペクトル幅は，5メガヘルツであった。コヒーレント状態の領域よりも狭いスペクトル幅が，ハイパー・コヒーレント状態である。つまり，1988年6月に得られた880ヘルツは，ハイパー・コヒーレント状態を実現したことを示している。

ールソン／R. E. スペロ／M. E. ズッカー「重力波天文台」サイエンス1987年8月号参照)。もし，鏡をつるしたおもりに重力波が当たれば鏡が揺れ，干渉した光の強度も変化するので，それを光検出器で測定することができる。

その測定感度は，干渉計の長さに比例するため，米国では人工衛星を使って，宇宙空間に長さ1万kmの干渉計を建設することを計画している。同時に大切なことは，光の波がなめらかなことである。したがって，前の例にもまして，ハイパー・コヒーレント光が必要不可欠なのである。

その他の科学分野での応用としては，相対論検証のための「ケネデイ・ソーンダイク実験」がある。また，工学分野での応用としては，新しい光通信方式のひとつである「コヒーレント光通信」がある。後者では，伝送したい情報に応じて光の波の周波数や位相を変調し，これを長距離伝送する。この方法を使うと伝送距離が稼げ，伝送可能な情報量も増加する。しかし，周波数や位相を変調するためには，光の波が十分になめらかでなければならないことから，ハイパー・コヒーレント光が要求されるのである。

## 新しい光を目指して

レーザー本体の光の波の揺らぎは，量子雑音によって制限されている。この制限を乗り越えるには，現在のところ2つの方法がある。1つはこれまで述べたような，ハイパー・コヒーレント光の発生である。これはコヒーレント光以上になめらかな波を作ることから，古典的な光の極限状態を目指すものともいえよう。すなわち，光を古典的な場として扱うのである。したがって，広い応用が可能で，使いやすい光でもある。

第2の方法はスクイーズド光の発生である。量子雑音を分散してしまうスクイーズド光は，古典的な場には対応しない。つまり，非古典的な新しい量子場である。この光の発生過程は，基礎物理分野での光の量子論の研究上，興味深い。現在行なわれている実験は，まだ初期段階なので，きわめて良質のスクイーズド光の発生は報告されていないし，その応用報告もわずかしかない。しかし，重力波検出には有力な道具となるといわれており，将来，このような非古典的な光の発生と応用とが進歩するだろう。

電子を制御・操作することで，なめらかな波の光を出すレーザー装置が，1960年に発明されてから，すでに四半世紀以上も経過している。今後は光，特にその量子的姿である光子を制御・操作することにより，人類は新しい光を手にするだろう。そのためには光の量子論，量子光学についての深い理解が一層必要である。そして，新しい光というフロンティアを目指し，世界各国の研究者が“開拓者”となって，日夜研究を進めているのである。（完）

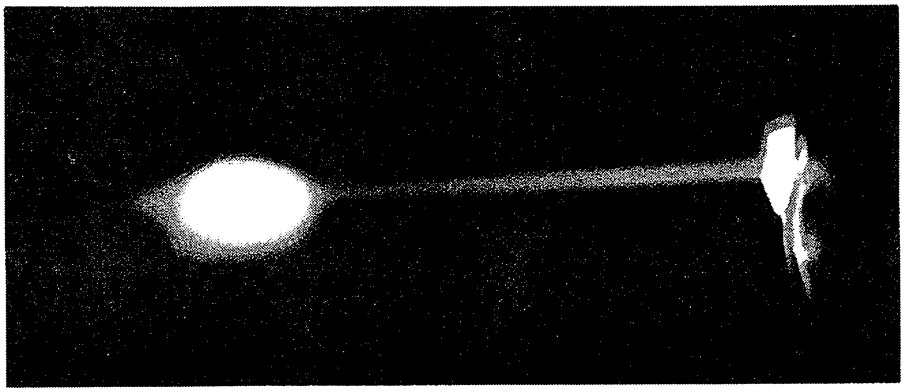

**真空中のナトリウム原子の冷却と静止**　なめらかな光の波をナトリウム原子にあてることにより，原子は冷却され，原子集団は「光による糖蜜」と呼ばれる状態となる。写真の中央で，オレンジ色に光っているのが，その状態である。右の方で光っているのは，真空中への，原子の噴き出し用スリットである。この実験は，AT＆Tベル研究所のチュー（Steven Chu）によって行なわれた。

**新しい光を目指したある“開拓者”グループ**　後列右から2人目で，西部開拓時代の衣装を身にまとっているのは，ヘリウム・ネオンレーザーの実験装置の考案者である，米国国立標準局のホール。左端は筆者（と妻，2人の娘）。2列目右から，電気通信大学の宅間宏（日本のレーザー研究の第一人者），東京大学の清水富士夫（ネオン原子の冷却と静止に初めて成功した），さらに，ホールの共同研究者である，米国国立標準局のバーガー（Rick L. Barger）が写っている。

# PROPOSAL OF HETERODYNE TYPE OPTICAL PHASE LOCKED LOOP BY SEMICONDUCTOR LASERS

KATSUHIKO KUBOKI, CHUL-HO SHIN, TORU KATO and MOTOICHI OHTSU
Graduate School at Nagatsuta, Tokyo Institute of Technology
4259, Nagatsuta, Midori-ku, Yokohama, Kanagawa 227, Japan
045-922-1111 ext. 2526

[Summary]

As a fundamental technique to realize ultra-high phase-stable lightwave, a heterodyne type optical phase-locked loop by semiconductor lasers [whose phase fluctuations are less than 1 (rad)] is proposed. A stable heterodyne signal is indispensable for a precise measurement of fundamental physical constants, an interferometer for the gravitation wave detection, and so on.

Figure 1 shows an experimental setup. As the first step, the spectral linewidth of the master laser (a 0.8 μm AlGaAs laser) was reduced by negative electrical feedback. A compact Fabry-Perot interferometer was used as a frequency discriminator. Theoretical estimations show that the linewidth can be reduced to a value narrower than that given by the Schawlow-Townes formula due to spontaneous emission noise (quantum noise) [1]. This implies that a very high coherent light can be artificially realized. The minimum linewidth obtained in the experiment was $\Delta\nu_{FB}$ = 100 kHz, which was 1/50 times as narrow as that of the free-running laser. As the linewidth broadening factor for AlGaAs lasers are $1.3 \leq \alpha \leq 5.4$ [2], this value of the linewidth was narrower than that determined from the magnitude of the spontaneous emission. The linewidth of 100 kHz corresponds that the phase fluctuations of the master laser are less than 1 (rad) for the integration time $\tau \leq 0.8$ μs. To extend the region of the integration time in which phase fluctuations are less than 1 (rad), for example $\tau \leq 1$ s (, which has been realized in the gas lasers [3],) the linewidth of $\Delta\nu$ = 0.3 Hz is required. It was confirmed by a computer simulation that such an ultra-narrow linewidth can be realized by using a super-high-finesse Fabry-Perot interferometer with the resonance linewidth of about 10 MHz as a frequency discriminator.

As the second step, the heterodyne signal between the master and the slave lasers was stabilized. For this purpose, the injection current of the slave laser in Fig.1 was controlled in order that the frequency of the heterodyne signal was locked to the stable radio frequency synthesizer. In other words, high coherence of the master laser could be transferred to the slave laser by this control. Two feedback loops were employed as shown in Fig.1. One was a narrowband feedback loop to reduce a long-term frequency drift of the heterodyne signal. The other was a wideband feedback loop to improve a short-term frequency stability. Figure 2(a) shows the square root of the Allan variance $\sigma^2_{yB}(\tau)$ of the heterodyne frequency fluctuations. Stabilized frequency fluctuations of curve B were considerably smaller than that under free-running laser of curve A. In particular, the very high stability of $\sigma_{yB} = 1.0 \times 10^{-14}$ was obtained at $\tau$ = 100 s, i.e., residual frequency fluctuations were only 3.7 Hz. Curve C in Fig.2(a) shows the value of $\sigma_{yB}$ which is required to realize the phase fluctuations of 1 (rad). To investigate the experimental conditions for realizing the value in curve C, the simulation by an electronic circuit model was carried out. As the result shown in Fig.2(b), it was found that the bandwidth of the phase-locked loop must be wider than twice the linewidth of the heterodyne signal. Furthermore, if the gain of 40~50 dB and the bandwidth of 2~3 MHz are the maximum attainable values for the active loop filter which are limited by a practical circuit design, the linewidth of the heterodyne signal must be narrower than 1 MHz. These conditions are technically reasonable ones, which can be realized by improving the performance of the presently employed system shown in Fig.1.

In conclusion, it can be claimed that the phase-stable semiconductor laser system [of which phase fluctuations of the master laser, heterodyne signal, and the slave laser are less than 1 (rad)] will be realized by negative electrical feedback.

[References]

1. M.Ohtsu, IEEE J. Lightwave Technol., vol. LT-6, January, 1988 in press
2. M.Osinski and J.Buss, IEEE J. Quantum Electron., vol. QE-23, pp. 9-29, 1987
3. D.Hils and J.L.Hall, Proc. IQEC '87, Bartimore, Maryland, pp. 102-103, 1987

[Figure Captions]

**Fig.1** Experimental setup.

**Fig.2(a)** The square root of the Allan variance $\sigma^2_{yB}(\tau)$ of the residual frequency fluctuations of the heterodyne signal.

**Fig.2(b)** Simulated result of a relation between the linewidth of heterodyne signal normalized to the bandwidth $\Delta\nu_h$ / $B_n$ and the square root of variance $\sigma\phi_B$ of the phase fluctuations of the heterodyne signal.

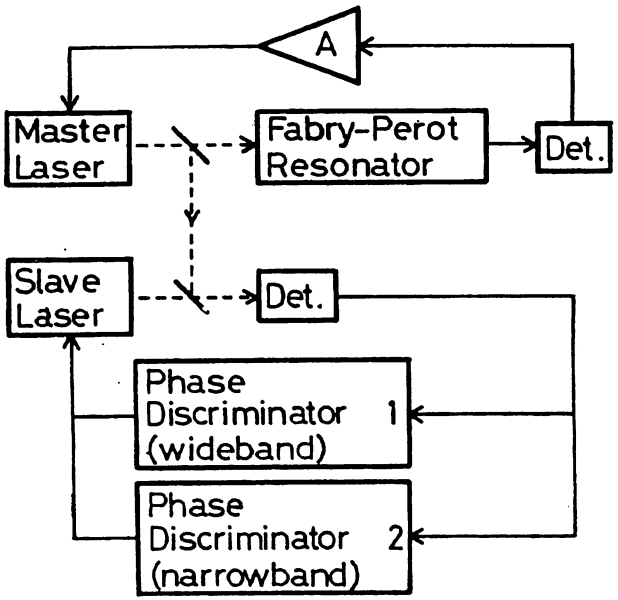


Fig.1

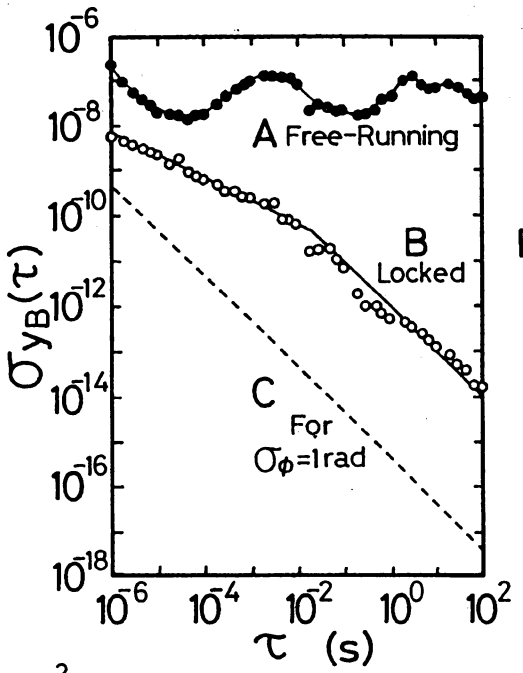


Fig.2(a)

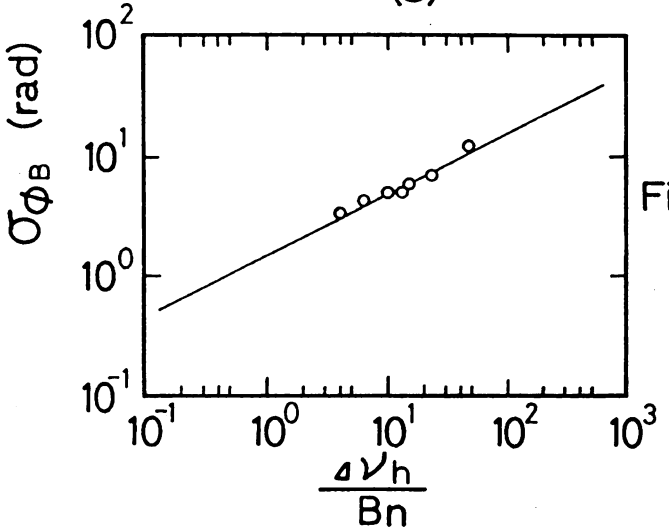


Fig.2(b)

# Frequency Control of Semiconductor Lasers

*M. Ohtsu, K. Kuboki, C.H. Shin, and M. Murata*

Graduate School at Nagatsuta, Tokyo Institute of Technology,
4259 Nagatsuta, Midori-ku, Yokohama, Kanagawa 227, Japan

## 1. Introduction

Frequency control of semiconductor lasers has become very important in recent years for several applications such as frequency standards, optical metrology, optical communication, and so on[1]. In the present work, a technique of electrical feedback was employed for the frequency control, because (a) stability and reliability of the feedback is high, (b) computer-aided-design (CAD) can be employed to realize the optimum feedback loop, and (c) magnitude of residual frequency fluctuations under the feedback can be reduced to a value which is far lower than that of the quantum noise limit of the free-running laser[2].

For practical applications, the following four problems should be solved simultaneously to improve the coherence of semiconductor lasers : (1) Stabilization of the center frequency of field spectrum of the master laser. (2) Linewidth reduction of field spectrum of the master laser. (3) Accurate frequency tracking of the slave laser to the master laser. (4) Stable and wideband frequency sweep of the slave laser. It should be important to develop a synthesized feedback system for solving these four problems simultaneously, which is possible by employing a technique of electrical feedback. In the following sections, experimental results for 0.8 μm wavelength AlGaAs laser ( CSP-type, Hitachi HL8312E ) on these four problems are presented.

## 2. Frequency Stabilization of the Master Laser

A slow electrical feedback loop with the bandwidth of 1 MHz was provided to the master laser to stabilize the center frequency of its field spectrum. The stability of $2 \times 10^{-12}$ was obtained at the integration time $\tau$ of 100 s by using the absorption spectral line in Rb vapor as a frequency reference. The frequency stability limited by the shot noise of the photodetector ( $= 1.7 \times 10^{-14}\ \tau^{-1/2}$ ) can be expected to accomplish by improving the performances of the feedback loop[2].



Frequency Standards and Metrology Editor: A. De Marchi

## 3. Linewidth Reduction of the Master Laser

The linewidth of the field spectrum of the master laser can be reduced by a fast electrical feedback loop if its bandwidth is wider than the linewidth of the free-running master laser. A slope of the resonance curve of the reflected light from a high finesse Fabry-Perot cavity was used as a sensitive frequency discriminator to realize a wideband feedback loop. Comparing the transfer characteristics of frequency discrimination of the reflected light with that of the transmitted light, the passband of frequency response is wider, and the slope of the transition band is improved by 20 dB/decade, and also phase-lead compensation is shown in the transition band, which allows to increase the feedback gain substantially. Thereby, it can be considered that the reflected light acts as the first order differentiator. This is why the reflected mode was chosen as the frequency discriminator.

The curve A in Fig. 1 represents the experimental result of the power spectral density $S_{FB}$ of frequency fluctuations obtained by using the feedback loop which was optimized by CAD. In this figure $S_{FB}$ was normalized to the power spectral density $S_{FR}$ of the free-running laser. The linewidth $\Delta\nu_{FP}$ of the resonant curve of the Fabry-Perot cavity used was 0.7 MHz ( finesse = 8,600 ). The curves B and C represent the results of computer simulations, where the values of $\Delta\nu_{FP}$ were assumed to be 10 MHz, and 0.1 MHz, respectively. It is seen from this figure that a wideband and large reduction of frequency fluctuations was realized, and that the magnitude of the reduction is larger by using a narrower $\Delta\nu_{FP}$. The minimum on the curve A was - 60 dB, and from such a large reduction of frequency fluctuations, a very narrow laser linewidth can be estimated. FFT program

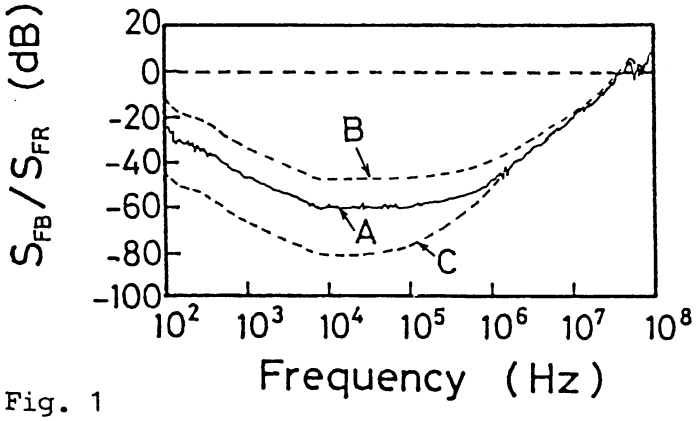


Fig. 1

Power spectral density $S_{FB}$ of frequency fluctuations under feedback, which is normalized to that of the free-running laser $S_{FR}$. A ; experimental result by using a Fabry-Perot cavity of 0.7 MHz linewidth. B, C ; the results of computer simulation by assuming the linewidths $\Delta\nu_{FP}$ of the Fabry-Perot cavity to be 10 MHz and 0.1 MHz, respectively.

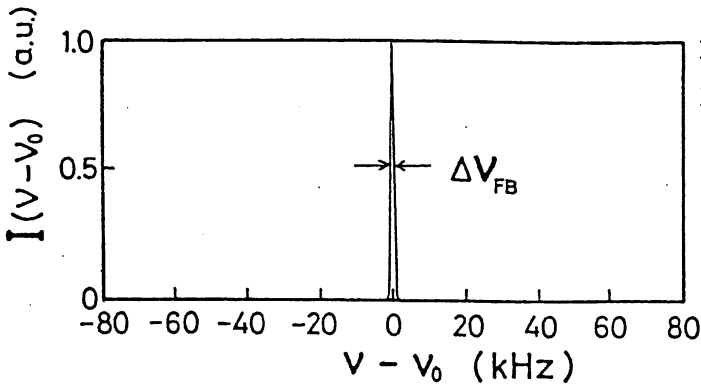


Fig. 2
Profile of the field spectrum of the laser obtained by electrical feedback. The linewidth $\Delta\nu_{FB}$ is 880 Hz.

was employed to estimate such a narrow linewidth by using the value of the curve A. The result is shown by Fig. 2. This figure shows that the linewidth of the field spectrum of the laser was reduced to 880 Hz, which is, to our knowledges, the world's record of the narrowest linewidth of semiconductor lasers. It can be estimated that the linewidth will be reduced to as narrow as 1 Hz by improving the performance of the electrical feedback loop and by utilizing the advanced technology of Opto-Electronic Integrated Circuit ( OEIC ) in the future.

## 4. Frequency Tracking of the Slave Laser

Frequency of the slave laser can be tracked to that of the master laser by employing the technique of frequency offset locking[3]. In the present experiment, the slave laser frequency was controlled by electrical feedback in order that the phase of the beat signal between the two lasers was locked to that of the signal from the local microwave oscillator. A slow and fast feedback loops were used simultaneously. The slow feedback loop was used to suppress the drift in the beat frequency. This loop had a digital phase comparator with a dynamic range as wide as $2\pi \times 2^{11}$ (rad) to realize a wide capture range of the tracking loop. The fast feedback loop had an analog phase comparator of the 5 MHz bandwidth. Figure 3 shows the experimental result of the square root of the Allan variance $\sigma_{yB}^2(\tau)$ of the beat frequency fluctuations. The minimum of $\sigma_{yB}(\tau)$ was $1.7 \times 10^{-15}$ at $\tau$ = 1000 (s), which corresponded to 0.6 Hz fluctuation. Since this value was far lower than the value of frequency fluctuations of the master laser ( see section 1 ), it was confirmed that the slave laser frequency tracked the master laser frequency accurately, or, in other words, high coherence of the master laser was transferred to the slave laser.

Capture range of this feedback loop depended on the division rate M of the beat frequency provided by the prescaler, and the maximum capture range was 1.8 GHz which was obtained at M = 2,000.
Furthermore, as will be shown in the next section, the locking range was 2GHz. The broken curve in this figure represents the beat frequency

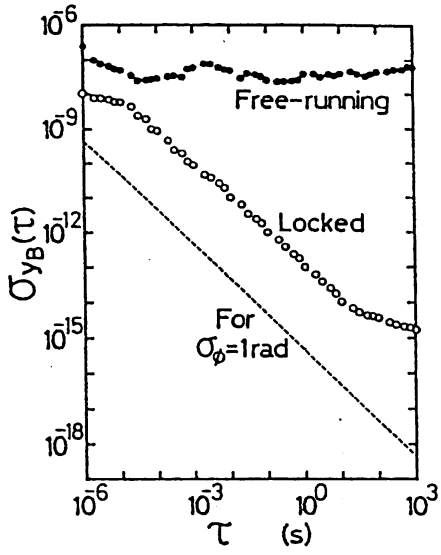


Fig. 3
The square root of the Allan variance $\sigma_{yB}{}^2(\tau)$ of the frequency fluctuations of the beat signal obtained by frequency tracking.

fluctuations which is required to realize 1 radian phase fluctuations of the beat signal. That is, the heterodyne-type optical phase locked loop can be realized if the beat frequency fluctuations will be reduced to this value. This experiment is now in progress[4].

## 5. Frequency Sweep of the Slave Laser

The beat frequency and the slave laser frequency can be swept accurately and in a very stable manner if the frequency of the local microwave oscillator is swept under the condition of the frequency tracking of the section 4. The beat frequency was swept continuously for the range of 2GHz in the present experiment. It corresponds to the locking range of the frequency tracking loop, which was limited by the bandwidth of the photodetector for the beat signal detection. The stability of the beat frequency was as high as that of Fig. 3, which was independent of the value of the beat frequency within this locking range.

The range of stable frequency sweep of the slave laser can be increased by achieving discrete tuning of the master laser frequency by locking it to successive frequencies of a frequency reference grid which are nearly equally spaced. For each locked frequency of the master laser, frequency tracking loop is applied to the slave laser. By this control scheme, a stable and accurate sweep of the slave laser frequency can be realized. In the present experiment, equally spaced resonance frequencies of a Fabry-Perot interferometer were used as a simple frequency reference grid. The master laser frequency was locked to 16 successive resonance frequencies, and as a result of it, the total range of the continuous sweep of the slave laser frequency was increased to 60 GHz. This range was limited by the discontinuous mode-hopping phenomenon of the AlGaAs laser[5]. If the improved single-longitudinal-mode laser, e.g., the DFB

laser will be used, it can be estimated that this range will be increased to as wide as 1 THz.

## 6. Summary

Table 1 summarizes the present status of the experimental results for the four problems and the estimated values which may be realized in the future. It is seen from this table that the performances of the semiconductor lasers have been improved to as high as, or even higher than, those of carefully designed gas or dye lasers. Further improvements can be expected by improving the electrical feedback loop and laser devices.

Table 1.
Present status of the experimental results for the four problems, and their estimated values which may be realized in the future.

| Problem | Present | Future |
|---|---|---|
| (1) Center frequency stabilization | $2 \times 10^{-12}$ ( at $\tau$ = 100 s ) | $1 \times 10^{-15}$ |
| (2) Linewidth reduction | 880 Hz | 1 Hz |
| (3) Frequency tracking | $1.7 \times 10^{-15}$ ( at $\tau$ = 1000 s ) | $1 \times 10^{-17}$ |
| (4) Frequency sweep | 60 GHz | 1 THz |

## Acknowledgments

The authors wish to thank Dr. L. Hollberg of NBS, Boulder, for many useful discussions regarding a high finesse Fabry-Perot cavity.

## References

1. M. Ohtsu and T. Tako, "Coherence in semiconductor lasers", in Progress in Optics, ed. by E. Wolf, Vol. XXV, ( Elsevier, Amsterdam, 1988 )
2. M. Ohtsu, J. Lightwave Technol., 6, 245 (1988)
3. K. Kuboki and M. Ohtsu, IEEE J. Quantum Electron., QE-23, 388 (1987)
4. C.H. Shin, K. Kuboki, and M. Ohtsu, Trans. IEE of Japan, 108-C, (1988), August issue, in press ( in Japanese )
5. M. Ohtsu, Y. Teramachi, Y. Otsuka, and A. Osaki, IEEE J. Quantum Electron., QE-22, 535 (1986)

**TUD4 Novel frequency control scheme for a 1.56-$\mu$m DFB laser using an internal second harmonic and an atomic rubidium line**

M. OHTSU, E. IKEGAMI, Tokyo Institute of Technology, Graduate School at Nagatsuta, 4259 Nagatsuta, Midori-ku, Yokohama, Kanagawa 227, Japan.

Frequency stabilization of 1.5-$\mu$m semiconductor lasers is important for coherent optical communication systems. Such stabilizations have been carried out by using gaseous organic molecules ($NH_3$,$H_2O$, etc.) as frequency references.[1] However, their low absorption coefficients and the difficulty of spectral assignments limit the sensitivity of frequency discrimination and frequency reproducibility. On the other hand, atomic spectra offer fewer, but relatively stronger lines, which can be easily identified to facilitate their use as reliable frequency references in lightwave communication systems. We propose a novel and simple method of frequency stabilization of a 1.5-$\mu$m DFB laser, whose internal second harmonic (ISH) frequency was locked onto an atomic rubidium ($^{87}$Rb) spectral line. Although the ISH itself has been observed for other semiconductor lasers,[2,3] the present work is, to our knowledge, the first report of the quantitative evaluation and application of the ISH of a 1.5-$\mu$m single-mode DFB laser.

Figure 1 shows a simple experimental setup. A single-longitudinal-mode 1.56-$\mu$m InGaAsP DFB laser[4] was used, and the temperature of its heat sink was regulated within 1 mK at room temperature. Since the laser material had a large second-order nonlinear susceptibility and the optical field strength in the laser cavity is strong enough, an ISH of 780-nm wavelength could be generated. By passing this ISH through a compact glass cell (35 mm long) of a $^{87}$Rb atomic vapor, the absorption spectral profile in $^{87}$Rb was measured. To lock the ISH frequency to the center of this spectral profile, the laser frequency was modulated by dithering the injection current, and a lock-in amplifier was used to obtain the first derivative of this spectral profile to use as the FM noise discriminator. After the output signal from the lock-in amplifier was processed by a proportional amplifier and an integrator, the error signal was added to the injection current. The output signal from the lock-in amplifier was sent also to the Allan variance real time processing system to estimate the frequency stability.

The measured relationship between the fundamental radiation power of the laser $P_f$ and its ISH power $P_{ish}$ was $P_{ish} = 2.0 \times 10^{-8} \times P_f^2$ ($P_f$, $P_{ish}$, expressed in watts). Although the maximum of $P_{ish}$ was as low as 2.0 pW, it was high enough to be measured by a conventional photomultiplier or even by a compact Si APD, which made the experimental setup simple.

Figure 2 shows the first derivative of the $^{87}$Rb $D_2$ spectral lines measured by the ISH. Two spectral components in this figure correspond to the transitions from the hyperfine levels of $F = 1$ and 2 in the ground state. It can be confirmed from this figure that the spectral profiles were measured with a high SNR. Frequency of the ISH was locked to the center of the transition from the $F = 2$ level (point $A$ in Fig. 2).

Figure 3 shows the square root of the Allan variance $\sigma_y^2(\tau)$ of the ISH frequency fluctuation, which corresponds also to the frequency stability of the 1.56-$\mu$m fundamental radiation. Comparison between curves $A$ and $B$ shows that the frequency stability was improved substantially by the present frequency control scheme. The minimum of $\sigma_y$ on curve $A$ was $9.0 \times 10^{-12}$ at an integration time $\tau$ of 100 s, which is 1/3 times that obtained by using the $NH_3$ molecular vapor as a frequency reference.[1] This is attributed to a strong absorption in $^{87}$Rb atoms, from which it was confirmed that the present method is very useful for realizing a high frequency stability. The present frequency control scheme by using ISH opens the possibility of frequency tracking of a 1.5-$\mu$m DFB laser to an AlGaAs laser, and thereby a frequency tuning range as wide as 10 THz is expected in the future by using a frequency offset locking technique.[5]

**(12 min)**

1. M. Ohtsu, H. Kotani, and H. Tagawa, Jpn. J. Appl. Phys. **22**, 1553 (1983).
2. T. Furuse and I. Sakuma, Opt. Commun. **35**, 413 (1980).
3. N. Ogasawara, R. Ito, H. Rokukawa, and W. Katsurashima, Jpn. J. Appl. Phys. **26**, 1386 (1987).
4. K. Kihara *et al.*, Electron. Lett. **23**, 941 (1987).
5. M. Ohtsu, IEEE/OSA J. Lightwave Technol. **LT-6**, 245 (1988).

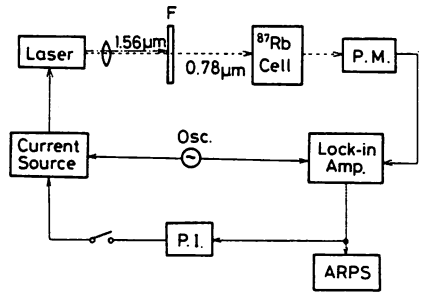


TUD4 Fig. 1. Experimental setup: *F*, infrared cut filter; *P.M.*, photomultiplier; *P.I.*, proportional amplifier and integrator; ARPS, Allan variance real time processing system.

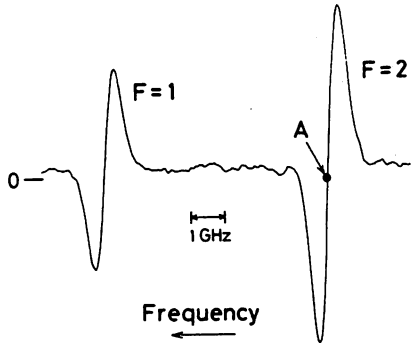


TUD4 Fig. 2. First derivative signal of the $^{87}Rb$ $D_2$ spectral line. The ISH frequency was locked at point *A*.

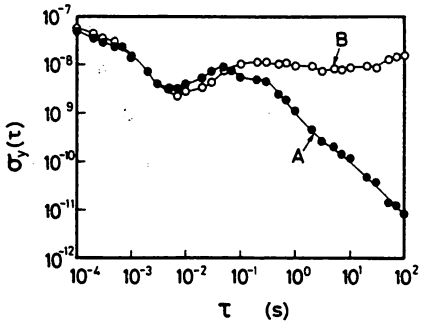


TUD4 Fig. 3. Square root of the Allan variance $\sigma_y^2(\tau)$ of the frequency fluctuations: *A*, frequency stabilized lasers; *B*, free-running laser.

**THK30 Subkilohertz linewidth of a semiconductor laser by electrical feedback and its network analysis**

M. OHTSU, M. MURATA, M. KOUROGI, Tokyo Institute of Technology, Graduate School at Nagatsuta, 4259 Nagatsuta, Midori-ku, Yokohama, Kanagawa 227, Japan.

Narrow linewidth semiconductor lasers are key devices for coherent optical measurement and communication systems. The authors believe that electrical feedback is a promising technique for reducing the linewidth in a very stable manner.[1] It is proposed that wideband electrical feedback can be realized by using reflected light from a high finesse Fabry-Perot cavity, and subkilohertz linewidths can be obtained. The experimental setup is shown in Fig. 1. A 0.8-$\mu$m wavelength AlGaAs laser (CSP type) was used. The slope of the resonance curve of the reflected light from a super Fabry-Perot cavity (finesse = 8600; linewidth of the resonance curve, $\Delta\nu_{F.P.}$ = 0.7 MHz) was used as a sensitive FM noise for the wideband feedback loop. Comparing the transfer characteristics of the frequency discrimination of the reflected light with that of the transmitted light, the passband of the reflected light is wider, and the slope of its transition band is improved by 20 dB/decade. Furthermore, phase-lead compensation is shown in the transition band, which allows a substantial increase in feedback gain and bandwidth.

Thus the reflected light acts as the first-order differentiator. This is why the reflected light was chosen as the frequency discriminator. Total delay time in the feedback loop was 1.2 ns. Transfer functions of the laser and associated feedback elements were estimated by measurement or calculation. By network analysis based on these results, optimum design of the phase compensating circuit was carried out to realize the maximum gain and bandwidth of the feedback.

Curve *A* of Fig. 2 represents the experimental result of the power spectral density $S_{FB}(f)$ of the residual FM noise obtained by using such an optimized feedback loop. In this figure, $S_{FB}(f)$ was normalized to the power spectrum density $S_{FR}(f)$ of the free-running laser. Curve *A'* represents the experimental result obtained by using the conventionally transmitted light from the same Fabry-Perot cavity as the frequency discriminator. Comparison between curves *A* and *A'* shows that a wider bandwidth and larger reduction of FM noise was realized by using the reflected light from the Fabry-Perot cavity. The minimum on curve *A* was −60 dB. A result of computer simulation by using a measured value of the loop transfer function agreed with curve *A*, which confirms the high accuracy of the present network analysis.

Curves *B* and *C* represent the results of a computer simulation by using reflected light from the Fabry-Perot cavity, where the values of $\Delta\nu_{F.P.}$ were assumed to be 10 and 0.1 MHz, respectively. Comparison among curves *A*, *B*, and *C* shows that a larger reduction of the FM noise is realized by using a narrower $\Delta\nu_{F.P.}$ while maintaining the feedback bandwidth almost constant. This is an advantage of using reflected light from the Fabry-Perot cavity.

A FFT program was employed to estimate accurately a profile of the field spectrum of the laser oscillation by using curve *A* of Fig. 2. The result is shown in Fig. 3. The linewidth of this spectral shape is 880 Hz, which is 1/1000 times that of the Schawlow-Townes limit. This can be, to the authors' knowledge, the world's record for the narrowest linewidth of semiconductor lasers including the results of various optical feedback techniques. Compared with the optical feedback technique, the present electrical feedback technique is more stable because it employs negative feedback. The narrow linewidth of Fig. 3 was maintained constant for several hours as long as the feedback loop was closed.

It can be estimated that the linewidth would be reduced to as narrow as 1 Hz (detector shot-noise-limited value[2]) by further reductions of the delay time of the feedback loop if an advanced technology OEIC is utilized. **(Poster paper)**

1. M. Ohtsu and S. Kotajima, IEEE J. Quantum Electron. **QE-21,** 1905 (1985).
2. M. Ohtsu, IEEE/OSA J. Lightwave Technol. **LT-6,** 245 (1988).

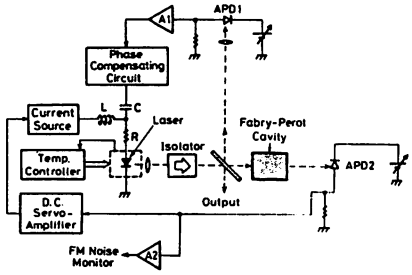


THK30 Fig. 1. Experimental setup.

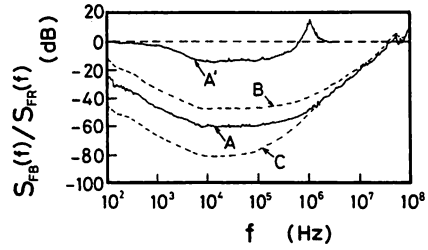


THK30 Fig. 2. Power spectral density $S_{FB}(f)$ of residual FM noise in feedback conditions. This value was normalized to the power spectral density $S_{FR}(f)$ of the free-running laser: *A*, *A'*, experimental results obtained by using the reflected light and transmitted light from the Fabry-Perot cavity of $\Delta\nu_{F.P.}$ = 0 7 MHz, respectively; *B*, *C*, results of computer simulation by using a reflected light from the Fabry-Perot cavity where the values of $\Delta\nu_{F.P.}$ were assumed to be 10 and 0.1 MHz, respectively.

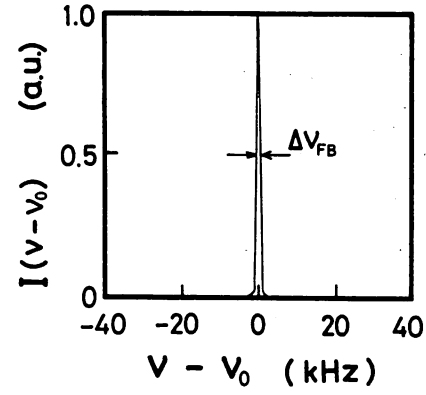


THK30 Fig. 3. Field spectrum of the laser oscillation under feedback, which was estimated by the FFT program based on the power spectral density given by curve *A* of Fig. 2. The linewidth $\Delta\nu_{F.B.}$ of this spectrum was 880 Hz.

**19A3-1** (Invited)

# Progress toward Highly Coherent Semiconductor Lasers

Motoichi Ohtsu

Graduate School at Nagatsuta, Tokyo Institute of Technology
4259 Nagatsuta, Midori-ku, Yokohama 227, Japan

<SUMMARY>

1. Introduction Highly coherent semiconductor lasers, especially coherent optical sweep generators, have been required for several applications such as optical communication, fiber gyroscopes, and so on[1]. We review here our recent studies on improvement of the coherence in semiconductor lasers. A technique of electrical feedback was employed because (a) stability and reliability of the feedback is high, (b) computer simulation can be employed to design the optimum feedback loop, (c) magnitude of the FM noise can be reduced to a value which is far lower than that of the quantum noise limit of the free-running laser. To realize a simple coherent laser modules, a technique of optical feedback was also used. Four problems given by the titles of the following sections should be solved simultaneously to realize a highly coherent optical sweep generator by using semiconductor lasers.

2. Frequency Stabilization of the Master Laser A slow electrical feedback was applied to the master laser to stabilize the center frequency of its field spectrum, and the stability of $2 \times 10^{-12}$ was obtained by using the absorption spectral line in Rb vapor as a frequency reference. The frequency stability limited by the shot noise of the photodetector ( $1 \times 10^{-15}$ ) can be expected to accomplish by improving the performances of the feedback loop[2]. For 1.5 μm InGaAsP lasers, a technique of second harmonic generation was employed to stabilize its frequency to a reliable reference frequency provided by the Rb vapor[3].

3. Linewidth Reduction of the Master Laser The linewidth of the field spectrum of the master laser can be reduced by a fast electrical feedback loop. A slope of the resonance curve of the reflected light from a high finesse Fabry-Perot cavity was used as a sensitive FM noise discriminator to realize a high-gain and wideband feedback loop. This is because the reflected light from the Fabry-Perot cavity acts as the first order differentiator for the fluctuating optical frequency. Figure 1 shows the experimental results for an AlGaAs laser obtained by using the optimized feedback loop. The curve A represents the power spectral density of the FM noise of a free-running laser. The curve B represents a preliminary result obtained by using a low finesse Fabry-Perot cavity. The curve C is the result obtained by using the high finesse Fabry-Perot cavity ( finesse =3,500 ). By comparing the curve C with the curve A, it is found that the FM noise reduction was as large as 80 dB. From such a large FM noise reduction, a very narrow linewidth of the field spectrum of the laser can be expected. FFT program was employed to estimate such a narrow linewidth by using the value of the curve C. As a result, it was found that the linewidth was reduced to 700 Hz. As shown by Fig. 2, this linewidth is far narrower than the quantum noise limit ( coherent state ) of the free-running laser, i.e., hyper-coherent state was realized. It can be estimated that the linewidth will be reduced to as narrow as 1 Hz by improving the performance of the electrical feedback loop and by utilizing the advanced technology of Opto-Electronic Integrated Circuit in the future.

As an alternative approach, optical feedback from an external Fabry-Perot cavity was used to reduce the linewidth. This technique provided the linewidth as narrow as 11 kHz, a good long-term locking stability, and frequency modulation capability. Its miniature-packaged version was devised by using a technique of fiber-optics or micro-optics. They would be useful as practical light sources for coherent lightwave system.

4. Frequency Tracking of the Slave Laser The slave laser can frequency-track the master laser by electrical feedback loop, in which the phase of the beat signal between the two lasers is locked to that of the signal from the local microwave oscillator. Figure 3 shows the measured value of the Allan variance of the beat frequency fluctuations. Its minimum was $1.7 \times 10^{-15}$ at the integration time of 1,000 (s), which corresponded to 0.6 Hz fluctuation. Since this value was far lower than the value of frequency fluctuations of the master laser, it was confirmed that the slave laser frequency tracked the master laser accurately. The capture range and locking range of this frequency tracking loop were as large as 1.8 GHz and 2 GHz, respectively. The broken curve in this figure represents the beat frequency fluctuations which is required to realize 1 radian phase fluctuation of the beat signal. That is, the heterodyne-type optical phase locked loop can be realized if the beat frequency fluctuation will be reduced to this value.

5. Frequency Sweep of the Slave Laser The beat frequency and the slave laser frequency can be swept accurately and in a very stable manner if the frequency of the local microwave oscillator

is swept under the condition of the frequency tracking given by the section 4. The beat frequency was swept continuously for the range of 64 GHz. This range was limited by mode-hopping of the AlGaAs laser. If the improved single-longitudinal-mode lasers and wavelength conversion by nonlinear optical effects will be used, it can be estimated that this range will be increased to as wide as 10 THz.

6. Summary Hyper-coherent state of the semiconductor lasers was realized by reducing its FM noise. The magnitude of this noise was as low as, or even lower than, those of carefully designed gas or dye lasers. Further improvements can be expected by improving the performances of the electrical feedback loop and laser devices. Table 1 summarizes the present status of the experimental results for the four problems and the estimated values which may be realized in the future.

References


[1] M. Ohtsu and T. Tako, "Coherence in Semiconductor Lasers", in Progress in Optics, ed. by E. Wolf, Vol. XXV, ( Elsevier, Amsterdam, 1988 )

[2] M. Ohtsu, J. Lightwave Technol., 6 (1988) pp.245-256

[3] M. Ohtsu and E. Ikegami, Electron. Lett., 25, (1989) pp.22-23


Table 1.
Present status of the experimental results for the four problems, and their estimated values which may be realized in the future.

| Problem | Present | Future |
|---|---|---|
| (1) Center frequency stabilization | $2 \times 10^{-12}$ | $1 \times 10^{-15}$ |
| (2) Linewidth reduction | 700 Hz | 1 Hz |
| (3) Frequency tracking | $1.7 \times 10^{-15}$ | $1 \times 10^{-17}$ |
| (4) Frequency sweep | 64 GHz | 10 THz |

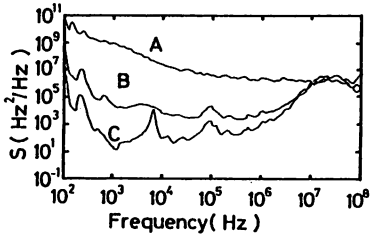


Fig. 1
Power spectral density of the FM noise of an AlGaAs laser. Curve A : Free-running. B : Result of preliminary electrical feedback using a low finesse Fabry-Perot cavity. C : Result of electrical feedback by using a high finesse Fabry-Perot cavity.

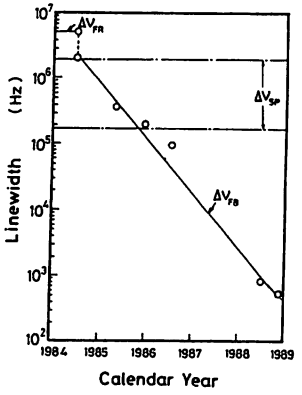


Fig. 2
Progress of the experiments on linewidth reduction by electrical feedback. $\Delta\nu_{FR}$ : Linewidth of the free-running laser. $\Delta\nu_{FB}$ : Linewidth obtained by electrical feedback. $\Delta\nu_{SP}$ : Linewidth limited by spontaneous emission, where the value of $\alpha$-parameter was assumed to be 1.3 ~ 5.4.

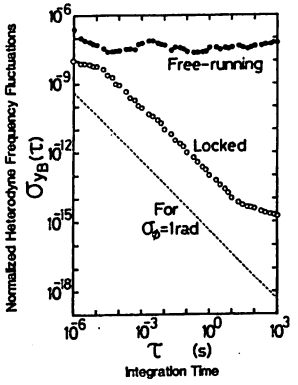


Fig. 3
The Allan variance of the beat frequency fluctuations in the frequency tracking loop.

21D4-5

# Modulatable, High Coherent and Compact Semiconductor Laser Modules

Chul-Ho Shin, Mitsuhiro Teshima, Motoichi Ohtsu,

Graduate School at Nagatsuta, Tokyo Institute of Technology
G2-806, 4259 Nagatsuta, Midori-ku, Yokohama 227, Japan

Tohru Imai, Junichi Yoshida, and Kenichi Nishide

Tokyo Aircraft Instrument Co.,Ltd.
35-1, Izumi-Honcho, 1-Chome, Komae-Shi, Tokyo 201, Japan

〈SUMMARY〉

Miniature-packaged semiconductor lasers(SL), which have frequency modulation (FM) capability and high spectral purity with long-term frequency stability, are required to use as optical local oscillators and/or light sources in coherent communication systems and optical measurements. In this presentation, we report semiconductor laser modules having such performances.

Fig.1 shows a basic experimental setup of the semiconductor laser module coupled off-axis with a confocal Fabry-Perot(CFP) cavity. Such an external cavity acts as an optical bandpass filter for the laser light which is spectrally purified by the resonance[1-4]. And then, a part of cleaned light field built within the cavity returns to the laser through the cavity input mirror at resonance. The oscillating frequency of the laser, thus, locks to the resonance of this CFP cavity, i.e., optical self-locking takes place. Thereby, spectral linewidth becomes very narrow, and center frequency is also stabilized substantially.

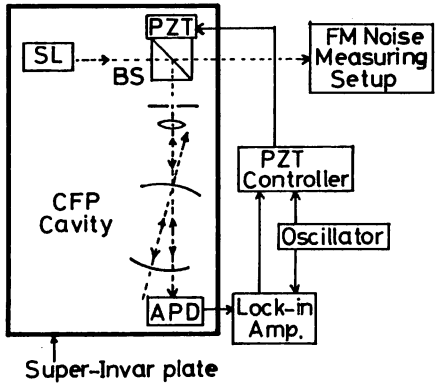


Fig.1 Schematic diagram of CFP-SL. Laser was a 0.83μm CSP-type commercial semi-conductor laser. The finesse of CFP cavity was 75.

The frequency locking range of the CFP-SL was as wide as about 500 MHz with moderate feedback level, where the free spetral range(FSR) of the CFP cavity was 1.5 GHz. The system can, thus, endure fluctuations of the injection current and the temperature of the laser mount. Furthermore, by the control of the voltage applied to the PZT attached under the beam splitter (BS) using the simple control loop as shown in Fig.1 , good phase locking was maintained stably during 3 hours until the time opened the loop. This loop was enough to absorb thermal and mechanical instabilities of the locking mechanism.

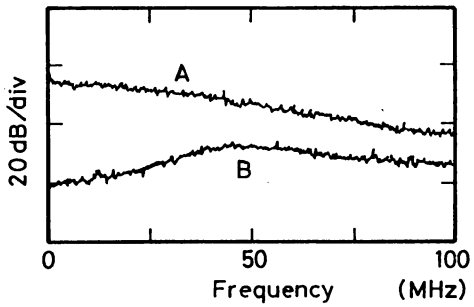


Fig.2 Power spectral density of FM noise. Curves A and B are for free-running and for optical locking, respectively.

The linewidth of the CFP-SL was 11 kHz at the bias level of 1.3-1.4 times the threshold current value. This linewidth was measured by heterodyning between two CFP-SLs. The linewidth at free running was about 25MHz. Fig.2 shows an example of power spectral density(PSD) of the frequency noise measured by using another FP cavity as a frequency discriminator. The reduction ratio of frequency noise of a part of Fourier frequency lower than 45 MHz is much larger than that of Fourier frequency higher than 45 MHz. The curve B in Fig.2 shows well the characteristics of optical bandpass filtering of the CFP cavity, of which the 3 dB bandwidth is about 10 MHz as seen from the curve B.

If the modulation frequency is a rational number times the FSR of the CFP cavity, the CFP-SL can be modulated with high efficiency at higher modulation speed. And, the CFP-SL can generate the high coherent

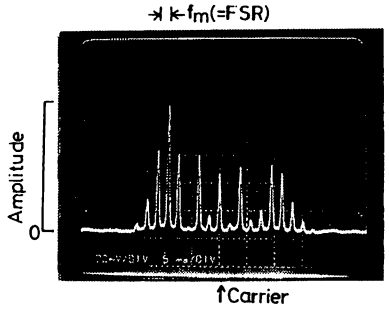


Fig.3 Coherent lightwave array generated by the direct modulation of the injection current. It was monitored by a scanning FP interferometer.

lightwave array (FM sidebands) with equal frequency interval by the direct modulation of the injection current. This is because optical sidebands at only those frequencies are simultaneously resonant with the cavity and are fed back to the laser with the carrier. Thereby every sidebands maintain the narrow linewidth and the center frequency stabilization. Fig.3 shows a coherent lightwave array, where the modulation frequency was equal to the FSR, and FM efficiency was as high as 1.1 GHz/mA. It can be pointed out that such the equally spaced coherent optical sidebands are applied as light sources of transmitters and optical local oscillators in FDM coherent communication systems.

Alternatives of the CFP-SL were devised. One is employing a hemisphere micro-cavity(HMC) in Fig.4(a), and the other is a fiber optics cavity(FOC) in Fig.4(b). The diameter of the HMC was 10mm, and the reflectivity was 90%. The reflectivity of the FOC was about 90% at Al coated both ends, and the length of the FOC was 1 m. The laser light was coupled with the FOC by a 9:1 fiber coupler, of which the coupling end with the laser and the output end were cut with inclines of 4 and 8 degrees, respectively, for preventing the direct reflection from fiber ends. The miniature-packaged HMC-SL module is shown in Fig.4(c). By this packaging, its performance became more stable and convenient to use.

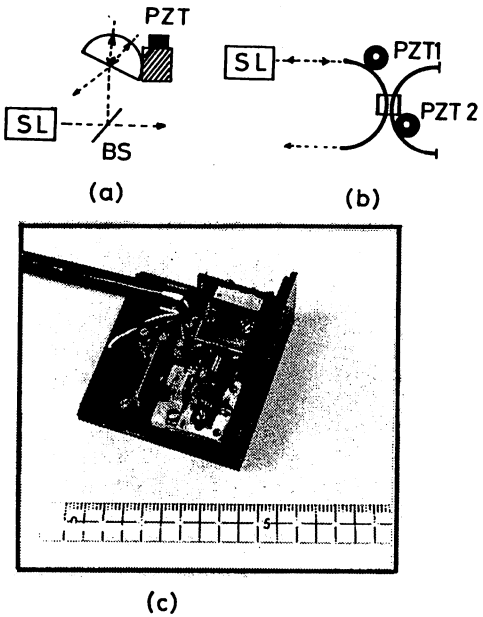


Fig.4 Alternatives of the CFP cavity in Fig.1. (a)Hemisphere micro-cavity(HMC). (b)Fiber optics cavity (FOC). (c) Miniature-packaged module of HMC-SL. Size 50 mm(L) x 50 mm(W) x 30 mm(H).

The frequency stability of FOC-SL can also be improved by packaging the FOC on the temperature controlled copper block, where the laser is mounted on.

Phases of feedback light from the HMC and the FOC could be controlled stably by the voltage control applied to the PZT in Fig.4(a) and PZT1 in Fig.4(b), respectively. In case of the FOC-SL, slower FM with the modulation frequency less than several kHz was possible by using the PZT2 in Fig.4(b). Such a slow modulation may be useful when it is used as the light source of optical measurement, e.g., a passive ring cavity fiber gyroscope[5] or in frequency/phase locking with another light signal. Linewidths of less than 40 kHz as shown in Fig.5 and less than 70 kHz were obtained by optical feedback from the HMC and the FOC, respectively.

In conclusion, we realized a CFP-SL having very good long-term locking stability, linewidth as narrow as 11 kHz, frequency modulation capability and devised the HMC-SL and the FOC-SL. Furthermore we developed the miniature-packaged version of the HMC-SL. It is expected that these high coherent semiconductor laser modules would be useful as light sources of the coherent lightwave systems.

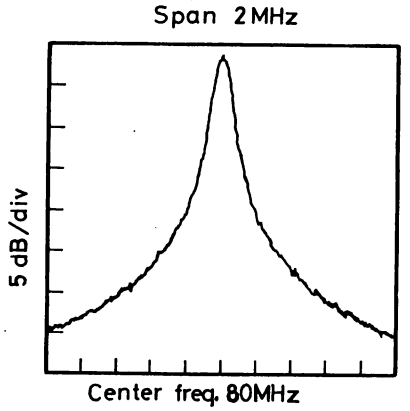


Fig.5 Beat note of the HMC-SL under locking measured by the delayed self heterodyne method with a optical fiber of 2 km long.

<REFERENCES>

[1]B.Dahmani, L.Hollberg and R.Drullinger, Opt.Lett.,12,876 ,1987
[2]L.Hollberg and M.Ohtsu, Appl.Phys.Lett.,53,944,1988
[3]Ph.Laurent,A.Clairon and Ch.Brent,IEEE JQE,to be published,1989
[4]C.H.Shin, M.Teshima and M.Ohtsu, Electron.Lett, 25, 27, 1989
[5]M.Ohtsu and S.Araki, Appl.Opt., 26, 464, 1987

# Analyses of Mode Partition and Mode Hopping in Semiconductor Lasers

MOTOICHI OHTSU, MEMBER, IEEE, AND YASUAKI TERAMACHI

*Abstract*—**This paper discusses mode power fluctuations in semiconductor lasers due to mode partition and mode hopping by comparing the results of precise measurements to those of theoretical analysis. The power dropout probability $P_e$ in the mode partition was measured for a wide range, $1.6 \times 10^{-6} \leqq P_e \leqq 1$, which decreased by increasing $I/I_{th}$ (the bias level; $I$ and $I_{th}$ are the dc injection current and its threshold value, respectively). The duration time $t_d$ of the power dropout depended on the bias level, which was approximately expressed as $t_d = 3.7 \times 10^{48} \exp[-118\,(I/I_{th})]$ for $1.065 \leqq I/I_{th} \leqq 1.104$. Power fluctuations exhibited specific characteristics around the threshold, which were similar to the critical slowing down in the phase transition phenomenon. An increase in the variance of the power fluctuations was observed when the laser oscillating condition was converted from mode partition to mode hopping. The unified stochastic model based on the Fokker–Planck approach described well both mode partition and mode hopping. By comparison between the experimental and theoretical results, it was found that characteristics of the power fluctuations at a high bias level can be estimated from the experimental results at a low bias level.**

## I. Introduction

POWER fluctuations in semiconductor lasers are one of the fundamental causes for limiting the performances of optical communication and optical measurement systems. For example, two longitudinal modes in a Fabry–Perot cavity-type semiconductor laser can oscillate when it is operated under CW conditions with certain values of dc injection current and heat sink temperature. However, in this case, temporal variations of the two mode powers exhibit random switching by nonlinear coupling between the two modes, i.e., the mode hopping phenomenon is observed [1]. On the other hand, this laser exhibits nearly single-longitudinal-mode oscillation with different values of injection current and heat sink temperature. In this case, temporal variation of the main mode power exhibits a power dropout phenomenon induced by the nonlinear coupling with the transiently oscillating side modes [2]. This phenomenon is called mode partition [3] and can be observed even in a carefully fabricated single-longitudinal-mode distributed feedback laser [4]. By this phenomenon, it should be noted that there are always unwanted vestigial side modes; single-longitudinal-mode semiconductor lasers can only be approximated. Therefore, analyses of mode coupling and mode power fluctuations should be considered as fundamental and important subjects to be investigated for designing stable semiconductor lasers and for understanding semiconductor laser dynamics.

Mode partition and mode hopping originate from random fluctuations of spontaneous emission as well as from nonlinear gain supression and mode coupling due to inter- and intraband relaxations of the carriers. Since power fluctuations due to mode partition would deteriorate the performance of optical communication systems [5], the statistical properties of these fluctuations have been measured [3]. Furthermore, a model based on rate equations has been presented for theoretical analysis [6]. However, unsolved problems in the previous work on mode power fluctuations can be listed as follows.

1) Criteria for designing single-longitudinal-mode lasers have been limited to giving a cavity loss difference between the competing longitudinal modes [7]. Furthermore, the effect of spontaneous emission fluctuations has been neglected. However, contributions from fluctuations of spontaneous emission should be taken into account for quantitative evaluation because these fluctuations work as the triggering forces for mode partition.

2) In the theoretical models presented so far [6], the origins of mode coupling have not been clearly shown.

3) Since experiments [3] and theoretical analysis [6] have been carried out by different authors, correspondence between them has not been sufficiently discussed.

4) Experimental results of power dropout probability $P_e$ for mode partition reported by several authors have been scattered, e.g., the results by Linke *et al.* are $1 \times 10^{-7} \leqq P_e \leqq 1 \times 10^{-4}$ [2] and those by Ohtsu *et al.* are $1 \times 10^{-3} \leqq P_e \leqq 1$ [8]. The causes of this scattering and the dependence of $P_e$ on the operating conditions of the lasers have not been fully discussed.

5) Experimental results on the duration time $t_d$ of power dropout reported by several authors have also been scattered. The values reported by Linke *et al.* are about 1 ns [2], while those by Ohtsu *et al.* [8] are about 1 $\mu$s [8]. The causes of this scattering have not been discussed.

6) Mode partition and mode hopping have been discussed separately. Theoretical models for describing both of these phenomena systematically have not been presented.

In the present work, discussions focused on points 1)–6) by comparing the results of precise measurements

Manuscript received August 16, 1988.

M. Ohtsu is with the Graduate School at Nagatsuta, Tokyo Institute of Technology, 4259 Nagatsuta, Midori-ku, Yokohama 227, Japan.

Y. Teramachi is with the Institute of Vocational Training, 1960 Aihara, Sagamihara, Kanagawa 229, Japan.

IEEE Log Number 8824380.

for power fluctuations and theoretical analysis based on the stochastic model. The relation between mode partition and mode hopping is also investigated. Furthermore, characteristics of the mode power fluctuations are discussed by analogy with the phase transition phenomenon in thermodynamics.

## II. Experimantal Apparatus

Fig. 1 shows the experimental apparatus. A Fabry–Perot cavity-type AlGaAs laser (channeled-substrate-planar type, Hitachi HL7802E) of 0.8 $\mu$m wavelength was employed for the experiments because this type of laser exhibits mode partition or mode hopping at appropriate values of dc injection current and temperature. The laser was installed in a small vacuum chamber, and the temperature of the heat sink for the laser, made of a copper block, was electronically controlled using a Peltier element and a thermistor sensor. As a result of this control, temperature fluctuations of the heat sink were reduced to $4 \times 10^{-4}$ K. The laser was driven by a low-noise dc current source with a current noise (root mean square (rms) value) of 0.6 nA/$\sqrt{\text{Hz}}$ at the Fourier frequency of 1 kHz. Average CW mode powers were measured by a conventional grating monochromator and a silicon avalanche photodiode (Si-APD) followed by a dc amplifier. For the measurements of the dynamic properties of mode power fluctuations, these mode powers were detected by Si-APD's after being separated spatially by a diffraction grating. After the photocurrent from the Si-APD was amplified by an amplifier of 100 MHz bandwidth, it was recorded by means of a two-channel digital memory or monitored by a wide-band oscilloscope. The bandwidth of the digital memory was 25 MHz. Although this bandwidth is narrower than that of the amplifier, it was enough for measuring the duration time $t_d$ of power dropout when the laser was operated at a low bias level. For a shorter duration time $t_d$ observed at a higher bias level, an oscilloscope of 350 MHz bandwidth was used for the measurements. It was confirmed by the preliminary experiments that results of these two measurements of $t_d$ agreed with each other at the crossover region of the bias level. The number of successive data points ($N_d$) stored in the digital memory was 2048, and the number of measurements ($N$) carried out repeatedly was 300. If stationarity of the system was assumed, the total sample number corresponded to $N_d \cdot N$. In this case, the resolution of the measurements of power dropout probability $P_e$ appearing in Section III was $1/N_d \cdot N = 1.6 \times 10^{-6}$.

## III. Experimental Results and Discussions

The open circles in Fig. 2(a) represent a temperature dependence of the threshold current $I_{th}$. The shaded areas given by the heat sink temperature $T$ and the dc injection current $I$ show the regions of individual single-longitudinal-mode oscillation of the laser. Here, the single-longitudinal-mode oscillation was defined as a situation in which the average CW powers of the satellite longitudinal modes were less than 5 percent of that of the main mode

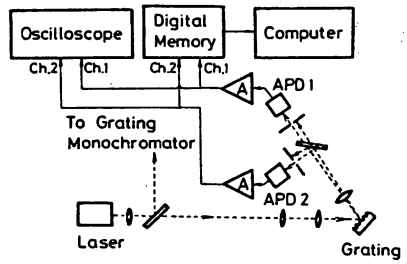


Fig. 1. Experimental apparatus. APD 1 and APD 2 are Si avalanche photodiodes.

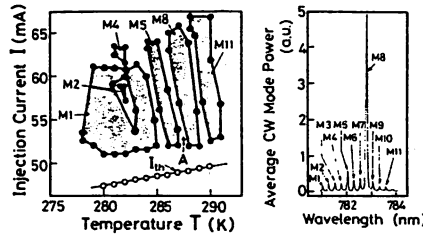


Fig. 2. (a) The shaded areas given by the heat sink temperature $T$ and the injection current $I$ show the regions of individual single-longitudinal-mode oscillation of the laser. Single-longitudinal-mode oscillation was defined as a situation in which the average CW powers of the satellite longitudinal modes were less than 5 percent of that of the main mode when they were measured by a grating monochromator. The numbers M1–M11 in this figure represent a series of longitudinal modes. Open circles in this figure represent the temperature dependence of the theshold current $I_{th}$. (b) Average CW mode power spectra of the longitudinal modes measured by the grating monochromator at point A in (a).

when they were measured by the grating monochromator. The numbers M1–M11 in this figure represent a series of longitudinal modes. Fig. 2(b) shows an example of the average CW power spectra of the longitudinal modes measured by the grating monochromator at the operating point outside of the meshed area, i.e., at point A in Fig. 2(a). Although a nearly single-longitudinal-mode oscillation of mode M8 was realized, several satellite longitudinal modes can still be seen in this figure.

In the following discussions, it is assumed that mode partition is induced by the nonlinear coupling between mode M8 (the main mode) and mode M5 (the side mode) of the second largest average CW power; i.e., the couplings between the main mode and other satellite modes are neglected. Figs. 3–5 show the results of measurements obtained to confirm the validity of this two-mode approximation. The measurements were carried out at operating point A in Fig. 2(a). Fig. 3(a) represents the results of simultaneous measurements of power fluctuations of the main mode (M8) and the side mode (M5) recorded using the digital memory. In this figure, one can see the mode partition phenomenon, i.e., a transient decrease of the main mode power (power dropout) and an increase of the side mode power. Fig. 3(b) gives a phase space, which represents the distributions of the temporal powers of both modes of Fig. 3(a) sampled at time intervals of 10 ns. The total number of data points used for this figure was 2048. It can be noted from this figure that the power fluctuations of both modes were strongly anticorrelated. A phase space

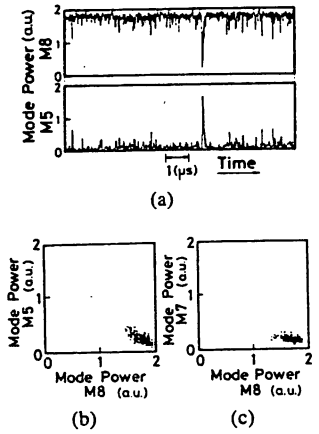


Fig. 3. (a) Results of simultaneous measurement of the power variations of the main mode (M8) and the side mode (M5) using the digital memory. (b) A phase space which represents the distributions of the temporal powers of the modes M8 and M5 of (a) sampled at time intervals of 10 ns. The total number of data points used was 2048. (c) A phase space for modes M8 (main mode) and M7 (one of the other satellite modes).

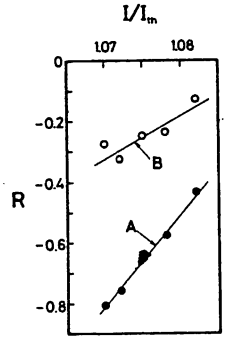


Fig. 4. Relation between the bias level $I/I_{th}$ and the cross-correlation coefficient $R$ between the power fluctuations of two modes. Curve A: Between modes M8 and M5. Curve B: Between modes M8 and M7.

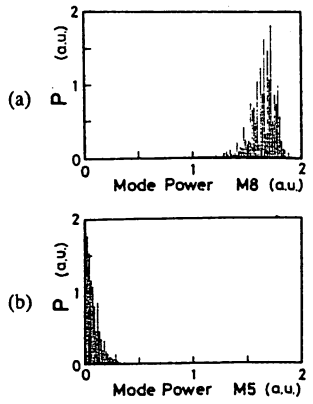


Fig. 5. Histogram, i.e., the probability distributions $P$ of powers obtained from the data points of Fig. 3(b). (a) Main mode (M8). (b) Side mode (M5).

for modes M8 (main mode) and M7 (one of the other satellite modes) is shown in Fig. 3(c). In this figure, however, anticorrelation between the power fluctuations of these two modes is not clearly seen, which means that the two mode powers vary almost independently. The value of cross-correlation coefficient $R$ between the power fluctuations of the two modes were $-0.81$ for Fig. 3(b) and $-0.38$ for Fig. 3(c), respectively; i.e., the absolute value of $R$ for Fig. 3(b) was more than twice that of Fig. 3(c), where all the data points in these figures were used for the calculations. Fig. 4 shows a dependence of $R$ on the bias level $I/I_{th}$ measured at around point A of Fig. 2(a). It is also noted from this figure that the absolute value of $R$ between modes M8 and M5 (curve A in Fig. 4) is always more than twice that between modes M8 and M7 (curve B in Fig. 4). Thus, the validity of the two-mode approximation mentioned above can be made clear from this result. Fig. 5 presents the histogram, i.e., the probability distributions $P$ of the main (M8) and side (M5) mode powers obtained from the data points of Fig. 3(b). The probability distribution of the main mode has a tail at its lower-power side. On the other hand, that of the side mode has a tail at its higher-power side. These tails can be further evidence of the anticorrelation between these modes. The probability distributions given by this figure have also been measured by Liu and Ogawa [3 fig. 1(b)].

The two kinds of measurements given below can be carried out by changing the injection current and temperature around point A in Fig. 2(a) under the conditions of the above-mentioned two-mode approximation. 1) The dependence of mode partition characteristics on the bias level can be measured by changing the bias level while the temperature is maintained constant. 2) The laser oscillating condition can be converted from the mode partition state to the mode hopping state by changing the ratio of average CW powers of the two modes, i.e., by changing the temperature while maintaining the bias level constant. Under this conversion, changes in the characteristics of mode power fluctuations can be measured.

Fig. 6 shows results of the first kind of measurements. This figure presents a relation between the threshold setting $\epsilon$ and the power dropout probability $P_e$ of the main mode. Here, $P_e$ was measured based on the following formula:

$$P_e = \sum_i t_i/T_m \qquad (1)$$

where $t_i$ is a time period in which the ratio between the average CW power $\langle I_1 \rangle$ of the main mode and the magnitude of deviation of the main mode power $I_1 - \langle I_1 \rangle$ exceeds the value $\epsilon$ (i.e., $(|I_1 - \langle I_1 \rangle|)/\langle I_1 \rangle > \epsilon$). $T_m$ represents the total time of a measurement. This measurement was carried out by fixing the bias level to several values around point A in Fig. 2(a) while the temperature was maintained constant. For this measurement, a sampling time $t_s$ for data acquisition by the digital memory was fixed at 10 ns. Linke *et al.* have measured the value of $P_e$ in the range of $1 \times 10^{-7} \leqq P_e \leqq 1 \times 10^{-4}$. (Reference [2, Fig. 2] shows that the measured values of the rate of power dropout events $r$ were between $1 \times 10^2$ ($s^{-1}$) and $1 \times 10^5$ ($s^{-1}$), and the duration time $t_d$ of power dropout measured was about 1 ns. From these values of $r$ and $t_d$, the value of $P_e$ can be estimated as the value given

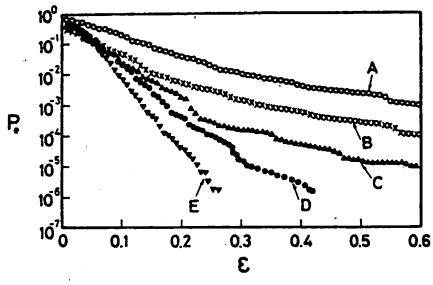


Fig. 6. A relation between the threshold setting $\epsilon$ and the power dropout probability $P_e$ of the main mode estimated using (1). The values of $I/I_{th}$ were A, 1.070; B, 1.072; C, 1.075; D, 1.078; and E, 1.082.

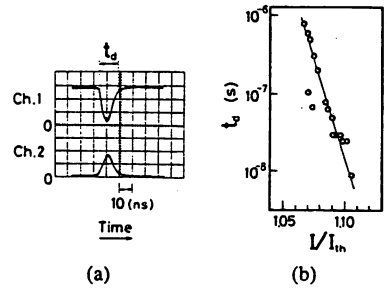


Fig. 7. (a) Oscilloscope traces of the waveforms of power fluctuations of the main and side modes when power dropout occurred. Ch. 1: Main mode, 20 mV/div. Ch. 2: Side mode, 10 mV/div. The duration time $t_d$ of power dropout is defined by the width of the pulse-shape-like waveform indicated in this figure. (b) A relation between the bias level $I/I_{th}$ and the duration time $t_d$.

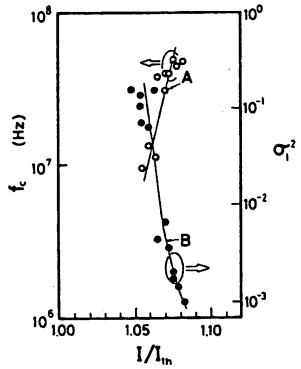


Fig. 8. Curve A (○): A relation between the bias level $I/I_{th}$ and the cutoff frequency $f_c$ of the Lorentzian power spectral density of power fluctuations of the main mode. Curve B (●): A relation between the bias level and the variance $\sigma_1^2$ of power fluctuations of the main mode.

above using a simple relation $P_e = r \cdot t_d$.) On the other hand, Ohtsu *et al.* have measured the values of $P_e$ in the range of $1 \times 10^{-3} \leqq P_e \leqq 1$ [8]. Therefore, the values of $P_e$ in the range of $1 \times 10^{-4} \leqq P_e \leqq 1 \times 10^{-3}$ have not yet been measured, and a relation between the results by Linke *et al.* [2] and by Ohtsu *et al.* [8] has not been made clear. In the present work, a wide range of $P_e$ (i.e., $1.6 \times 10^{-6} \leqq P_e \leqq 1$) could be measured, which covered both of the ranges measured by Linke *et al.* [2] and Ohtsu *et al.* [8] and bridged the gap between these previous works. This figure shows that $P_e$ decreases by increasing $\epsilon$, which agrees with the experimental results by Linke *et al.* [2] and Ohtsu *et al.* [8]. This figure also shows that $P_e$ decreases by increasing $I/I_{th}$, which means that the mode power fluctuations are less sensitive to agitation by spontaneous emission at a higher bias level.

Fig. 7(a) shows the waveforms of power fluctuations of the main and side modes observed by the oscilloscope when the power dropout occurred. The duration time $t_d$ of power dropout can be defined by the width of the pulse-shape-like wave form in this figure. The dependence of $t_d$ on the bias level was measured and is shown in Fig. 7(b). It can be noted that $t_d$ strongly depended on the bias level, which is approximately expressed as $t_d = 3.7 \times 10^{48} \exp [-118 (I/I_{th})]$ (s) for $1.065 \leqq I/I_{th} \leqq 1.104$. Linke *et al.* [2] and Henry *et al.* [6] claimed that the value of $t_d$ took a constant value of about 1 ns, while the value reported by Ohtsu *et al.* [8] was several microseconds. Fig. 7(b) indicates that the difference between these values is due to the different bias level of the laser used for the measurements. Therefore, the characteristics of a fast power dropout phenomenon in a highly biased laser can be estimated by measurements of the characteristics of a slow power dropout phenomenon at a low bias level. Measurements of a slow power dropout phenomenon can be easily carried out using inexpensive narrow-band measuring instruments.

A noticeable increase in $t_d$ observed around the threshold in Fig. 7(b) corresponds to the critical slowing down [9] around the critical point in the phase transition phenomenon. To clarify this correspondence, the power spectral density of the power fluctuations of the main mode was calculated from the data stored in the digital memory. The profile of this power spectral density was approximated as a Lorentzian with a cutoff frequency $f_c$. This cutoff frequency $f_c$ corresponds to the inverse of the correlation time of the power fluctuation characteristics, i.e., an inverse of the duration time of power dropout $1/t_d$ [10]. Curve A of Fig. 8 shows a dependence of the measured $f_c$ on the bias level. It can be noted from this figure that $f_c$ decreases by decreasing $I/I_{th}$. Furthermore, the variance $\sigma_1^2 [= (\langle I_1^2 \rangle - \langle I_1 \rangle^2)/\langle I_1 \rangle^2]$ of the power fluctuations of the main mode was calculated, and its dependence on the bias level is shown by curve B of Fig. 8. Analog data stored in the digital memory were sampled with a sampling time of 10 ns and were used for the calculation, as for Fig. 3(b) and (c). Curve B of Fig. 8 shows that the value of $\sigma_1^2$ increases with decreasing $I/I_{th}$. The decrease in $f_c$ and increase in $\sigma_1^2$ around the threshold shown in Fig. 8 are evidence of the fact that the behavior of power fluctuations corresponds to the critical slowing down [9].

For the second measurement, the ratio of the average CW power of the main and side modes $\langle I_1 \rangle / \langle I_2 \rangle$ was changed by changing the temperature at around point A in Fig. 2(a) while the bias level was maintained constant. As shown in Fig. 9(a), mode hopping was observed at $\langle I_1 \rangle / \langle I_2 \rangle \cong 1$. Mode hopping follows the stochastics of a Poisson process, as was pointed out by Ohtsu *et al.* [1], and the power spectral density of power fluctuations exhibits a Lorentzian profile. Its cutoff frequency $f_c$ represents the average frequency of mode hopping. Curve A

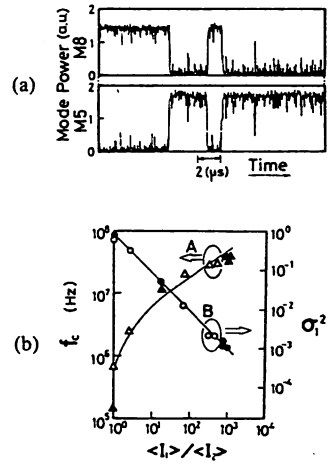


Fig. 9. (a) Results of simultaneous measurements of power variations of modes M8 and M5 when mode hopping occurred at around point A in Fig. 2(a) where $\langle I_1 \rangle / \langle I_2 \rangle \cong 1$. (b) Curve A (▲, △): A relation between the ratio of average CW mode power $\langle I_1 \rangle / \langle I_2 \rangle$ and the cutoff frequency $f_c$ of the power spectral density of power fluctuations of the main mode. Curve B (●, ○): A relation between the ratio of average CW mode powers and the variance $\sigma_1^2$ of the power fluctuations of the main mode. ▲, ●: $I/I_{th} = 1.082$. △, ○: $I/I_{th} = 1.070$.

of Fig. 9(b) shows a relation between the average CW mode power ratio $\langle I_1 \rangle / \langle I_2 \rangle$ and the measured value of $f_c$. Curve B of this figure shows a relation between $\langle I_1 \rangle / \langle I_2 \rangle$ and the measured value of the variance $\sigma_1^2$ of power fluctuations of the main mode. The method for calculating $\sigma_1^2$ was the same as that for Fig. 8. It can be noted from this figure that the cutoff frequency $f_c$ decreases by decreasing $\langle I_1 \rangle / \langle I_2 \rangle$, i.e., by the conversion from mode partition to mode hopping. It can also be noted that the value of $\sigma_1^2$ increases by decreasing $\langle I_1 \rangle / \langle I_2 \rangle$. At $\langle I_1 \rangle / \langle I_2 \rangle = 1$, the value of $\sigma_1^2$ takes unity, which is a specific value of $\sigma_1^2$ for the above-mentioned Poisson process.

## IV. Theoretical Analysis

A unified stochastic model for describing both the mode partition and mode hopping phenomena will be presented in this section by comparison to the experimental results given in the previous section. This stochastic model is based on the rate equations for the amplitudes of electric fields of the two modes ($\tilde{E}_i$, $i = 1, 2,$) and for the carrier density $\bar{n}^{(0)}$ in the active layer of the laser cavity. These equations are derived from the density matrix formulation, and details of these equations have been given in [1]. Since each coefficient in these equations is calculated by using the structural and material constants of the semiconductor laser, quantitative comparisons between the theoretical and experimental results are possible.

Noise terms are added to the rate equations for $\tilde{E}_i$ to represent the contributions from spontaneous emission fluctuations, which work as random triggering forces for mode partition and mode hopping. Here, it is assumed that the carrier density fluctuations are negligible, and the value of the carrier density can be approximated to its stationary value $\bar{n}_{st}^{(0)}$ because the total stimulated emission rate can be kept constant all the time. This assumption is based on the experimental observation that the total power was maintained constant with time even though each mode power fluctuated in an anticorrelated fashion due to mode partition or mode hopping. The validity of this assumption has been confirmed in [1] and [8] for mode hopping and mode partition, respectively, by comparing experimental and theoretical results. By this assumption, the rate equation for carrier density can be excluded in the following discussions. Thus, the equation to be solved for the following discussions is only the rate equation for $\tilde{E}_i$ with the noise terms due to spontaneous emission. In this formulation, it is interpreted that occurrences of mode partition and mode hopping are caused by fluctuations of spontaneous emission and by nonlinear mode coupling due to spectral hole burning induced by intraband relaxation of the carrier in the conduction band. The value of its relaxation time $\tau_{in}$ has been reported as about 0.1–0.3 ps [11].

By normalizing the rate equations for $\tilde{E}_i$, a set of nonlinear Langevin equations can be derived, which is expressed as [1], [8]

$$\frac{dE_i}{d\tau} = (a_i - |E_i|^2 - \xi |E_j|^2) E_i + q_i(\tau) \qquad (i, j = 1, 2;\ i \neq j) \tag{2}$$

where $E_i$ is the normalized amplitude of the electric field of the $i$th mode and $\tau$ is the normalized time. The quantity $a_i$ is the pump parameter corresponding to the stationary mode power normalized to the rms value of the power fluctuations of spontaneous emission. Therefore, the pump parameter $a_i$ is proportional to the small signal gain and depends on the bias level and temperature. The quantity $\xi$ represents the mode coupling constant between the two modes and is expressed as

$$\xi = \tfrac{4}{3} / [1 + (2\pi c \tau_{in} \Delta\lambda / \lambda^2)^2] \tag{3}$$

where $c$ is the speed of light, $\lambda$ is the wavelength, and $\Delta\lambda$ is the wavelength separation between the two modes. Substitution of $\Delta\lambda = 0.79$ nm, $\lambda = 783$ nm, and $\tau_{in} = 0.2$ ps into this equation gives a value of the mode coupling constant $\xi$ of 1.08, which is larger than unity and represents a strong coupling between the two modes [12]. The quantities $q_i(\tau)$ $(i = 1, 2)$ are Langevin noise terms which represent the fluctuations of spontaneous emission. They are supposed to be delta-correlated Gaussian random processes with zero mean and

$$\langle q_i^*(\tau) \cdot q_j(\tau') \rangle = 4 \cdot \delta_{ij} \cdot \delta(\tau - \tau') \qquad (i, j = 1, 2) \tag{4}$$

where * means the complex conjugate, $\delta_{ij}$ is the Kronecker delta, and $\delta(\tau - \tau')$ is the delta function. If $\xi < a_1/a_2$, a set of Langevin equations given by (2) has a set of stationarily stable solutions of $(|E_1|^2, |E_2|^2) = (a_1, 0)$, and the two mode powers fluctuate around these values by fluctuations of spontaneous emission. These power fluctuations correspond to the mode partition phenome-

non. If $1/\xi < a_1/a_2 < \xi$, on the other hand, these equations have two sets of stationarily stable solutions, i.e., $(a_1, 0)$ and $(0, a_2)$. Fluctuations of spontaneous emission drive the two mode powers from one of the solutions to the other at random points in time. Each mode power therefore tends to jump randomly between zero and nonzero values, which corresponds to the mode hopping phenomenon. Both of the phenomena can therefore be described by these equations if the values of the pump parameters are appropriately adjusted. In the experiments, these adjustments are performed by changing the bias level and the temperature.

If we express the normalized complex field amplitude $E_i$ in terms of real and imaginary parts,

$$E_k = x_k + i \cdot y_k \qquad (k = 1, 2), \tag{5}$$

the vector $\vec{x}\,[= (x_1, x_2, y_1, y_2)]$ represents the state of the laser, and its components obey a set of coupled Langevin equations given by (2). These multidimensional nonlinear Langevin equations can be transformed to the linear Fokker–Planck equation describing the probability density $p(\vec{x}, \tau)$, which is expressed as [10]

$$\frac{\partial}{\partial \tau} p(\vec{x}, \tau) = \sum_{i=1}^{2} \left[ -\frac{\partial}{\partial x_i} A_i^{(x)} p - \frac{\partial}{\partial y_i} A_i^{(y)} p + \left( \frac{\partial^2}{\partial x_i^2} + \frac{\partial^2}{\partial y_i^2} \right) p \right] \tag{6}$$

where

$$A_i^{(\eta)} = [a_i - (x_i^2 + y_i^2) - \xi(x_j^2 + y_j^2)]\eta_i \qquad (i, j = 1, 2;\ i \neq j;\ \eta = x, y). \tag{7}$$

The steady-state solution $p_s(\vec{x})$ is given by [10]

$$p_s(\vec{x}) = B^{-1} \cdot \exp\,[-U(\vec{x})] \tag{8}$$

where $B$ is the normalized constant. The quantity $U(\vec{x})$, called a potential, is expressed as

$$U(\vec{x}) = \tfrac{1}{4}(I_1^2 + I_2^2 + 2\xi I_1 I_2) - \tfrac{1}{2}(a_1 I_1 + a_2 I_2) \tag{9}$$

where $I_i$ is the normalized mode power given by $x_i^2 + y_i^2$ $(= |E_i|^2)$. Forms of the potential are shown in Fig. 10(a) and (b) for two values of $a_1/a_2$. The potential has one minimum at point $M_1$ in Fig. 10(a) for $\xi < a_1/a_2$ and two minima at points $M_1$ and $M_2$ in Fig. 10(b) for $1/\xi < a_1/a_2 < \xi$. These minima correspond to the stationarily stable solutions of (2). Therefore, mode partition and mode hopping can be described by means of the potential of Fig. 10(a) and (b), respectively. The shape of the potential can be continuously changed from one to the other given by these figures by changing the injection current and temperature. Therefore, this unified stochastic model can describe both mode partition and mode hopping. It can also be seen from this figure that a relation between $a_1/a_2$ and $\xi$ is important for single-frequency operation. The values of $a_1/a_2$ can be controlled by controlling injection current and temperature. The value of $\xi$ can be controlled by controlling $\tau_{in}$ at the stage of laser device fabrication, as can be said from (3).

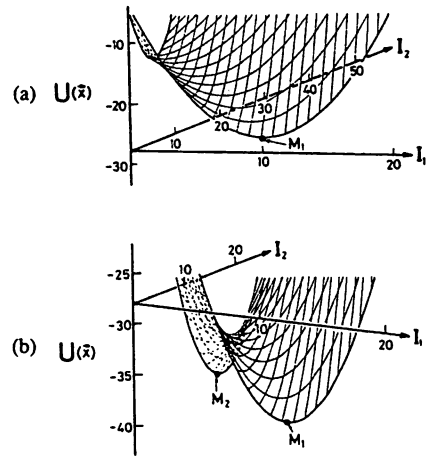


Fig. 10. Forms of the potential $U(\vec{x})$. (a) For mode partition. $a_1 = 10$ and $a_2 = 7$, i.e., $\xi < a_1/a_2$. (b) For mode hopping. $a_1 = 12$ and $a_2 = 12$, i.e., $1/\xi < a_1/a_2 < \xi$. The points $M_1$ and $M_2$ represent the positions of the minima of the potential.

The histogram, i.e., the probability distribution $P(I_i)$ of the $i$th mode power, is given by

$$P(I_i) = \int_0^\infty p_s(\vec{x}) \cdot dI_j \qquad (i, j = 1, 2;\ i \neq j). \tag{10}$$

Fig. 11(a) and (b) shows this probability distribution calculated by using numerical values of the experimental parameters at point A of Fig. 2(a). For this calculation, the rms value of spontaneous emission fluctuations is necessary to determine the values of $a_1$ and $a_2$. However, this rms value cannot be measured directly in the experiments. Then, the rms value estimated by Ohtsu *et al.* [1, Fig. 11] was employed; i.e., the employed rms value of the fluctuating electric field of spontaneous emission was $2.8 \times 10^2$ (V/m). Fig. 11(a) and (b) represents the power distributions of the main and side modes, respectively, which corresponds to the experimental results of Fig. 5(a) and (b). Agreement between the calculated and experimental results can be seen from these figures. These distributions have also been measured by Liu and Ogawa [3] and have been analyzed by Henry *et al.* [6]. It was claimed in [3] and [6] that the power distribution of the side mode resembled a Gaussian profile. However, it should be noted from the present analysis that the distribution in Fig. 11(b) is not necessarily approximated to a Gaussian profile, but has a profile which depends on the form of the potential of Fig. 10(a).

The time-dependent solution of the Fokker–Planck equation is expressed as [10]

$$p(\vec{x}, \tau) = p_s(\vec{x}) \cdot \sum_{n_1, n_2, m_1, m_2} C_{n_1, n_2, m_1, m_2} \cdot \exp\,(-g_{n_1, n_2, m_1, m_2} \cdot \tau)\, V_{n_1, n_2, m_1, m_2}(\vec{x}) \tag{11}$$

where the coefficient $C_{n_1, n_2, m_1, m_2}$ is determined from the

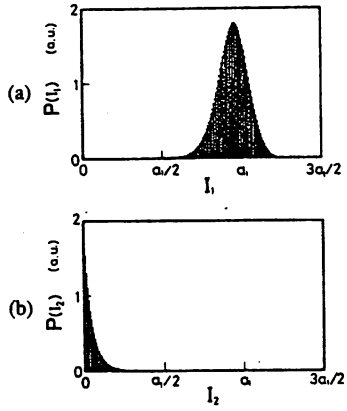


Fig. 11. Histogram, i.e., probability distributions of powers. (a) Main mode. (b) Side mode. The values of $a_1$ and $a_2$ used for this calculation were 17.0 and 15.5, respectively, which corresponded to the value at point A of Fig. 2(a).

boundary conditions and $V_{n_1,n_2,m_1,m_2}(\vec{x})$ is the eigenfunction of the Fokker–Planck operator corresponding to the eigenvalue $g_{n_1,n_2,m_1,m_2}$. The eigenvalue is expressed as

$$g_{n_1,n_2,m_1,m_2} = 2n_1 \cdot a_1 + (m_1^2/a_1) + (2 \cdot n_2 + |m_2|) \cdot |a_2 - \xi \cdot a_1| \quad (n_1, n_2, m_1, m_2 = 0, 1, 2, 3, \cdots). \tag{12}$$

The eigenvalue of the lowest-order $g_{0,0,0,0}$ is zero, which means that the Fokker–Planck equation has the steady-state solution given by (8).

To derive the probability $P_e$ given by (1), the method proposed by Bonifacio *et al.* [13] is employed. This method is based on the time-dependent solution given by (11). Since the details of the derivation by following this method has been given in [4] and [8], only the final form of the expression is presented here. It is

$$P_e = 1 - P(\infty) \tag{13}$$

where

$$P(\infty) = \iint_D p_s(\vec{x})\, dI_1 dI_2. \tag{14}$$

The region $D$ is bounded by

$$D: \begin{cases} a_1(1-\epsilon) \leqq I_1 \leqq \infty \\ 0 \leqq I_2 \leqq \infty. \end{cases} \tag{15}$$

The quantity $\epsilon$ can be called the threshold setting to calculate $P(\infty)$, as was shown in Fig. 6. Fig. 12 shows a relation between $\epsilon$ and $P_e$ calculated using (13)–(15). Comparison between Figs. 6 and 12 shows that the dependences of $P_e$ on $I/I_{th}$ and $\epsilon$ are described well by the present model, from which the validity of the present stochastic model is confirmed.

The theoretical expression of the variance $\sigma_i^2$ shown in Figs. 8 and 9(b) can be given by

$$\sigma_i^2 = (\langle I_i^2 \rangle - \langle I_i \rangle^2)/\langle I_i \rangle^2 \quad (i = 1, 2) \tag{16}$$

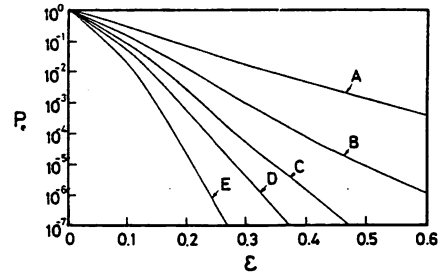


Fig. 12. Calculated relation between the threshold setting $\epsilon$ and the power dropout probability $P_e$. Here, the values of the pump parameters $a_1$ and $a_2$ used for this calculation are given as follows: A, $a_1 = 17.0$ and $a_2 = 15.4$; B, $a_1 = 22.0$ and $a_2 = 20.0$; C, $a_1 = 26.0$ and $a_2 = 24.0$; D, $a_1 = 29.0$ and $a_2 = 26.9$; E, $a_1 = 35.0$ and $a_2 = 32.4$.

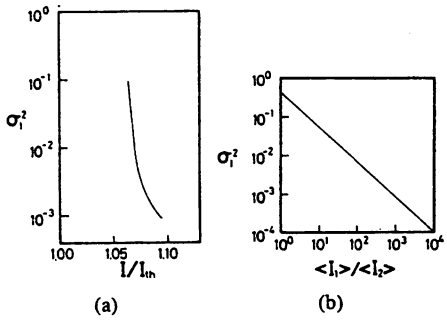


Fig. 13. (a) A calculated relation between the bias level $I/I_{th}$ and the variance $\sigma_1^2$ of the power fluctuations of the main mode. (b) A calculated relation between the ratio of average CW mode power $\langle I_1 \rangle / \langle I_2 \rangle$ and the variance $\sigma_1^2$.

where

$$\langle I_i^n \rangle = \int\int_0^\infty p_s(\vec{x})\, I_i^n \cdot dI_1 \cdot dI_2 \quad (n = 1, 2). \tag{17}$$

Fig. 13(a) and (b) shows calculated results of $\sigma_1^2$. Fig. 13(a) indicates the noticeable increase in the variance $\sigma_1^2$ when the bias level approaches the threshold, which agrees quantitatively with the experimental result of curve B of Fig. 8. It is also seen that the results of Fig. 13(b) agree with that of the curve B of Fig. 9(b).

The cutoff frequency $f_c$ of the power spectral density of power fluctuation corresponds to the inverse of the correlation time of fluctuations. This is given by the lowest nonzero eivenvalue $g_{1,0,0,0}$. Equation (12) indicates that $g_{1,0,0,0} = 2 \cdot a_1$, i.e., $g_{1,0,0,0}$ is proportional to the bias level, which agrees with the fact given in Fig. 8 that the cutoff frequency $f_c$ decreases by decreasing $I/I_{th}$.

From the agreement between the experimental and theoretical results obtained above, it can be claimed that the unified stochastic model presented in this section describes characteristics of both the mode partition and mode hopping phenomena.

## V. Summary

The discussions given in the previous sections can be summarized as follows.

1) The power dropout probability $P_e$ in the mode par-

tition was measured for a wide range, $1.6 \times 10^{-6} \leqq P_e \leqq 1$. This measurement covered the ranges of $P_e$ which have been reported in [2] and [8] and bridged the gap between the two previous works.

2) It was found that the duration time $t_d$ of power dropout depended on the bias level, which was approximately expressed as $t_d = 3.7 \times 10^{48} \exp[-118(I/I_{th})]$ (s) for $1.065 \leqq I/I_{th} \leqq 1.104$.

3) Power fluctuations exhibited specific characteristics around the threshold, which were similar to the critical slowing down in the phase transition phenomenon.

4) An increase in the variance of power fluctuations was observed when the laser oscillating condition was converted from mode partition to mode hopping.

5) A stochastic model was derived directly from the structural and material constants of the laser. Fluctuations of spontaneous emission were introduced into this model to represent the random triggering forces for mode power fluctuations. This unified model described both mode partition and mode hopping phenomena.

6) By the comparisons between the experimental and theoretical results, it was found that characteristics of the power fluctuations at a high bias level can be estimated from the experimental results at a low bias level.

## Acknowledgment

The authors thank T. Nakahara of the Tokyo Institute of Technology for his experimental support.

## References

[1] M. Ohtsu, Y. Teramachi, Y. Otsuka, and A. Osaki, "Analyses of mode-hopping phenomena in an AlGaAs laser," *IEEE J. Quantum Electron.*, vol. 22, pp. 535-543, 1986.

[2] R. A. Linke, B. L. Kasper, C. A. Burrus, Jr., I. P. Kaminov, J. S. Ko, and T. P. Lee, "Mode power partition events in nearly single-frequency lasers," *J. Lightwave Technol.*, vol. LT-3, pp. 706-712, 1985.

[3] P. L. Liu and K. Ogawa, "Statistical measurements as a way to study mode partition in injection lasers," *J. Lightwave Technol.*, vol. LT-2, pp. 44-48, 1984.

[4] M. Ohtsu and K.-Y. Liou, "Mode stability of a two-wavelength Fabry-Perot/distributed feedback laser," *J. Lightwave Technol.*, vol. 6, pp. 47-51, 1988.

[5] K. Ogawa, "Semiconductor laser noise: Mode partition noise," in *Semiconductors and Semimetals, Vol. 22*, W. T. Tsang, Ed. New York: Academic, 1985, ch. 8.

[6] C. H. Henry, P. S. Henry, and M. Lax, "Partition fluctuations in nearly single-longitudinal-mode lasers," *J. Lightwave Technol.*, vol. LT-2, pp. 209-216, 1984.

[7] Y. Suematsu, S. Arai, and K. Kishino, "Dynamic single-mode semiconductor lasers with a distributed reflector," *J. Lightwave Technol.*, vol. LT-1, pp. 161-176, 1983.

[8] M. Ohtsu, Y. Teramachi, and T. Miyazaki, "Mode stability analysis of nearly single-longitudinal-mode semiconductor lasers," *IEEE J. Quantum Electron.*, vol. 24, pp. 716-723, 1988.

[9] A. B. Pippard, *Response and Stability, An Introduction to the Physical Theory*. London, UK: Cambridge Univ. Press., 1985, ch. 6.

[10] F. T. Hioe and S. Singh, "Correlations, transients, bistability, and phase-transition analogy in two-mode lasers," *Phys. Rev. A*, vol. 24, pp. 2050-2074, 1981.

[11] M. Yamada, H. Ishiguro, and H. Nagato, "Estimation of the intraband relaxation time in undoped AlGaAs laser," *Japan. J. Appl. Phys.*, vol. 19, pp. 135-142, 1980.

[12] M. Sargent III, M. O. Scully, and W. E. Lamb, Jr., *Laser Physics*. Reading, MA: Addison-Wesley, 1974, ch. 9.

[13] B. Bonifacio, L. Lugiato, J. D. Farina, and L. M. Narducci, "Long time evolution for a one-dimensional Fokker-Planck process: Absorptive optical bistability," *IEEE J. Quantum Electron.*, vol. QE-17, pp. 357-364, 1981.

**Motoichi Ohtsu** (M'88) was born in Kanagawa, Japan, on October 5, 1950. He received the B.S., M.S., and Ph.D. degrees in electronics engineering from the Tokyo Institute of Technology, Tokyo, Japan, in 1973, 1975, and 1978, respectively.

In 1978 he was appointed a Research Associate and in 1982 became an Associate Professor at the Tokyo Institute of Technology. From September 1986 to July 1987, while on leave from the Tokyo Institute of Technology, he joined the Crawford Hill Laboratory, AT&T Bell Laboratories, Holmdel, NJ. His main fields of interest are the frequency control of lasers, analysis of the dynamic behavior of lasers and its applications to coherent optical measurements, optical communications, and microwave atomic clocks.

Dr. Ohtsu has written over 70 papers and received 2 patents. He is the author or coauthor of 8 books. He is a member of the Institute of Electronics, Information and Communication Engineers of Japan, the Institute of Electrical Engineers of Japan, the Japan Society of Applied Physics, and the Optical Society of America. In 1982 he was awarded a prize from the Japan Society of Applied Physics. He was also awarded the Issac Koga Gold Medal from the International Union of Radio Science (URSI) in 1984.

**Yasuaki Teramachi** was born in Japan in 1947. He received the Doctor's degree in electrical engineering from the Tokyo Institute of Technology, Tokyo, Japan, in 1975.

In 1976 he was appointed a Research Associate in the Department of Applied Electronics, Tokyo Institute of Technology. In 1986 he became an Associate Professor in the Department of Information Engineering, the University of Industrial Technology. He has been involved in the research program on the body surface potential mapping system and on nonlinear instability of lasers.

Dr. Teramachi is a member of the Physical Society of Japan, the Japan Society of Medical Electronics and Biomedical Engineering, and the Laser Society of Japan.

# A Simple Interferometric Method for Monitoring Mode Hopping in Tunable External-Cavity Semiconductor Lasers

M. OHTSU, K.-Y. LIOU, E. C. BURROWS, C. A. BURRUS, FELLOW, IEEE, AND G. EISENSTEIN, MEMBER, IEEE

*Abstract*—A problem in frequency tuning of external-cavity lasers is mode hopping between neighboring external cavity modes. An interferometric method is proposed for monitoring mode hopping in external-cavity semiconductor lasers. The mode-hopping events in a 1.3-μm grating-tuned external-cavity laser were analyzed using this method. The average frequency of mode hopping for a 7.5-cm external-cavity length was estimated and was expressed as $f_c = 2.7 \times 10^6 \times \exp[-1.7/(I/I_{th} - 1)]$ (hertz) for $0.07 \leq (I/I_{th} - 1) \leq 0.8$ ($I$ = injection current and $I_{th}$ = threshold current). The mode-hopping monitoring signal was negatively fed back to the laser using an automatic control circuit which maintained single-mode operation while the wavelength of the grating external-cavity laser was tuned.

## I. INTRODUCTION

NARROW-LINEWIDTH and wide-band tunable semiconductor lasers are needed for coherent optical communication, multicolor coherent optical sensing, and so on. A narrow linewidth often can be obtained by adding an external cavity to the semiconductor laser (e.g., [1]–[4]). By using a diffraction grating as a dispersive mirror in the external cavity configuration, wide-band tunability can be achieved by rotating the grating [2], [3]. Monolithic integrated devices with a distributed Bragg reflector (DBR) that can be tuned by current injection have also been demonstrated [5], although the tuning range is about 10 times smaller than that of the hybrid external grating laser.

A problem in frequency tuning of external cavity lasers, however, is mode hopping between successive external cavity modes. Mode hopping occurs in both the hybrid grating-tuned external-cavity laser and the integrated external-cavity DBR laser. In the case of the grating-tuned external-cavity laser, the lasing frequency is changed by grating rotation, but the continuous tuning range is limited by the longitudinal mode spacing of the external cavity. The mode spacing is inversely proportional to the cavity length. For an external cavity length of a few centimeters, which is required for a linewidth of about 100 kHz, the mode spacings are several gigahertz. These closely spaced longitudinal modes can not be resolved by a grating monochromator. Although a Fabry–Perot interferometer has sufficient resolution, the instrument is bulky, and the stability is influenced by changes in the alignment.

We propose in this paper a simple method for monitoring mode hopping in external cavity lasers using a fiber Mach–Zehnder interferometer. Hopping between two longitudinal modes results in a beat signal at a frequency equal to the difference between the oscillation frequencies of the two modes. For a few gigahertz frequency separation in the case of an external cavity laser, the beat signal of two neighboring longitudinal modes can be detected with a wide bandwidth photodiode located after the interferometer. Using this method, we have analyzed mode-hopping events in a hybrid grating-tuned external-cavity laser emitting at 1.3-μm wavelength and have estimated the average mode-hopping frequency in the laser. Finally, a control scheme that monitors mode-hopping and maintains single-mode operation in the laser by negative feedback of the monitoring signal to the laser is demonstrated. This control method can be applied to a monolithic integrated external-cavity DBR laser, which is expected to have a longitudinal mode behavior similar to the grating-tuned external cavity laser used in this experiment.

## II. PRINCIPLE OF MODE-HOPPING DETECTION FOR EXTERNAL-CAVITY LASERS

### A. Theoretical Analysis

A Mach–Zehnder interferometer was used for monitoring mode hopping in a grating-tuned external-cavity laser. A single-mode fiber was employed as a delay line in one of the interferometer arms. The experimental setup is shown in Fig. 1(a). Fiber directional couplers were used to combine the two interferometer arms. In this figure, components for negative feedback, which will be described in Section V, are also illustrated.

When mode hopping occurs between two external cavity modes, the electric field of the total laser light is expressed as the sum of that of the two modes

$$E(t) = \alpha_1(t) \cdot E_1(t) + \alpha_2(t) \cdot E_2(t) \qquad (1)$$

where

Manuscript received September 24, 1987; revised November 30, 1987.

M. Ohtsu is with AT&T Bell Laboratories, Crawford Hill Laboratory, Holmdel, NJ 07733, on leave from Tokyo Institute of Technology, The Graduate School at Nagatsuta, Midori-Ku, Yokohama 227, Japan.

K.-Y. Liou, E. C. Burrows, C. A. Burrus, and G. Eisenstein are with AT&T Bell Laboratories, Crawford Hill Laboratory, Holmdel, NJ 07733.

IEEE Log Number 8821126.

0733-8724/89/0100-0068$01.00 © 1989 IEEE

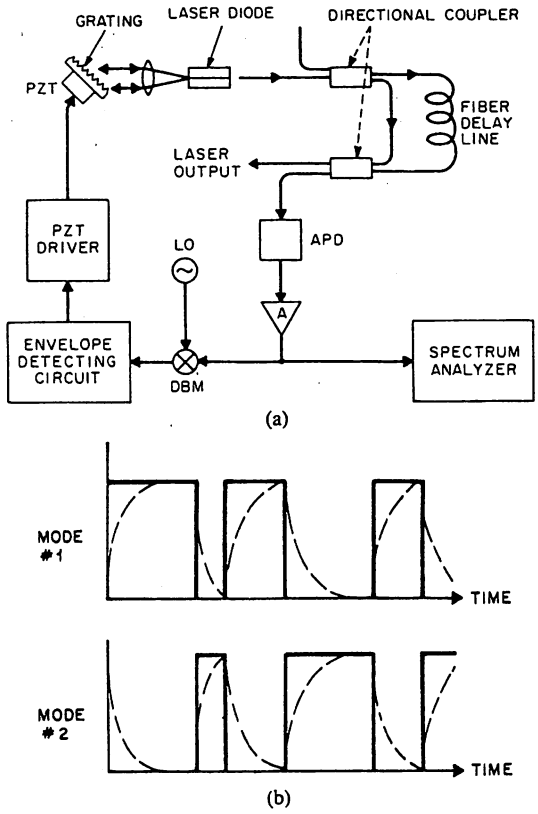


Fig. 1. (a) Experimental apparatus. LO is a local oscillator, DBM is a double balanced mixer, and APD is an avalanche photodiode. (b) Diagrammatic waveforms for illustration of the field amplitudes of the two modes under mode-hopping condition.

$$E_k(t) = \sqrt{P_k} \cdot \cos\left\{\omega_k t + \phi_k(t)\right\} \quad (k = 1, 2) \quad (2a)$$

and

$$\alpha_2(t) = 1 - \alpha_1(t). \quad (2b)$$

The notations $P_k$, $\omega_k$, and $\phi_k$ are the light power, angular frequency, and phase of the $k$th mode, respectively. Temporal mode hopping is represented by the two variables $\alpha_1(t)$ and $\alpha_2(t)$. Although mode intensities are measured in the experiment, the field amplitudes are used in the theory because mode amplitudes are more fundamental variables than mode intensities for the analysis of multimode phenomena. Equation (2b) simply represents that the field amplitudes of the two modes are anticorrelated in time when mode hopping occurs.

The frequency difference between the adjacent external cavity modes, $(\omega_1 - \omega_2)/2\pi$, is a few gigahertz for an air external-cavity length of a few centimeters. It can be expected [6] that these two closely spaced modes exhibit strong coupling because $|\omega_1 - \omega_2| < 1/\sqrt{3} \cdot \tau_{in}$, where $\tau_{in}$ is the intraband relaxation time of the semiconductor laser material. Under this condition, complete mode changes occur during mode hopping, i.e., the variables $\alpha_1$ and $\alpha_2$ take a value of either 1 or 0, and they follow the stochastics of a Poisson process, which has been confirmed for solitary semiconductor lasers [6]. This mode-hopping behavior is illustrated diagrammatically by the solid line in Fig. 1(b).

In the case of an external-cavity laser, however, the mode-switching rise and fall times are longer than that of a solitary laser because both the photon lifetime and the resonance build-up time are increased by the long external-cavity length. Therefore, the actual mode-hopping waveforms in a grating external-cavity laser can deviate from rectangular waves. This is illustrated diagrammatically by the dashed curves with finite rise and fall times in Fig. 1(b). An effect of the long rise and fall times on mode-hopping monitoring will be discussed in Section IV. For the following discussion in this section, it is assumed for simplicity that the mode-hopping waveforms are rectangular.

From (1), the photocurrent of the square-law detector located after the interferometer is given by

$$i_d = i_{do} + i_{db} \quad (3)$$

where

$$i_{do} \propto \alpha_1(t) \cdot \alpha_1(t - \tau_d) \cdot P_1 \cdot \cos\left\{\omega_1 \tau_d + \phi_1(t) - \phi_1(t - \tau_d)\right\} + \alpha_2(t) \cdot \alpha_2(t - \tau_d) \cdot P_2 \cdot \cos\left\{\omega_2 \tau_d + \phi_2(t) - \phi_2(t - \tau_d)\right\} \quad (4)$$

$$i_{db} \propto \alpha_1(t) \cdot \alpha_2(t - \tau_d) \cdot \sqrt{P_1 P_2} \cdot \cos\left\{(\omega_1 - \omega_2)t + \omega_2 \tau_d + \phi_1(t) - \phi_2(t - \tau_d)\right\} + \alpha_1(t - \tau_d) \cdot \alpha_2(t) \cdot \sqrt{P_1 P_2} \cdot \cos\left\{(\omega_1 - \omega_2)t - \omega_1 \tau_d + \phi_1(t - \tau_d) - \phi_2(t)\right\}. \quad (5)$$

In these equations, $\tau_d$ represents the delay time for light propagation through the fiber delay line. The $\cos\{\omega_k \tau_d + \phi_k(t) - \phi_k(t - \tau_d)\}$ term in $i_{do}$ of (4) gives the field spectrum of the $k$th mode at the frequency $f = 0$ on a spectrum analyzer [7]. However, the peak height of the field spectrum fluctuates due to mode hopping, which is described by the $\alpha_k(t) \cdot \alpha_k(t - \tau_d)$ term. The magnitude of this fluctuation is large if $\tau_d \lesssim 1/f_c$, where $f_c$ is the average mode-hopping frequency, because the anticorrelation between the random variables $\alpha_1$ and $\alpha_2$, i.e., $\alpha_1 \cdot \alpha_2 = 0$, is still preserved at the output port of the interferometer. For $\tau_d >> 1/f_c$, on the other hand, the fluctuation decreases because the anticorrelation between $\alpha_1$ and $\alpha_2$ is removed by a sufficiently long delay time, resulting in a stable profile of the field spectrum on the spectrum analyzer. Therefore, when the laser oscillates with a single mode, $i_{do}$ gives the profile of the field spectrum of this mode at $f = 0$ on the spectrum analyzer. If mode-hopping occurs, the spectral profile at $f = 0$ is the superposition of the field spectra of the two hopping modes.

For the present work, we are interested in the photocurrent $i_{db}$ in (3), which gives the mode-hopping signal. From (5), $i_{db} \cong 0$ for $\tau_d < 1/f_c$ because the anticorrelation between $\alpha_1$ and $\alpha_2$ is still preserved at the output port of the interferometer, i.e., $\alpha_1 \cdot \alpha_2 \cong 0$. However, $\alpha_1 \cdot \alpha_2 \neq 0$ for $\tau_d >> 1/f_c$ because the anticorrelation of these two random variables is violated by the long delay time. Therefore, a signal appears at $f = (\omega_1 - \omega_2)/2\pi$ in the

frequency domain shown by the spectrum analyzer. This signal can be used as a sensitive indicator of mode hopping because it appears only when mode hopping occurs. Since the average frequency of mode hopping $f_c$ estimated in Section III, is around 1 MHz, a fiber delay line of several hundred meters will be sufficient to satisfy the $\tau_d > 1/f_c$ condition for mode-hopping detection. However, it is possible to monitor mode hopping even without the delay line due to the effect of the slow rise and fall times of mode hopping, as will be discussed in Section III.

### B. Experiment

A grating-tuned external-cavity laser at 1.3-$\mu$m wavelength was used in the experiment to demonstrate the mode-hopping detection method. The diffraction grating had 1200 lines/mm, and the blaze wavelength was 0.75 $\mu$m. The grating was located 7.5 cm away from the laser diode to form the external cavity. One facet of the diode was AR coated ($R \lesssim 1$ percent) and the output light was collimated by an objective lens of 0.85 numerical aperture for optical coupling to the diffraction grating. The threshold current of this external cavity laser was 28 mA near room temperature. The grating was mounted on a piezoelectric transducer (PZT) for fine adjustment of the cavity length. Wide-band frequency tuning was obtained by rotating the grating, and fine tuning was done by adjusting the PZT voltage. All the components of the laser were fixed on a brass plate and installed in a shield box to achieve mechanical stability. The temperature of the laser diode was stabilized at 23 $\pm$ 0.001°C. The longitudinal mode spacing for this external cavity laser of 7.5-cm length was about 2 GHz.

A. 2.8-km single mode fiber was used as a delay line for the Mach–Zehnder interferometer shown in Fig. 1(a). Output light from the interferometer was detected by an avalanche photodiode, and its photocurrent was monitored by a spectrum analyzer after a wide-band amplifier. The longitudinal mode spectra were simultaneously monitored by a scanning Fabry–Perot interferometer with a free spectral range of 150 MHz. The external cavity length is controlled by the PZT voltage $V_{PZT}$ which can be varied to introduce mode-hopping events.

The rate of frequency change by varying $V_{PZT}$ was measured to be 194 MHz/V. For a large change in $V_{PZT}$ the laser will hop periodically to successive external cavity modes. The same periodic mode hop occurs when the grating is rotated. In principle, the change in $V_{PZT}$ and the grating rotation can be synchronized to increase the continuous frequency tuning range. However, this well-behaved periodic mode-hopping characteristic may not always be the case for a complicated external-cavity configuration. An example of irregular mode hopping behavior when $V_{PZT}$ was varied is shown in Fig. 2, and we will show that the proposed mode-hopping control method can be applied even to this case.

Fig. 2 shows an observed relationship between $V_{PZT}$ and the mode-hopping signal level at 2 GHz ($= (\omega_1 - \omega_2)/2\pi$), measured with a spectrum analyzer. The injection current of the laser was fixed at 45 mA. For several values of $V_{PZT}$, Fig. 3(a) shows the longitudinal mode spectra observed with a scanning Fabry–Perot interferometer. Fig. 3(b) and (c) shows the corresponding monitoring signals at $f = 2$ GHz and at $f = 0$, respectively, recorded using a spectrum analyzer. For $V_{PZT} < 250$ V, the laser showed single-mode oscillation, and no mode-hopping signal at $f = 2$ GHz was detected. For $V_{PZT} \geq 250$ V, however, mode hopping began and the detected signal at $f = 2$ GHz can be seen clearly in Fig. 2 and Fig. 3(b). For $V_{PZT} > 550$ V, the laser returned to single mode oscillation, and the signal at $f = 2$ GHz disappeared. At $V_{PZT} = 620$ V, a mode-hopping signal, 5 dB higher than the noise level, appeared again. This signal is clearly seen in Fig. 3(b), even though the Fabry–Perot interferometer measurement in Fig. 3(a) shows a nearly single mode spectrum with a very weak side mode. This indicates that the present method has a better sensitivity than the scanning Fabry–Perot interferometer for monitoring mode-hopping.

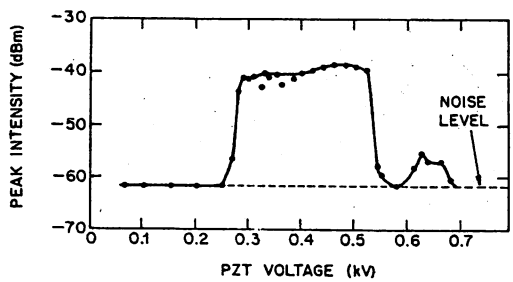


Fig. 2. The intensity of the mode-hopping signal at $f = 2$ GHz as a function of $V_{PZT}$.

Several alternative ways for monitoring mode hopping were compared, experimentally, with the present method. One of them is to measure the jump in the total output power of the laser [8]. The laser output power was simultaneously monitored when Fig. 2 was recorded, and the results are shown in Fig. 4. The output power exhibits discontinuities, at $V_{PZT} = 250$ and 550 V, which are consistent with those of Fig. 2. However, it cannot be recognized which side of the discontinuity corresponds to the mode-hopping region. Furthermore, in this figure, the mode hop at $V_{PZT} = 620$ V, observed in Fig. 2, is not seen clearly. The present mode-hopping detection method is clearly more sensitive than monitoring the total output power. Mode hopping also can be monitored by measuring the variation of the voltage $V_{p\text{-}n}$ across the p-n junction of the laser diode [9]. Again we found that the measurements of $V_{p\text{-}n}$ or its derivatives do not provide a clear signal for mode-hopping control in the case of a long external cavity laser. From these comparisons, it was concluded that the present scheme is much more sensitive than the previous methods.

## III. Estimation of the Average Mode-Hopping Frequency

The rise and fall times of power switching between the two modes during mode hopping were assumed to be neg-

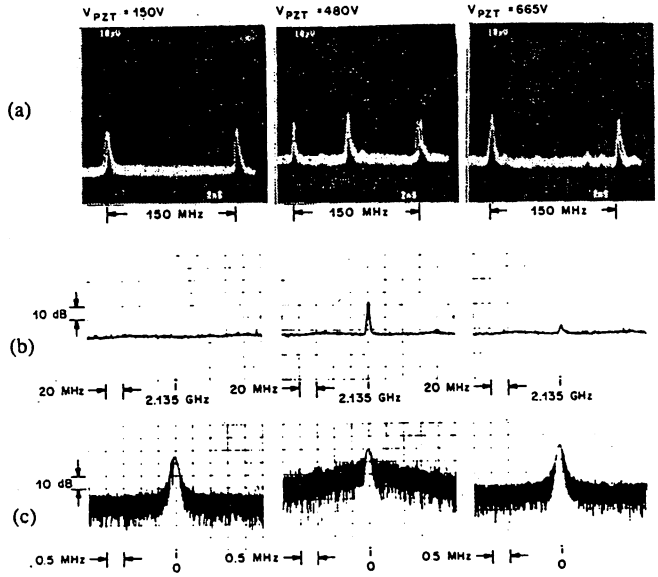


Fig. 3. (a) Mode spectra observed by a scanning Fabry-Perot interferometer with a 150-MHz free spectral range. (b) Mode-hopping signal near 2 GHz shown on analyzer. (c) Signal at $f = 0$ Hz observed by a spectrum analyzer.

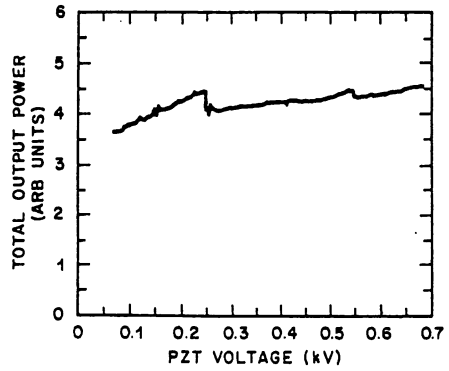


Fig. 4. The total output power of the laser as a function of $V_{PZT}$.

ligible in Section II to simplify the discussion of the mode-hopping detection method. In this section, we analyze the effects of the finite rise and fall times on the detected mode-hopping signal. The average frequency of mode hopping in the external-cavity laser will be estimated. In the case of long rise and fall times due to a sufficiently long external cavity, we will discuss the possibility of monitoring mode hopping without using the fiber delay line, i.e., without the Mach-Zehnder interferometer.

Curve *A* in Fig. 5 shows a mode-hopping signal at $f =$ 2 GHz observed by using a 2.8-km fiber delay line in the Mach-Zehnder interferometer. The mode-hopping signal could still be detected, but with a smaller intensity, when the fiber delay line was removed. The result without the delay line is shown by curve *B* in Fig. 5. Because the switching waveforms of the two modes represented by $\alpha_1(t)$ and $\alpha_2(t)$ are not completely rectangular due to the finite transient times, $\alpha_1(t) \cdot \alpha_2(t) \neq 0$. Both the photon lifetime and the buildup time for cavity resonance can be increased by a long external cavity. We will show that the average frequency of mode hopping in the external-cavity

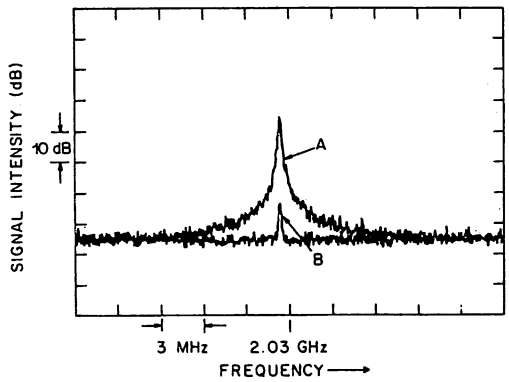


Fig. 5. Spectral profiles of the signal at $f = 2$ GHz. Curve *A*: The signal obtained by using a 2.8-km fiber delay line and curve *B*: without using the delay line.

laser can be estimated from the ratio of the intensities of the two mode-hopping signals *A* and *B* in Fig. 5.

The intensity of the heterodyned signal with zero delay time can be written as

$$I_0 \equiv \frac{1}{T}\int_0^T \left\{\alpha_1(t) \cdot \sqrt{P_1}\right\} \cdot \left\{\alpha_2(t) \cdot \sqrt{P_2}\right\} dt \quad (6)$$

where $T$ is the averaged value of the pulse duration time of the waveforms in Fig. 1(b) and is related to the average frequency of mode-hopping $f_c$ [6] by

$$T = 1/2f_c. \quad (7)$$

With an infinite delay time, the intensity of the heterodyned signal is expressed as

$$I_\infty = \lim_{\tau_d \to \infty} \frac{1}{T}\int_0^T \left\{\alpha_1(t) \cdot \sqrt{P_1}\right\} \cdot \left\{\alpha_2(t - \tau_d) \cdot \sqrt{P_2}\right\} dt. \quad (8)$$

The values of $I_0$ and $I_\infty$ can be estimated by computer simulation, similar to those previously done for a solitary semiconductor laser by Ohtsu *et al.* [6]. A simple first-order approximation is used here, however, to avoid the tedious procedure of computer simulation. That is, although the temporal behavior of mode hopping is dependent on the magnitudes of the nonlinear gain coefficients [10], it is approximated here that $\alpha_1(t)$ and $\alpha_2(t)$ vary exponentially with time during a mode-hopping transient with a rise time of $\tau_r$.

As we have pointed out earlier, the rise and fall times of longitudinal mode switching are slowed down by the long external cavity due to its effects on the photon lifetime and the build-up time for external-cavity resonance. The photon lifetime is increased by the external cavity because the normalized internal loss and the normalized mirror loss are both reduced by the air external cavity. The buildup time for resonance at one of the external cavity modes is also increased by the length of the cavity. Since the cavity buildup time is of the order of the round trip time in the external cavity, it is an order of magnitude smaller than the photon lifetime for the laser under consideration. The rise and fall times are therefore deter-

mined by the photon lifetime, and a single time constant $\tau_r$ can be used to describe the transient stage of mode hopping. Under this approximation, we can write

$$\alpha_1(t) = (1 - e^{-t/2\tau_r})/(1 - e^{-T/2\tau_r}) \quad (9a)$$

and

$$\alpha_2(t) = (e^{-t/2\tau_r} - e^{-T/2\tau_r})/(1 - e^{-T/2\tau_r})\ (0 \le t \le T). \quad (9b)$$

The value of $I_0$ then can be evaluated easily using (9). On the other hand, $I_\infty$ is approximated as follows: Since no temporal correlation exists between $\alpha_1(t)$ and $\alpha_2(t)$ after an infinite delay time, $I_\infty$ can be approximated as the average of the values of $I_\infty$ for the correlated case and the anticorrelated case. This is expressed as

$$I_\infty \cong \left[\frac{1}{T}\int_0^T \frac{(\alpha_1\sqrt{P_1})^2 + (\alpha_2\sqrt{P_2})^2}{2}\,dt + \frac{1}{T}\int_0^T (\alpha_1\sqrt{P_1})(\alpha_2\sqrt{P_2})\,dt\right]\Big/2. \quad (10)$$

During mode-hopping in the laser, $\alpha_1(t)$ and $\alpha_2(t)$ are anticorrelated, i.e., $\alpha_1\alpha_2 = 0$ except during the turn on and turn off periods. This relationship is removed by the delay line. The first and the second integral represent the value of $I_\infty$ when $\alpha_1(t)$ and $\alpha_2(t)$ vary in a correlated fashion and when they are anticorrelated, respectively.

The ratio of $I_0$ and $I_\infty$, $\epsilon$ ($\equiv I_0/I_\infty$), is then given by

$$\epsilon = \frac{2[1 - (T/\tau_r)e^{-T/2\tau_r} - e^{-T/\tau_r}]}{(T/2\tau_r)(1 + e^{-T/\tau_r} - 2e^{-T/2\tau_r})}. \quad (11)$$

Fig. 6 shows the calculated $\epsilon$ versus $T/\tau_r$ relationship. The value of $\epsilon$ decreases with increasing $T/\tau_r$ because the waveforms of $\alpha_1$ and $\alpha_2$ become rectangular (solid curve in Fig. 1(b)) when $T/\tau_r$ approaches infinity. On the other hand, $\epsilon$ should approach unity in the $T/\tau_r \to 0$ limit. However, Fig. 6 shows that $\epsilon$ equals 0.67 when $T/\tau_r$ approaches 0. The error is caused by the approximation made for the calculations of $\alpha_1$ and $\alpha_2$ in (9) and $I_\infty$ in (10). Since the difference between 0.67 and the exact value 1.0 is only 2 dB, the accuracy of the approximation is good enough for the present discussions.

Fig. 7 shows the measured relationship between $\epsilon$ and the injection current $I$ normalized by the threshold current $I_{th}$. The 2.8-km fiber delay line was used in the measurements and it is approximated as an infinitely long delay line in the calculations. This figure shows that the value of $\epsilon$ decreased with increasing injection current in the range of $0.07 \le I/I_{th} - 1 \le 0.8$. A least square fit of the measured $\epsilon$ can be made by assuming the following functional form for $\epsilon$:

$$\epsilon = A(I/I_{th} - 1)^{-1} \exp[-B(I/I_{th} - 1)]. \quad (12)$$

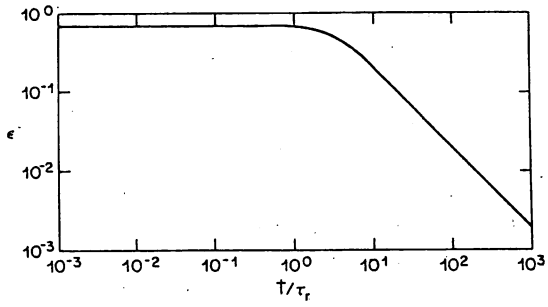


Fig. 6. Relation between $T/\tau_r$ and $\epsilon$ calculated by using (11).

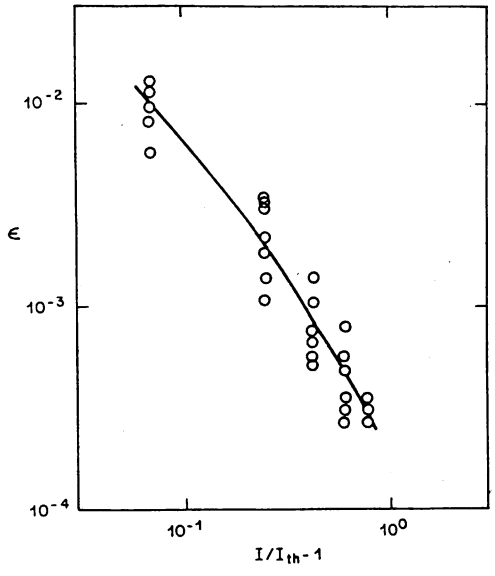


Fig. 7. Relation between $I/I_{th} - 1$ and $\epsilon$. Open circles represent the experimental results. A solid curve represents a least-square fit to the experimental results.

This function was employed in order that the average frequency of mode-hopping $f_c$ estimated in the following, decreases exponentially as a function of $(I/I_{th} - 1)$. This exponential decrease of $f_c$ has been shown experimentally and theoretically for solitary lasers in which mode-hopping follows a stochastic Poission process driven by the fluctuation of spontaneous emission [6]. The least-square fit of the experimental data gives $A = 8.4 \times 10^{-4}$ and $B = 1.7$ for the constants in (12).

Since the range of $\epsilon$ in Fig. 7 is smaller than $1 \times 10^{-2}$, Fig. 6 shows that $\epsilon$ can be approximated as

$$\epsilon \cong 2/(T/\tau_r). \quad (13)$$

From (7) and (13) the mode-hopping frequency is given by

$$f_c \cong \epsilon/4\tau_r. \quad (14)$$

The rise time $\tau_r$ in (13) depends on the difference between the small signal gain and the cavity loss, and can be approximately expressed as [6]

$$\tau_r = \tau_p/(I/I_{th} - 1) \quad (15)$$

where $\tau_p$ is the photon lifetime. Since $\tau_p$ is inversely proportional to the cavity loss, $\tau_r$ is given by

$$\tau_r = 1\Big/\left[(I/I_{th} - 1)\cdot c \cdot \left\{\frac{nl}{L}\cdot\alpha_{in} + \frac{1}{2L}\cdot\ln\left(\frac{1}{R_1 T_l^2 R_2}\right)\right\}\right] \quad (16)$$

where $n$ is the refractive index, $l$ is the length, $\alpha_{in}$ is the internal loss of the laser diode, $c$ is the speed of light in vacuum, $L$ is the length of the external cavity, $R_1$ is the reflectivity of the uncoated laser diode facet, $R_2$ is the reflectivity of the external grating, and $T_l$ is the transmissivity of the objective lens in the cavity. By substituting (12) and (16) into (14) and using the parameters in the experiments ($l$ = 300 $\mu$m, $n$ = 3.5, $\alpha_{in}$ = 20 cm, $L$ = 7.5 cm, $R_1$ = 0.3, $R_2$ = 0.6, $T_l$ = 0.8), we obtain the mode-hopping frequency

$$f_c = 2.7 \times 10^6 \times \exp\left[-1.7(I/I_{th} - 1)\right] \quad \text{(Hz)}. \quad (17)$$

The value of $f_c$ is in the range of 0.69 MHz $\leq f_c \leq$ 2.4 MHz for 0.07 $\leq (I/I_{th} - 1) \leq$ 0.8, which is shown in Fig. 7.

The minimum delay time in the interferometer ($\tau_d > 1/f_c$) required to violate the anticorrelation between $\alpha_1$ and $\alpha_2$ is 1.5 $\mu$s. This corresponds to a 320-m length of fiber delay line, for a fiber refractive index of 1.4. This means that the 2.8-km fiber used in the experiment provided a sufficiently long delay time.

The mode-hopping detection system becomes more compact if a sufficiently large signal can be obtained without using the fiber delay line. Fig. 5 shows that mode hopping can be detected without using the delay line, but the signal intensity is much lower than that obtained with the 2.8-km fiber delay line. The signal intensity without the delay line increases if the degree of anticorrelation between $\alpha_1$ and $\alpha_2$ is decreased. This can be achieved by increasing the rise and fall times with a long photon lifetime. Since the photon lifetime is proportional to the length of the external cavity, the signal intensity without the delay line depends on the cavity length. Fig. 6 shows that $\epsilon$ is a constant nearly equal to unity for $T/\tau_r < 1$. This indicates that the signal intensity without the fiber delay line approaches that with a long fiber delay line for $T/\tau_r \leq 1$. The minimum cavity length $L_m$ required for $T/\tau_r < 1$ can be derived from (7) and (16), and is given by

$$L_m = \frac{c}{2f_c}\cdot(I/I_{th} - 1)\cdot\left\{nl\alpha_{in} + \frac{1}{2}\ln\left(\frac{1}{R_1 T_l^2 R_2}\right)\right\}. \quad (18)$$

Curve $A$ in Fig. 8 shows $L_m$ calculated using (17) and (18). Curves $B$, $C$, and $D$ in this figure show the values of cavity lengths required to get a mode-hopping signal intensity with $\epsilon = 10^{-1}$, $10^{-2}$, and $10^{-3}$, respectively, calculated using (13). Fig. 8 also shows that without the fiber delay line the signal intensity is higher if the external-cavity laser is operated at a lower bias level.

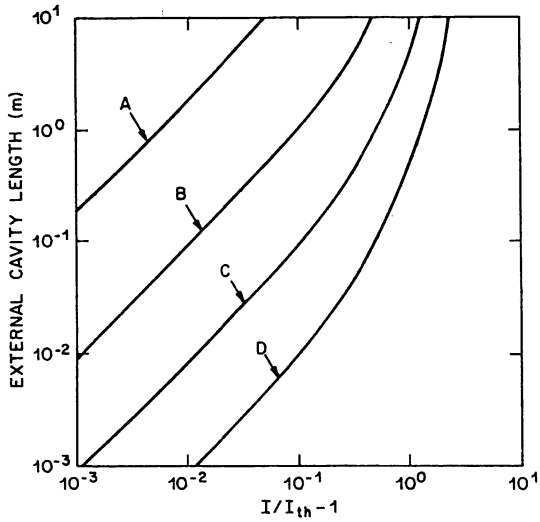


Fig. 8. Relation between $I/I_{th} - 1$ and the external cavity length for $\epsilon$ equals ($A$) 1, ($B$) $10^{-1}$, ($C$) $10^{-2}$, and ($D$) $10^{-3}$. $\epsilon$ is the ratio of the mode-hopping signal levels detected without and with an infinitely long delay line.

## IV. A Negative Feedback Circuit for Automatic Mode-Hopping Control

### *A. Demonstration of the Feedback Circuit*

In principle, control of the PZT voltage can be synchronized to the rotation of the grating so that mode hopping is prevented in the external-cavity laser when the laser frequency is tuned. In practice, however, external cavity lasers are complicated and a negative feedback circuit is almost always necessary to prevent mode hopping. We demonstrate here that our mode-hopping detection method can be utilized in a automtic mode-hopping control circuit.

The experimental apparatus for the negative feedback loop is shown in Fig. 1(a). The output signal from the Mach–Zehnder interferometer was amplified and heterodyned with a 2-GHz microwave local oscillator. The amplitude of this down-shifted low-frequency signal from the double balanced mixer was monitored by an envelope detecting circuit. The output signal from this circuit was applied to a control circuit for the PZT driver. When a mode-hopping signal was detected, the external cavity length was automatically shifted in one direction by the PZT driver until the mode-hopping signal disappears.

In this experiment, the angle of the grating was fixed and the PZT voltage was scanned to introduce mode hopping. The negative feedback circuit then was turned on to demonstrate mode-hopping prevention. The laser operating with the mode-hopping behavior shown in Fig. 2, which is an example of a nonideal external-cavity behavior, was used in this demonstration. When the feedback loop was open and $V_{PZT}$ was increased by the PZT driver, mode-hopping occurred at several values of $V_{PZT}$ as shown in Fig. 2. The monotonic increase of $V_{PZT}$ with time is shown in Fig. 9(a). When the feedback loop was closed, the corresponding $V_{PZT}$ curve in Fig. 9(b) shows an irregular variation with time, indicating the function of the mode-hopping control circuit that maintained single-mode

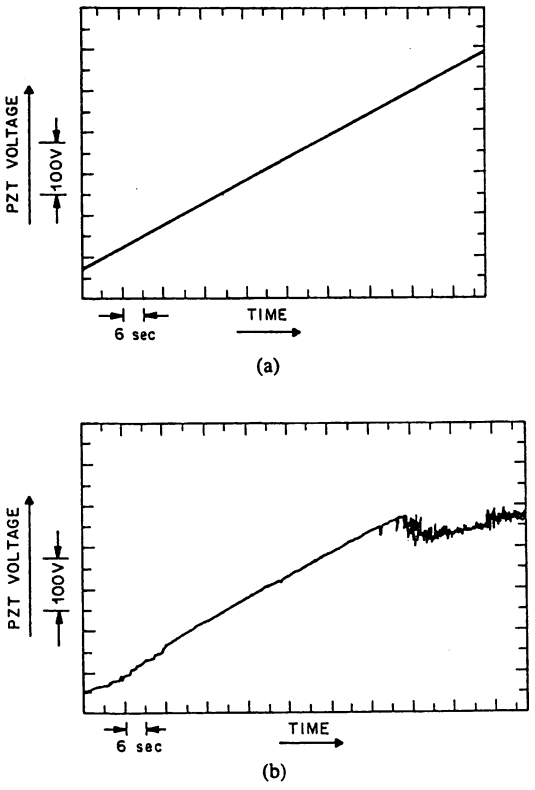


Fig. 9. Time dependences of $V_{PZT}$ which was swept at a constant speed. (a) The feedback loop was open. (b) The feedback loop was closed.

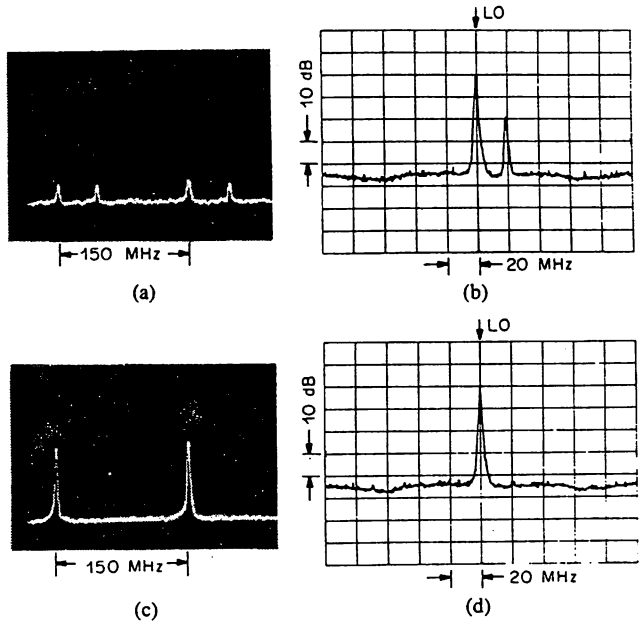


Fig. 10. Longitudinal mode spectra (a) and the monitoring signal from the Mach–Zehnder interferometer (b) when the feedback loop was open. (c) and (d) are those when the feedback loop was closed. In (b) and (d), the spectral line marked by LO is from the 2-GHz local oscillator in the control circuit. The peak on the higher frequency side of the LO peak in (b) is the mode-hopping signal.

oscillation in the laser for the whole range of the PZT voltage sweep. Fig. 10(a) and (b) shows a longitudinal mode spectrum during mode hopping and the corresponding mode-hopping signal from the Mach–Zehnder interferometer when the feedback loop was open. The free spectral range of the scanning Fabry–Perot interferometer is 150 MHz. When the feedback loop was closed, Fig. 10(c) and (d) shows the controlled single-mode operation when $V_{PZT}$ was swept. Single longitudinal mode oscillation was confirmed by both the longitudinal mode spectrum from the scanning Fabry–Perot interferometer and the spectrum analyzer display after the Mach–Zehnder interferometer. The peaks marked by LO in Fig. 10(b) and Fig. 10(d) are from the microwave local oscillator in the control loop.

Since the mode-hopping characteristics in the external cavity laser had hysteresis with respect to the variation of $V_{PZT}$ and were also sensitive to mechanical vibration, the variation of $V_{PZT}$ with the feedback loop closed (Fig. 9(b)) during mode-hopping control was complicated and might not be reproducible if the alignment of the external cavity changed. However, mode hopping was always suppressed and a single longitudinal mode oscillation was maintained as long as the negative feedback loop was closed.

The same mode-hopping control technique we have demonstrated may be employed for monolithic integrated devices with a distributed Bragg reflector (DBR) [5] if the laser has a passive-cavity section longer than about 0.5 cm. The current applied to the passive cavity section in the integrated device corresponds to $V_{PZT}$ in our experiment and the current applied to the DBR section for frequency tuning corresponds to the grating rotation. For an integrated device, however, the internal loss of the long semiconductor cavity is much higher than that of an air external cavity; therefore the photon lifetime should be treated differently. However, the same negative feedback circuit can be used as long as the longitudinal mode spacing is at a low enough frequency detectable with a photodiode.

### *B. Applications*

Although the mode-hopping control circuit demonstrated here is relatively simple, the application to lasers in heterodyne detection systems is dependent on the system bandwidths. We discuss here examples where the method is applicable and some limitations of this technique.

The control loop detects mode hopping and uses it as the feedback signal to reset the laser operating point for single-mode oscillation. At the time when mode hopping is detected and before the laser is reset, the bit-error rate in a high-data-rate communication system may increase. The bandwidth of the feedback loop is mainly limited by the average mode-hopping frequency, which is estimated in Section III to be of the order of 1 MHz. This is true in the case of an integrated external-cavity DBR laser, which can be electrically tuned at a high speed by current changes. For a grating external-cavity laser, the speed of the PZT element also contributes to the bandwidth of the feedback loop. With a 1-MHz bandwidth, the control loop is not fast enough to stabilize a laser used as the source in an optical communication system, which is typically specified to have a less than $1 \times 10^{-9}$ bit-error rate.

However, the feedback circuit can be used for controlling a local oscillator laser in the receiver used in a multichannel coherent-detection system. When a local oscillator is tuned by the user to different channels over a wide frequency range, mode hopping occurs; but the noisy period during tuning, before communication is established, is acceptable. This is similar to tuning an AM/FM radio to different channels. The acquiring time for tuning the local oscillator to one channel frequency is typically much longer than 1 $\mu$s. Once the local oscillator is tuned to a selected frequency, however, the automatic control circuit monitors mode hopping and sets the laser at an optimum single-mode operation point at a speed faster than the channel acquiring time.

The present mode-hopping control circuit can also be applied to the lasers used in coherent optical sensing systems. The measurement times in sensing systems are usually much longer than one microsecond. Mode hopping that occurs at a hopping rate of about 1 MHz can be detected by the control loop which resets the laser for single mode operation. This does not affect the accuracy of optical measurements because the speed of the mode-hopping control loop is higher than the sensing system.

We should note that, in general, two control variables are required for the local oscillator, because the local oscillator should track the signal laser and maintains single-mode operation at the same time. In the case of the grating-tuned external-cavity laser, the required two degrees of freedom can be obtained by controlling both the grating angle and the PZT voltage. When the laser is fine tuned, change in $V_{PZT}$ varies the frequency of the lasing longitudinal mode and at the same time the grating angle can be controlled to follow the frequency change to avoid mode hopping. The channel frequency, or the signal laser frequency, is assumed to be fixed. If a tunable external-cavity laser is used as the local oscillator, $V_{PZT}$ can be adjusted by an intermediate-frequency locking circuit to lock the local oscillator to the signal laser, and the grating angle can be controlled by the mode-hopping control circuit to maintain single-mode operation. In the case of an integrated external-cavity DBR laser, the corresponding two control parameters are the two currents applied to the DBR section and the passive external-cavity section.

## V. Summary

An interferometric method was proposed to monitor mode hopping between successive longitudinal modes in external-cavity semiconductor lasers. The experimental results for a 1.3-$\mu$m grating-tuned external-cavity laser showed that this mode-hopping detection method is much more sensitive than previously proposed methods related to measurements of the light-current or voltage-current characteristics. The average frequency of mode hopping, for a 7.5-cm external-cavity length, was estimated from the ratio of the mode-hopping signals obtained with and without a delay line in the interferometer. The estimated hopping frequency is dependent on the dc injection current to the laser, and it can be expressed as $f_c = 2.7 \times 10^6 \times \exp[-1.7(I/I_{th} - 1)]$ (hertz) for $0.07 \leq (I/I_{th} - 1) \leq 0.8$. The monitoring signal was negatively fed back to the grating-tuned external-cavity laser to prevent mode hopping. With this control circuit, single-longitudinal-mode oscillation was automatically maintained while the external grating was adjusted by a PZT element for wavelength tuning.

## References


[1] S. Saito and Y. Yamamoto, "Direct observation of lorentzian lineshape of semiconductor laser and linewidth reduction with external grating feedback," *Electron. Lett.*, vol. 17, pp. 325-326, 1981.

[2] R. Wyatt and W. J. Devlin, "10-kHz linewidth 1.5-$\mu$m InGaAsP external cavity laser with 55-nm tuning range," *Electron. Lett.*, vol. 19, pp. 110-112, 1983.

[3] N. A. Olsson and J. P. van der Ziel, "Performance characteristics of 1.5-$\mu$m external cavity semiconductor lasers for coherent optical communication," *J. Lightwave Technol.*, vol. LT-5 pp. 510-515, 1987.

[4] K.-Y. Liou, Y. K. Jhee, G. Eisenstein, R. S. Tucker, R. T. Ku, T. M. Shen, U. K. Chakrabarti, and P. J. Anthony, "Linewidth characteristics of fiber-extended-cavity distributed-feedback lasers," *Appl. Phys. Lett.*, vol. 48, pp. 1039-1041, 1986.

[5] S. Murata, I. Mito, and K. Kobayashi, "Over 720 GHz (5.8-nm) frequency tuning by a 1.5-$\mu$m DBR laser with phase and Bragg wavelength control regions," *Electron. Lett.*, vol. 23, pp. 403-405, 1987.

[6] M. Ohtsu, Y. Teramachi, Y. Otsuka, and A. Osaki, "Analyses of mode-hopping phenomena in an AlGaAs laser," *IEEE J. Quantum Electron.*, vol. QE-22, pp. 535-543, 1986.

[7] L. E. Richter, H. I. Mandelberg, M. S. Kruger, and P. A. McGrath, "Linewidth determination from self-heterodyne measurements with subcoherence delay times," *IEEE J. Quantum Electron.*, vol. QE-22, pp. 2070-2074, 1986.

[8] N. A. Olsson and W. T. Tsang, "Transient effects in external cavity semiconductor lasers," *IEEE J. Quantum Electron.*, vol. QE-19, pp. 1479-1481, 1983.

[9] R. W. Dixon, "Derivative measurements of light-current-voltage characteristics of AlGaAs double-heterostructure lasers," *Bell Syst. Tech. J.*, vol. 55, pp. 973-980, 1976.

[10] M. Sargent III, M. O. Scully, and W. E. Lamb, Jr., *Laser Physics*. Reading, MA: Addison-Wesley, 1974, ch. 8.


*


**Motoichi Ohtsu** was born in Kanagawa, Japan, on October 5, 1950. He received the B.S., M.S., and Ph.D. degrees in electronics engineering from the Tokyo Institute of Technology, Tokyo, Japan, in 1973, 1975, and 1978, respectively.

In 1978, he was appointed a Research Associate, and in 1982, became an Associate Professor at the Tokyo Institute of Technology. From September 1986 to July 1987, on leave of absence from Tokyo Institute of Technology, he joined AT&T Bell Laboratories, Crawford Hill Laboratory, Holmdel, NJ. His main fields of interest are the frequency control of lasers, analysis of dynamic behavior of lasers, and its applications to coherent optical measurements, optical communications, and microwave atomic clocks. He has written seven books.

Dr. Ohtsu is a member of the Institute of Electronics, Information, and Communication Engineers of Japan, the Institute of Electrical Engineers of Japan, the Japan Society of Applied Physics, and the Optical Society of America. In 1982, he was awarded a prize from the Japan Society of Applied Physics. He was also awarded the Issac Koga Gold Medal from the International Union of Radio Science (URSI) in 1984.

**Kang-Yih Liou** received the B.S. degree in physics from National Taiwan University, Taipei, Taiwan, in 1970, the M.S. degree in physics from Temple University, Philadelphia, PA, in 1974, and the Ph.D. degree in materials science from University of Wisconsin at Madison in 1978.

From 1979 to 1980, he was a Research Scientist at Argonne National Laboratory, Argonne, IL, where he contributed to theories and experiments of radiation modified thermodynamics of solids, ion implantation, and defects in crystals. He joined AT&T Bell Laboratories at Allentown, PA, in October 1980, where he did work on semiconductor lasers and transmitters, and single-frequency coupled cavity lasers. Since 1984 he has been with the Crawford Hill Laboratory of AT&T Bell Laboratories at Holmdel, NJ. His current research interests include semiconductor lasers and related optoelectronic integrated circuits and devices for lightwave systems.

*

**Ellsworth C. Burrows** was born in Nassau, The Bahamas, on November 14, 1963. He received the A.A.S. degree in electronic technology from Technical Career Institute, New York, in 1985.

Currently he is a Technical Associate at AT&T Bell Laboratories Crawford Hill Laboratory, Holmdel, NJ, in the Photonic Devices Research Department.

**Charles A. Burrus, Jr.** (SM'63–F'74) was born in Shelby, NC in 1927. He received the B.S. degree *cum laude* from Davidson College in 1950, the M.S. degree from Emory University in 1951, and the Ph.D. degree from Duke University in 1955, all in physics. At Duke he studied under Texas Company and Shell Company fellowships, and was employed in the Physics Department as a Research Associate during 1954–1955.

In 1955 he joined the Technical Staff of AT&T Bell Laboratories, Holmdel, NJ, where his work initially was concerned with the millimeter- and submillimeter-wave region of the spectrum (microwave spectroscopy and various types of semiconductor diodes for millimeter-wave use), and later with sources and detectors for lightwave communications (fiber-compatible LED's, lasers, and p-i-n photodiodes), single-crystal active fibers, and the effects of deuterium and hydrogen in optical fibers. Currently he is engaged in work on high-speed semiconductor devices for lightwave communications in the 1- to 1.6-$\mu$m wavelength region.

Dr. Burrus is a member of Phi Beta Kappa, Sigma Pi Sigma, and Sigma Xi. He is a Fellow of the American Association for the Advancement of Science, the American Physical Society, and the Optical Society of America. He is the recipient of the 1982 David Richardson Medal in applied optics from the Optical Society of America and the Distinguished Technical Staff Award (1982) from AT&T Bell Laboratories.

*

**Gadi Eisenstein** (S'80–M'80) was born in Haifa, Israel, on June 20, 1949. He received the B.Sc. degree from the University of Santa Clara, Santa Clara, CA, in 1975 and the M.Sc. and Ph.D. degree from the University of Minnesota in 1977 and 1980, respectively, all in electrical engineering.

He joined the AT&T Bell Laboratories in 1980 where he is a Member of the Technical Staff in the Photonic Devices Research Department. His work is in the area of mode-locking and high-frequency modulation of semiconductor lasers, composite-cavity lasers, thin-film technology, optical amplifiers, and electrooptic waveguide devices.

# Power Partition Fluctuations in Two-Mode-Degenerate Distributed-Feedback Lasers

K.-Y. LIOU, M. OHTSU, C. A. BURRUS, JR., FELLOW, IEEE, U. KOREN, AND T. L. KOCH

*Abstract*—**We present measurements and theoretical analysis of power partition fluctuations in a distributed feedback (DFB) laser operating CW with the two DFB degenerate modes as the only significant longitudinal modes. The power ratio of the two modes was varied from 1:1 to 2500:1 by electrical control using a novel two-electrode DFB laser. The laser was observed to exhibit 1) transient power dropouts and 2) two-mode relaxation oscillation. The dropout depths were less than 30 percent of the main-mode power in all cases, except when the laser was subjected to external optical feedback. The relaxation oscillations of the two mode powers are anticorrelated, which is different from the well-known relaxation oscillation of the total output power due to photon-carrier interaction. The calculated result based on a Fokker–Planck analysis agrees with the experiment, except for the two-mode relaxation oscillation, which was not considered in the theory.**

## I. INTRODUCTION

DISTRIBUTED-FEEDBACK (DFB) injection lasers, due to their single-longitudinal-mode characteristics, are potentially useful for optical fiber communication and interferometric optical sensing. In practice, however, the stability of single-mode operation in DFB lasers can still be affected by unwanted side modes. These additional side modes in a DFB laser are either Fabry–Perot resonances due to facet reflections or other DFB resonances. The Fabry–Perot modes can be suppressed, for example, by antireflection coatings on the end facets. For an ideal DFB laser without facet reflections, however, it is known that the two lowest order DFB modes have equal threshold gains and that they are equally likely to oscillate [1]. Two-mode oscillation in the DFB laser has been found to cause error-rate flooring in a high-bit-rate long-distance transmission system even at the 1.3-$\mu$m minimum fiber dispersion wavelength [2]. Although a phase shifted grating [3]–[6] or asymmetric facet structures [7], [8] can be designed into the DFB laser to remove the two-mode degeneracy, the stability of single-mode operation as the lasers degrade has not yet been confirmed.

Mode power fluctuations in DFB lasers, under the condition that the two degenerate DFB modes are the only competing longitudinal modes, have not been investigated previously, although such information is important for understanding the behavior of DFB lasers and for designing reliable optical fiber systems. We present in this paper measurements and a theoretical analysis of power partition fluctuations in a DFB laser due to the characteristic two-mode degeneracy. The two degenerate DFB modes are the only two significant longitudinal modes in the experiment, and the same condition is treated in the theory. A novel DFB laser in which the two-mode degeneracy can be electrically controlled was used in the experiment to simulate the mode behavior of a conventional DFB laser. The laser, which we have reported previously [9], [10], is a 1.3-$\mu$m DFB laser with two separate electrodes. Adjustment of the two currents applied to the two electrodes allows active control of the oscillations of the two degenerate modes [9]. High-speed wavelength switching between the two modes and optical logic operations by current control of such a two-electrode DFB laser have also been demonstrated previously [10].

In the present experiment, the power ratio of the two degenerate DFB modes under continuous wave (CW) operation was varied from 1:1 to 2500:1 by controlling the currents applied to the two electrodes of the DFB laser. The wavelengths of the two modes were separated by a 20-Å stopband of the DFB resonator [1]. Power partition fluctuations of the laser under the two-mode condition and power dropouts of the dominant DFB mode in the nearly single-mode cases were measured. The measured power dropout rates were in good agreement with calculated results. However, a two-mode power relaxation oscillation phenomenon was observed in the experiment, which was not considered in the theory and may account for some discrepancy between calculated results and the experiment. This two-mode relaxation oscillation was not reported in previous investigations on partition fluctuations in DFB lasers [11] or other nearly single-mode Fabry–Perot lasers [12]–[14], probably because the dominant lasing mode in those cases was influenced by more than one competing side mode.

## II. EXPERIMENT

The DFB laser used in the experiment is of the semi-insulating planar buried heterostructure (SIPBH) [15] type. The laser was grown by metalorganic chemical vapor deposition (MOCVD) with an emitting wavelength near 1.3 $\mu$m. A first order grating was processed by hol-

Manuscript received February 16, 1988; revised May 16, 1988.

K.-Y. Liou and C. A. Burrus are with AT&T Bell Laboratories, Crawford Hill Laboratory, Holmdel, NJ 07733.

M. Ohtsu was with AT&T Bell Laboratories Crawford Hill Laboratory, Holmdel, NJ 07733, on leave from Tokyo Institute of Technology, Tokyo, Japan.

U. Koren and T. L. Koch are with AT&T Bell Laboratories, Holmdel, NJ 07733.

IEEE Log Nubmer 8824811.

0733-8724/89/0400-0632$01.00 © 1989 IEEE

ography and chemical etching. The grating coupling constant $\kappa$, estimated from the scanning electron micrographs of the corrugation, was about 100 $cm^{-1}$. The separated contact pads were metallized on the p side of the laser, which was cleaved and then mounted p-side up on a copper heat sink.

Fig. 1(a) shows a shematic diagram of the DFB laser with the two electrodes which are used for electrical control of the power ratio of the two degenerate modes. The two-mode degeneracy is a characteristic of an ideal DFB laser which is symmetrical along the axial direction and has no reflections from the end facets. The non-uniform current densities applied to a two-electrode DFB laser vary the profile of refractive index and gain coefficient along the laser cavity, which introduces axial asymmetry in the DFB resonator and removes the two-mode degeneracy [9], [10]. Facet reflections can also introduce asymmetry and can stabilize one of the two modes [16] but the effect is dependent on the phase of the DFB grating relative to the positions of the end facets, which are cleaved randomly without control of their locations. The two-electrode method, however, permits active control of the two-mode degeneracy even for a laser with reflections from randomly cleaved facets, as in the present case.

Fig. 1(b) shows examples of the longitudinal mode spectra recorded by a grating spectrometer for a DFB laser under CW operation with two injection currents, $I_1$ and $I_2$, applied to the two electrodes at 25°C. When $I_1$ was fixed at 35 mA while $I_2$ was increased from 8 to 10 mA, the spectrum changed continuously from oscillation at the $\lambda_{+1}$ mode to simultaneous $\lambda_{-1}$ and $\lambda_{+1}$ two-mode oscillation. Further increase in $I_2$ switched to single mode operation at $\lambda_{-1}$. The two degenerate DFB modes, $\lambda_{-1}$ = 12976 Å and $\lambda_{+1}$ = 12996 Å, were separated by a 20-Å stopband, which was confirmed by the spontaneous emission spectrum below threshold. The lengths of the two electrodes of this laser were $L_1$ = 197 $\mu$m and $L_2$ = 76 $\mu$m. The gap between the two sections was 32 $\mu$m, providing an 80 Ω electrical isolation.

The output powers from the two facets of a two-electrode DFB laser are not equal, especially when the two sections are unequally pumped. Even for a conventional single-electrode DFB laser, it is known that the front face and back face output powers are different, simply because of the different grating phases at the randomly cleaved facets [17]. The same asymmetric grating phase effect may also influence the spectrum because one side of the laser may be more transparent for one DFB mode than the other. For the two-electrode DFB laser used for measurements, we found that when the power ratio of the two DFB modes was 1:1 from one facet, it was about 3:2 from the other. However, the difference between the front face and back face output spectra became negligible when the main-to-side mode ratio was higher than 20:1. In the experiment, the output from the facet of the longer section of a two-electrode DFB laser was used.

For the power partition measurement, the power ratio of the $\lambda_{+1}$ and $\lambda_{-1}$ modes, $P_{+1}/P_{-1}$, was varied from

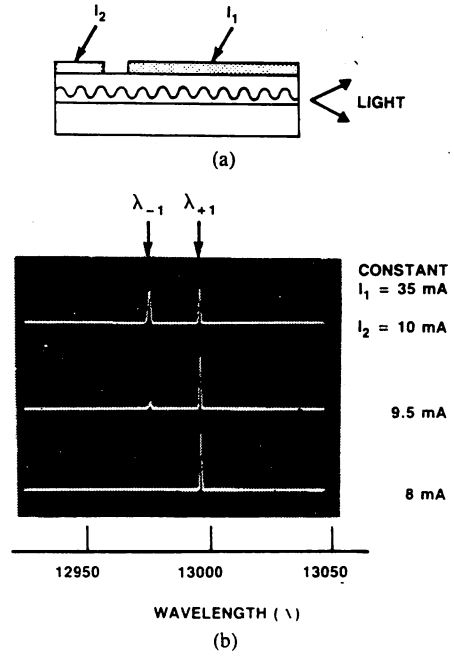


Fig. 1. (a) The schematic diagram of a two-electrode DFB laser, and (b) CW longitudinal mode spectra showing electrical control of the two degenerate DFB modes.

1:1 to 2500:1 by adjusting $I_1$ and $I_2$. All the other side modes, including the Fabry–Perot modes, were suppressed relative to the main mode by more than a 4000:1 ratio for the laser (Fig. 1) chosen for the measurement. The Bragg wavelength of this laser was close to the peak of the gain spectrum. Therefore, the two DFB modes had about the same material gain, and the $\lambda_{+1}$ mode was chosen arbitrarily as the main mode in the experiment. The laser was CW operated at a constant power of 2 mW from the output facet while the $P_{+1}/P_{-1}$ ratio was varied.

Power partition (dropout) events of the main DFB mode were analyzed by a method similar to that used by Linke *et al.* for nearly single-mode short-cavity Fabry–Perot lasers [12]. Using this method, a grating monochromator was used as a mode filter to pass only the $\lambda_{+1}$ mode or the $\lambda_{-1}$ mode. The passed single mode was detected with a wide-band InGaAs p-i-n photodiode. The detected light intensity was amplified with a broad-band (dc to 3.2 GHz) amplifier and then analyzed using a real-time oscilloscope with a 1-GHz bandwidth. The power partition events were used to trigger the oscilloscope, and a delay line was used to display the dropout events near the center of the oscilloscope trace. At the same time, the rate of the dropout events was measured by triggering a frequency counter using the gate output from the oscilloscope.

Two optical isolators were used in series with the laser to provide about 60 dB of optical isolation from external reflections. Also, the p-i-n detector was tilted to decouple the laser from light reflected from the surface of the photodiode. These precautions were found to be necessary for suppressing reflection-induced mode power fluctuations that were observed for the DFB laser.

Fig. 2 shows an example of the power partitioning in

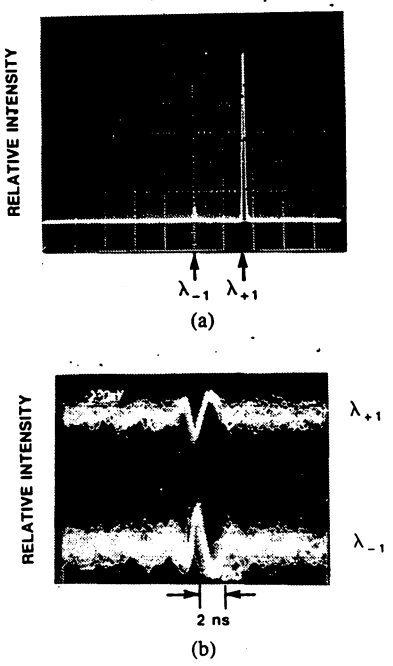


Fig. 2. Partition dropout events in the DFB laser at 2-mW output. (a) CW spectrum with a 14:1 power ratio, all the other side modes are suppressed by more than 4000:1 ratio relative to the main mode. (b) Oscilloscope display of the two-mode partition events.

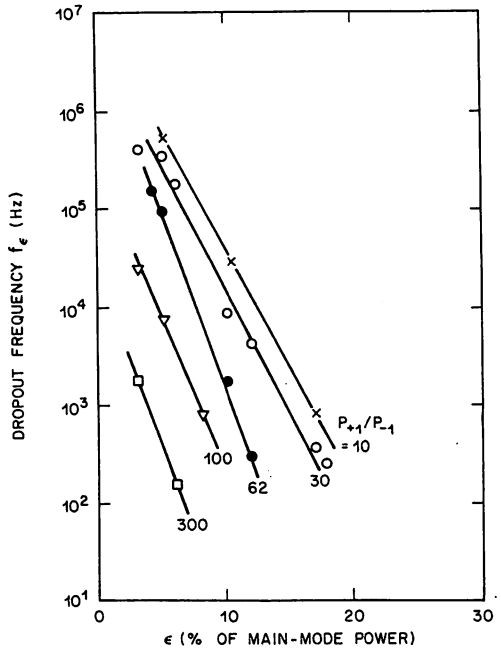


Fig. 3. Measured rates of dropout events $f_\epsilon$ with dropout depths deeper than a fraction $\epsilon$ of the main-mode power. $f_\epsilon$ is plotted as a function of $\epsilon$ for different power ratios of the two degenerate DFB modes at constant 2-mW total output power.

the DFB laser. In this case, the main lasing mode is the $\lambda_{+1}$ mode, and the $\lambda_{-1}$ mode is the only significant side mode, as can be seen in the CW spectrum in Fig. 2(a). The main-to-side mode power ratio $P_{+1}/P_{-1}$ is 14. Fig. 2(b) shows the real-time oscilloscope traces of the dropout events. When the power of the main mode drops, the power of the side mode increases. However, the total output power of the laser remains nearly constant in time. In Fig. 2(b), the amplitude of power fluctuations of the $\lambda_{-1}$ mode appears to be higher than the fluctuation amplitude of the $\lambda_{+1}$ mode. This was found to be caused by a small difference in the optical coupling efficiencies of the two modes to the p-i-n detector in the experiment due to an alignment drift.

The measured power dropout frequencies $f_\epsilon$ of the main mode are plotted in Fig. 3 as a function of the dropout depth $\epsilon$ for various main-to-side mode power ratio $P_{+1}/P_{-1}$. Here $\epsilon$ is defined as the fraction of the average power of the main mode and $f_\epsilon$ is the rate of dropout events of the main mode deeper than $\epsilon$. The total output from the laser was kept constant at about 2 mW for all $P_{+1}/P_{-1}$ values. For $P_{+1}/P_{-1}$ higher than 500, the dropout rates became too low to be measured accurately. The depths of the dropout events were found to be less than about 30 percent, even for $P_{+1}/P_{-1} = 1$. This indicates that the two DFB modes, 20 Å apart, are oscillating simultaneously without complete mode change.

Mode power fluctuations with more than 30-percent power changes between the two modes or even complete mode switching were observed only when the optical isolators were removed in the experiment and optical feedback from the detector to the laser was introduced intentionally. Changes in the side mode suppression ratio with optical feedback were also observed. Reflections were not calibrated in the experiment to quantify feedback induced fluctuations since optical feedback had been shown previously to have various effects on DFB lasers depending on the feedback level (e.g., [18], [19]). For studying the properties of DFB lasers, an optical isolation of about 60 dB is generally required to suppress the reflection effects.

In addition to the transient dropout events in the DFB laser, anticorrelated periodic oscillations of the two mode powers were observed. As can be seen in Fig. 2(b), the power level of both the $\lambda_{+1}$ and $\lambda_{-1}$ mode are noisy at all times before and after the dropout events. This amplitude noise is revealed by the single sweep oscilloscope traces in Fig. 4 for the case where the two modes have about the same average power. Fig. 4(a) and (b) for the $\lambda_{+1}$ and $\lambda_{-1}$ mode, respectively, were recorded at different times. The powers of the two modes shown in the figure are both oscillating at a frequency of about 1.3 GHz. The amplitude noise spectra under this two-mode condition were measured using a spectrum analyzer. The noise spectrum for a single mode, the $\lambda_{+1}$ mode shown in Fig. 5 for example, shows clearly a peak near 1.3 GHz (and a smaller second-harmonic peak near 2.5 GHz). A similar noise spectrum with a 1.3-GHz peak was observed for the $\lambda_{-1}$ mode. However, the 1.3-GHz oscillation peak disappears in the noise spectrum of the total output power in Fig. 5, indicating that the power oscillations of the two DFB modes are anticorrelated. The noise spectrum of the total output is similar to the background noise when the laser is off, except a weak noise peak is still noticeable at 1.3 GHz in Fig. 5. This weak residual noise peak exists in

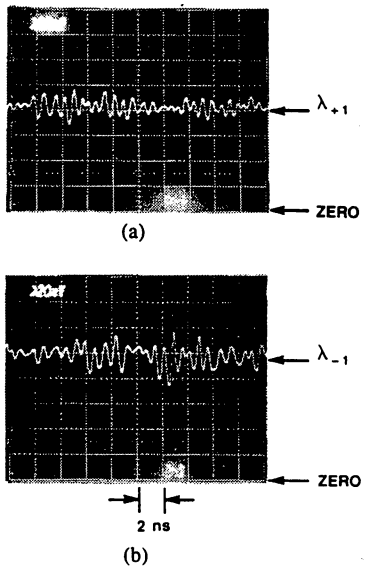


Fig. 4. Single-sweep oscilloscope trace of (a) the $\lambda_{+1}$ mode power and (b) the $\lambda_{-1}$ mode power, showing two-mode relaxation oscillation; (a) and (b) are not recorded at the same time. The two modes have about the same average power in this case; they oscillate in an anticorrelated fashion even when they have unequal powers.

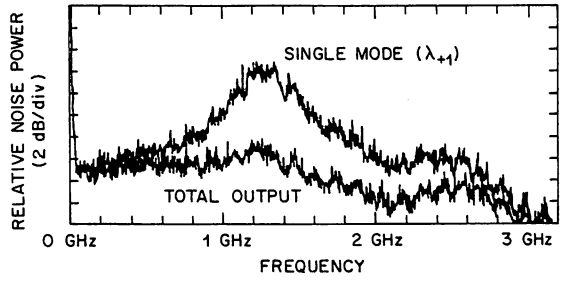


Fig. 5. Amplitude noise spectra showing a two-mode relaxation oscillation peak at 1.3 GHz for a single mode, while the total output power of the laser remains nearly a constant. The laser is operated under the same condition as in Fig. 4.

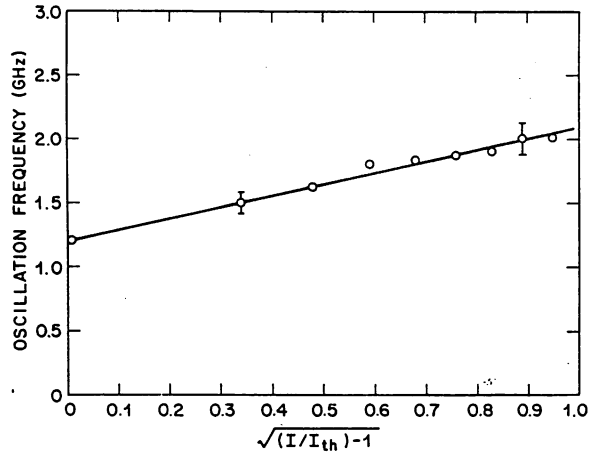


Fig. 6. Measured frequency of two-mode oscillation versus $\sqrt{(I/I_{th}) - 1}$ for $P_{+1} = P_{-1}$. The total current $I = I_1 + I_2$, and $I_{th}$ is the total threshold current.

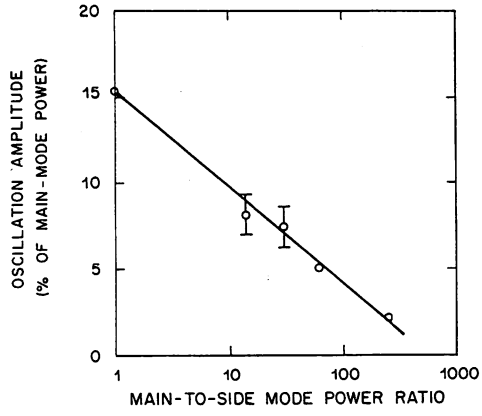


Fig. 7. Measured amplitude (one half the maximum peak-to-peak range) of the two-mode relaxation oscillation versus the power ratio of the two degenerate DFB modes at a constant total output of 2 mW.

the total output spectrum probably because the anticorrelated oscillations of the two DFB modes do not follow each other perfectly.

The frequency of the two-mode relaxation oscillation was measured as a function of the pumping level. Since the two facets have unequal output powers and the intracavity optical power is not easily measurable, the total injection current was used. Fig. 6 shows the measured oscillation frequency versus $[(I/I_{th}) - 1]^{1/2}$. The total current, $I = I_1 + I_2$, was varied while maintaining $P_{+1} = P_{-1}$ for the plot in Fig. 6 and $I_{th}$ is the total current at threshold. A decrease in the oscillation frequency, but less than 0.5 GHz, was observed when the mode power ratio $P_{-1}/P_{+1}$ was reduced. However, the two mode powers oscillated only when the side mode was significant. Fig. 7 shows the measured oscillation amplitudes, defined as one half of the maximum peak-to-peak range of power oscillation of the main mode. The oscillation amplitude decreases from 15 percent of the main-mode power for $P_{+1}/P_{-1} = 1$ to about 2.5 percent for $P_{+1}/P_{-1} = 300$. From the plot in Fig. 7, the two-mode relaxation oscillations disappears when the DFB laser operates with a single mode with a main-to-side mode ratio equal to or higher than about 500 : 1.

To verify that the observed two-mode relaxation oscillation is not a characteristic only of the DFB laser with two electrodes, a conventional DFB laser with a single electrode was tested. The selected single-electrode DFB laser oscillated with two degenerate DFB modes in a certain current range near room temperature. The same two-mode power relaxation oscillation phenomenon was observed for the single-electrode DFB laser. Although two-mode operation conditions at a constant total power for the single-electrode DFB laser cannot be controlled as precisely as with the two-electrode laser, the power partitioning behavior of the two lasers appeared to be similar. This observation confirms that the measured results for the two-electrode DFB laser are representative of conventional single-electrode DFB lasers.

## III. Theory

We consider in this section power partition fluctuations of a laser whose CW spectrum consists of only two sig-

nificant longitudinal modes. A stochastic approach based on a Fokker–Planck equation is used to compute the rates of partition (dropout) events for various power ratios of the two modes. In the numerical calculation, the separation between the two modes is chosen to be 20 Å, which is the width of the stop band of the DFB laser used in the experiment in Section II. Although two-current adjustment was used in the experiment for active control of two-mode operation, the theory considers the simple case of a conventional single-electrode DFB laser that oscillates with two modes under uniform current injection. The calculated result will be compared with the experiment.

A theory we developed earlier for a two-wavelength Fabry–Perot/DFB laser [20] is modified here for the case of a DFB laser that oscillates with the two degenerate DFB modes. In [20], oscillation of a DFB mode detuned from the gain peak and a Fabry–Perot mode near the gain peak with equal mode powers was analyzed for the design of a two-wavelength semiconductor laser. Here we analyze the power fluctuations of the two degenerate DFB modes that are separated by the stopband and may have equal or unequal mode powers. We write the rate equations for the electric fields of the two modes, $\tilde{E}_i$, and for the carrier density, $n^{(0)}$, in the density matrix formalism [21] as

$$\frac{d\tilde{E}_i^2}{dt} = \frac{1}{n\sqrt{\epsilon_0\mu_0}}\left[\tilde{\alpha}_i^{(1)} - \alpha_{thi} - \tilde{\alpha}_i^{(3)}\tilde{E}_i^2 - \tilde{\alpha}_{ij}^{(3)}\tilde{E}_j^2\right]\tilde{E}_i^2 \qquad (i, j = 1, 2;\ i \neq j) \tag{1}$$

$$\frac{dn^{(0)}}{dt} = -n\sqrt{\frac{\epsilon_0}{\mu_0}}\left(\frac{2}{\hbar\omega_1}\tilde{\alpha}_1^{(1)}\tilde{E}_1^2 + \frac{2}{\hbar\omega_2}\tilde{\alpha}_2^{(1)}\tilde{E}_2^2\right) - \frac{n^{(0)}}{\tau_s} + \frac{I}{V_e} \tag{2}$$

where the subscripts $i = 1$ and 2 represent the two DFB modes $\lambda_{+1}$ and $\lambda_{-1}$, respectively. In the equations, $n$ is the refractive index, $\epsilon_0$ and $\mu_0$ are the dielectric constant and the permeability in vacuum, $\hbar\omega$ is the photon energy, $\tau_s$ is the spontaneous lifetime, $V$ is the volume of the laser cavity, $I$ is the injection current, and $e$ is the electric charge. The parameter $\alpha_{thi}$ is the loss of the laser cavity, and $\tilde{\alpha}_i^{(1)}$, $\tilde{\alpha}_i^{(3)}$, $\tilde{\alpha}_{ij}^{(3)}$, are respectively the linear gain, the self-saturation coefficient, and the cross-saturation coefficient, which are all dependent on the carrier density $n^{(0)}$. The third order terms with $\tilde{\alpha}_i^{(3)}$ and $\tilde{\alpha}_{ij}^{(3)}$ are included in (1) to consider gain saturation due to intraband relaxation [21].

Using the approach of [20] in assuming that the carrier density is a constant in time, (1) is decoupled from (2). A constant carrier density is a good approximation for a laser under CW operation above threshold with a constant output power. This is the case of our experiment and previous observations [12], [22]. Even when the dropout event occurs, the total mode power of the laser remains constant in time. The total power is partitioned into the two DFB modes, which fluctuate in an anticorrelated fashion. However, the observed two-mode relaxation oscillation near 1.3 GHz may contribute to small errors in the numerical result calculated with the constant-carrier-density approximation, which will be discussed in Section IV.

The coefficients $\tilde{\alpha}_i^{(1)}$, $\tilde{\alpha}_i^{(3)}$, and $\tilde{\alpha}_{ij}^{(3)}$ in (1) can also be approximated as time independent constants when the carrier density is approximated as a constant. We can then derive from (1) the Langevin equations for the normalized electric field $E_i$,

$$\frac{dE_i}{d\tau} = \left(a_i - |E_i|^2 - \xi|E_j|^2\right)E_i + q_i(\tau) \qquad (i, j = 1, 2;\ i \neq j) \tag{3}$$

with

$$\xi = \tilde{\alpha}_{ij}^{(3)}/\tilde{\alpha}_i^{(3)} = \tfrac{4}{3}/\left[1 + (2\pi c\tau_{in}\Delta\lambda/\lambda^2)^2\right] \tag{4}$$

where $\tau$ in (3) is a normalized time, $q_i(\tau)$ is a random Langevin noise term caused by spontaneous emission, $\tau_{in}$ in (4) is the intraband relaxation time [21], $c$ and $\lambda$ are the light velocity and wavelength in vacuum, and $\Delta\lambda$ is the wavelength separation between the two modes. The quantity $a_i$ is a pump parameter of the $i$th mode and is proportional to the ratio of the average mode power to the root-mean-square intensity of spontaneous emission into that mode. Since the spontaneous emission rates for the two DFB modes, spaced by 20 Å, are nearly the same, $a_1/a_2$ equals the power ratio of the two modes.

The state of the laser oscillating with two modes can be represented by a vector $\vec{x} = (x_1, x_2, y_1, y_2)$, where $x_i$ and $y_i$ are the real and imaginary part of the normalized complex field $E_i$ of the $i$th mode. The partition fluctuations caused by spontaneous emission events can be described by fluctuations in $\vec{x}$ due to the random driving force $q_i(\tau)$ in (3). This stochastic process is similar to the Brownian motion which can be analyzed by the method of Fokker–Planck [e.g., (23)–(25)]. The Fokker–Planck equation for the probability density $p(\vec{x}, \tau)$ associated with the Langevin equations of motion in (3) is given by

$$\frac{\partial}{\partial\tau}p(\vec{x}, \tau) = \sum_{i=1}^{2}\left[-\frac{\partial}{\partial x_i}A_i^{(x)}p - \frac{\partial}{\partial y_i}A_i^{(y)}p + \left(\frac{\partial^2}{\partial x_i^2} + \frac{\partial^2}{\partial y_i^2}\right)p\right] \tag{5}$$

where

$$A_i^{(\eta)} = \left[a_i - (x_i^2 + y_i^2) - \xi(x_j^2 + y_j^2)\right]\eta_i \qquad (i, j = 1, 2;\ i \neq j,\quad \eta = x, y). \tag{6}$$

The solution of the Fokker–Planck equation can be expressed as

$$p(\vec{x}, \tau) = p_s(\vec{x}) \cdot e^{-\gamma\tau} \cdot V(\vec{x}) \tag{7}$$

where $V(\vec{x})$ is the eigenfunction of the Fokker–Planck operator belonging to the eigenvalue $\gamma$, and $p_s(\vec{x})$ is the

steady-state solution, given by

$$p_s(\vec{x}) = B^{-1} \exp [-U(\vec{x})] \quad (8)$$

with

$$U(\vec{x}) = \tfrac{1}{4}(I_1^2 + I_2^2 + 2\xi I_1 I_2) - \tfrac{1}{2}(a_1 I_1 + a_2 I_2) \quad (9)$$

where $B$ is a normalization constant, $I_1 = x_1^2 + y_1^2$ and $I_2 = x_2^2 + y_2^2$ are the intensities of the two modes.

The spectral behavior of the laser is determined by the probability distribution $p(\vec{x}, \tau)$ by (7). Here $p(\vec{x}, \tau)\, d\vec{x}$ is the probability of finding the state of the laser in the range of $\vec{x}$ to $(\vec{x} + d\vec{x})$ at time $\tau$. The longitudinal mode spectrum of the laser is given by the steady-state solution $p_s(\vec{x})$. It has been shown in [20] that the stability of two-mode operation is dependent on the two-mode coupling constant, $\xi$ in (4), which is proportional to the wavelength separation between the two modes. In the present case, the wavelength separation is set equal to the stopband width of the DFB laser to calculate the transient power partitioning between the two degenerate DFB modes. In general, the statistics of partition fluctuations we are interested in can be described by

$$P(\tau) = \iint_D p(\vec{x}, \tau)\, dI_1\, dI_2 \quad (10)$$

where the integration is carried over a region $D$ in the four dimensional space $(x_1, x_2, y_1, y_2)$. We call $P(\tau)$ the "occupation" probability, which is the probability for the laser mode intensities $(I_1, I_2)$ being in the range $D$ at time $\tau$. The "dropout" probability that $(I_1, I_2)$ exceeds $D$ is then given by $(1 - P(\tau))$.

To compare the theory with measurement, some simplification based on experimental observations can be made. Within the accuracy of our measurements, the durations of the dropout event for the same laser appear to be independent of the dropout depth and the power ratio of the two modes $(P_{+1}/P_{-1})$. Although a small fluctuation has slower rise and fall than a large fluctuation, the dropout durations are the same, indicating that this observation is not due to limited measurement bandwidth. The same observation was also reported by Linke *et al.* [12]. If $\Delta t$ is the constant dropout duration, we can then relate the dropout probability $P_\epsilon$ to the dropout frequency $f_\epsilon$ by

$$P_\epsilon = f_\epsilon \Delta t. \quad (11)$$

Here $P_\epsilon$ is defined as the probability for a dropout event deeper than a fraction $\epsilon$ of the main mode power, and $f_\epsilon$ is the rate per second that the events occur. In the experiment, $f_\epsilon$ was measured as a function of $\epsilon$ for various values of $(P_{+1}/P_{-1})$ with $P_{+1}$ as the main mode.

The dropout probability $P_\epsilon$ in (11) is independent of time, and it can be expressed using (10) as [20]:

$$P_\epsilon = 1 - \iint_D p_s(\vec{x})\, dI_1\, dI_2 \quad (12)$$

where $p_s(\vec{x})$ is the steady-state solution of the Fokker–Planck equation. The integration is carried over the range of $P_{+1}$ between $(1 - \epsilon)\langle P_{+1}\rangle$ and $(1 + \epsilon)\langle P_{+1}\rangle$, where $\langle P_{+1}\rangle$ is the time average of $P_{+1}$. It is found from numerical calculations that $P_\epsilon$ can be approximated as

$$\log_{10} P_\epsilon = -17.9 \cdot \log_{10} \epsilon - 0.145 \cdot a_2 \cdot (a_1/a_2) - 15.5 \quad (13)$$

where $a_1$ and $a_2$ are the pump parameters in (3). Equation (13) is accurate to within a few percent for $a_1/a_2 > 10$.

The ratio $(a_1/a_2)$ is equal to $(P_{+1}/P_{-1})$ in the experiment. However, $a_2$ is not known from the experiment. To test the accuracy of the theory, $a_2$ was used as a fitting parameter to fit the experimental data. In the experiment, the full width at half maximum of the transient dropout pulses for the laser tested was about 1 ns. We then set $\Delta t = 1$ ns for converting the calculated $P_\epsilon$ to $f_\epsilon$ using (11). Fig. 8 shows the calculated dropout frequency $f_\epsilon$ as a function of $\epsilon$ with $a_2$ chosen to fit the data in Fig. 3. The experimental fit parameter $a_2$ becomes smaller than 1, i.e., average side-mode power lower than the root-mean-square intensity of spontaneous emission into the side mode, only for $P_{+1}/P_{-1} = 100$ and 300 in Fig. 8 ($a_2 = 0.8$ for $P_{+1}/P_{-1} = 100$, and 0.4 for $P_{+1}/P_{-1} = 300$). If $a_2$ is much smaller than 1, the accuracy of (3) is poor because the spontaneous emission can no longer be considered as a small Langevin noise term, $q_i(\tau)$. However, for $P_{+1}/P_{-1} = 100$ and 300, where the side mode is close to lasing threshold, $a_2$ is still close enough to 1 and (3) is still valid.

Different characteristics of two-mode partitioning, depending on the coupling between the two modes, can be predicted by the Fokker–Planck analysis. Both the measured data in Fig. 3 and calculated curves in Fig. 8 show that the two degenerate DFB modes, separated by a 20-Å stopband, are oscillating simultaneously without 100-percent mode hops. From our analysis of two-mode stability [20], two-mode competition with complete mode hopping occurs in the strongly coupled case when the coupling coefficient $\xi$ in (4) is larger than 1. The two modes become decoupled and oscillate independently without correlated power fluctuations when $\xi$ approaches 0. In the present case, $\xi$ is still larger than 1 but is close to 1, i.e., $\xi \gtrsim 1$. Since the wavelength separation $\Delta\lambda = 20$ Å, (4) gives an intraband relaxation time $\tau_{in} \lesssim 0.26$ ps. This value derived by the present new method agrees well with the values estimated previously from spectral hole burning. The theory, therefore, describes very well the experimental observations.

Comparing the calculated $f_\epsilon$ in Fig. 8 with experimental result in Fig. 3, we note that the slopes of measured $f_\epsilon$ curves are different from the calculated $f_\epsilon$ curves. This discrepancy may be caused by the two-mode relaxation oscillation observed in the experiment, which is not considered in the theory. The carrier density may oscillate due to the mode power oscillation and may induce addi-

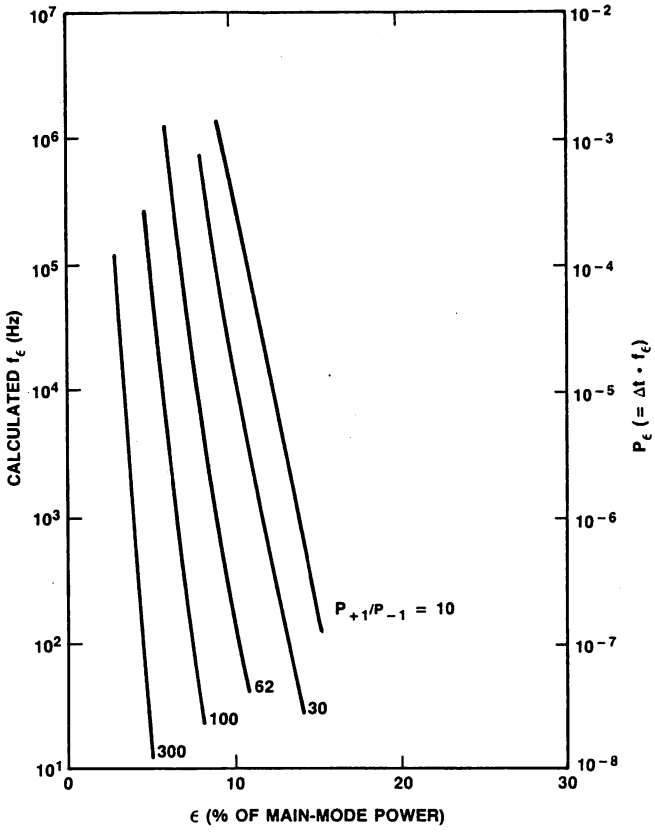


Fig. 8. Dropout frequency (number of events deeper than abscissa per second) versus dropout depth, calculated by the Fokker-Planck analysis.

tional dropout events, while in the present Fokker-Planck model the carrier density is assumed to be constant in time.

## IV. Discussion and Summary

The measurement of the power partition fluctuations of the two-mode-degenerate DFB laser under CW operation is of practical importance. The DFB laser is of potential interest for use as the source and local oscillator in coherent optical detection systems. Both the source laser and the local oscillator laser are operated CW for various modulation and detection schemes. In a high-speed long-haul direct detection system, a CW operated DFB laser with external amplitude modulation can be used to reduce the wavelength chirp that degrades the performance of the communication system caused by fiber dispersion. All these systems require that the DFB laser operate with a single longitudinal mode, which may fail, however, due to the intrinsic two-mode degeneracy of a DFB resonator. On the other hand, DFB laser oscillating with two wavelengths simultaneously is a convenient light source for interferometric sensing.

The two-mode-degenerate DFB laser was observed to exhibit: 1) transient power dropouts and 2) two-mode relaxation oscillation. The transient dropout events are similar to that first reported by Linke *et al.*, for nearly single-mode short-cavity Fabry-Perot lasers [12]. One difference, however, is the observation that the depths of the dropout events in the SIPBH DFB laser are less than about 30 percent of the main-mode power for all values of the $P_{+1}/P_{-1}$ ratio. Large dropout events of 50 to 100 percent depths occurred in the DFB laser only when the laser was influenced by external optical feedback.

The observed anticorrelated two-mode relaxation oscillation is different from the well-known relaxation oscillation of the total power due to photon-carrier interaction that follows a step change in the excitation current. In the latter case, the oscillation of the powers of the main mode and the side modes are in phase [26]. Also, the resonance frequency approaches zero at threshold, which is not observed in the measurements shown in Fig. 6. Although it is not clear at this time, it is possible that the anticorrelated two-mode oscillation is generated by fluctuations in the local carrier density. We have shown that variation in the profile of carrier density along the laser cavity changes the power ratio of the two DFB modes [9], [10]. By modulating the carrier density profile using a two-electrode DFB laser we can switch the two DFB modes. Small fluctuations in the local carrier density in a conventional DFB laser may therefore generate anticorrelated two-mode oscillation. Fluctuations in the local carrier density may be triggered by transient dropout events due to the relation between the mode power ratio and the carrier density profile. The local carrier density may oscillate before it reaches steady state. On the other hand, the two-mode relaxation oscillation probably can also trigger additional dropout events.

The two-mode relaxation oscillation occurs in the gigahertz range. If a DFB laser is operated with two modes for interferometric sensing, the performance of the sensor is not affected because the oscillation frequency is much higher than the bandwidth of the sensing system. For optical communications, however, the DFB laser should have a higher than 500 : 1 main-to-side mode ratio, where the two-mode relaxation oscillation becomes negligible and the power dropout frequency also decreases.

## Acknowledgment

The authors would like to thank E. C. Burrows for technical assistance and R. M. Jopson for providing the optical isolators used in the experiment.

## References

[1] H. Kogelnik and C. V. Shank, "Coupled-wave theory of distributed feedback lasers," *J. Appl. Phys.*, vol. 43, pp. 2327-2335, 1972.
[2] M. Shikada, S. Fujita, N. Henmi, I. Mito, K. Taguchi, and Minemura, "Long-distance gigabit-range optical fiber transmission experiments employing DFB-LD's and InGaAs-APD's," *J. Lightwave Technol.*, vol. LT-5, pp. 1488-1497, 1987.
[3] K. Sekartedjo, N. Eda, K. Furuya, Y. Suematsu, F. Koyama, and T. Tanbunek, "1.5-$\mu$m phase-shifted DFB lasers for single-mode operation," *Electron. Lett.*, vol. 20, pp. 80-81, 1984.
[4] F. Koyama, Y. Suematsu, K. Kojima, and K. Furuya, "1.5-$\mu$m phase

adjusted distributed reflector laser for complete dynamic single-mode operation," *Electron. Lett.*, vol. 20, pp. 391-393, 1984.
[5] K. Utaka, S. Akiba, K. Sakai, and Y. Matsushima, "λ/4-shifted InGaAsP/InP DFB lasers by simultaneous holographic exposure of positive and negative photoresists," *Electron. Lett.*, vol. 20, pp. 1008-1010, 1984.
[6] K. Utaka, S. Akiba, K. Sakai, and Y. Matsushima, "λ/4-shifted InGaAsP/InP DFB lasers," *IEEE J. Quantum Electron.*, vol. QE-22, pp. 1042-1051, 1986.
[7] T. Matsuoka, Y. Yoshikuni, and H. Nagai, "Verification of the light phase effect at the facet on DFB laser properties," *IEEE J. Quantum Electron.*, vol. QE-21, pp. 1880-1886, 1985.
[8] K. Utaka, S. Akiba, K. Sakai, and Y. Matsushima, "Effect of mirror facets on lasing characteristics of distributed feedback InGaAsP/InP laser diodes at 1.5-μm range," *IEEE J. Quantum Electron.*, vol. QE-20, pp. 236-245, 1984.
[9] K.-Y. Liou, C. A. Burrus, U. Koren, and T. L. Koch, "A two-electrode distributed feedback injection laser for single-mode stabilization and electrooptical switching," *Appl. Phys. Lett.*, vol. 51, pp. 634-636, 1987.
[10] K.-Y. Liou, C. A. Burrus, U. Koren, and T. L. Koch, "Electrooptical logic operations with two-electrode distributed feedback injection lasers," *Appl. Phys. Lett.*, vol. 51, pp. 1777-1779, 1987.
[11] S. Yamamoto, H. Sakaguchi, and N. Seki, "Measurement of mode partition in DFB lasers," *J. Lightwave Technol.*, vol. LT-4, pp. 672-679, 1986.
[12] R. A. Linke, B. L. Kasper, C. A. Burrus, I. P. Kaminow, J.-S. Ko, and T. P. Lee, "Mode power partition events in nearly single-frequency lasers," *J. Lightwave Technol.*, vol. LT-3, pp. 706-711, 1985.
[13] C. H. Henry, P. S. Henry, and M. Lax, "Partition fluctuations in nearly single-longitudinal-mode lasers," *J. Lightwave Technol.*, vol. LT-2, pp. 209-216, 1984.
[14] P.-L. Liu, L. E. Fencil, J.-S. Ko, I. P. Kaminow, T. P. Lee, and C. A. Burrus, "Amplitude fluctuations and photon statistics in InGaAsP injection lasers," *IEEE J. Quantum Electron.*, vol. QE-19, pp. 1348-1351, 1983.
[15] B. I. Miller, U. Koren, and R. J. Capik, "Planar buried heterostructure InP/GaInAs lasers grown entirely by OMVPE," *Electron. Lett.*, vol. 22, pp. 947-949, 1986.
[16] W. Streifer, R. B. Burnham, and D. R. Scifres, "Effect of external reflectors on longitudinal mode of distributed feedback lasers," *IEEE J. Quantum Electron.*, vol. QE-11, pp. 154-161, 1975.
[17] G. P. Agrawal, N. K. Dutta, and P. J. Anthony, "Linewidth of distributed feedback semiconductor lasers with partially reflecting facets," *Appl. Phys. Lett.*, vol. 48, pp. 457-459, 1986.
[18] N. Ogasawara, R. Ito, M. Kato, and Y. Takahashi, "Mode switching in injection lasers induced by temperature variation and optimal feedback," *Jap. J. Appl. Phys.*, vol. 22, pp. 1684-1690, 1983.
[19] R. W. Tkach and A. R. Chraplyvy, "Regimes of feedback effects in 1.5-μm distributed feedback lasers," *J. Lightwave Technol.*, vol. LT-4, pp. 1655-1661, 1986.
[20] M. Ohtsu and K.-Y. Liou, "Mode stability of a two-wavelength Fabry-Perot/distributed-feedback laser," *J. Lightwave Technol.*, vol. LT-6, pp. 47-51, 1988.
[21] M. Yamada and Y. Suematsu, "Analysis of gain suppression in undoped injection lasers," *J. Appl. Phys.*, vol. 52, pp. 2653-2664, 1981.
[22] M.Ohtsu, Y. Teramachi, Y. Otsuka, and A. Osaki, "Analysis of mode-hopping phenomena in an AlGaAs laser," *IEEE J. Quantum Electron.*, vol. QE-22, pp. 535-543, 1986.
[23] G. E. Uhlenbeck and L. S. Ornstein, "On the theory of the Brownian motion," *Phys. Rev.*, vol. 36, pp. 823-841, 1930.
[24] M. C. Wang and G. E. Uhlenbeck, "On the theory of the Brownian Motion II," *Rev. Modern Phys.*, vol. 17, pp. 323-342, 1945.
[25] R. Bonifacio, L. Lugiato, J. D. Farina, and L. M. Narducci, "Long-time evolution for a one-dimensional Fokker-Planck process: Application to absorptive optical bistability," *IEEE J. Quantum Electron.*, vol. QE-17, pp. 357-365, 1981.
[26] D. Marcuse and T. P. Lee, "On approximate analytical solutions of rate equations for studying transient spectra of injection lasers," *IEEE J. Quantum Electron.*, vol. QE-19, pp. 1397-1406, 1983.

**Kang-Yih Liou** received the B.S. degree in physics from National Taiwan University, Taipei, Taiwan, in 1970, the M.S. degree in physics from Temple University, Philadelphia, PA, in 1974, and the Ph.D. degree in materials science from University of Wisconsin at Madison in 1978.

From 1979 to 1980, he was a Research Scientist at Argonne National Laboratory, Argonne, IL, where he contributed to theories and experiments of radiation modified thermodynamics of solids, ion implantation, and defects in crystals. He joined AT&T Bell Laboratories at Allentown, PA, in October 1980. Since 1984 he has been with the Crawford Hill Laboratory of AT&T Bell Laboratories at Holmdel, NJ. He has worked on lightwave transmitters, single-frequency composite-cavity lasers, distributed feedback lasers, and photonic integrated circuits.

*

**Motoichi Ohtsu** was born in Kanagawa, Japan, on October 5, 1950. He received the B.S., M.S., and Ph.D. degrees in electronics engineering from the Tokyo Institute of Technology, Tokyo, Japan, in 1973, 1975, 1978, respectively.

In 1978, he was appointed a Research Associate, and in 1982, became an Associate Professor at the Tokyo Institute of Technology. From September 1986 to July 1987, on leave of absence from Tokyo Institute of Technology, he joined AT&T Bell Laboratories, Crawford Hill Laboratory, Holmdel, NJ. His main fields of interest are the frequency control of lasers, analysis of dynamic behavior of lasers, and its applications to coherent optical measurements, optical communications, and microwave atomic clocks. He has written seven books.

Dr. Ohtsu is a member of the Institute of Electronics, Information, and Communication Engineers of Japan, the Institute of Electrical Engineers of Japan, the Japan Society of Applied Physics, and the Optical Society of America. In 1982, he was awarded a prize from the Japan Society of Applied Physics. He was also awarded the Issac Koga Gold Medal from the International Union of Radio Science (URSI) in 1984.

*

**Charles A. Burrus, Jr.** (SM'63-F'74) was born in Shelby, NC, in 1927. He received the B.S. degree *cum laude* from Davidson College in 1950, the M.S. degree from Emory University in 1951, and the Ph.D. degree from Duke University in 1955, all in physics. At Duke he studied under Texas Company and Shell Company Fellowships, and was employed in the Physics Department as a Research Associate during 1954-1955.

In 1955 he joined the Technical Staff of AT&T Bell Laboratories, Holmdel, NJ, where his work initially was concerned with the millimeter- and submillimeter-wave region of the spectrum (microwave spectroscopy and various types of semiconductor diodes for millimeter-wave use); and later with sources and detectors for lightwave communications (fiber-compatible LED's, lasers, and pin photodiodes), single-crystal active fibers, and the effects of deuterium and hydrogen in optical fibers. Currently he is engaged in work on high-speed semiconductor devices for lightwave communications in the 1- to 1.6-μm wavelength region.

Dr. Burrus is a member of Phi Beta Kappa, Sigma Pi Sigma, and Sigma Xi. He is a Fellow of the American Association for the Advancement of Science, the American Physical Society, and the Optical Society of America. He is the recipient of the 1982 David Richardson Medal in applied optics from the Optical Society of America and the Distinguished Technical Staff Award (1982) from AT&T Bell Laboratories.

*

**V. Koren,** photograph and biography not available at time of publication.

*

**T. L. Koch,** photograph and biography not available at time of publication.

UDC 621.373.8 : 621.382 : 621.375.826.018.4

論　文

# $^{87}$Rb 原子発振器のためのレーザ分光および半導体レーザの周波数制御

正員　橋本　実　(東京工業大)
正員　大津元一　(東京工業大)

## 1. まえがき

セシウム，水素，と並んで，ルビジウム原子発振器は最も一般的な原子発振器である。特に，近年，ルビジウム原子発振器は GPS (Grobal Positioning System) 衛星搭載用の基準周波数源などとしての用途を拡大しつつある[1]。このルビジウム原子発振器の性能向上を図るために，半導体レーザを従来の $^{87}$Rb ランプに代わる励起光源として用いることは，早くから提唱され[2]，いくつかの予備的な実験が行われている[3][4]。また周波数掃引が可能であって，コヒーレント光を発生する半導体レーザは，高分解能分光用光源としても利用できる。特に，波長 0.78 μm 帯の半導体レーザはルビジウム原子の $D_2$ 線の分光に適している。そして，大津らによって半導体レーザを $^{85}$Rb 原子の飽和吸収分光に利用する試みが既になされている[5]。

しかし，半導体レーザを使った $^{87}$Rb-$D_2$ 線の高分解能分光や半導体レーザを原子発振器システムの一要素として組み込むための性能向上実験などに関する系統的な研究はほとんど行われてこなかった。

本研究では，最初に $^{87}$Rb-$D_2$ 線において，ドップラーフリー分光の一種である飽和吸収分光を行った結果を報告する。すなわち，励起状態の超微細構造を半導体レーザを用いて，高精度で分解する。この際，飽和吸収スペクトルの計算機シミュレーション結果と対照することによって半導体レーザの持つ線幅を推定する。また，$^{87}$Rb-$D_2$ 線に半導体レーザの発振周波数を安定化する実験を行った。更に，周波数安定化時の出力変動を評価し，周波数安定化によってフリー・ランニングに比べ出力変動が大きくなることを調べた。

最後に，半導体レーザをルビジウム原子発振器の励起光源としてシステムに組み込む際に必要とされる条件を考察した。

Laser Spectroscopy and Frequency Stabilization of a Semiconductor Laser for a $^{87}$Rb Atomic Clock. By *Minoru Hashimoto*, Member & *Motoichi Ohtsu*, Member (The Graduate School at Nagatsuta, Tokyo Institute of Technology).
橋本　実：正員，東京工業大学総合理工学研究科物理情報工学専攻
大津元一：正員，東京工業大学総合理工学研究科物理情報工学専攻

## 2. 飽和吸収分光

$^{87}$Rb-$D_2$ 線のエネルギー準位を図1に示す。$^{87}$Rb 原子核が核スピン ($I$=3/2) を持つので，$^{87}$Rb-$D_2$ 線は基底状態 ($5S_{1/2}$) で2準位，励起状態 ($5P_{3/2}$) で4準位の超微細準位に分離する。ここでは，超微細準位間の各遷移に対して，周波数の低い順に $o$～$t$ までの記号を割り当てた。基底状態の超微細分裂は約 6.8 GHz である。これに対して，励起状態の超微細分裂の大きさは，常温 ($T$=296 K) におけるドップラー幅 ($\Delta\nu_D$=500 MHz) よりかなり小さい．そのため，線形吸収分光によって励起状態の超微細構造を明らかにすることはできない。そこで，ドップラー・フリーの

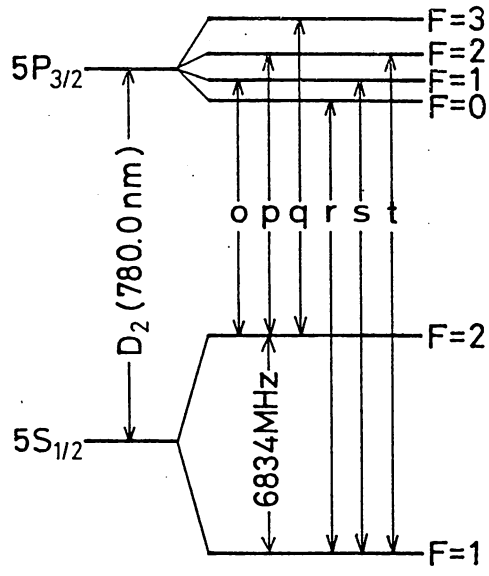


図1　$^{87}$Rb-$D_2$ 線のエネルギー準位
Fig. 1. Energy-level diagram of $^{87}$Rb-$D_2$ line.

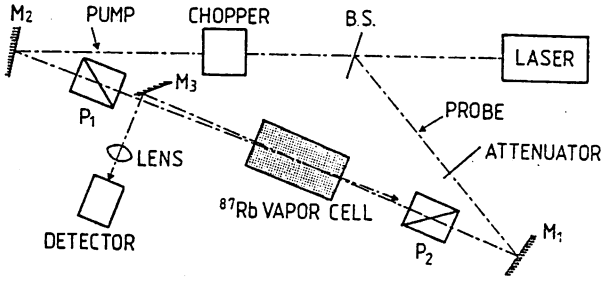


図 2 飽和吸収分光実験系

Fig. 2. Experimental setup for saturation spectroscopy.

スペクトルを得るために飽和吸収分光を行った。

〈2・1〉 実 験 $^{87}$Rb ガスは，端面に平坦な板ガラスを二枚張り合わせた円筒形のガラス製セル（長さ 35 mm，直径 30 mm$\phi$）に封入されている。半導体レーザ（日立，HL 7802 E）の動作温度は，アルコール恒温槽とペルチエ素子によって制御され，温度変動の大きさは 1 mK 以内に抑えられている。半導体レーザの注入電流は低雑音の定電流源によって制御されている。飽和吸収スペクトルを観測するために図 2 のように，レーザ光をビーム・スプリッター (BS) でふたつにわけてから互いに反対向きになるように $^{87}$Rb ガスセルに入射させた。このとき，一方のレーザ光で原子の吸収を飽和させ，他方のレーザ光をプローブとして飽和吸収スペクトルを観測した。吸収を飽和させるのに用いられるレーザ光は，ポンプ光と呼ばれ，観測用の光はプローブ光と呼ばれる。セルを透過した後，プローブ光は光検出器 (PIN フォトダイオード) で受光される。注入電流掃引により，レーザ周波数を掃引しながらプローブ光強度を観測することによって得られる原子の吸収スペクトルは，ポンプ光による飽和吸収スペクトルとプローブ光自身の線形吸収スペクトルとの重なりからなる。このスペクトルから飽和吸収スペクトルのみを取り出すために，ポンプ光を低周波 (170 Hz) でチョップして，これと同期して変化するプローブ光のみをロックインアンプを使って検出した。なお，半導体レーザは完全に直線偏光しているが，念のため，グラントムソン・プリズムを用いてポンプ光およびプローブ光の直線偏光方向を合わせている。

〈2・2〉 結 果 測定結果を図 3 (a) に示す。このときの，ポンプ光強度およびプローブ光強度は，レーザの発振周波数が基底状態の超微細準位 $F=1$ と励起状態の超微細準位との間の遷移周波数に等しいとき，それぞれ 216 $\mu$W/cm$^2$ および 57.6 $\mu$W/cm$^2$ であった。

ここで，ガスセル内で熱運動する原子の速度ベクトルの，レーザ光ビームに水平な方向の成分を $V_z$ とする。

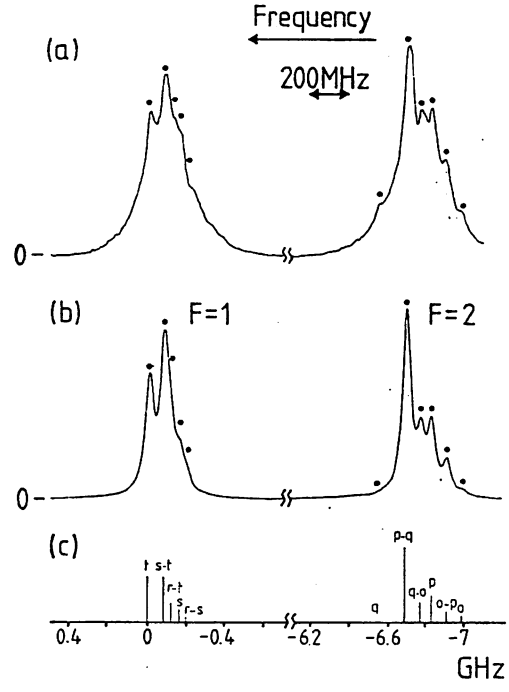


図 3 (a) 観測された飽和吸収スペクトル，(b) 理論計算から求められた飽和吸収スペクトル，(c) 超微細遷移線の相対的な強度と位置

Fig. 3. (a) Observed saturated absorption spectral shapes. (b) Calculated saturated absorption spectral shapes. (c) Ralative intensity and position of hyperfine resonance spectral lines.

飽和吸収スペクトルは $V_z=0$ の原子による超微細共鳴（主共鳴）と $V_z\neq 0$ の原子による crossover 共鳴として観測できる。主共鳴では，ポンプ光とプローブ光が共鳴する超微細遷移が等しいので，共鳴する周波数は遷移 $o$〜$t$ のいずれかに相当する。これに対して，crossover 共鳴では，ポンプ光とプローブ光が共鳴する超微細遷移は異なるので，共鳴する周波数はふたつの超微細遷移周波数の平均値となる。ポンプ光の共鳴する超微細遷移とプローブ光の共鳴する超微細遷移の周波数軸上での相対的な位置や強度，更に基底状態と励起状態の超微細準位間の角運動量選択則によって，crossover 共鳴の強度は主共鳴の強度よりも大きくなる場合がある。そのため，飽和吸収スペクトルを構成する多数の超微細共鳴線を同定するのは直観的には容易ではない。そこで，$^{85}$Rb-$D_2$ 線の飽和吸収スペクトルに対する理論モデル[6]に従って，計算機シミュレーションを行った。飽和吸収を与える原子の複素感受率は 3 準位原子系の密度行列の運動方程式を解くことによって得られる。複素感受率は，主共鳴と crossover 共鳴を表すローレンツ関数の和として定義され

ている。超微細共鳴を表すローレンツ関数の半値全幅 $\gamma$ は超微細共鳴ごとに異なる。しかし，おおまかなシミュレーションを行うために，これらを単一の値で代表させた。実測結果図3(a)とシミュレーション・スペクトルが一致するように，$\gamma$ の値をパラメータにとった。視察により，$\gamma$ が 50 MHz のときに最良のフィッティングが得られた。結果を図3(b)に示す。また，主共鳴と crossover 共鳴の位置と強度を図3(c)に示す。実験結果図3(a)とシミュレーション結果図3(b)の全体のプロフィールは非常によく一致している。このことは，文献[6]の理論モデルの妥当性を示している。しかし，より細かくみると，実験結果では 11 本の超微細遷移を観測できたのに対し，シミュレーション結果では8本しか明確には観測できていない。これは，理論モデルの精度に起因しているので，理論モデルが更に高精度になればより良いフィッティングが得られる。

図3(a)と図3(b)との対比から，実験によって観測できた超微細共鳴は次の 11 本であることがわかった。

(基底状態 $F=1$ を共通の下準位とする超微細共鳴)

$r-s,\ s,\ r-t,\ s-t,\ t$

(基底状態 $F=2$ を共通の下準位とする超微細共鳴)

$o,\ o-p,\ p,\ p-q,\ q-o,\ q$

ただし，$i-j$ $(i\neq j;\ i,j=0,p,q,r,s,t)$ は crossover 共鳴を定義するもので，$i$, $j$ はポンプ光とプローブ光が共鳴するふたつの超微細遷移を表す。

このように，飽和吸収分光によって，超微細共鳴線の同定を高確度に行えることが示された。この結果，超微細共鳴線を，レーザ周波数安定化のための信頼できる光周波数標準として利用することが可能になった。また，半値全幅 $\gamma$ は，自然幅，遷移時間幅，レーザ線幅，パワー広がり幅，残留ドップラー幅の和で与えられるので，半導体レーザの線幅は 50 MHz 以下であることが結論できる。

## 3. 周波数安定化

半導体レーザの発振周波数は，自然放出光揺らぎ，キャリア密度揺らぎ，動作温度の変動，および注入電流の変動によって，わずかに揺らいでいる。特に，動作温度変動に起因する周波数揺らぎが最も大きい。半導体レーザをルビジウム原子発振器の励起光源として用いるためには，この周波数揺らぎを抑えなければならない。そこで，$^{87}$Rb 原子の吸収スペクトルを周波数基準として，半導体レーザの周波数安定化を行った。$^{85}$Rb-$D_2$ 線や $^{87}$Rb-$D_1$ 線を用いた周波数安定化は既に行われているが[5][7]，ルビジウム原子発振器励起に必要な $^{87}$Rb-$D_2$ 線に安定化したのは今回が初めてである。

〈3・1〉 実 験　周波数安定化のための基準セルとして2種類のガスセルを使用した。ひとつはバッファガスを封入した $^{87}$Rb ガスセル（セルA），もうひとつはバッファガスを封入していない $^{87}$Rb ガスセル（セルB）である。バッファガスは，$^{87}$Rb 原子のマイクロ波遷移の吸収線のドップラー広がりを減少させるために封入される不活性気体であり，本研究では，アルゴン原子（Ar）と窒素分子（$N_2$）を 1.65/1.0 の比で 43 Torr 封入したものを用いている。原子発振器はセルAを基準としてマイクロ波周波数を制御するので，セルAを基準とした半導体レーザの周波数安定化実験は，実際の応用上，非常に大きな意味を持つ。

半導体レーザは注入電流に変調信号を重ねることにより，周波数変調されている。変調周波数は 2 kHz である。変調振幅は，線形吸収スペクトルおよび飽和吸収スペクトルを周波数弁別曲線として用いる場合には，それぞれ 60 MHz および 20 MHz である。

吸収スペクトルの種類によって光学装置の配置は異なる。線形吸収スペクトルを周波数弁別に用いる場合は，レーザ光はガスセルを透過した後，直ちに，光検出器で受光される。飽和吸収スペクトルを周波数弁別に用いる場合には，2章で使われた飽和吸収分光系よりも単純な方法を使う。すなわち，レーザ光は強いポンプ光として一度ガスセルを透過した後，反射鏡によってその一部はプローブ光として再びポンプ光とは反対方向からガスセルに入射され，光検出器で受光される。

検出された信号は，ロックインアンプによって同期検波される。ロックインアンプの出力は，近似的に，吸収スペクトルの1次微分曲線となり，周波数弁別曲線として用いられる。周波数弁別曲線から得られる誤差電圧は，PID コントローラを介して注入電流源に負帰還される。このフィードバック系全体の時定数 $(\tau_F)$ は，ロックインアンプ出力段のローパスフィルタの時定数によって決まり，その値は 1 ms である。

周波数揺らぎの大きさを評価するために，アラン分散の平方根 $\sigma_y(\tau)$[8] を用いた。ただし，$\tau$ は積分時間である。具体的には，誤差電圧の時間変動を V/F コンバーターによってパルス列に変換し，ARPS（アラン分散実時間測定システム）[9] を使用してその周波数揺らぎを計算した。

〈3・2〉 結 果　周波数弁別曲線として用いた吸収スペクトルの一次微分曲線を図4，5，6に示す。ま

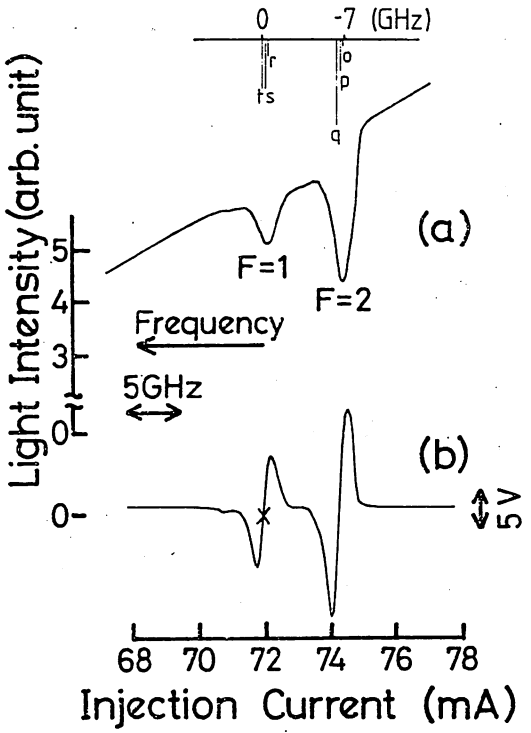


図 4 バッファガス入りの $^{87}$Rb ガスセルを用いて観測された(a)線形吸収スペクトルと(b)その微分曲線

Fig. 4. (a) Linear absorption spectral shapes observed and (b) its first derivative by using $^{87}$Rb cell with buffer gases.

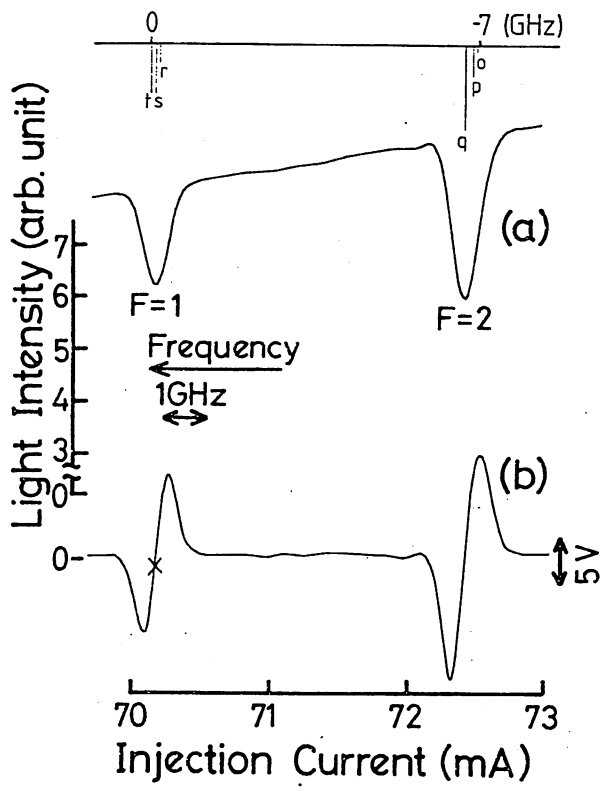


図 5 バッファガスなしの $^{87}$Rb ガスセルを用いて観測された(a)線形吸収スペクトルと(b)その微分曲線

Fig. 5. (a) Linear absorption spectral shapes observed and (b) its first derivative by using $^{87}$Rb cell without buffer gases.

た，注入電流負帰還による周波数安定化の結果を，非制御時の結果と共に図7に示す。フリーランニング時の半導体レーザの周波数安定度（図7の曲線A）はアラン分散の平方根を用いて以下のような式で近似できる。

$$\sigma_y(\tau)=5.7\times10^{-9}\tau^{0.32}$$
$$(100\,\mathrm{ms}\leqq\tau\leqq100\,\mathrm{s}) \quad \cdots\cdots(1)$$

図4および図5において，セルAとセルBの線形吸収スペクトルを周波数弁別曲線に用いて周波数安定化を行った際には，(×)でマークされた超微細遷移 $r$, $s$, $t$ が重なった吸収スペクトルの中心にレーザ周波数は安定化された。図4においては，バッファガスの圧力（43 Torr）が高いため，$^{87}$Rb 原子同士の衝突よりむしろバッファガス原子と $^{87}$Rb 原子との衝突が支配的となり，線形吸収スペクトルは 2 GHz 程度の圧力幅を持つ。

これに対して，図5のようにバッファガスがない場合には，$^{87}$Rb 原子の熱運動に基づくドップラー効果により 線形吸収スペクトルの線幅は常温で 500 MHz 程度である。このときの周波数安定化結果（図7の曲線BとC）も次式のように近似できる。

セルA：$\sigma_y(\tau)=4.4\times10^{-11}\tau^{-1}$
$$(10\,\mathrm{ms}\leqq\tau\leqq100\,\mathrm{s}) \quad \cdots\cdots(2)$$
セルB：$\sigma_y(\tau)=2.3\times10^{-11}\tau^{-1}$
$$(10\,\mathrm{ms}\leqq\tau\leqq100\,\mathrm{s}) \quad \cdots\cdots(3)$$

図6において，セルBの飽和吸収スペクトルを周波数弁別曲線に用いて周波数安定化を行った際には，(×)でマークされた，crossover 共鳴 $s$-$t$ にレーザ周波数は安定化された。このときの周波数安定結果（図7の曲線D）は次のように近似される。

セルB：$\sigma_y(\tau)=1.8\times10^{-11}\tau^{-1}$
$$(10\,\mathrm{ms}\leqq\tau\leqq100\,\mathrm{s}) \quad \cdots\cdots(4)$$

周波数安定化の結果，積分時間 $\tau=50$ s 付近ではいずれの場合（図7の曲線 B～D）でも周波数安定度は，$\sigma_y=2\times10^{-12}$ まで達している。すなわち，フリーランニング時の周波数安定度に比べて4桁改善されていることがわかる。特に，曲線Dは曲線Cに比べて，$\tau<1$ s の範囲で周波数安定度が向上している。これは，飽和吸収スペクトルの線幅がドップラー幅に比べて，狭いためと考えられる。周波数安定度のより一層の向上は，制御回路の最適化によって達成可能である。

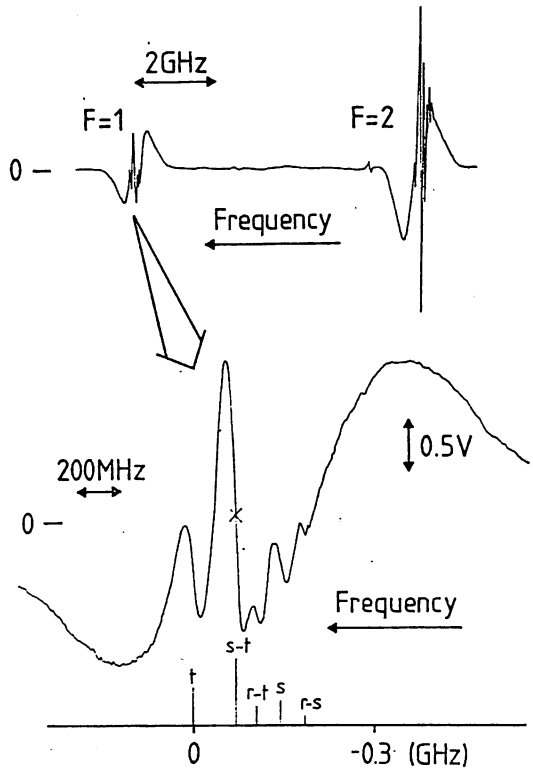


図 6 バッファガスなしの $^{87}$Rb ガスセルを用いて観測された飽和吸収スペクトル

Fig. 6. Saturated absorption spectral shapes observed by using $^{87}$Rb cell without buffer gases.

## 4. 周波数安定化時の出力変動

3章において，注入電流制御により，$^{87}$Rb-$D_2$ 線を周波数基準としたフィードバック系を構成することができた。しかし，この制御方式では，主に半導体レーザの動作温度のドリフトを注入電流の増減によって補償しているため，レーザ自身の光出力特性に起因した出力変動がフリーランニング時に比べて大きくなる。

ここでは，周波数安定化に伴う出力変動の大きさを正確に評価する。

〈4・1〉 実 験　周波数安定化されたレーザ光の一部をビームスプリッターによって取り出し，光検出器で受光する。光出力に比例する電圧の時間変動を $V/F$ コンバーターによってパルス列に変換し，3章と同様に ARPS を使用して出力変動のアラン分散の平方根 $\sigma_y(\tau)$ を計算した。

〈4・2〉 結 果　出力変動のアラン分散の平方根を図8のように測定した。フリーランニング時の出力変動（図8の曲線A）は以下のような式で近似できる。

$$\sigma_y(\tau)=5.0\times10^{-5}\tau^{-1}(\tau<1\,\mathrm{s})$$
$$5.0\times10^{-5}\tau^{0.11}(\tau\geqq1\,\mathrm{s}) \quad \cdots\cdots(5)$$

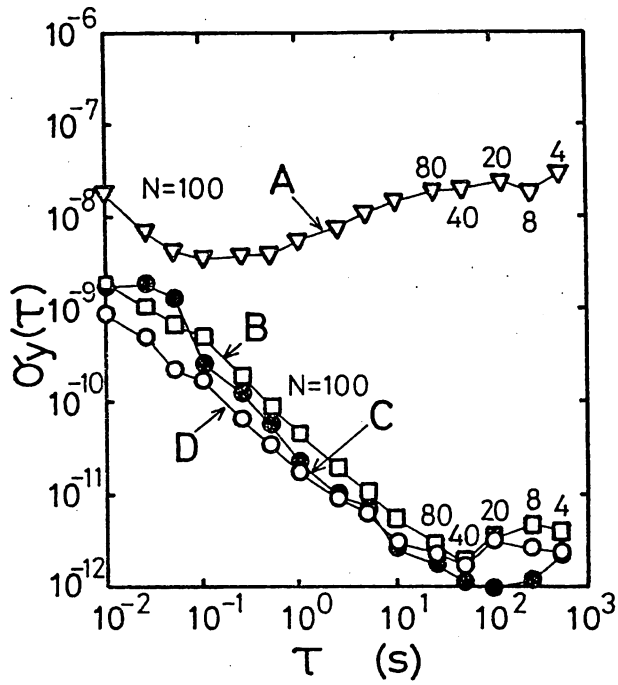


図 7 $^{87}$Rb-$D_2$ 線を基準として半導体レーザの周波数安定化を行った結果

A：フリーランニング時
B：バッファガス入りの $^{87}$Rb セルの線形吸収スペクトル
C：バッファガスなしの $^{87}$Rb セルの線形吸収スペクトル
D：バッファガスなしの $^{87}$Rb セルの飽和吸収スペクトル
ただし，$N$ はサンプル数

Fig. 7. Results of the frequency stabilization of a semiconductor laser by using the $^{87}$Rb-$D_2$ line as a frequency reference.

A : Free-running.
B : Stabilized; $^{87}$Rb with buffer gases, linear absorption.
C : Stabilized; $^{87}$Rb without buffer gases, linear absorption.
D : Stabilized; $^{87}$Rb without buffer gases, saturated absorption.
$N$ represents a number of data.

また，セルBの線形吸収スペクトルを周波数弁別曲線に使って周波数安定化を行ったときの出力変動（図8の曲線B）は

$$\text{セルB}：\sigma_y(\tau)=1.3\times10^{-4}\tau^{-1/2}(\tau<1\,\mathrm{s})$$
$$1.3\times10^{-4}\tau^{0.17}(\tau\geqq1\,\mathrm{s})\ldots(6)$$

で近似できる。(5)式と(6)式を比較すると，周波数安定化を行うとフリー・ランニングに比べ2～3倍出力変動が大きくなることがわかる。

## 5. ルビジウム原子発振器励起のためのレーザの条件

2～4章までの実験は，レーザ単体の性能向上を図るものであった。周波数安定化された半導体レーザはルビジウム原子発振器を励起するのに用いられるから，高精度なシステムを構成するためには特別な条件が必要とされる。本章では，それら条件を考察する。

原子発振器の性能を表す典型的な項目は周波数確度

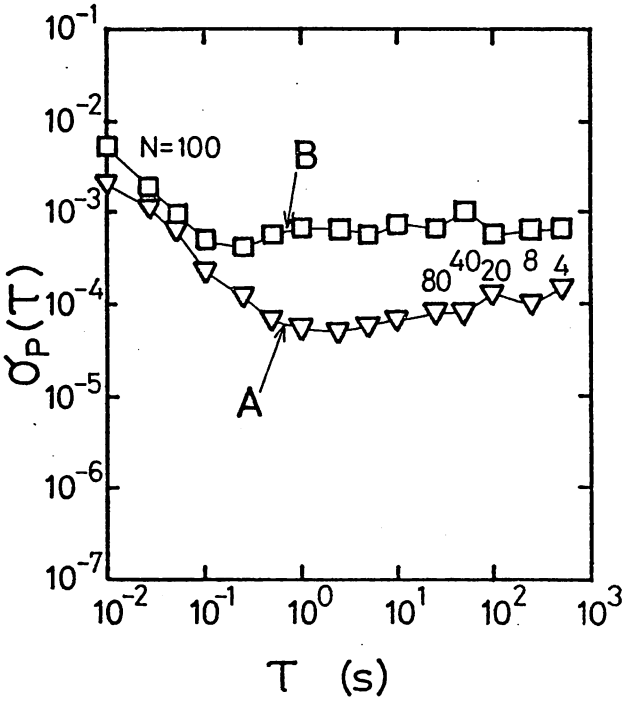


図 8　レーザパワーの安定度

A：フリーランニング時
B：バッファガス入りの $^{87}$Rb セルの線形吸収スペクトルを基準にして半導体レーザーの周波数を安定化したとき。
ただし，$N$ はサンプル数

Fig. 8. Stabilities of the laser power.

A : Free-running.
B : Frequency stabilized conditions when a semiconductor laser was locked to linear absorption of $^{87}$Rb with buffer gases.
$N$ represents a number of data.

と周波数安定度である。原子発振器の基準周波数である $^{87}$Rb 原子の基底状態の超微細準位間のマイクロ遷移周波数（約 6.8 GHz）は，ポンピング光の周波数およびパワーによってわずかにシフトすることが知られている[10]。この効果は光シフトと呼ばれ，ルビジウム原子発振器の周波数確度を制限してきた。従来のルビジウム原子発振器は，インコヒーレントな光を発生する $^{87}$Rb ランプを励起光源として用いているので，自分自身ではこのシフト量を計算できない。このために，ルビジウム原子発振器は，二次周波数標準器としての用途しか持たなかった。しかし，半導体レーザ励起を行うことによってこの光シフト特性は定量的に求められるようになった[11][12]。文献[12]から得られる，レーザ周波数の真の光遷移周波数から離調（$\Delta\nu_L$）に比例してシフトするマイクロ波共鳴周波数の量（$\Delta\nu_{HFS}$）は，ほぼ以下に示すような値である。

$$\Delta\nu_{HFS}/\Delta\nu_L = -0.11\,\mathrm{Hz/MHz} \quad \cdots\cdots(7)$$

(7)式で定義される光シフト係数を使って，商用可搬型セシウム原子発振器と同等のマイクロ波周波数確度 $1\times10^{-12}$ を達成するために必要なレーザ周波数の真の光遷移周波数からの離調の最大値を計算することができ，その値は約 45 kHz である[13]。つまり，レーザ周波数は，真の光遷移周波数，すなわち，光シフトが零になる周波数から

$$\Delta\nu_L = \pm 45\,\mathrm{kHz} \quad \cdots\cdots(8)$$

の範囲に固定されなければならない。この条件を達成するためには，マイクロ波周波数確度を高める特別な自己同調系を組むか[14]，あるいは2章で得られた飽和吸収スペクトルの線幅より更に狭い 45 kHz 以下の鋭い周波数弁別曲線にレーザ周波数を安定化する必要がある。

また，この周波数確度が得られる状態で，達成し得るマイクロ波周波数安定度の大きさを考える。レーザ周波数の短期の揺らぎは，光シフト特性を介して，観測されるマイクロ波共鳴信号の FM 雑音を増加させる。そこで，例えば，積分時間 $\tau=1$ s において水素メーザに匹敵するマイクロ波共鳴周波数安定度 $1\times10^{-13}$ を実現するために必要なレーザ周波数安定度は，(7)式で定義される値を用いて

$$\sigma_y(\tau) = 1.6\times10^{-11}(\tau=1\,\mathrm{s}) \quad \cdots\cdots(9)$$

と算出できる。この値は3章で得られたレーザ周波数安定度に近く，十分に達成可能である。

## 6. ま と め

飽和吸収分光を行った結果，基底状態の $F=1$ および $F=2$ を共通の下準位とする超微細共鳴を，それぞれ5本および6本分解できた。この際，計算機シミュレーションによって半導体レーザの持つ線幅を推定することができ，その値は 50 MHz 以下であった。また，$^{87}$Rb-$D_2$ 線に半導体レーザの発振周波数を安定化する実験を行った。その結果，線形吸収スペクトルを周波数基準に用いたときには周波数変動のアラン分散の平方根として $\sigma_y(\tau)=2.3\times10^{-11}\tau^{-1}$（$\tau$は積分時間，10 ms$\leqq\tau\leqq$100 s）が得られた。飽和吸収スペクトルを用いたときには $\sigma_y(\tau)=1.8\times10^{-11}\tau^{-1}$ (10 ms$\leqq\tau\leqq$100 s) とより良好な結果が得られた。更に，周波数安定化時のレーザの出力変動を評価し，周波数安定化によってフリー・ランニングに比べ2～3倍出力変動が大きくなることがわかった。最後に，半導体レーザをルビジウム原子発振器の励起光源としてシステムに組み込む際に必要とされる条件を考察し，マイクロ波周波数確度 $1\times10^{-12}$ を達成するために，レーザ周波数の離調の大きさは 45 kHz 以内でなければならないことがわかった。また，マイクロ周波数安定度 $1\times10^{-13}$($\tau=1$ s) を実現するのに必要なレーザ周波数の安定度は $1.6\times10^{-11}$ ($\tau=1$ s) であることもわかった。

謝辞　御指導，御討論いただいた富士通，五雲寺氏，千葉氏，日本 IBM，狩野博士，京都工繊大，中山博士，本学，大浦助教授，倉持博士に感謝いたします。　（昭和 63 年 2 月 25 日受付）

## 文　献


(1) 塩見：「GPS 利用超精密測位システム」，電子情報通信学会誌，521 (昭 62-5)

(2) J.L. Picque: "Hyperfine Optical Pumping of a Cesium Atomic Beam, and Applications", *Metrologia*, **13**, 115 (1977)

(3) L.L. Lewis & M. Feldman: "Optical Pumping by Lasers in Atomic Frequency Standards", Proc. 35th Annu. Freq. Control Symp., Monmouth, NJ, 612 (May-1981)

(4) M. Ohtsu, M. Hashimoto & H. Ozawa: "A Highly Stabilized Semiconductor Laser and Its Application to Optically Pumped Rb Atomic Clock", Proc. 39th Ann. Freq. Control Symposium, Philadelphia, PA, 43 (May-1985)

(5) H. Tsuchida, M. Ohtsu & T. Tako: "Frequency Stabilization of AlGaAs Semiconductor Laser Based on the $^{85}Rb$-$D_2$ Line", *Jpn. J. Appl. Phys.*, **21**, L561 (1982)

(6) S. Nakayama: "Theoretical Analysis of Rb and Cs $D_2$ Lines in Saturation Spectroscopy with Optical Pumping", *Jpn. J. Appl. Phys.*, **23**, 879 (1984)

(7) 山口・鈴木：「Rb原子発振器の光ポンピングへの半導体レーザの応用」，第1回レーザ・原子発振器の周波数制御と応用，F-4 (昭 59-12)

(8) D.W. Allan: "Statistics of atomic frequency standards", Proc. IEEE, 54, 221 (1966)

(9) 椎尾・大津・田幸：「レーザ周波数安定度の実時間測定装置の測定」，電子通信学会論文誌(C)，204 (昭 56-1)

(10) B.S. Mathur, H. Tang & W. Happer: "Light Shifts in the Alkali Atoms", *Phys. Rev.*, **171**, 11 (1968)

(11) M. Hashimoto & M. Ohtsu: "Experiments on a Semiconductor Laser Pumped Rubidium Atomic Clock", *IEEE J. Quantum Electron.*, **QE-23**, 446 (1987)

(12) M. Hashimoto, M. Ohtsu & H. Furuta: "Ultra-Sensitive Frequency Discrimination In a Diode Pumped $^{87}Rb$ Atomic Clock", Proc. 41th Annu. Freq. Control Symp., Philadelphia, PA, 25 (June-1987)

(13) 中桐・渋木・占部・石津：「セシウム原子周波数標準器」，電波研究所季報，**29**，97 (1983)

(14) 橋本・古田・大津：「半導体レーザ励起ルビジウム原子発振器」，第2回レーザ・原子発振器の周波数制御と応用，B-1，(1987-11)

# Improvements in Short- and Long-Term Frequency Stabilities of Diode Laser Pumped Rubidium Atomic Clock

*M. Hashimoto and M. Ohtsu*

Graduate School at Nagatsuta, Tokyo Institute of Technology,
4259 Nagatsuta, Midori-ku, Yokohama, Kanagawa 227, Japan

## 1. Introduction

Highly stable rubidium (Rb) atomic clocks have been used popularly for global positioning system, microwave communication system, and so on. We have carried out several experiments for the developing a diode laser (DL) pumped Rb atomic clock, and have demonstrated for the first time that a sensitive detection of the optical-microwave double resonance signal in Rb atoms was possible by using a technique of frequency modulation (FM) spectroscopy[1].

In the present paper, we report results of experiments to improve the short- and long-term frequency stabilities of a DL pumped Rb atomic clock.

## 2. Improvement in Short-Term Frequency Stability

The square root of the Allan variance for the short-term stability of the microwave frequency is expressed as[2]

$$\sigma_y(\tau) = \frac{0.11}{Q\,(S/N)}\,\tau^{-1/2}, \qquad (1)$$

where $\tau$ is the integration time, $S/N$ is the signal-to-noise ratio of resonance signal. The quantity $Q$ is a quality factor of frequency discriminator which is defined by $Q = (\omega_{12}/2\pi)/\Delta\nu$, where $\Delta\nu$ is the linewidth of frequency discriminator, and $\omega_{12}/2\pi$ is the microwave transition frequency (6.8GHz). Therefore, the short-term frequency stability can be improved by increasing the values of $Q$ and of $S/N$. For this purpose, we employed a technique of FM spectroscopy by using a coherent optical pumping by DL. The optimum values of $S/N$ and $\Delta\nu$ obtained by this technique were 73 dB and 220 Hz, respectively. Substituting these values into eq.(1), the value of $\sigma_y(\tau)$ of a DL pumped Rb atomic clock was estimated as $\sigma_y(\tau) = 7.9\times10^{-13}\tau^{-1/2}$ which is about 1/10 times that of conventional Rb atomic clocks[3]. Further improvements of the short-term frequency stability of a DL pumped Rb atomic clock are possible by increasing the $S/N$ value by applying a technique of the electrical negative feedback to DL[4].

## 3. Improvement in Long-Term Frequency Stability

The optical Stark effect by the electric field of pumping light would reduce light shift, i.e., the shift of the microwave transition frequency[5]. If the light shift is induced, the profile of double resonance spectral shape is deformed and become asymmetric, which results from inhomogeneous distribution of laser intensity in the Rb gas cell[6]. The light shift as well as buffer gases would limit the frequency accuracy of Rb atomic clock. Furthermore, the light shift would induce microwave frequency drifts, which have not been reduced yet in conventional Rb atomic clocks. We propose here a new technique to improve long-term frequency



Frequency Standards and Metrology Editor: A. De March

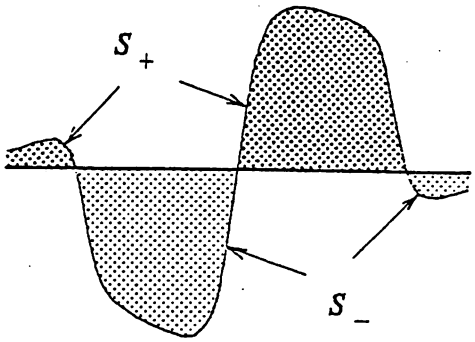


Fig.1 The definition of the asymmetrical factor $\Delta S$.

$$\Delta S = S_+ - S_-$$

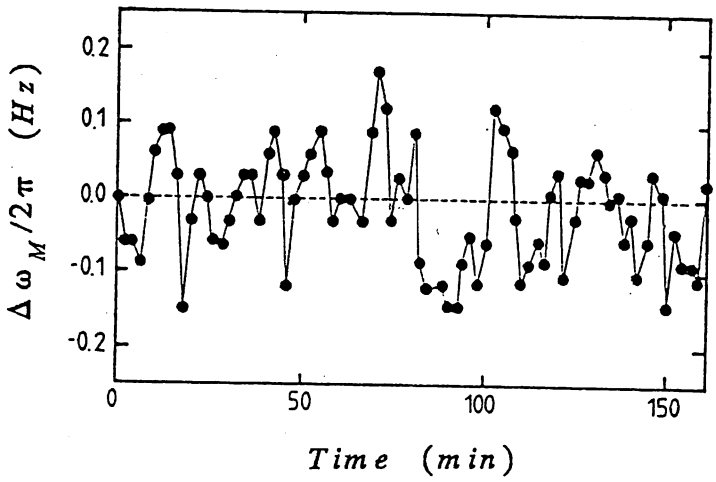


Fig.2 Reduction of microwave frequency drift by a self-tuning system.
$\Delta\omega_M/2\pi$ : Microwave frequency drift.

stability. We defined the asymmetical factor $\Delta S$ as a difference between the areas $S_+$ and $S_-$ of the double-resonance spectral profile, which are schematically given in Fig.1. Since the value of $\Delta S$ is proportional to the magnitude of the light shift, the microwave frequency drift caused by the light shift can be reduced by controlling the laser frequency so that the measured value of $\Delta S$ can be maintained zero. It should be noted that this system does not require any additional reference frequency sources. Therefore, this system can be referred as a self-tuning system.

In order to reduce the microwave frequency drift caused by the light shift, the laser frequency was controlled by this self-tuning system at every 120s. The result is shown by Fig.2. The value of $\sigma_y(\tau)$ at $\tau$ =120s was $1.2\times10^{-11}$, which is 1/10 times that of conventional Rb atomic clocks[3]. This result confirms that the present method is feasible for the improvement of the long-term stability.

## 4. Summary

The short-term frequency stability of Rb atomic clock was improved to as high as $\sigma_y(\tau) = 7.9\times10^{-13}\tau^{-1/2}$ by using a technique of FM spectroscopy. A self-tuning system was developed to reduce the frequency drift caused by the light shift. The long-term frequency stability obtained by using this system was $\sigma_y(\tau = 120s) = 1.2\times10^{-11}$.

## REFERENCE

1. M.Hashimoto and M.Ohtsu:IEEE J.Quantum Electron.,QE-23,446(1987)
2. J.Vanier and L.G.Bernier:IEEE Trans.Instrum.Meas.,IM-13,221(1981)
3. H.Hellwig:Proc.28th Annu.Freq.Control Symposium,612(1974)
4. M.Ohtsu:J.Lightwave Technol.,6,245(1988)
5. W.Happer and B.S.Mathur:Phys.Rev.,163,12(1967)
6. J.C.Camparo,R.P.Frueholz, and C.H.Volk:Phys.Rev.,27 ,1914(1983)

特別寄稿

UDC 621.375.826：621.383.2：621.396.6

# コヒーレント光通信・計測用半導体レーザの周波数安定化

東京工業大学　助教授
大津　元一
（工学博士）

この特別寄稿は，大津先生が当社で行った講演の録音をもとに，編集事務局が原稿を作成して掲載するものです。

## 1 波のそろっている光の利用

可視から赤外付近の光というのは電磁波の一種ですが，このような光を出す発振器としてレーザがあります。レーザから出てくる光は非常に波がそろっており，これを使うとどのように良いことがあるか，ということを簡単に書いたのが図1です。

まず，気体レーザの光は，一つは計測関係に，宇宙開発関係ですと人工衛星追尾，VLBI用の基準クロックとして将来的には使えるようになると期待され，航法への利用の可能性もあります。更に科学技術の基礎分野では分光分析，重力波検出へ利用され，時間又は周波数の標準への使用可能性もあります。

より実用的な話として，半導体レーザを使うと，最近実用化研究が活発になっているコヒーレント光通信，光センシングの一つであるファイバジャイロスコープ，血管中の血流測定のドップラー流速計，公害計測での公害ガス分析のレーザレーダ，マイクロ波の原子発振器用のルビウムやセシウムの光励起など，に使えるようになると考え

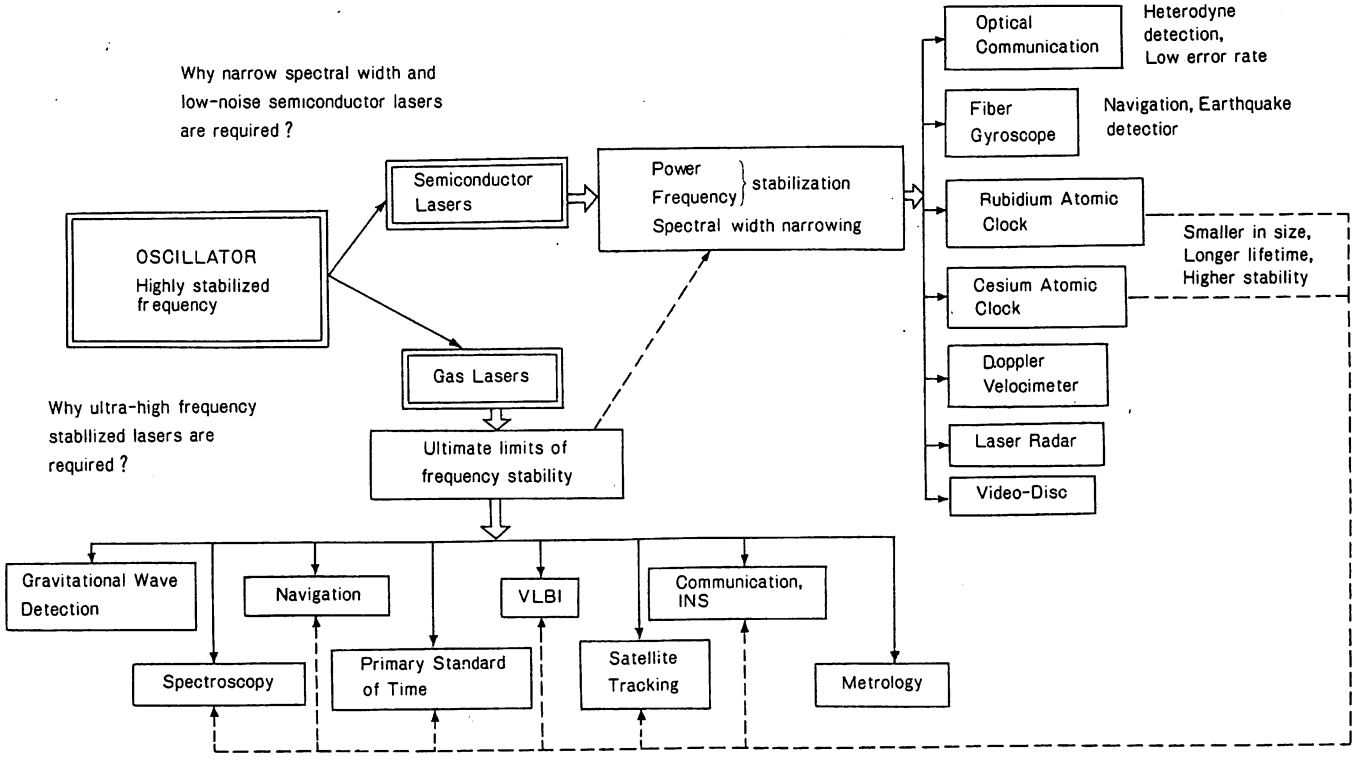


図1　波がそろっている光の利用

られます。

これらは今すぐに全部実用化するとは考えられませんけれども，このような部分の幾つかが近い将来実用化されるのではないかという状況です。

## 2 レーザ光はどのぐらい安定か

現状で，レーザから出てくる光はどのくらい安定か，ということを検討するために簡単に書いたのが図2です。同図で $\sigma$ は，時間的にレーザの周波数が変動している大きさを $\nu_0$ という平均値に対して規格化した値です。この図ではその $\sigma$ の対数値を，いろいろな発振器やレーザについて書いてあります。例えば，非常に性能の高い水晶発振器などですと，この $\sigma$ の対数値は $10^{-8}$ から $10^{-11}$ になっております。ルビジウムとかセシウの発振器ですと $10^{-8}$ から $10^{-12}$ の値で，水素メーザですと $10^{-14}$ に達します。先ほどの半導体レーザの先輩格の気体レーザですと，大体 $10^{-12}$ から $10^{-16}$ の値に達していますし，AlGaAs 半導体レーザのチャンピオンデータとして $10^{-12}$ に達しています。可能性として，非常に性能の高い発振器になり得るということが，気体レーザ及び半導体レーザの持っている特性です。

光の領域に話を限り，先に定義した $\sigma$ という値が気体レーザの場合にはどのくらいの大きさになっているかを図3から見ることにします。横軸に西暦で年号を表しており，縦軸は $\sigma$ の値です。1960年にレーザが発明された当時には，$\sigma$ の値は大体 $10^{-7}$ ぐらいでした。レーザの光の周波数は大体 100 THz すなわち $10^{14}$ Hz ですから，$10^{-7}$ ということは約 10 MHz の変動分があったことを意味します。

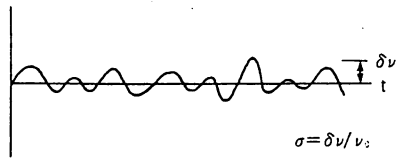


Definition of frequency (in) stability

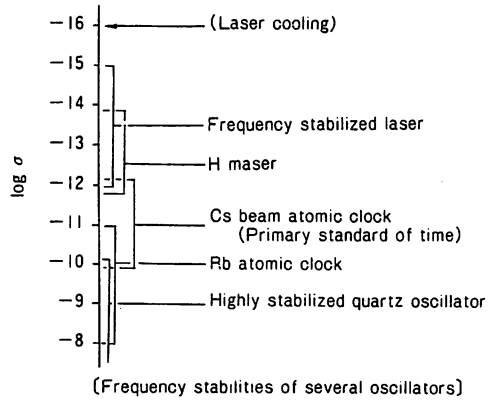


(Frequency stabilities of several oscillators)

図2 レーザ光の周波数はどのくらい安定か

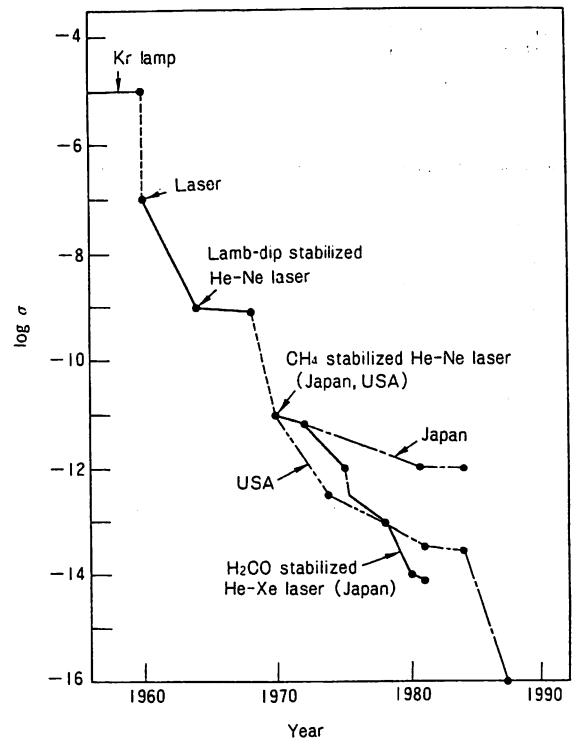


図3 レーザ光の周波数安定度の推移

1960年から継続された世界的な努力によって $\sigma$ の値が小さくなり，1987年7月の段階では $10^{-16}$ に達しております。これは気体レーザについての世界のトップデータで，要するにレーザの周波数は約 1/100 Hz ぐらいしか変動しない状態に達しているということです。

現在の技術を延長して行けば2000年の段階で，大体 $10^{-18}$ から $10^{-21}$ の $\sigma$ 値のレーザが実現できるだろうという技術予測がされております。それらの値がどれぐらい精度の高いデータといいますと，大体 $10^{-18}$ ぐらいの揺らぎで図1にありました重力波の検出ができる程度といわれていますから，光の性能は相当に向上するわけです。重力波の検出のためには，$\sigma$ の値以外にも性能を向上させなくてはいけない要因があるのですが，光学的な方法で重力波を検出しようとしますと，光源に関してはあと2桁，すなわち $10^{-18}$ に達すれば，可能になるという現状にきています。

## 3 きれいな波を出す半導体レーザは存在するか

世の中に先ほどのようなきれいな波を出す半導体レーザが，例えばシステム設計者の要求にかなうような半導体レーザが，果たしてありますでしょうか。以下ではこの話題について簡単に御紹介します。

### 3.1 副モードの発生

最近は，半導体レーザの活性層の上に回折格子を切った図4に示す，いわゆるDFBレーザというのがよく開発されています。これ

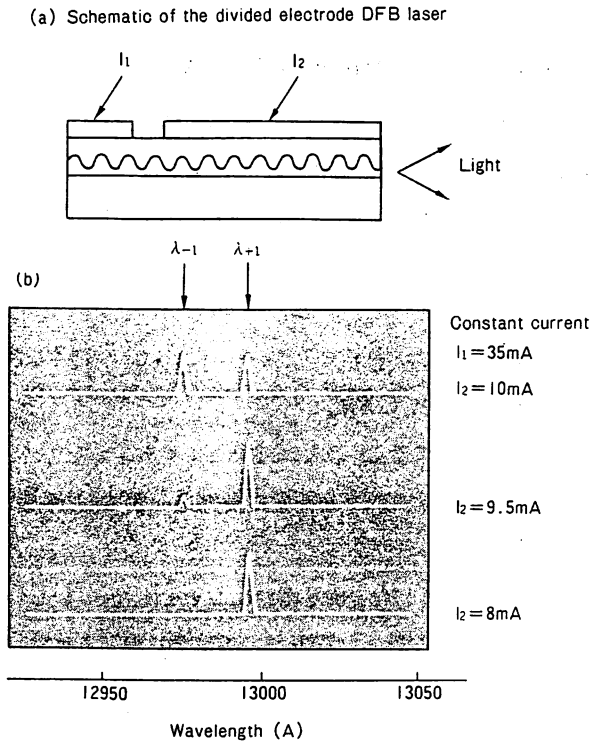


図4　分割電極形DFBレーザの断面とスペクトル特性の例

を回折格子分光器を使って直流的に測定しますと，一つの波長だけが出てくるような結果が得られますので，これをもとにこのレーザは単一モードレーザといわれております。果たしてそうかどうかということで更に注意深く調べてみますと，同図の下のような横軸に波長をとり，縦軸にDFBレーザから出てくる光のパワーをとった発振スペクトルでは，非常に強く発振している主モードのわきに非常に小さい副モードがしばしば観測されます。

これはレーザの端面の反射率がゼロでなく有限なことによる，いわゆるファブリペロー共振をしているために出てくる副モードであったり，又はDFBレーザの構造が完全に対称性が優れているということからくる，縮退したもう一つのモードであったりします。いずれにしましても，主モードのわきに非常に低いレベルですが副モードが発生します。そうすると，この副モードにより主モードの発振の利得が抑圧されてしまって，主モードが瞬間的に発振を止めてしまうのです。この現象をパワードロップアウトといい，これはレーザの発振に伴って発生する自然放出光のパワーが非常に不規則に揺らぐこと，更に半導体レーザの利得の非線形性に起因します。

これらの理由により現在のところ，まだ非常に厳密な意味での単一モードレーザはなく，例えばDFBレーザにおける回折格子の結合度を大きくするとか，端面の反射防止膜のコーティングを強化するとか，という努力をもう少し続けないと，厳密な意味での単一モード性というのは保証されないのが実情です。

### 3.2　周波数のドリフト

単一モード性が非常に高いレーザが仮に得られたとしても，もう一つ問題になるのは，非常にゆっくりした時間スケールでの単一モードの周波数のドリフトです。図5において横軸に時間をとり，レーザを作った時刻をゼロとしまして，それからずっとレーザを使い始めてから600時間，更に半年経過した時点を下の図のゼロとして，そこから600時間をとります。縦軸は単一モードレーザの周波数をとります。レーザの温度揺らぎを100万分の1ぐらい，レーザの電流揺らぎを大体0.6 nA/$\sqrt{\text{Hz}}$ の非常に安定化したような状況でレーザを駆動しても，長期にわたってドリフトがあります。上の図のように大体1時間当たり平均して40 MHzぐらいのドリフトがあり，さらに，時々不連続な飛びも発生します。下の図のように半年もしますとドリフトも少なくなってきますが，不連続な飛びは依然としてあります。

現在知られているところでは，半導体レーザの電極づけのボンディング層のインジュウムのはんだが，電流をずっと流しているときに一度溶けなおして，そこでの熱抵抗値が時間経過とともに変化していくことからくる，レーザの周波数の不連続な飛びであるといわれます。

### 3.3　周波数の揺らぎを解析する

式(1)は半導体レーザの周波数の揺らぎ $\delta\nu(t)$ が，どのような量子雑音，すなわちレーザ固有の雑音源によって与えられているかということを表しています。

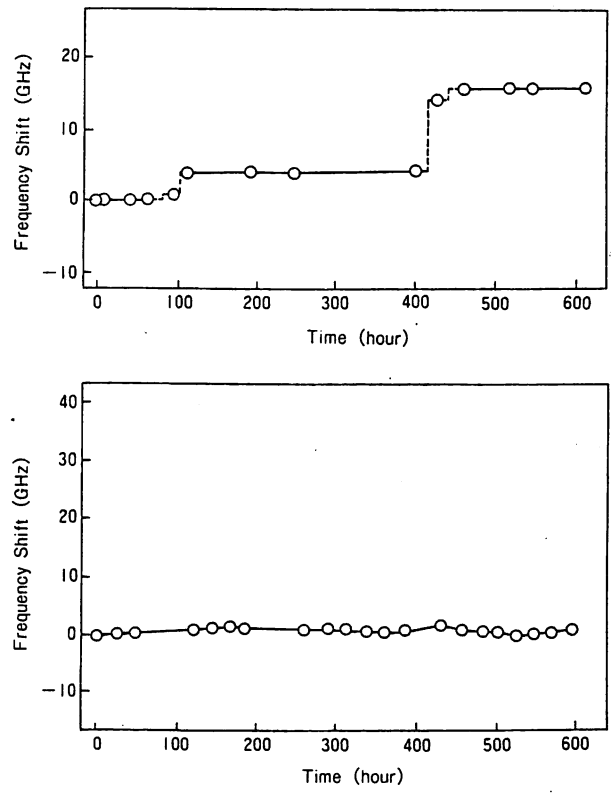


図5　周波数の長期ドリフト

$$\delta\nu(t)=\underbrace{K\,[\Gamma_s(t)}_{\text{Cavity loss}}+\underbrace{\Gamma_c(t)]}_{\text{キャリヤ密度変動}}-\int_0^{\infty}\underbrace{h(\tau)}_{\text{制御系応答}}\{\delta\nu(t-\tau)+\underbrace{\Gamma_n(t)}_{\text{制御系ノイズ}}\}\,d\tau$$

自然放出

外部からの負帰還

……(1)

第1項目は自然放出です。レーザを発振させるには自然放出が必要ですから，これによる雑音はどのようなレーザにも混入してきます。

第2項目はキャリア密度の変動です。これは自然放出に起因して発生するのですが，活性層の中のキャリアの密度が時間的に変化すると，半導体レーザの屈折率が変わりますから，周波数を変化させるという効果があります。この二つの効果に，比例係数としてレーザの共振器の損失の大きさが掛って，半導体レーザの周波数を揺らす原因となっています。

この揺らぎの量を小さくする一つの方法は，共振器を大きくすることです。これは半導体レーザの外側に鏡(かがみ)を置きレーザ光を当てて，戻ってきた光をまたレーザに戻してやるものです。

制御系応答 $h(\tau)=0$ のときのレーザ光のスペクトル線幅 $\Delta\nu$ は式(2)で表され，自然放出の効果とキャリヤ密度変動の効果の値として，数 MHz から 100 MHz ぐらいあります。

$$\Delta\nu=\Delta\nu_{SP}(1+\alpha^2)+\Delta\nu_{PI}\quad[h(\tau)=0\text{のとき}]\quad\cdots\cdots(2)$$

ここに，式(1)との関連において

$$\left.\begin{aligned}K\cdot\Gamma_s(t)&\rightarrow\Delta\nu_{SP}\\K\cdot\Gamma_0(t)&\rightarrow\Delta\nu_{SP}\cdot\alpha^2\end{aligned}\right\}\rightarrow\text{外部 Cavity により 10 kHz}$$

$$\text{電子数揺らぎ}\rightarrow\Delta\nu_{PI}\simeq\text{数 MHz}$$

鏡を設けることにより共振器構造を変化させて共振器の $Q$ を上げますと，この値は大体 10 kHz ぐらいに小さくなります。しかしながらこの方法は，発振状態に不安定さが残る，パワードロップアウトの現象がある，周波数の直接変調効率が著しく減少する，という欠点があります。

この辺りのことを解決する一つの方法は，外からの負帰還制御をかけて，雑音の大きさを補償してやるものです。つまり式(1)の積分記号の中の雑音の大きさを光電的に検出しまして，全体の揺らぎの大きさがゼロになるように，レーザの電流などを調節してやるのです。要するに，量子雑音そのものはレーザの周波数の揺らぎを決める本質的なものではなくて，非常に高い利得を持つ負帰還制御系を使えば，周波数の揺らぎが低い光の状態を人工的に実現できるのです。

## 4 半導体レーザ光を利用するための課題

レーザに関する今まで述べた背景をもとにしまして，実用的な光源である半導体レーザの光の波の性能を，つまり波のきれいさを向上させまして，図1に示したいろいろな種類の応用に利用しようとするときに，まず何をすべきかということですが，その課題は四つあると考えられます。

(1) 発振しているレーザ光のフィールドスペクトルの中心周波数を非常に安定にする。

(2) スペクトルの揺らぎの大きさを表す，いわゆるスペクトル線幅（以下線幅と略す）を非常に狭くする。要するに単色性を上げる。

(3) このような優れた光源を得たら，これを主発振器として，従発振器の周波数を主発振器の周波数に追随させる。つまり，光のトラッキングジェネレータを実現する。

(4) このように性能の高い発振器の周波数を広帯域に掃引する。つまり，光周波数のシンセサイザを実現する。

肝心なことは，これらのことをある程度同時に行うような統合的なシステムを開発すべきである，ということです。ところで，これを半導体レーザに対して実行するときに，半導体レーザは次の二つの特徴を持っているので，統合的に実行することは可能であります。

第1の特徴としては，半導体レーザは非常に小さい発振器ですから，それを構成している共振器の $Q$ が非常に小さいことです。このため半導体レーザの光に混入してくる量子的な雑音，すなわち自然放出による雑音のレベルは非常に高くなります。したがってこのような半導体レーザの固有の量子雑音を，古典的な光電的な方法である干渉法とかヘテロダイン法で直接検出できます。

第2の特徴として，半導体レーザの固有の量子雑音を適当に補償するような負帰還制御の手法が考えられることです。また負帰還制御をかけるときに都合が良いのは，半導体レーザの注入電流を適当に変調してやりますと，非常に効率良く周波数を変調できるということです。

この量子雑音の検出と，それを補償するための負帰還制御の効率が非常に高いことにより，先に数式で説明しましたように半導体レーザの周波数の揺らぎは本質的にはゼロになります。

## 5 四つの課題を解決する総合的な手法

四つの課題を解決するために，中心周波数の安定化，線幅の狭窄化，周波数のトラッキング及び掃引ということを，統合的に負帰還

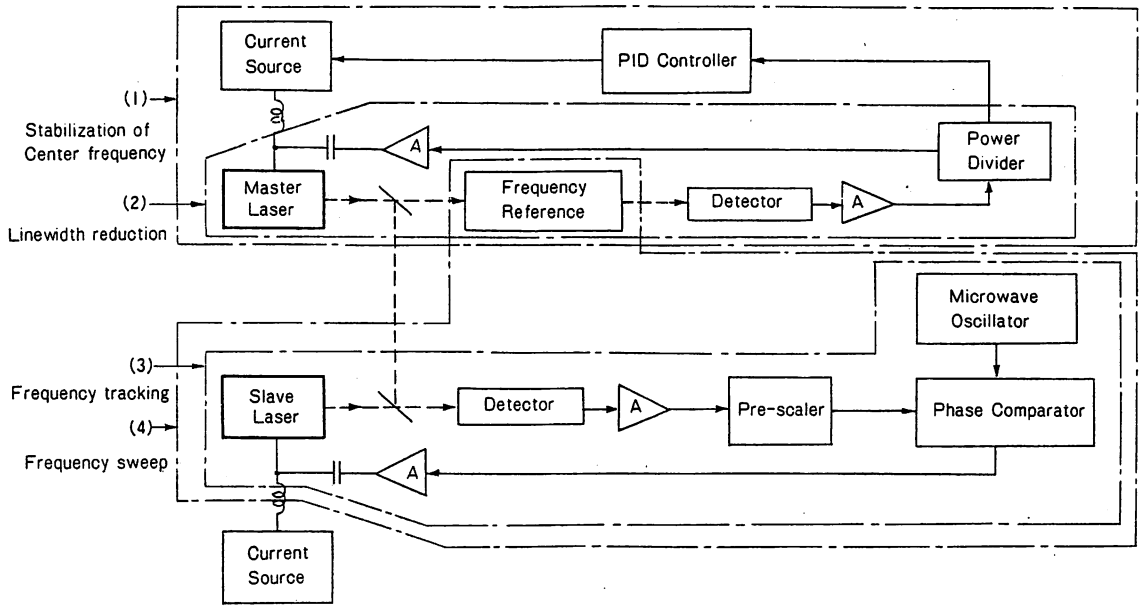


図6　負帰還制御回路の構成

制御を使って行う場合，一つ考えられる手段として図6のような構成があります。すなわち，主レーザに外付けの光電回路であるブロック(1)によって負帰還制御をかけることで周波数を安定化して，更に広帯域の負帰還制御をブロック(2)でかけることで線幅を抑圧します。これで時間的なコヒーレンス，すなわち波のきれいさを増してやることができます。

そのような状態のレーザを主レーザとしまして，2番目のレーザすなわち従レーザを持ってきます。ブロック(3)で従レーザの周波数を主レーザに追随させながら，ブロック(4)で従レーザの周波数を掃引させるということが可能です。

### 5.1　中心周波数を安定化する

第1番目の課題である中心周波数を安定化する装置は，図7のとおりの簡単なもので，どんな発振器でもこのやり方で実行できます。まず，レーザから出てくる光の周波数の揺らぎを適当な周波数の基準である周波数の復調器で検出し，ここで周波数の揺らぎを透過光のパワーに直すような変換をしてやります。これを光の検出器で受けて，検出量に応じた量だけレーザの電流に負帰還してやります。周波数の復調器の種類にもよりますけれども，図8のように，周波数の安定性としては現在のところ一番よいデータとして，$10^{-12}$ぐらいの値が得られています。

図8では縦軸は周波数の揺らぎの大きさを表すσで，横軸はこのσを測定するときの積分時間です。積分時間が長い所では，非常にゆっくりした揺らぎの成分を観測していることになります。図中で曲線の$A_1$，$B_1$，$C_1$，Dは，負帰還制御を施さないフリーランニング状態でのデータです。この状態で$10^{-8}$から$10^{-9}$ぐらいの揺らぎ

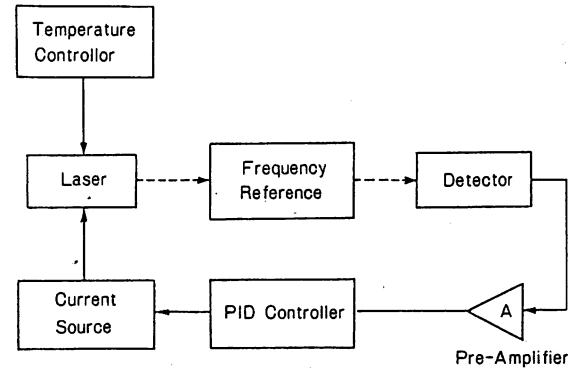


図7　中心周波数を安定化する装置の構成

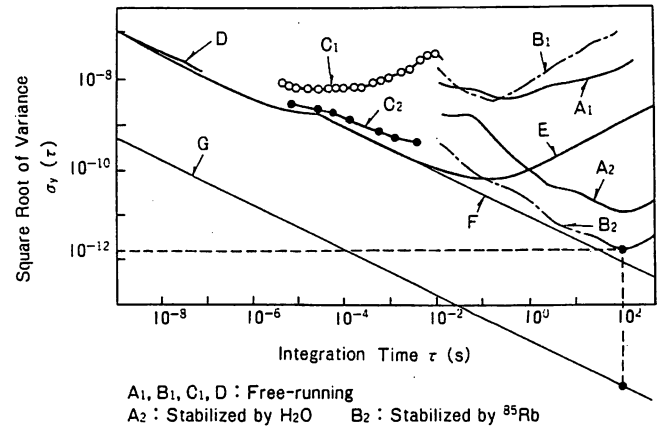


$A_1$, $B_1$, $C_1$, D：Free-running
$A_2$：Stabilized by $H_2O$　　$B_2$：Stabilized by $^{85}Rb$
$C_2$：Stabilized by a rigid Fabry-Perot interferometer
E：Free-running laser including external noises
F：Quantum noises in free-running laser
G：Detector noise limited
(M. Ohtsu, et. al.：Jpn. J. Appl. Phys., 22 (1983) p. 1157)

図8　周波数安定度のデータ

になっていること，すなわち数 100 kHz から数 MHz の揺らぎが，どのように外部の環境を整えてやっても，発生しているということです。これに対して負帰還制御をかけてやりますと，曲線 $A_2$，$B_2$，$C_2$ のように，量子雑音限界ぎりぎりのところまで達します。

現在のシステムで，制御系の性能向上によってどのぐらいまで安定度が上がるかというのが，この理論曲線の G です。現在よりも大体 2 桁半ぐらい安定度は向上することが可能です。すなわち，積分時間が 100 s において大体 $10^{-15}$ ということです。これは水素メーザの短期安定度とそれほど遜色のないデータが，半導体レーザにおいても期待されるということを意味しています。

### 5.2 線幅を狭窄化する

線幅の狭窄化は，図 6 のブロックの(2)で行うことができ，具体的な回路は図 9 のとおりです。レーザは戻り光の影響を抑えるためにアイソレータなどを使い，さらに，周波数の復調器として小形のファブリペロー干渉計を使っています。そこからの透過光を光検出器で受けるのですが，この透過光パワーの揺らぎが周波数の揺らぎに対応しています。これを適当な広帯域の増幅器と帯域を広げるための位相補償回路を通して，レーザに負帰還してやります。ここではコヒーレントな主レーザを用意するので，先ほどの 1 番目の課題である中心周波数も同時に安定化させるために，ファブリペロー干渉計からの反射光を受けておきます。この反射光パワーの揺らぎを中心周波数の揺らぎの大きさに比例する信号として利用し，低域の負帰還制御を同時にかけます。

このような系を使いまして実際にレーザの FM 雑音を測ってみますと，図 10 のような結果を得ます。縦軸が FM 雑音のパワースペクトル密度ですが，低周波の方ではキャリヤの易動度の揺らぎにもとづくフリッカ雑音が現れています。大体 100 kHz 以上では白色雑音，すなわち量子雑音が現れています。こうしてキャリヤ密度揺らぎと自然放出にもとづく揺らぎが実際に検出できましたので，この量を負帰還してやればよいわけです。

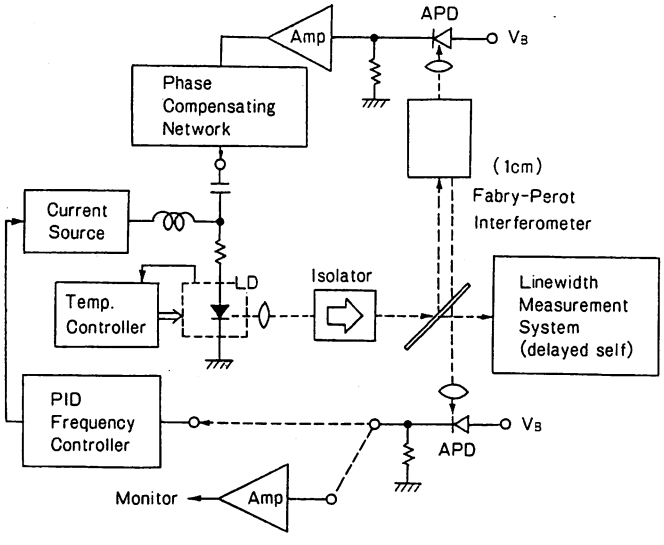


図 9　線幅を狭窄化するための回路の構成

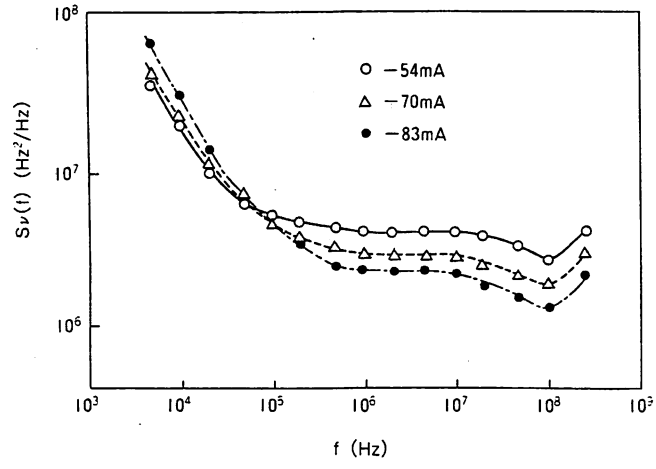


図10　半導体レーザの周波数揺らぎを表すパワースペクトル密度

負帰還制御のときに肝心なのは，レーザの電流を変調したとき実際のレーザ光の周波数がどのぐらいの振幅で変調するかという周波数偏移に関する特性と，電流をある周波数 $f$ で変調したときの電流の変化に対して光の周波数がどのような位相差を持って，すなわちどのぐらいの位相遅れで，変化するかという位相遅れ特性の二つが重要なパラメータとなっていることです。

図 11 のように1.5 $\mu$m 帯のレーザに関しましては，フリーランニン

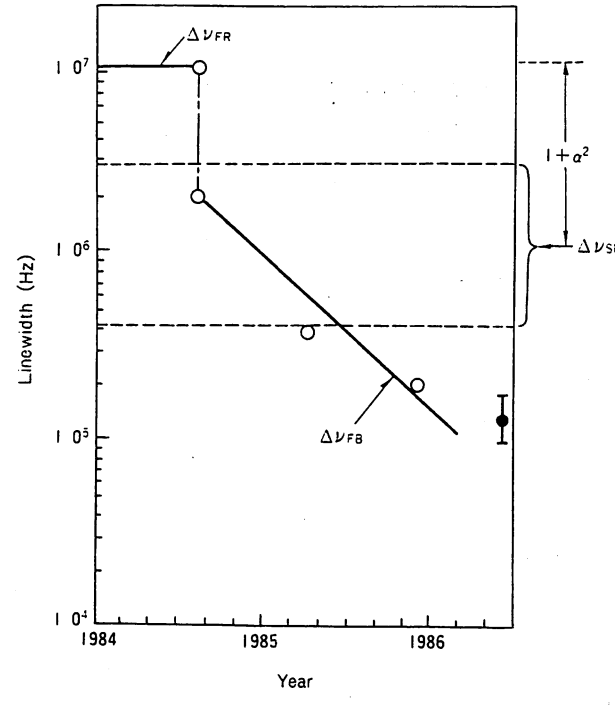


図11　1.5 $\mu$m InGaAsP レーザの線幅の推移

グのときに線幅が 10 MHz であったものが，年々制御系の性能が上がりまして現在のところでは 100 kHz から 80 kHz ぐらいの値に達しています。横軸に水平な二つの破線に囲まれた範囲というのは，実はフリーランニングの値を基に推定した，自然放出によって決まるレーザ固有の量子雑音限界です。この値よりも現在は線幅が狭くなっているということは，負帰還制御によって線幅は，レーザ固有の自然放出雑音によって制限されるような線幅の値以下に，また人工的なコヒーレントといいますか光の波のきれいな状態が，実際に実現できていることを表しています。

現在のところ実は線幅 80 kHz というのは，もっと狭くなる可能性があります。どのくらい狭くなるかを示すのが図 12 で，先ほどのレーザの周波数の揺らぎを表すパワースペクトル密度を測定したときのデータです。横軸はフーリエ周波数で，適当な復調器を用いてレーザの周波数揺らぎのパワースペクトル測定をしますと，曲線 A のような形になります。高周波では白色雑音，低周波ではフリッカ雑音になります。これに対して復調器から発生する測定系の雑音の大きさは曲線 B です。

この両者を比較しますと周波数揺らぎの測定の際の SN 比は大体 28 dB ぐらいあります。言い換えますと，現在の制御系を使いますと原理的にはフリーランニングの状態の−28 dB ぐらいの狭い線幅が実現できることを，この図は表しています。28 dB は大体 1/630 ぐらいですから，1 kHz を切るぐらいの線幅が実際に得られるはずです。しかし，現在のところまだ最小値は 80 kHz です。この差は何からくるかといいますと，制御系の帯域が十分広くないということです。

更に回路解析をしまして，もう少し線幅を狭くするような方法を考えます。一番簡単な方法は，制御系の発振ピークを減らしてやるといいますか，高周波の方へ持っていってその高さを低くしてやります。そのためには全体の負帰還制御系の遅延時間を短くしてやることが有効です。結論を申しますと，遅延時間が0.6 ns 以内ですと，先ほどの SN 比の値−28 dB に合致するような狭い線幅がこの負帰還制御系によって実現できると推定できます。

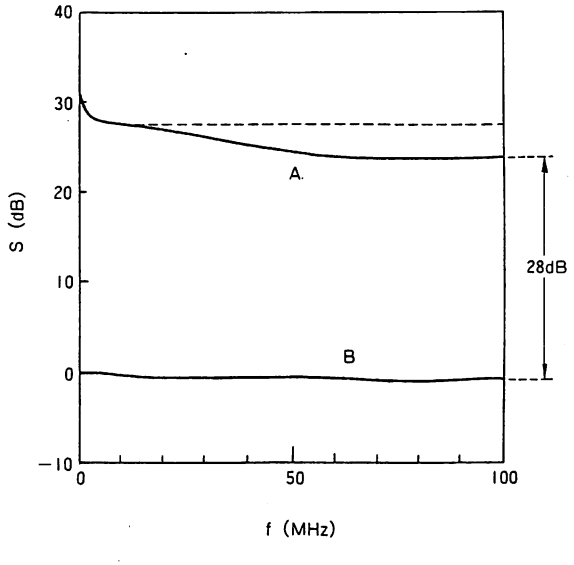


図12　1.5 μm InGaAsP レーザの周波数揺らぎを表すパワースペクトル密度

0.6 ns という値を作ることは現在の技術では難しくなくて，例えば GaAs のサーボアンプを使いますと，このアンプの遅延時間自身が 0.2 ns ぐらいになります。また電気的なケーブルの長さ，光学的な光路長の和を大体 12 cm 以下にしてやりますと，これらによる遅延時間は 0.4 ns になります。このようなことで，遅延時間は 0.6 ns にできるという予想が立ちます。このことは逆にいいますと，最近盛んに研究されている OEIC（Opto-Electronic IC）や集積化技術を使わなくても，市販のディスクリートのコンポーネントを使いまして，先ほどの 28 dB すなわち 1/630 の線幅が実現できることを物語っております。

ここまでが主レーザとしての中心周波数の安定化と線幅の狭窄化についての話です。

### 5.3　従レーザの周波数を追随させる

これまで述べましたような比較的質の高いレーザが完成しますと，これを主レーザとして第 2 番目に従レーザを持ってきて，このレーザの周波数を主レーザの周波数に追随させることが考えられます。この原理は図 13 のように非常に簡単で，ヘテロダイン方式の周波数スタビライザのような回路を設けてやればよいのです。要するに 2 台のレーザのヘテロダイン信号の周波数が，別に用意するマイクロ波シンセサイザの周波数と一致するように，従レーザの注入電流を制御してやるというわけです。この方式から決まる従レーザの周波数は，主レーザの周波数とマイクロ波シンセサイザの周波数（実際にはこれをプリスケーラの分周率倍した値）との和で与えられます。

我々が行っている実験では，追随精度を上げるために，ヘテロダイン信号の周波数ではなくて位相をマイクロ波シンセサイザの位相と合わせるという，いわゆる光領域の位相同期ループのようなことを実行しています。

実際のヘテロダイン信号の周波数の揺らぎは図 14 の大きさになっていて，横軸は積分時間 $\tau$，縦軸は周波数の揺らぎの平方根 $\sigma$ です。積分時間が大体 100 s ですと $\sigma$ は数 Hz で，これは $10^{-14}$ という非常に小さい値になります。この値は一番目の課題である主レーザの中心周波数の安定度の値よりも大分小さい値になっています。すなわち，ヘテロダイン信号の周波数の揺らぎ大きさというのは主レーザの周波数揺らぎに比べて 2 桁ぐらい小さい値ですので，従レーザは主レーザに十分精度よく追随していることが分かります。

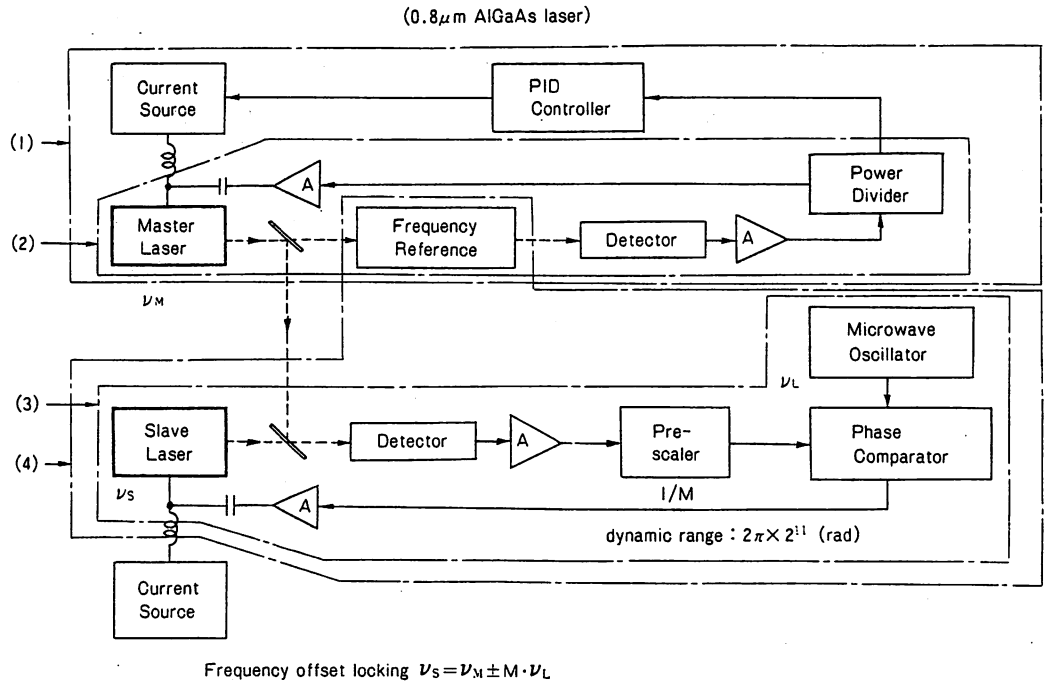


図13　従レーザの周波数追随回路の構成

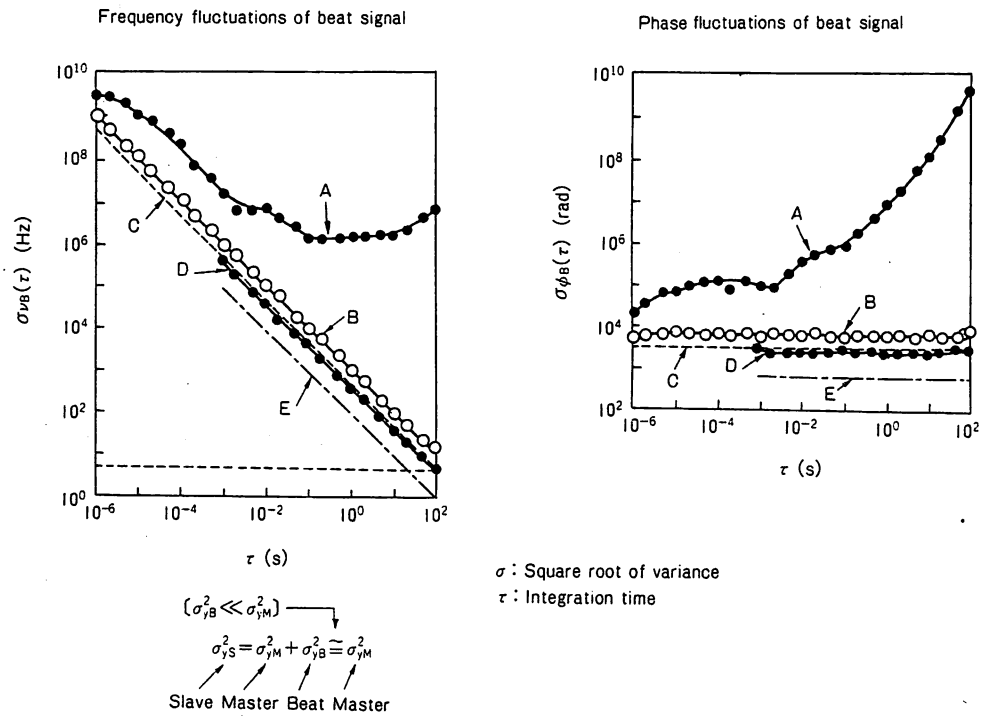


図14　ヘテロダイン信号の周波数の揺らぎ

### 5.4　周波数を掃引する

最後に4番目の課題として周波数の掃引ということですが，先ほどの光トラッキングジェネレータといいますか，光位相同期ループの技法をそのまま流用することができます。図15のように主レーザと従レーザがありまして，従レーザの周波数を主レーザに追随させながら，マイクロ波シンセサイザの周波数をずっと掃引していきますと，ヘテロダイン信号の周波数がこれに応じて掃引されます。すなわち，従レーザの周波数も掃引されるということです。

一例としまして図16のように，大体5sおきぐらいにマイクロ波シンセサイザの周波数を20 MHzステップで掃引していきますと，ヘテ

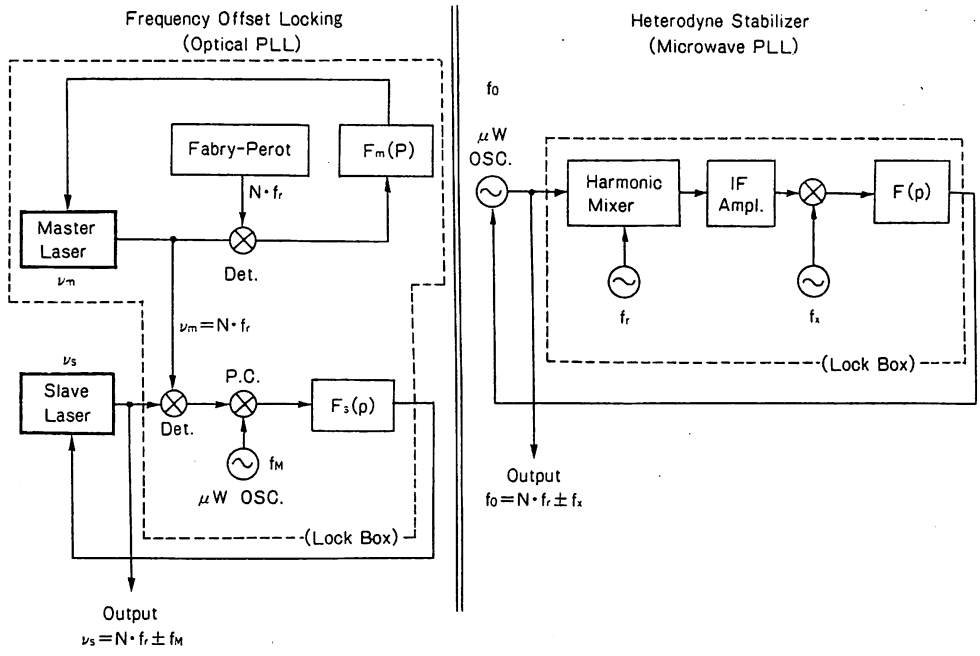


図15　周波数掃引回路の構成

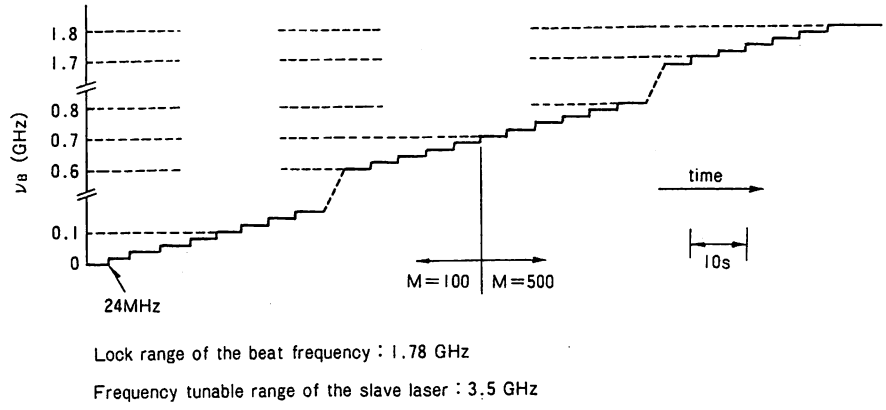


Lock range of the beat frequency : 1.78 GHz

Frequency tunable range of the slave laser : 3.5 GHz

図16　ヘテロダイン周波数の掃引周波数範囲

ロダイン信号の周波数もそれに合わせて掃引されまして，結局ヘテロダイン信号の測定の際の光検出器の帯域いっぱいぐらいまで，大体 1.8 GHz ぐらいまで一回で掃引されます。実際には符号を＋の方に掃引するのと，－の方へ掃引するのと両方ありますから，その 2 倍の 3.6 GHz ぐらい一回で掃引できることになります。そのときの周波数設定精度は，先ほどいいましたように $10^{-14}$ ぐらいになっています。

更に周波数の掃引範囲を広げるために，図15の主レーザの周波数を先ほどの周波数の基準，すなわち周波数の復調器としてのファブリペロー干渉計の共振周波数に次々に固定していって，その状態で主レーザの周波数に対して光位相同期を保ちながら従レーザの周波数を掃引していきますと，更に従レーザの周波数可変範囲が広がります。

このように周波数の基準となる主レーザの周波数基準のグリッドとして最近よく使われますのは，1.5 μm 帯とか 0.8 μm 帯ですと，アンモニア，水蒸気という非常に希薄なガスの持つ吸収スペクトルです。

簡単なグリッドとして，実際にファブリペロー干渉計の共振曲線を使って，次々に主レーザの周波数をこれにロックしながら従レーザ周波数を掃引していきますと，現在のところ大体 50 GHz ぐらいの連続周波数掃引が可能です。この 50 GHz というのは実際には主レーザのモードの飛び，すなわちモードホッピング現象により制限を受けています。このモードの飛びがないようなレーザを使いますと，原理的にはこのような技術で 1 THz ぐらいの掃引範囲にわたって連

続掃引が可能となります。

## 6 実験的なデータ，理論的な限界値のまとめと本手法の特徴

四つの課題を解決する手法を簡単に説明申し上げましたけれども，実験的なデータ，理論的な限界値をまとめると，以下のようになります。

（1） 中心周波数の安定度の実験結果は $2\times10^{-12}$。理論的には約 $10^{-15}$ の値が可能であろう。

（2） 線幅の狭窄化の実験結果は 100 kHz。理論的には約 1 Hz の値が可能であろう。

（3） 周波数トラッキング精度の実験結果は $3\times10^{-14}$。理論的には約 $1\times10^{-16}$ の値が可能であろう。

（4） 連続周波数掃引の実験結果は約 50 GHz。理論的には約 1 THz の値が可能であろう。

さらに，いままで説明してきた手法の特徴を述べます。

（1） 負帰還制御ですから安定性と再現性が高い。

（2） コヒーレンスの度合いが，レーザの共振器構造そのものを変更することなく，制御利得を可変することで調節できる。

（3） 制御系の設計には，電子回路との類推によって，いわゆるCAD ができる。要するになにも実験をやらなくても計算機の上で光電系の伝達関数を計算してやれば，大体線幅の値が何 kHz ぐらいになるかということを予測できる。

（4） OEIC との適合性が良い。要するに OEIC が可能であれば制御系のループが非常に短くなる。更にまた遅延時間が小さくなるから，制御帯域を拡大することによって，性能が向上できる。

（5） このような方法はコヒーレントな光センシングにはもちろん利用できるし，ローカルエリアネットワークなどに使うようなコヒーレント光通信（低ビットレートから中ビットレートのもの），更にまた 1000 チャネル程度の周波数多重度を要求するような，将来の周波数超多重のコヒーレント光通信の信号には適していると考えられる。

## 7 むすび
（コヒーレンスの高い半導体レーザの将来構造）

これまで非常に良いことずくめの話をしてきましたが，最初の話のように現在のところは，そもそも単一モードの半導体レーザとして必ずしも十分性能が高いものが得られていないという問題が依然として残っています。デバイスの構造からいいますと，そのようなことをある程度克服して，先ほどの四つの技法を十分生かせるようなレーザ構造が望ましいのです。将来の半導体レーザデバイスの構造として，従来から在ります非常にコヒーレンスの高いレーザ，すなわち気体レーザとか色素レーザの構造との類推から，次に述べるような方向に進むのが一つの手法ではないかと考えます。

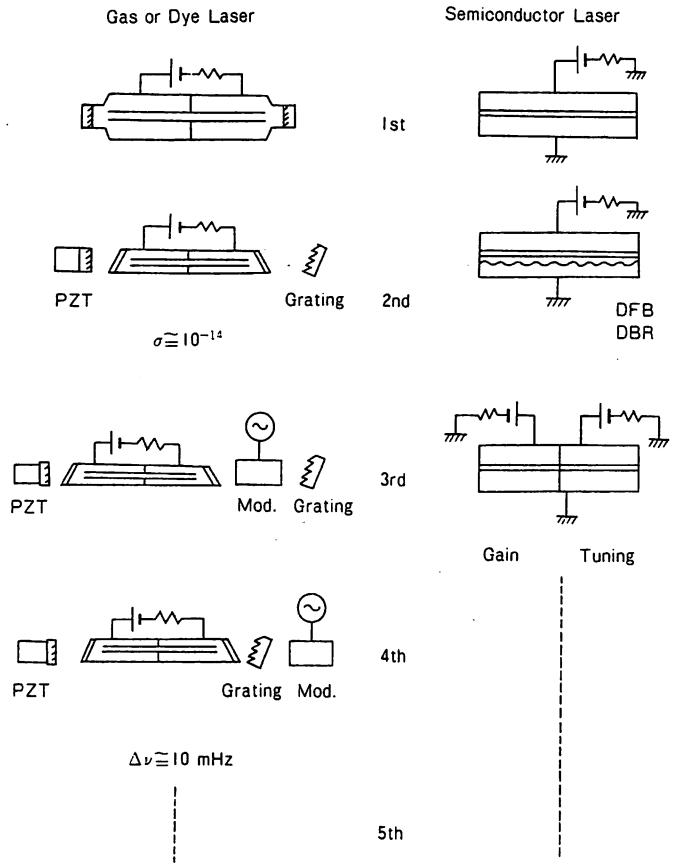


図17 レーザ構造の推移

図 17 の左側は従来の性能の高い気体レーザあるいは色素レーザで，右側は半導体レーザの構造の推移を示します。

気体レーザあるいは色素レーザにおいて1960年代の第 1 世代のレーザとしては，とにかく発振して光が出てくれれば良いということで，レーザ媒質の両側に鏡が直接固定されたような非常に単純な構造であったのです。しかし，1980年代の冒頭ぐらいまでには第 2 世代になりまして，周波数のコヒーレンスと周波数の安定度を向上するために，例えばグレーティングを使って単一モードを保ったり，共振器長を変調するための適当な変調器を設けて負帰還制御がかかるようなことをしまして，周波数の安定性としては $10^{-14}$ ぐらいの値を得ています。

1980年代の半ばころになりますと，制御系の帯域を広げるために共振器の中に変調器を入れて高速化するということをしました。つい最近では，変調器を共振器の外に置きまして，位相を変調しながら

パワーをある程度一定に保つという方法で制御の精度を上げて，周波数の安定性で $10^{-16}$，線幅で 10 mHz というチャンピオンデータを，第 4 世代のレーザとして得ております。

同じようなことを半導体レーザに対していえば，普通の闢開（へきかい）で作ったファブリペロー共振器形のレーザというのが第 1 世代になりますし，最近一部は市販されるようになった動的単一モードレーザすなわち DFB レーザというのが第 2 世代になります。

図 18 のように，周波数変調特性を向上させるために発振の利得部分と位相制御の部分を二つに分けたレーザが，実験室段階で最近試作されており，これが第 3 世代に相当します。将来的には第 4 世代のものに進むこと，すなわちレーザの共振器の外側に位相変調器を設けて精度を上げることが，より一層の性能向上の一つの方法でないかと思います。

## 参考文献


1) K. Kobayashi, and I. Mito, "Progress in narrow-linewidth tunable laser sources", Proc. OFC/IOOC '87, WC1, Reno, Nevada, January 1987

2) S. Murata, I. Mito, and K. Kobayashi, "Over 5.8-nm continuous wavelenth tuning of 1.5 $\mu$m wavelength tunable DFB laser", Proc. OFC/IOOC '87, WC3, Reno, Nevada, January 1987


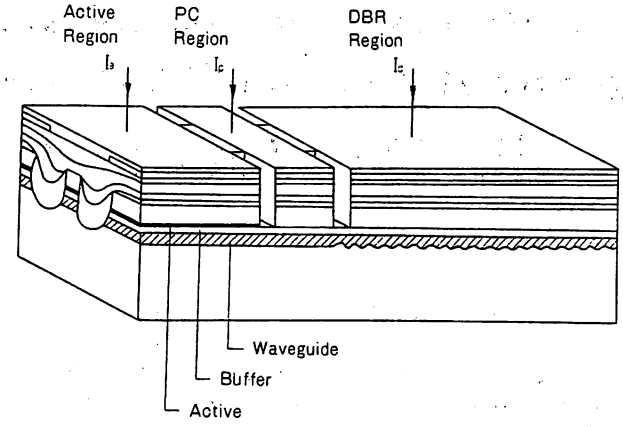



● K. Kobayashi, and I. Mito, "Progress in narrow-linewidth tunable laser sources", Proc. OFC/IOOC'87, WC1, Reno, Nevada, January 1987.

● S. Murata, I. Mito, and K. Kobayashi, "Over 5.8-nm continuous wavelenth tuning of 1.5um wavelength tunable DFB laser", Proc. OFC/IOOC'87, WC3, Reno, Nevada, Junuary 1987.


図18　半導体レーザの将来構造の一例


講演者の略歴

大津　元一　（おおつ　もといち）

1978年　東京工業大学大学院を卒業

同　年　工学博士

1984年　電波科学国際連合 (URSI) より I. Koga Gold Medal を受賞

1986年　米国ベル研究所において研究に従事

現　在　東京工業大学大学院総合理工学研究科物理情報工学専攻助教授

## Research and Studies on Optical Control in Japan

# III. Development of a Hyper-coherent Optical

### Introduction

A laser is an oscillator which generates clean optical waves, and can be used in various ways as shown in Figure 1. When gas lasers are used, for example, highly precise optical measurement, satellite tracking, navigation, maintenance of time standard, gravitational wave detection, etc., can be carried out. When more practical light sources, i.e., semiconductor lasers are used, coherent optical communication systems including inter-satellite links, fiber gyroscopes, Doppler velocimeters, and optical pumping of microwave atomic oscillators become possible. In this article, generation of hyper-coherent light by controlling semiconductor laser frequency and experiments on realizing a system to sweep the optical frequency over a wide spectral range, that is, an optical sweep generator, are introduced.[1-3)]

*Motoichi Ohtsu was born in Kanagawa, Japan, in 1950. He received his B.S., M.S. and Ph.D. degrees in electronics engineering from the Tokyo Institute of Technology in 1973, 75 and 78, respectively.*

*In 1982, he was appointed Associate Professor at the same Institute. From 1986 to 87, he joined AT&T Bell Laboratories, Crawford Hill Laboratory. His main fields of interest are frequency control of lasers, analysis of dynamic behavior of lasers and their application to coherent optical measurement, optical communications and microwave atomic clocks.*

*Dr. Ohtsu received a prize from the Japan Society of Applied Physics in 1982, the Issac Koga gold medal from the International Union of Radio Science (URSI) in 1984, and the Japan IBM Science Award in 1988.*

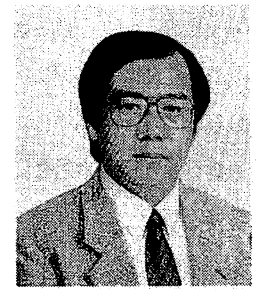

### Semiconductor Laser Frequency Fluctuation and Control Limits

Optical frequency fluctuation of a semiconductor laser is a measure indicating the smoothness of the optical waves. The magnitude of fluctuation is dependent on the fundamental fluctuation source originating from the quantum mechanical principle (spontaneously emitted light fluctuation, in other words, the quantum noise source)

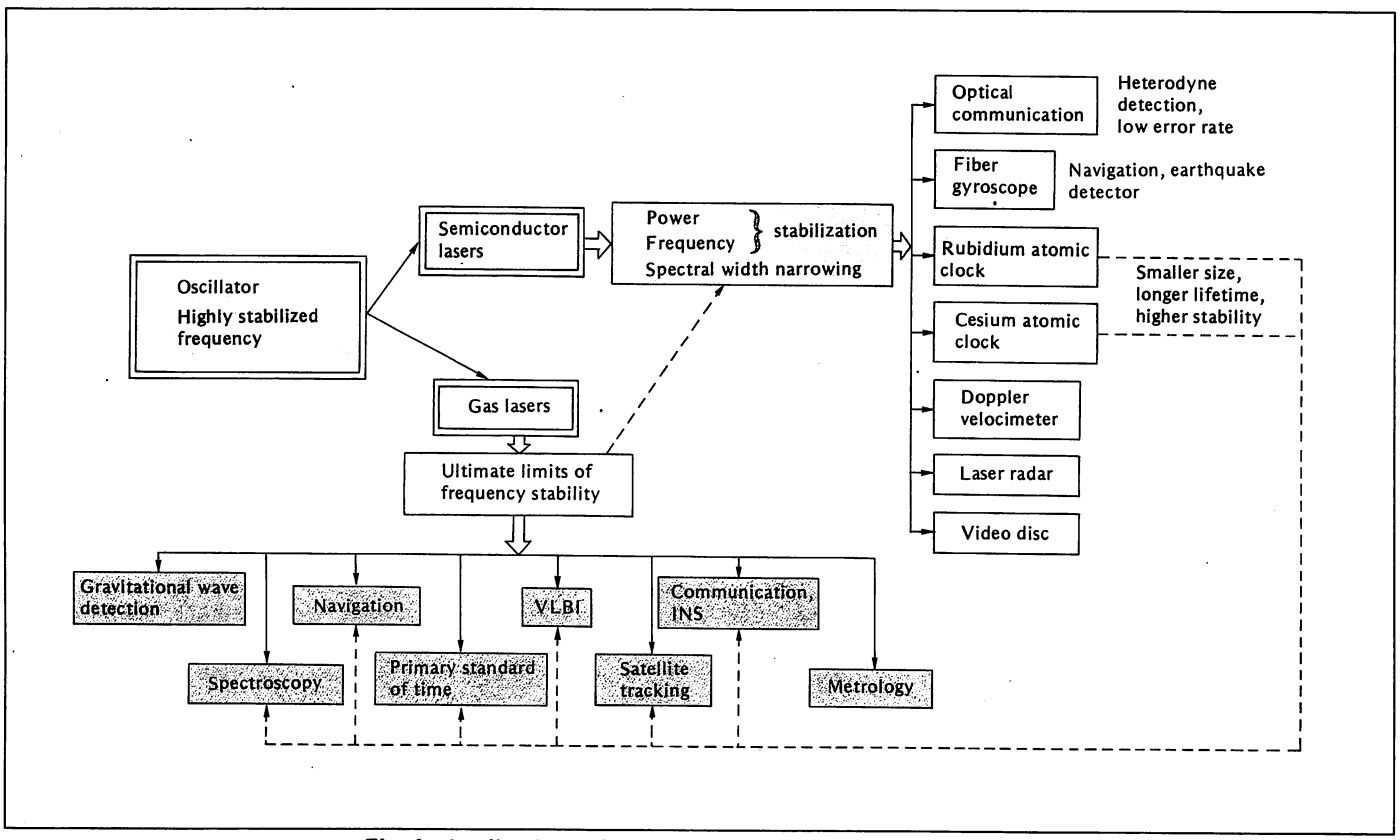


**Fig. 1. Applications of lasers having low frequency fluctuation**

# Sweep Generator Using Semiconductor Lasers

By Dr. Motoichi Ohtsu,
Tokyo Institute of Technology

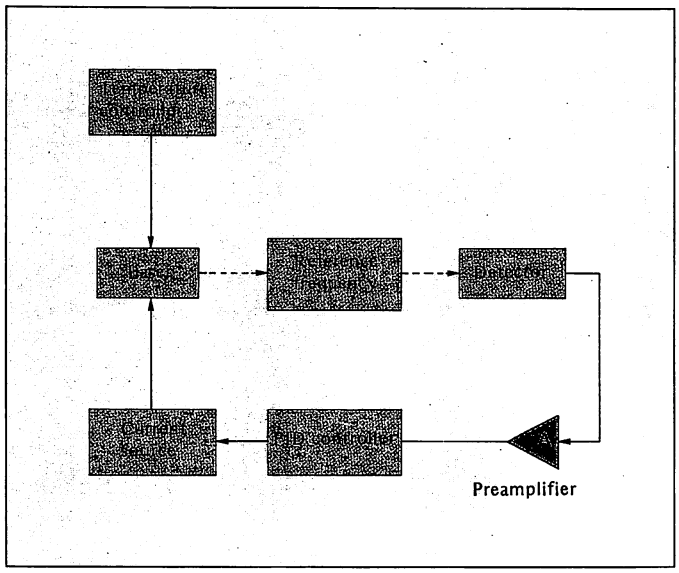


**Fig. 2. Principle of the negative electrical feedback control method for reducing semiconductor laser frequency fluctuation**

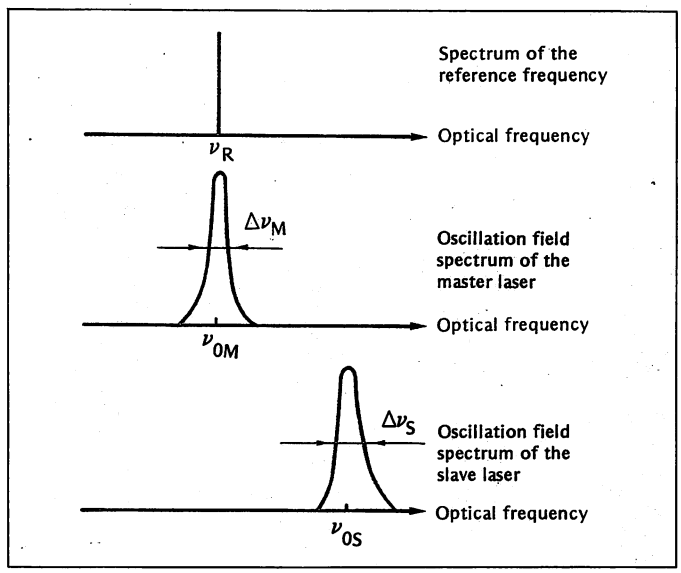


**Fig. 3. Problems to be solved to realize a hyper-coherent optical sweep generator**

and from the carrier density fluctuation intrinsic to the semiconductor laser. Magnitudes of these fluctuations are also proportional to the amount of loss of a laser resonator. The field spectral linewidth of a semiconductor laser is as wide as several megahertz because of these fluctuation sources, and as long as it has such a wide linewidth, the above-mentioned applications are difficult to achieve.

When the laser current is negative feedback controlled to reduce the frequency fluctuation using the system shown in Figure 2, in an extreme situation where the control gain is infinite, the magnitude of fluctuation can be reduced to the value which is limited by the noise magnitude generated by the control system.[1-3] Therefore, if a high-gain, low-noise control system is used, the magnitude of frequency fluctuation becomes lower than the quantum noise level of a free-running laser. This low-noise state of the laser can be referred to as the hyper-coherent state.[3]

## Problems in Realizing an Optical Sweep Generator

For a hyper-coherent optical sweep generator to be realized, it is first necessary to reduce the semiconductor laser frequency fluctuation in order to realize the hyper-coherent state, and second, the optical frequency should be swept over a wide spectral range. In other words, the following four problems must be solved as shown in Figure 3.

(1) Center frequency $\nu_{0M}$ of the field spectrum of the master laser must be controlled so as to be locked to stable reference frequency $\nu_R$.
(2) The field spectral linewidth $\Delta\nu_M$ of the master laser must be narrowed.
(3) Center frequency $\nu_{0S}$ and linewidth $\Delta\nu_S$ of the field spectrum of the slave laser must track those of the master laser.
(4) Frequency $\nu_{0S}$ of the slave laser must be swept, while maintaining the conditions described in (1) to (3).

We have proposed using the negative electrical feedback control method as shown in Figure 4, which solves all four above-mentioned problems simultaneously.[1-3] The devices shown in blocks (1) to (4) solve the above-mentioned problems (1) to (4), respectively. Although the overall system looks rather complicated, its size can be kept compact. The beneficial characteristics of this system are: high stability and reproducibility; ability to reduce the magnitude of frequency fluctuation below the quantum noise limit, that is, an optical hyper-coherent state can be realized; and optimum design of the control system can be made by using computer simulation. Experimental results obtained using this system are introduced below.

### 1. Stabilization of the Center Frequency

In order to solve problem (1) mentioned above, it is essential to find a stable reference frequency $\nu_R$. Since molecular gases such as ammonium and water vapor have many absorption spectral lines in the wavelength range between 0.7 to 1.6$\mu$m, they can be used as convenient reference frequencies for a semiconductor laser.[4] These spectral lines, however, exhibit weak absorption. On the other hand, at a wavelength of around 0.8$\mu$m, absorption spectral lines are found in rubidium and cesium atomic vapor, etc. These spectral lines have the advantage of offering high absorption[5] and low frequency shift caused by disturbance,[6] making it

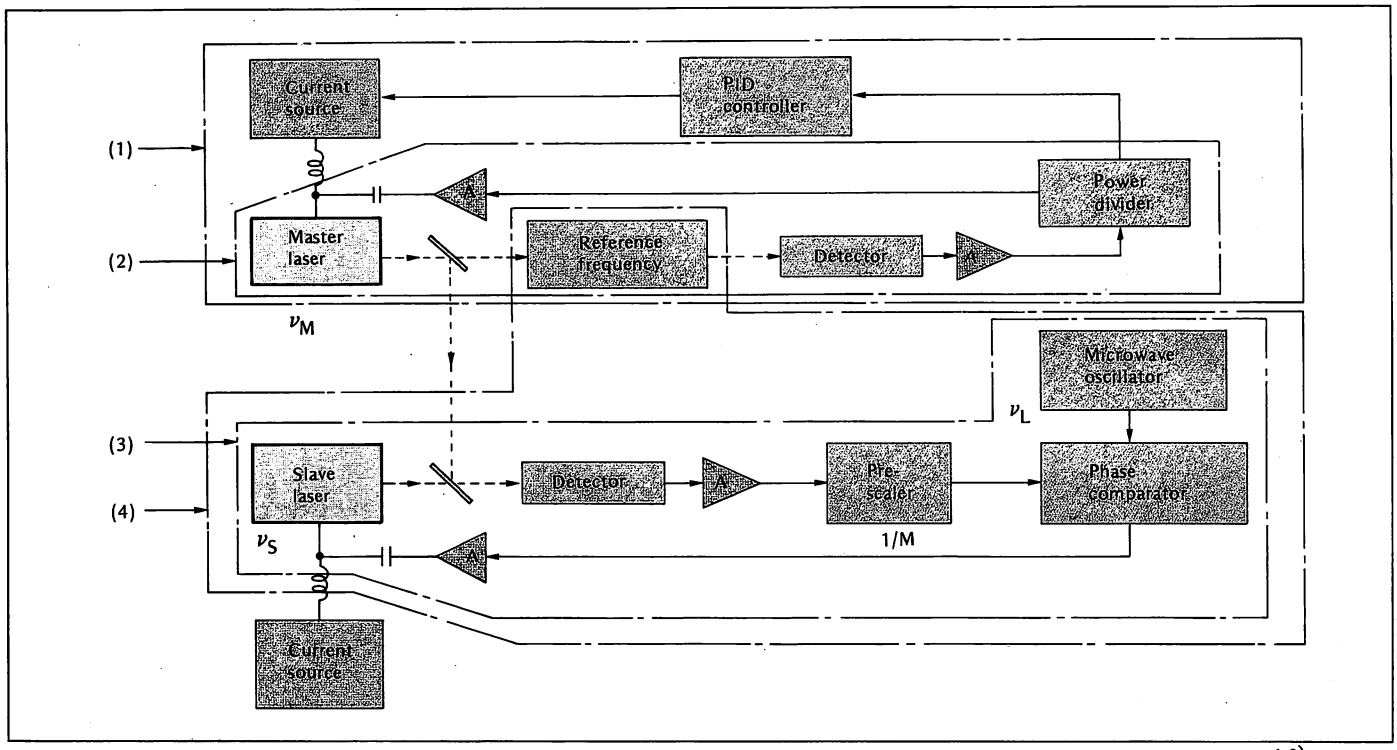


**Fig. 4. A synthesized negative electrical feedback control system which solves all four problems simultaneously[1,2]**

a very stable reference frequency. Using one of these spectral lines as the reference frequency, stabilization of a 0.8$\mu$m AlGaAs laser frequency was carried out using device (1) in Figure 4, and a stability of 2 x $10^{-12}$ (at an integration time of 100 seconds) was obtained.[1,2,7]

As mentioned in "Semiconductor Laser Frequency Fluctuation and Control Limits," the noise generated from the control system limits ultimate stability, which is estimated as being 1 x $10^{-15}$. For a 1.5$\mu$m InGaAsP laser, which is used as a light source for coherent optical communications systems, stabilization using its internal second harmonic and rubidium reference frequency has also been carried out.[6,8]

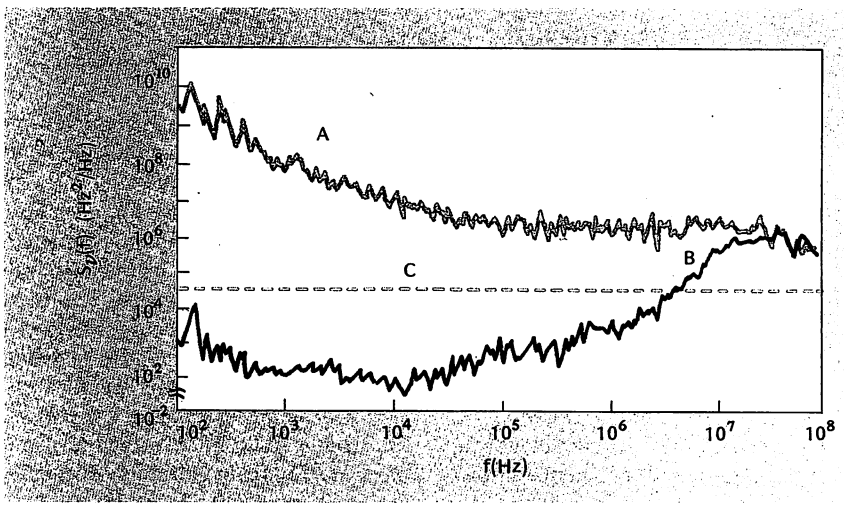


**Fig. 5. Measured values of power spectral density $S_\nu(f)$ of the frequency fluctuation in a 0.8$\mu$m AlGaAs laser.[9] A: Free-running; B: Negative electrical feedback controlled; C: Quantum noise limit of the free-running laser.**

## 2. Narrowing of the Spectral Linewidth

The spectral linewidth can be reduced by applying fast negative electrical feedback control using device (2) in Figure 4. In this case, we used the resonance frequency of a high-performance Fabry-Perot interferometer having a finesse of 3,500 as a frequency discriminator. In order to apply fast feedback control, wide band detection of frequency fluctuation is required. For this purpose, a laser beam was incident into the interferometer, and the fluctuation of the reflected light power was measured. Since a differential amount of frequency fluctuation is included in the power fluctuation of the reflected light, the frequency fluctuation detection bandwidth can be wider than that for measuring the power fluctuations of the transmitted light. Using this method, a fast, high-gain

control system was realized.[9]

The power spectral density of frequency fluctuation in a 0.8$\mu$m AlGaAs laser is shown in Figure 5. Curve A shows the values in the free-running condition, and curve B when under controlled conditions. By comparing these two curves, it can be seen that a fluctuation reduction of more than 60dB can be realized. Dotted line C indicates the quantum noise limit of the free-running laser. By comparing curve B and dotted line C, it can be seen that in the Fourier frequency range between 100Hz and 4.4MHz, frequency fluctuation is below the quantum noise limit, and a hyper-coherent condition is obtained. From this, justification of the discussion mentioned in "Semiconductor Laser Frequency Fluctuation and Control Limits" is proved.

Figure 6 shows the field spectral profile of a laser estimated from the values produced by curves A and B in Figure 5. Although the half-width of the spectrum is 4.5MHz in the free-running condition, it is shown to be narrowed to only 560Hz by feedback.[9] This is the narrowest value reported so far.

By comparing curves A and B in Figure 5, it can be seen that the bandwidth of negative electrical feedback control was 40MHz, and the control gain-bandwidth product reaches as high as 40THz. Furthermore, Figure 6 shows that the power of the optical carrier of the controlled laser is about 30dB larger than that of the free-running laser. From these results, it can be concluded that such a hyper-coherent laser can be very effective for coherent optical sensing as well as for low-to-medium bit rate coherent optical communication systems. Through further improvements of the control system, the spectral linewidth is expected to be reduced down to approximately 1Hz.[10]

### 3. Frequency Tracking

The hyper-coherent laser obtained by the methods described above is used as the master laser, and the frequency of a second laser, i.e., the slave laser, is made to track that of the master laser using device (3) in Figure 4. The heterodyne signal between the master and of the slave laser is electrically negative feedback controlled so that the heterodyne signal frequency $\nu_{0S} - \nu_{0M}$ is locked to the frequency $\nu_L$ of the microwave oscillator which is used as a stable local oscillator.

If the division factor of the frequency divider for heterodyne frequency detection is represented by M, the frequency of the slave laser will be: $\nu_{0S} = \nu_{0M} + M \cdot \nu_L$. This means that the slave laser frequency tracks that of the master laser with an offset of $M \cdot \nu_L$. By measuring the fluctuation of the heterodyne frequency, tracking errors can be estimated and the results are shown in Figure 7. These are square roots of the fluctuation variance. Curve A shows the values in the free-running condition. Curve B shows the results of frequency tracking, and the value of $5 \times 10^{-16}$ at an integration time of 50 seconds is smaller than the frequency fluctuation of the master laser.[11] This means that the frequency of the slave laser tracks that of the

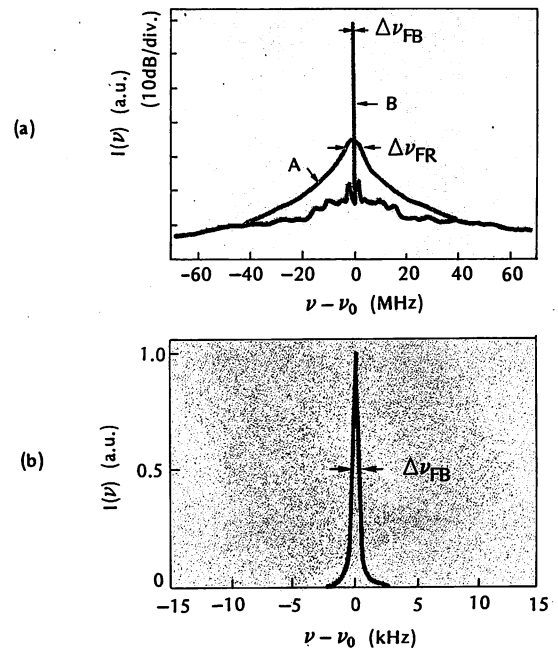


**Fig. 6. A profile of the field spectrum of a 0.8$\mu$m AlGaAs laser.[9] In (a), A: Free-running; Half-width $\Delta\nu_{FR}$ = 4.5MHz; B: Negative electrical feedback controlled. (b) Magnified profile of curve B in (a). Half-width $\Delta\nu_{FB}$ = 560Hz.**

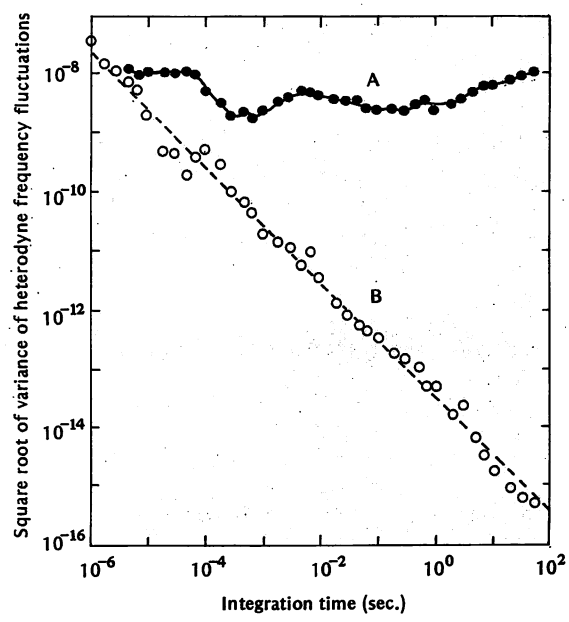


**Fig. 7. Measured values of the square root of the fluctuation variance of a heterodyne signal between master and slave lasers.[11] A: Free-running; B: Negtive electrical feedback controlled.**

master laser with high precision. In other words, the very high coherence in the master laser is transferred to the slave laser. Therefore, a heterodyne-type optical frequency-locked loop has been realized.

At present, however, phase-fluctuation of a heterodyne signal still remains larger than 1 radian. By improving the system, further reduction to less than 1 radian is possible, and it is expected that a heterodyne-type phase-locked loop will be realized in the near future.

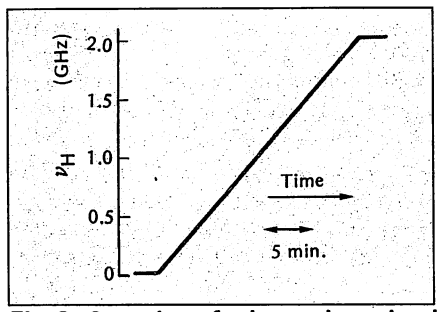


**Fig. 8. Sweeping of a heterodyne signal frequency $\nu_H$ between master and slave lasers[12)]**

### 4. Frequency Sweep

Stable sweep of the frequency of the slave laser was achieved using device (4) in Figure 4, while maintaining the performance obtained in sections 1 to 3. For this purpose, frequency $\nu_L$ of the microwave oscillator should be swept under heterodyne-type frequency-locked loop conditions. In this way, as shown in Figure 8, a 2GHz range can be swept at one time. By repeating this process, a total range as wide as 64GHz was obtained.[12)] However, the range was limited by the mode hopping phenomenon of the AlGaAs laser used.

It is estimated that the sweep range can be increased to 1THz if a dynamic single-mode laser such as a DFB laser is used.[12)] Furthermore, if parametric wavelength conversion using an organic nonlinear optical waveguide, which we are trying to fabricate, is employed, the sweep range is expected to be increased up to 10THz. With such an improvement, realization of an extremely high performance hyper-coherent optical sweep generator is expected.

## Comparison with Other Methods

In addition to the negative electrical feedback method already explained, the following two methods have also been proposed to reduce the frequency fluctuation of a semiconductor laser. However, it should be noted that a hyper-coherent state is not realized by these methods because they reduce the fluctuation by decreasing the laser resonator loss.

(1) Optical feedback method.
(2) Method of developing a laser device having a low-loss resonator.

With the optical feedback method, light transmitted from the laser is injected into the laser by an external reflector to decrease the loss of the laser resonator in order to suppress frequency fluctuation. Since this is a simple method, it has been employed for a long time. The control bandwidth is determined by the photon life time in the resonator, which is medium scale. Control gain is also medium scale. Problems are induction of deterministic instability, hopping between longitudinal modes, and a decrease in modulation efficiency.

For practical use, the optical feedback method in Figure 9 is proposed, since it has relatively little instability, in which an external Fabry-Perot cavity is used as an external reflector. Using this method, the bandwidth was expanded to 100MHz, and the spectral linewidth of the laser was reduced to 40kHz. The external Fabry-Perot cavity was fabricated by the micro-optics or fiber-optics technique, and the entire

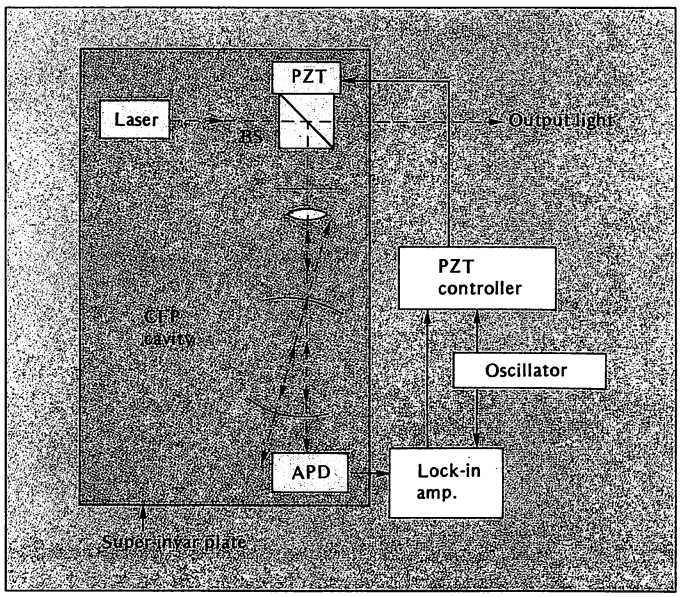


**Fig. 9. A system for reducing laser frequency fluctuation by optical feedback from an external confocal Fabry-Perot cavity**

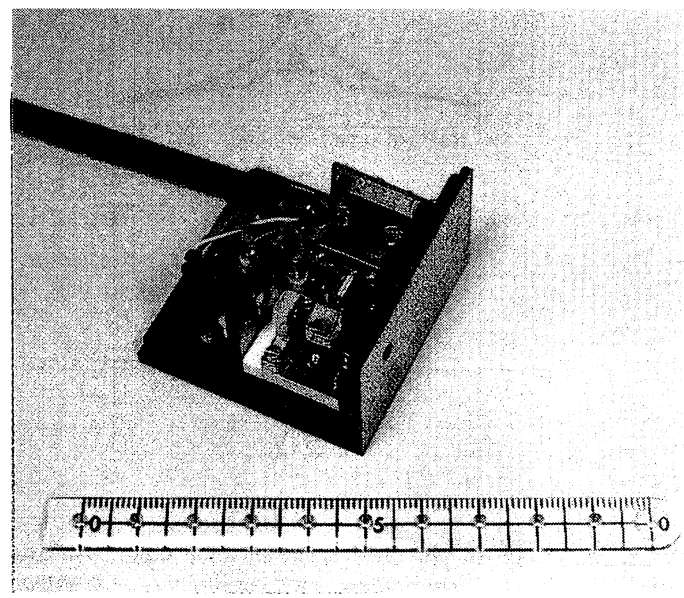

Fig. 10. A compact laser module using the micro-optics technique, which has the same performance as that in Fig. 9[11)]

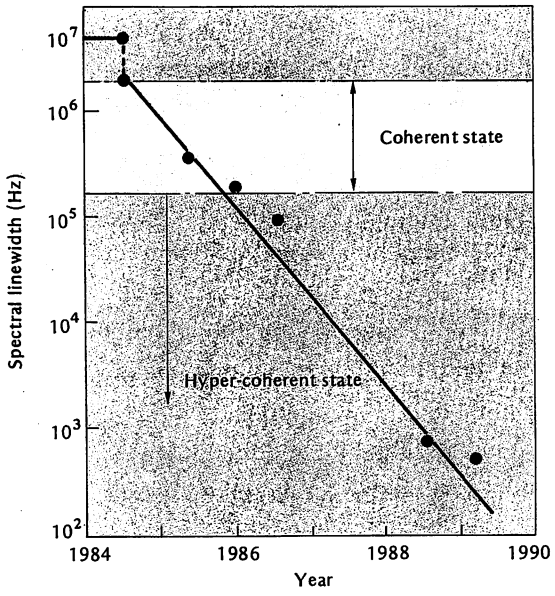


**Fig. 11. Progress in narrowing of the spectral linewidth employing the negative electrical feedback control method**

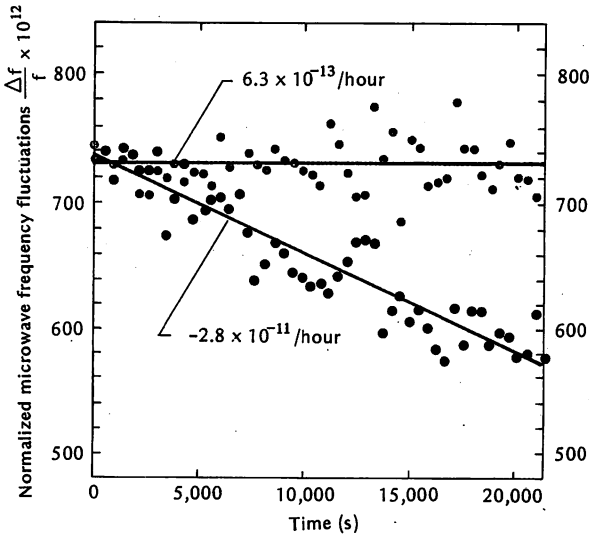


**Fig. 12. Temporal change in the microwave output signal frequency (6.8GHz) of a rubidium atomic oscillator.[14] ●: When a frequency controlled semiconductor laser is used. ●: When a free-running semiconductor laser is used.**

system was made compact as shown in Figure 10.[11]

With method (2), which involved developing a laser device having a low-loss resonator, the control bandwidth is wide, however, the control gain is as low as 10dB. At present, a laser device having a spectral linewidth of less than 1MHz is under development.[13] If a processing method can be developed to decrease resonator loss, it may be possible to increase the gain up to 20dB, resulting in the narrowing of the spectral linewidth to approximately 0.1MHz. To realize further narrowing of the spectral linewidth, use of the negative electrical feedback method mentioned earlier is indispensable.

## Conclusion and Future Prospects

Figure 11 shows the progress made in spectral linewidth narrowing using the experimental negative electrical feedback method. As can be seen, hyper-coherent light exceeding the quantum noise limit, in other words, extremely clean optical waves have been achieved. Further improvements of the characteristics is possible in the future. To accomplish this, improvements in the performance of laser devices themselves and development of opto-electric integrated circuits (OEICs) are required. The light obtained by employing these advanced technologies will be effectively used in various fields such as frequency-division-multiplexed coherent optical communications systems and optical sensing, as well as in the development of basic sciences, e.g., atomic physics and gravitational wave detection.

Finally, an example of the effective use of the high-performance semiconductor laser system just described is demonstrated in Figure 12.[14] The figure shows the measured values of the drift in the microwave output signal frequency (6.8GHz) of a semiconductor laser pumped rubidium atomic oscillator that we developed. As can be seen, the drift was decreased to less than 1/40 that of conventional devices by using a semiconductor laser.


REFERENCES

1) M. Ohtsu: Realization of ultrahigh coherence in semiconductor lasers by negative electrical feedback, J.Lightwave Technol., 6, pp. 245-256, 1988.
2) M. Ohtsu and T. Tako: Coherence in semiconductor lasers, Progress in Optics XXV (Ed. by E. Wolf), Elsevier Science Publishers, Amsterdam, pp.193-278, 1988.
3) M. Ohtsu: Generation of hyper-coherent light, Japanese version of Scientific American, pp.64-73, Mar., 1989. (in Japanese)
4) M. Ohtsu, H. Kotani and H. Tagawa: Spectral measurement of $NH_3$ and $H_2O$ for pollutant gas monitoring by 1.5$\mu$m InGaAsP/InP lasers, Jpn. J. Appl. Phys., 22, pp.1553-1557, 1983.
5) M. Hashimoto and M. Ohtsu: Laser spectroscopy and frequency stabilization of a semiconductor laser for a $^{87}$Rb atomic clock, Trans. IEE Japan, 108-C, pp.706-712, 1988. (in Japanese)
6) M. Ohtsu and E. Ikegami: Novel frequency control scheme for a 1.5$\mu$m DFB laser by using internal second harmonic and an atomic rubidium line, Conference on Lasers and Electro-Optics (CLEO '89), Baltimore, ML, TuD4, Apr. 1989.
7) M. Ohtsu: Frequency stabilization in semiconductor lasers, Opt. & Quantum Electron., 20, pp.283-300, 1988.
8) Ohtsu and E. Ikegami: Frequency stabilization of 1.5$\mu$m DFB laser by using internal second harmonic and $^{87}$Rb line, Electron. Lett., 25, pp.22-23, 1989.
9) M. Ohtsu, M. Murata and M. Kourogi: Subkilohertz linewidth of a semiconductor laser by electrical feedback and its network analysis, Conference on Lasers and Electro-Optics (CLEO '89), Baltimore, ML, ThK30, Apr. 1989.
10) M. Ohtsu and N. Tabuchi: Electrical feedback and its network analysis for linewidth reduction of a semiconductor laser, J. Lightwave Technol., 6, pp.357-369, 1988.
11) C.H. Shin, M. Teshima, M. Ohtsu, T. Imai, J. Yoshida and K. Nishide: Modulatable, high coherent and compact semiconductor laser module, to be presented at International Conference on Integrated Optics and Optical Fiber Communication (100C '89), Kobe, Japan, Jul., 1989.
12) K. Kuboki and M. Ohtsu: A synthesized method to improve coherence in semiconductor lasers by electrical feedback, to be published in IEEE J. Quantum Electron.
13) S. Takano, T. Sasaki, H. Yamada, M. Kitamura and I. Mito: Narrow linewidth (<1MHz) 1.5$\mu$m SCH-QW-DFB LD, Extended Abstracts of the 49th Autumn Meeting, The Japan Society of Applied Physics, Toyama, Japan, Oct. 1988.
14) M. Hashimoto and M. Ohtsu: A novel method to compensate for the effect of the light shift in rubidium atomic clock pumped by a semiconductor laser, submitted to IEEE Trans. on Instrum. & Meas.